Forward genetic analysis of mammalian immunity

Owen M. Siggs

Lincoln College
University of Oxford

and

The Scripps Research Institute





Submitted for the degree of Doctor of Philosophy (Joint Oxford/TSRI)

Trinity Term 2012

Statement

The research contained within this thesis was performed in the laboratories of Professor Bruce Beutler and Professor Richard Cornall between August 2007 and August 2012. The work presented is my own, with all contributions from others stated in the acknowledgments and methods.

Owen M. Siggs

September 2012

Acknowledgements

To be paid to do science is a special privilege, and I'm very grateful to the private and public donors that continue to support it. In my case, these have included The General Sir John Monash Foundation and the Skaggs Family. I'm also grateful for the efforts of Ian Wilson and Raymond Dwek, who have allowed me to conduct this research in two strikingly different environments: The Scripps Research Institute and the University of Oxford.

My mentor at Scripps, Bruce Beutler, has been a great inspiration. Here he ran a well-oiled and well-financed mutagenesis machine, providing me with technical resources and support that many scientists would only dream of. I was given the freedom to focus exclusively on science, and explore any problem (immunological or otherwise) that interested me. His steady stream of awards, capped off by a share of the 2011 Nobel Prize in Medicine and Physiology, has served as great motivation for those around him. Following his footsteps will be a lofty goal, but I hope at the very least to learn to recognise an important and underappreciated problem, and have the courage and persistence to chase it.

There were many others at Scripps who made my life there a breeze: Yu Xia for his outstanding bioinformatics support; Nengming Xiao for teaching me the TLR screen and for identifying and mapping the *sinecure* mutant; Xiaohong Li for blastocyst injections and ICSI, without which I never would've found the *scanT* mutation; Christine Domingo, Liz Hanley and Elaine Pirie for ENU injections and pedigree generation; Kevin Kovananth and Chip Ross for robotic sequencing and mapping; Pei Lin for SOLiD sequencing; Xin Du for outstanding technical know-how; Mercedes Gutierrez for taking excellent care of my mice; Terrence Robinson and Sara Kalina for genotyping; Lei Sun for ES cell and cloning advice; Carrie Arnold for all things immunisation, and for the identification of the *spelling* allele of *Atp11c*; Kasper, Micha, Philippe, Celine, Sungyong, Kathi, Wataru, Amanda, Hua and all the other Beutler lab postdocs; Nancy, Betsy and Cindy for administrative support; and David Nemazee, Michael Oldstone and Ari Theofilopoulos for their support as my thesis committee members (with some unofficial but highly valued guidance from Chris Goodnow).

At Oxford, I couldn't be more grateful for the generosity and kindness of Richard Cornall. Richard has helped me at every step of the way, and given me the freedom to continue projects that I'd started at Scripps. Thank you also to Katherine Bull for teaching me everything I know about bioinformatics; Tanya Crockford for keeping the lab running smoothly; and Greg, Delphine, Sophia, Daian, Billur and Consuelo for their help and company around the lab.

Thank you to my friends and family for their encouragement, and most of all, thank you to those who have patiently followed me around the world. It's been a great adventure.

Forward genetic analysis of mammalian immunity

Owen M. Siggs

Lincoln College

Doctor of Philosophy (Joint Oxford/TSRI)

Trinity Term 2012

Abstract

Mutation, whether spontaneous or induced, is the premier tool for understanding gene function. One approach is to create mutations in a specific gene, and then use the resulting cell or organism to search for a phenotype. An alternative is to create mutations at random, and focus first on the identification of phenotypes. The mutation that underlies a phenotype can then be tracked down, forming the foundation of testable hypotheses.

Using random chemical mutagenesis in mice, I have identified 20 heritable phenotypes affecting either the innate or adaptive branches of immunity. The genetic basis of 18 of these phenotypes was solved, caused by mutations in at least 16 unique genes. Five of these genes were not previously known to be involved in immunity, and a detailed analysis of four of them is provided in this thesis. These include genes encoding the following proteins: the inactive rhomboid protease iRhom2, which is specifically required for the secretion of tumour necrosis factor alpha; the hypothetical phospholipid flippase ATP11C, required for B cell development in the adult bone marrow; the folliculin-interacting protein FNIP1, also required for B cell development; and the zinc finger transcription factor ZBTB1, essential for the development of all lymphocyte lineages.

These findings uncover new entry points for the understanding of mammalian immunity, and highlight the value of mouse forward genetics in the understanding of mammalian phenomena in general.

Contents

1. INTRODUCTION 1

1.1. Genomes & gene function 2

1.1.1. Reverse and forward genetics 2

1.1.2. Human genetics 3

1.1.3. Experimental genetics and the mouse 3

1.2. Mouse reverse genetics 5

1.2.1. Transgenesis 5

1.2.2. Embryonic stem cells 5

1.2.3. Homologous recombination in mouse ES cells 5

1.2.4. RNA interference 6

1.2.5. Sequence-specific nucleases 6

1.3. Mouse forward genetics 8

1.3.1. Spontaneous mutation 8

1.3.2. Radiation mutagenesis 10

1.3.3. Chemical mutagenesis 10

1.3.4. Transposable elements 11

1.4. Forward genetic screening methods 13

1.4.1. Germline mutagenesis 13

1.4.2. Somatic cell mutagenesis 15

1.4.3. ES cell mutagenesis 16

1.5. Germline ENU mutagenesis 17

1.5.1. ENU administration & action 17

1.5.2. Linkage analysis 17

1.5.3. Mutation isolation by whole-genome sequencing 18

1.5.4. Validation of cause and effect 19

1.6. Immunity and the application of germline ENU mutagenesis 20

1.6.1. Adaptive immunity and lymphocyte development 20

1.6.2. Innate immunity and Toll-like receptor signalling 22

2. MATERIALS & METHODS 26

2.1. Mice, mutagenesis and mutation identification 27

2.1.1. Inbred, outbred & congenic strains 27

2.1.2. Transgenic strains 27

2.1.3. Mutant strains 28

2.1.4. Genotyping 31

2.1.5. ENU mutagenesis 31

2.1.6. Positional cloning & targeted sequencing 32
2.1.7. Whole genome sequencing 33
2.2. Macrophage isolation, stimulation and analysis 34
2.2.1. Peritoneal cell isolation 34
2.2.2. TLR stimulation 34
2.2.3. NALP3 stimulation 34
2.2.4. dsDNA stimulation 35
2.2.5. TNF bioassay 35
2.2.6. Type I IFN bioassay & cytokine ELISA 35
2.2.7. Western blotting 36
2.3. *In vivo* challenges 37
2.3.1. Infections 37
2.3.2. DSS-induced colitis 37
2.4. Flow cytometry 38
2.4.1. Ex vivo B cell culture 39
2.4.2. Quantitative RT-PCR 39
2.5. Immunisations & ELISAs 40
2.6. Haematopoietic stem cell assays 41
2.6.1. Haematopoietic chimeras and colony-forming unit assay 41
2.6.2. Retroviral transductions 41
2.7. Histology 42
2.8. Data analysis 42

3. FORWARD GENETIC ANALYSIS OF INNATE IMMUNITY 43
3.1. Innate immune receptor screen 44
3.1.1. Toll-like receptor screen 44
3.1.2. NALP3-inflammasome screen 44
3.1.3. Cytoplasmic DNA screen 47
3.2. A mutation of *Ikbkg* causes immune deficiency without impairing degradation of IκBα 48
3.2.1. NEMO and NF-κB signalling 48
3.2.2. Identification of the panr2 phenotype 49
3.2.3. panr2 mice have a mutation in Ikbkg 49
3.2.4. $Ikbkg^{panr2}$ impairs adaptive immunity 52
3.2.5. Impairment of p65 translocation, but not IκBα degradation 58
3.2.6. Discussion 58
3.3. iRhom2 is necessary for the secretion of TNFα 63
3.3.1. TLR-induced TNFα secretion 63
3.3.2. Mutation of Rhbdf2 reduces secretion of TNFα 63
3.3.3. Discussion 68

4. FORWARD GENETIC ANALYSIS OF ADAPTIVE IMMUNITY 70
4.1. Lymphocyte development screens 71
4.1.1. Blood lymphocyte screen 71
4.1.2. Competitive bone marrow chimera screen 71
4.2. The P4-type ATPase ATP11C is essential for B lymphopoiesis in adult bone marrow 75
4.2.1. B cell development 75
4.2.2. A heritable B cell deficiency 76
4.2.3. A cell-intrinsic failure of adult B lymphopoiesis 78
4.2.4. Compromised responsiveness to IL-7 81
4.2.5. Partial correction of B cell deficiency by a BCR transgene 83
4.2.6. Mutation of Atp11c 86
4.2.7. A context-sensitive requirement for ATP11C 92
4.2.8. Discussion 92
4.3. ZBTB1 is a determinant of lymphoid development 97
4.3.1. Lymphocyte development 97
4.3.2. Severe T cell lymphopenia 97
4.3.3. Mutation of a previously uncharacterized zinc finger protein 99
4.3.4. Defects in lymphoid but not myeloid development 103
4.3.5. A cell-intrinsic defect 105
4.3.6. Uncompromised haematopoietic progenitor function 105
4.3.7. Discussion 105
4.4. Folliculin-interacting protein 1 is required for B cell development 110
4.4.1. Birt-Hogg-Dubé syndrome and folliculin 110
4.4.2. A cell-intrinsic B cell deficiency 111
4.4.3. Mutation of Fnip1 111
4.4.4. Discussion 116

5. DISCUSSION 119
5.1. Summary 120
5.2. The future of mouse genetics 121
5.2.1. Forward genetics in mouse and man 121
5.2.2. Systematic reverse genetics and new tools in forward genetics 121
5.2.3. The mouse as a model of human disease 122
5.2.4. Outstanding immunological phenomena 123
5.3. Conclusions 124

6. REFERENCES 125

7. APPENDICES 148
7.1. Genotyping conditions 150
7.2. Whole-genome mapping panel markers 151
7.2.1. C57BL/6J vs C3H/HeN 151
7.2.2. C57BL/6J vs C57BL/10J 154
7.3. Publications 156

1. Introduction

1.1. Genomes & gene function

Genomes are the molecular blueprints of life. Our own genome sequence (Lander et al., 2001; Venter et al., 2001) has the potential to revolutionise our understanding of health, and the genetic variation between us will explain a substantial part of our susceptibility to disease. We each share ~21,000 protein-coding genes, and several thousand more non-protein-coding genes, but the function of the vast majority of them is a mystery. To capitalise on our knowledge of the human genome sequence, we must therefore address a challenge of interpretation. This challenge can be encapsulated by three specific questions: where are the functional elements in the genome, what are their biological roles, and what are the consequences of variation within them?

1.1.1. Reverse and forward genetics

When faced with a biological phenomenon, the genetic approach uses mutation to understand it. There are two general ways in which mutations might be exploited. The first is to introduce a defined mutation into the genome, with the expectation that it might affect the phenomenon of interest. First applied in bacteriophage (Flavell et al., 1974), this 'reverse genetic' approach involves the modification or inactivation of individual genes, the effects of which can then be studied in isolation. It also requires knowledge of where the genetic elements themselves are, which might not always be known at the outset. MicroRNA genes, for example, were not previously known to have a biological function (Lee et al., 1993), and there may still be other functional elements left to find (ENCODE Project Consortium et al., 2012).

A second approach is forward genetics, which holds no assumptions about which genes are important for a given phenomenon, nor does it require knowledge of where they are. Forward genetics begins with the identification of phenotypes: inherited variations in the phenomenon of interest. This might be an unusual behaviour or physical appearance, or a propensity to develop a disease. Where the phenotype is monogenic, the genetic cause can be tracked down, and only then does hypothesis generation begin. Pioneered in *Drosophila* (Muller, 1927), forward genetics has been applied with great success to understand many biological phenomena, including cell division (Hartwell et al., 1970), embryonic development (Nüsslein-Volhard and Wieschaus, 1980), coordination (Brenner, 1974) and cell death (Ellis and Horvitz, 1986).

1.1.2.Human genetics

The human population is rich in genetic and phenotypic diversity, and therefore ideally suited to forward genetics. Current estimates suggest that each of us harbours at least 100 loss-of-function variants in protein-coding genes (MacArthur et al., 2012), some of which can lead to a monogenic inherited phenotype (McKusick, 2006). These inherited phenotypes are typically rare, yet solving their genetic cause can tell us much about normal physiology, and even about more common disease mechanisms (Brown and Goldstein, 1976).

The availability of the human genome reference sequence and massively parallel sequencing technology has transformed Mendelian gene discovery, to the point at which causative rare variants can be found within a matter of weeks for a only a few thousand dollars (Lupski et al., 2010; Ng et al., 2010). Our understanding of polygenic diseases has also benefitted from testing increasingly large patient cohorts for variant-specific associations (Wellcome Trust Case Control Consortium, 2007).

Mutation is also a driving force behind cancer and other somatic genetic diseases. These diseases, too, are susceptible to massively parallel sequencing (International Cancer Genome Consortium et al., 2010), and carry the advantage of a normal reference sequence with which to compare the diseased cell genome. Distinguishing disease-causing "driver" mutations from incidental "passenger" mutations may be difficult at first, but will become increasingly easier as recurrent mutations are observed within the same genes.

1.1.3.Experimental genetics and the mouse

Once a candidate mutation is found, linking mutation to phenotype requires experimentation. Mutations affecting a cell-intrinsic process can be relatively straightforward to examine in patient cells *ex vivo* (Li et al., 2011a), so long as the cell type in question is accessible. An alternative is to create induced pluripotent stem cells (Takahashi et al., 2007; Yu et al., 2007) and engineer the mutation within them (Hockemeyer et al., 2009; Zou et al., 2009). This gives a potentially unlimited supply of mutant and control cells on a uniform genetic background, which can be differentiated into a wide array of cell types *in vitro*.

For those disease processes that cannot be replicated *in vitro*, a physiological model is required. This might be as simple as a worm or fruit fly, or as complex as a zebrafish or mouse, although it is usually preferable to study a phenomenon in the simplest system available. Since many phenomena are

unique to mammals, the mouse is often the most suitable experimental organism. More than 99% of human genes have a direct counterpart in the mouse genome (Mouse Genome Sequencing Consortium et al., 2002), making the mouse an experimentally tractable tool for understanding the human genome. The mouse has many other advantages as a model organism: modest size, short generation time, high fecundity, a wide array of inbred strains, and an assortment of tools for genetic modification. Forward and reverse genetics are practiced widely in the mouse, and will be described in the following paragraphs.

1.2. Mouse reverse genetics

1.2.1. Transgenesis

The ability to specifically modify the mouse genome originated with transgenesis. Fertilised mouse oocytes could be injected with a transgene element, and following random integration into the genome, the transgene would be transmitted to the offspring (Gordon et al., 1980; Brinster et al., 1981). A similar outcome could be achieved by infecting an early mouse embryo with a murine retrovirus (Jaenisch, 1976). A variety of transgenes could be introduced, including oncogenic transgenes, which could be driven by tissue-specific promoters (Adams et al., 1985). Although transgenesis was well suited to ectopic expression of certain genes, it could not reliably silence them, and alternative approaches were necessary.

1.2.2. Embryonic stem cells

The first mouse embryonic stem (ES) cell lines were isolated from 3.5 day-old blastocysts (Evans and Kaufman, 1981). These ES cell lines could be cultured indefinitely, and retained their capacity to form endodermal, ectodermal and mesodermal cell types (in the form of a teratocarcinoma) when injected into syngeneic mice (Evans and Kaufman, 1981). When injected into blastocysts (Gardner, 1968), the same ES cells contributed to multiple cell types in the resulting chimeric animals, including cells of the germ line (Bradley et al., 1984). This allowed for the heritable transmission of retroviral insertions made in ES cells *in vitro* (Robertson et al., 1986), including specific loss-of-function mutations in the X-linked *Hprt* gene, which could be selected for in male cells with 6-thioguanine (Kuehn et al., 1987).

1.2.3. Homologous recombination in mouse ES cells

A core requirement of reverse genetics is the ability to make targeted modifications. Yeast geneticists established that exogenous DNA with homology to chromosomal sequences could recombine stably and specifically at the homologous chromosomal locus (Orr-Weaver et al., 1981). This was later applied to the β-globin locus in human cells (Smithies et al., 1985), and eventually also to the *Hprt* locus in 6-thioguanine-selected mouse ES cells (Doetschman et al., 1987; Thomas and Capecchi, 1987). Gene targeting could also be achieved without direct selection of the mutant phenotype, and many other targeted loci soon followed (Johnson et al., 1989; Joyner et al., 1989; Koller and Smithies, 1989;

Schwartzberg et al., 1989). More discrete point mutations could also be created by a two step insertion and reversion method (Hasty et al., 1991).

Methods of genetic modification became increasingly sophisticated, co-opting genetic tools from other organisms. One of these is the Cre-*loxP* system of bacteriophage P1 (Sternberg and Hamilton, 1981), which permits site-specific recombination (Sauer and Henderson, 1988). Combined with an ability to introduce transmissible transgenes (Gordon et al., 1980; Brinster et al., 1981), Cre transgene-mediated recombination allowed mutations to be made selectively *in vivo*, including in specific cells (Lakso et al., 1992; Orban et al., 1992; Gu et al., 1994), or in an interferon-inducible manner (Kühn et al., 1995). The ability to perform homologous recombination in mouse ES cells has formed the foundation of mouse reverse genetics, with large-scale efforts now underway to construct conditional alleles of all mouse genes (Skarnes et al., 2011).

1.2.4.RNA interference

The discovery of RNA interference arose from observations in plants, in which expression of a transgene led to the silencing of an endogenous pigmentation gene (Napoli et al., 1990). This was subsequently explained in *Caenorhabditis elegans* (Fire et al., 1998), and has since been applied for gene silencing in transgenic mice (Carmell et al., 2003; Dickins et al., 2007). RNA interference is generally inferior to mutation as a means of understanding gene function, given the associated off-target effects and incomplete silencing, but has been a powerful tool for systematic reverse genetic screens in *Caenorhabditis elegans* (Fraser et al., 2000) and some mammalian cell lines (Berns et al., 2004; Ngo et al., 2006).

1.2.5.Sequence-specific nucleases

Bacterial restriction enzymes serve an important function in bacterial immunity, recognising and cleaving DNA sequences that are absent from the host genome, yet present in the genomes of viruses and other bacterial species (Arber, 1965; Smith and Wilcox, 1970). No such counterpart is known to exist in mammalian cells, although a similar enzyme can be engineered with modular DNA binding domains. One of these is the zinc-finger domain (Miller et al., 1985), which is the most common DNA-binding domain encoded by our genome (Klug, 2010). By combining a series of zinc-finger domains with the *Fok*I

endonuclease domain, zinc-finger nuclease enzymes can create double-stranded breaks at a defined site (Kim et al., 1996).

A second modular sequence-recognition domain comes from the bacterial plant pathogen genus *Xanthomonas*. Transcription activator-like (TAL) effector proteins promote pathogenesis by binding to specific host DNA sequences and activating gene expression (Römer et al., 2007). Unlike zinc-finger domains which typically recognise trinucleotides, each TAL effector repeat recognises a single nucleotide (Boch et al., 2009; Moscou and Bogdanove, 2009). As with zinc-finger nucleases, assembly of TAL effector repeats with the *Fok*I endonuclease domain can direct sequence-specific cleavage (Christian et al., 2010). Both zinc-finger and TAL effector nucleases are becoming indispensable tools for genome engineering in multiple species, and seem likely to supersede conventional homologous recombination as the method of choice for gene targeting in the mouse.

1.3. Mouse forward genetics

Forward genetics starts with no assumptions about how a given phenomenon might work, or which regions of the genome might be involved, but relies only on the creation of phenotypes by random mutagenesis. Reverse genetics, too, can be performed on a systematic scale, with engineered cells or animals screened for phenotypes of interest (Gates et al., 2011). Systematic overexpression of genes, which led to the discoveries of the pluripotency gene *Nanog* (Chambers et al., 2003) and later to cellular reprogramming (Takahashi and Yamanaka, 2006), could also be considered a form of genetic screen. The distinction between forward genetics and systematic reverse genetics can often become blurred, although there is still an element of bias inherent in the latter, since it begins with the assumption that all functional genetic elements are known. Forward genetics begins instead with random mutation, which may occur spontaneously (as it does in people), or can be conducted in the laboratory (as summarised in **Table 1.1**).

1.3.1. Spontaneous mutation

Genetic diversity is abundant in the human population, as it is in laboratory mice. Part of this is a consequence of environmental mutagens, with the remainder being a simple consequence of error-prone DNA replication. Inherited genetic variation had been recognised ever since the rediscovery of Mendel's laws (Mendel, 1866) and their application to coat colour alleles in mice (Cuénot, 1902; 1903). We owe much of our knowledge of mammalian genetics to mouse fanciers of the 18th, 19th and 20th centuries, particularly Miss Abbie Lathrop, who assembled diverse collections of allelic variants (Silver, 1995). From these stocks emerged the inbred mouse strains as we know them today.

One set of allelic differences between inbred strains occurred at the major histocompatibility locus: the understanding of which led to the development of clinical organ transplantation (Snell, 1948). Other variants have arisen more recently, and revealed the genetic basis of phenomena such as appetite control (Zhang et al., 1994), the sensing of infection (Poltorak et al., 1998), and the control of autoimmunity (Watanabe-Fukunaga et al., 1992; Brunkow et al., 2001). Polygenic phenotypes have been more difficult to solve, although libraries of recombinant inbred strains are being produced to help deconstruct them (Churchill et al., 2004).

Table 1.1 | Mutagenic agents for forward genetic screens.
Examples are presented for each of the four major classes of mouse mutagen, along with the type of mutation they induce, any mutagenic biases they show, and the contemporary method used for their discovery. CGH, comparative genomic hybridisation; MuLV, murine leukemia virus; GOF, gain of function; LOF, loss of function.

mutagen	**example**	**mutation classes**	**mutation sites**	**mutation discovery**
radiation	X-ray	deletions, insertions, rearrangements	unbiased	CGH
chemical	ENU	point mutations	unbiased	whole-genome sequencing
retrovirus	MuLV	insertions (GOF or LOF)	biased	splinkerette PCR
transposon	*Sleeping Beauty, piggyBac, Tol2*	insertions (GOF or LOF)	biased	splinkerette PCR

1.3.2.Radiation mutagenesis

To accelerate the discovery of inherited phenotypes, mutations can also be induced. X-rays were the first mutagenic agent to be defined, based on their ability to create phenotypes in *Drosophila* associated with visible chromosomal changes (Muller, 1927). Ultraviolet light had similar effects (Altenburg, 1928), and both X-rays and radium were found to induce mutations in maize (Stadler, 1928). The type of mutation induced will depend upon the radiation source, with UV irradiation primarily creating pyrimidine dimers, some of which lead to point mutations after incorrect repair. Ionising radiation, on the other hand, induces double-stranded breaks, which after repair can lead to deletions, duplications, rearrangements, or translocations.

Radiation mutagenesis is equally effective in mice (Snell, 1935), and an important tool used to define the transmissible mutation rate was the *T*-stock: a strain of mice homozygous for a series of seven visible recessive mutations (Russell, 1951). Six of these mutations affect coat colour: *nonagouti*, *brown*, *chinchilla*, *dilute*, *pink-eyed dilution*, *piebald-spotting*; while one affects ear morphology: *short-ear*. By breeding mutagenised male mice with *T*-stock females, new recessive mutations at any of the loci could be visibly observed in the F1 progeny. This technique, known as the specific locus test, became the gold-standard method for quantification of heritable mutations in mice.

1.3.3.Chemical mutagenesis

The first mutagenic chemical to be identified was mustard gas (Auerbach et al., 1947). Dozens have been discovered since and used extensively in forward genetic screens (Brenner, 1974; Nüsslein-Volhard and Wieschaus, 1980), although most were inferior to the mutagenic effects of X-rays. One exception is *N*-ethyl-*N*-nitrosourea (ENU), which acts by transferring its ethyl group to nucleophilic nitrogens or oxygens within nucleic acids. Single base substitutions are the most common outcome of this modification, resulting in a diverse array of alleles.

Specific locus test experiments determined that ENU was 5 times more mutagenic than the optimal dose of X-rays, and 15 times more mutagenic than procarbazine, the most mutagenic chemical known at the time (Russell et al., 1979). ENU became a "mutagen of choice" for random mutagenesis in the mouse (Russell et al., 1979), and was applied in early experiments to reveal dominant mutations which predisposed mice to cancer (Moser et al., 1990) or disrupted circadian rhythm (Vitaterna et al.,

1994). Large-scale ENU mutagenesis screens soon followed for the isolation of recessive mutations (Justice et al., 1999).

1.3.4. Transposable elements

DNA elements can themselves be used as mutagens. One such element is the transposon, first discovered as the agent of mosaic kernel pigmentation in maize (McClintock, 1950). These elements encode a transposase enzyme, flanked on either side by short repetitive sequences, which catalyses the excision and reintegration of the transposon element elsewhere in the genome. This system can also be engineered: the contents of the transposon can be modified (within certain size limits), and an exogenous transposase enzyme can drive transposition in an inducible or tissue-restricted manner.

Depending on the insertion site and contents of the transposable element, an insertion may either activate or inactivate a gene. If the insertion occurs within an exon, for instance, the gene product is usually disrupted. Elements containing a splice-acceptor site can also silence a gene if positioned within an intron, while promoter-bearing elements can activate expression of gene if positioned in the correct upstream orientation. This is especially useful for studies of tumorigenesis, in which both types of mutations are often necessary for the transition to disease (Dupuy et al., 2005).

Various transposons are active in mammalian cells, including *Tol2* (Koga et al., 1996), *Sleeping Beauty* (Ivics et al., 1997) and *piggyBac* (Ding et al., 2005). Each has its own advantages, with *piggyBac* generally considered to be the most versatile of the three. Among its advantages are a large cargo capacity (Li et al., 2011b), high transposition efficiency (Liang et al., 2009), absence of an excision "footprint" that is characteristic of other transposons, and relative lack of local hopping effects (Wang et al., 2008). Viruses can also act as insertional mutagens, transcribing their RNA genome into DNA (Baltimore, 1970; Temin and Mizutani, 1970) before integrating it into the host genome. The mutagenic potential of retroviruses was clear from their ability to induce cancer (Rous, 1911; Stehelin et al., 1976), and was one of the first mutagens applied for phenotypic screens in mouse ES cells (Kuehn et al., 1987).

Compared to radiation- and chemically-induced mutations, insertional mutations have been relatively straightforward to locate. Various PCR-based methods can be used to amplify sequences surrounding the insertion site, revealing the insertion boundary (Uren et al., 2009). Yet both transposons

and retroviruses exhibit biases with respect to their insertion sites, which are often restricted to expressed genes.

1.4. Forward genetic screening methods

A forward genetic screen relies upon the creation of phenotypes by mutation. Like almost all mammals, mice are diploid, and therefore have two alleles of every autosomal gene in each somatic cell. Phenotypes can result from mutations in one or both alleles of a gene, respectively classified as dominant or recessive. A dominant mutation might cause a phenotype simply by inactivating the gene product, or alternatively, by conferring an entirely new function (Muller, 1932). Screens for dominant phenotypes are therefore the most straightforward to conduct, since they require mutation of only one allele in cells or in animals.

Most mutations, however, are recessive: that is, their phenotypic effect is masked by the wild-type allele (Fisher, 1928; Wilkie, 1994). This poses a problem for genetic screens, as these genes require both alleles to be mutated before a phenotype can be observed. Experimental geneticists have developed various methods to circumvent this problem, some of which will be described in the following sections.

1.4.1. Germline mutagenesis

The earliest forward genetic screens were performed in whole organisms (Muller, 1927). These relied upon the transmission of mutations through the germline, usually by inducing mutations in male spermatogonia. ENU is the most efficient germline mutagen known in the mouse (Russell et al., 1979), although both radiation and transposable elements are also effective. The progeny of a mutagenised male can then be screened for phenotypes, either in the first generation (for dominant phenotypes), or in later generations after inbreeding (for dominant and recessive phenotypes)(**Figure 1.1A**).

While inbreeding is the most straightforward way to bring recessive mutations to homozygosity, the use of balancer chromosomes can accelerate their selection. First applied in *Drosophila*, balancer chromosomes allow for the selection of mutations within defined chromosomal intervals (Muller, 1918). An engineered inversion of mouse chromosome 11, for example, promotes transmission of an intact mutant chromosome by suppressing recombination (Zheng et al., 1999). The inverted chromosome can be followed by a dominant coat colour transgene, allowing the mutagenised chromosome to easily be brought to homozygosity. This has proven to be an effective way of isolating recessive mutations (Kile et al., 2003), although it is limited by the availability of engineered chromosomal inversions (van der Weyden and Bradley, 2006).

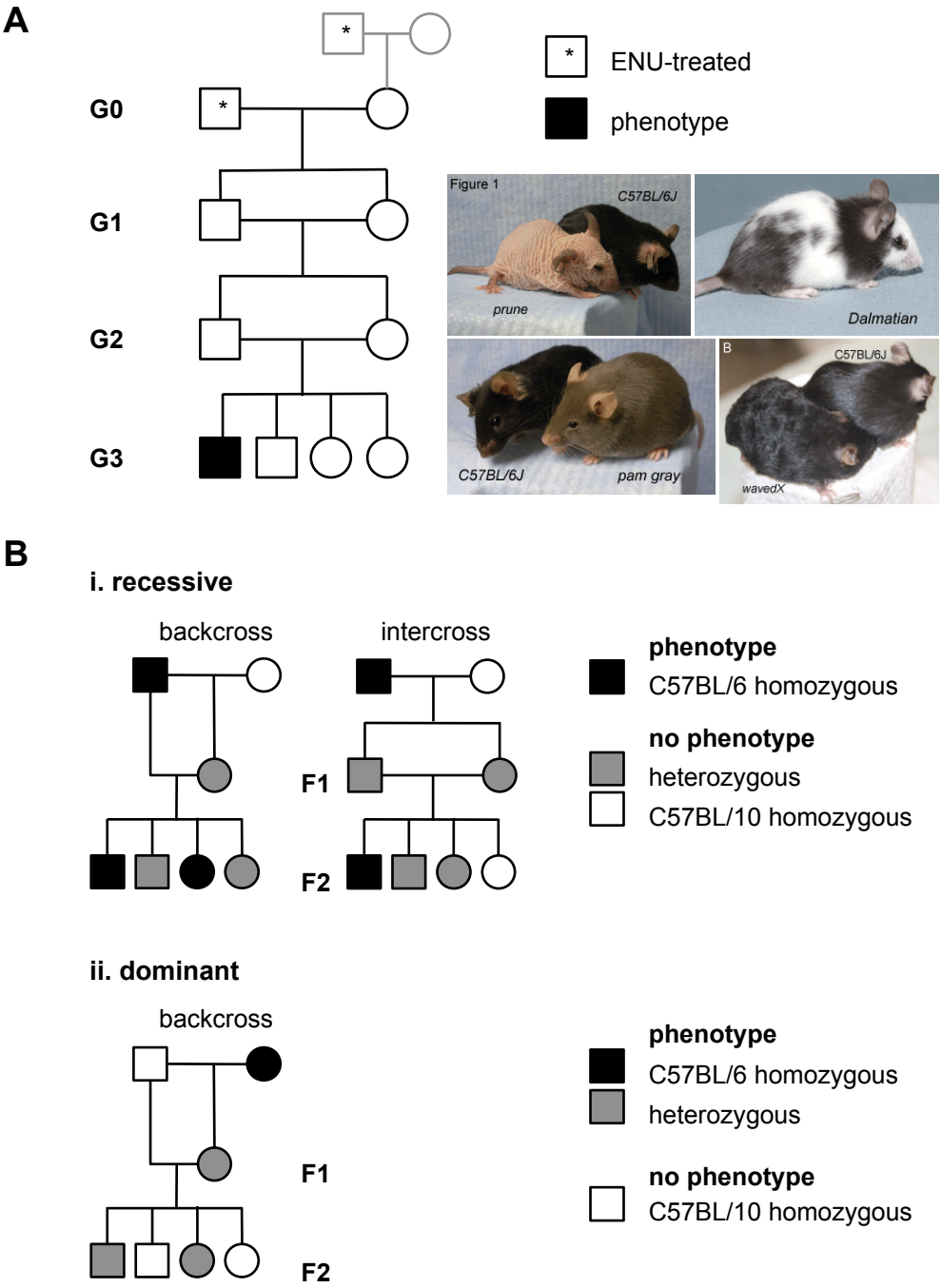


Figure 1.1 | Pedigree structures for ENU mutagenesis and positional cloning. ENU-treated males are bred to untreated C57BL/6J females, or to the daughters of a different ENU-treated male. After two generations of brother-sister mating, third generation progeny (G3) are screened for dominant and recessive phenotypes. Examples of visible phenotypes are shown alongside. (B) Having identified a phenotype, the mutation can be isolated by outcross-based mapping. The pedigree structure will depend upon the inheritance pattern of the phenotype, but may involve either backcross or intercross strategies. F2 mice are then screened for the phenotype, and genotyped at a series of polymorphic markers to test for linkage.

Under certain rare reproductive circumstances, mutations can be brought to homozygosity within a single generation. Gynogenesis is a reproductive phenomenon in which an oocyte is activated by sperm, without any genetic contribution from the sperm itself. This has been exploited in zebrafish to produce large numbers of homozygous progeny (Streisinger et al., 1981), and now represents a valuable tool in zebrafish germline mutagenesis screens. A related phenomenon is parthenogenesis, in which embryogenesis proceeds from an oocyte in the complete absence of sperm. It occurs naturally in several species of plants and invertebrates, but only rarely in vertebrates such as the Komodo dragon (Watts et al., 2006). Since diploid parthenotes arise exclusively from the haploid oocyte genome, parthenogenesis is a means of quickly bringing recessive mutations to homozygosity. Artificial parthenogenesis has been achieved in several organisms including engineered mice (Kono et al., 2004), although parthenogenetic mice have yet to be used in genetic screens.

1.4.2.Somatic cell mutagenesis

For those phenotypes that are cell-intrinsic, mutagenesis of the cells themselves can be an efficient alternative. It also allows the identification of mutations that would otherwise be lethal in a developing embryo, and therefore not detectable in traditional germline mutagenesis screens. Somatic mutagenesis can be performed either *in vitro* or *in vivo*, usually under conditions that favour survival of mutant cells. In this respect, somatic mutagenesis is especially well suited to the identification of tumorigenic mutations, since cells with the correct set of mutations are clonally expanded. If a selective agent is not available, mutant clones can also be screened in isolation. Both *in vitro* and *in vivo* approaches generally favour the identification of dominant or sex chromosome-linked mutations, unless the dose of mutagen is sufficiently high to mutate both alleles independently.

Certain cell lines, including Chinese hamster ovary cells (Tjio and Puck, 1958), are known to be functionally hemizygous at many loci despite being diploid (Siminovitch, 1976). This permits the identification of mutations that would otherwise be recessive, and has been used to study various cellular phenotypes including DNA repair. Haploid cells are more useful still, and a partially haploid subclone isolated from a human myeloid leukemia line (Andersson et al., 1995) (haploid at all chromosomes except chromosome 8 (Kotecki et al., 1999)) has become a powerful genetic screening tool for many cell-intrinsic phenotypes (Carette et al., 2009).

Unlike germline mutations, which can be separated by meiotic recombination, somatic mutations can be difficult to isolate. Cell fusion experiments can establish if a mutation is recessive or dominant, but systematic cDNA complementation has traditionally been the only way to expose a causative mutation. Massively parallel sequencing is beginning to change this, shifting the bottleneck from identification to validation. For most current applications, transposable elements are the most suitable somatic mutagen, due to the ease with which they can be found (Uren et al., 2009).

1.4.3.ES cell mutagenesis

Forward genetic screens may also be conducted in ES cells. A key advantage is that mutagenised ES cells may be differentiated into an array of different cell types *in vitro* (Williams et al., 2012), and may also be transmitted to the mouse germline for *in vivo* analysis or meiotic mapping (Chen et al., 2000; Munroe et al., 2000).

Diploidy, again, is an issue for ES cell mutagenesis screens. Yet unlike many cell lines, specific mutations can be engineered in mouse ES cells, including those that increase spontaneous loss of heterozygosity. Inactivation of the mouse ortholog of the Bloom syndrome gene (Ellis et al., 1995), for example, leads to increased loss of heterozygosity (Luo et al., 2000). This allows for the creation of homozygous mutations in diploid ES cells, and has successfully been applied in recessive phenotypic screens (Guo et al., 2004; Yusa et al., 2004).

A more preferable alternative to *Blm* mutation is the use of haploid ES cell lines. Haploid cell mutagenesis has been a staple of yeast genetics (Hartwell et al., 1974), and has shown recent success in a human cancer cell line (Carette et al., 2009). Haploid ES cell lines have only recently been isolated, first from *Medaka* fish (Yi et al., 2009), and subsequently from parthenogenetic mouse embryos (Elling et al., 2011; Leeb and Wutz, 2011). These came many years after the first observations of haploid mouse ES cells (Kaufman et al., 1983), due in part to the development of specialised culture conditions (Ying et al., 2008). Androgenetic haploid ES cells have also been established, derived from enucleated oocytes injected with haploid sperm heads (Yang et al., 2012). Like their parthenogenetic counterparts these cells can be mutagenised *in vitro* and contribute to multiple tissues after blastocyst injection, including, importantly, the germ line (Leeb et al., 2012; Yang et al., 2012). Given that it is already possible to create

parthenogenetic human embryos and ES cells (Strain et al., 1995; Kim et al., 2007; Revazova et al., 2007), it seems inevitable that human haploid ES cell lines will soon exist.

1.5. Germline ENU mutagenesis

For the study of physiological phenotypes there is often no substitute for the mouse, and with the exception of screens for cancer-causing mutations, germline mutagenesis is the most suitable approach. ENU is the most effective germline mutagen known in the mouse (Russell et al., 1979), and the approach to creating and discovering ENU-induced mutations will be described below.

1.5.1. ENU administration & action

As with radiation (Russell, 1962), administering ENU in a fractionated dose is more effective than a single administration of the total dose (Hitotsumachi et al., 1985). A common administration schedule for C57BL/6 male mice is three weekly intraperitoneal injections of 100 mg/kg ENU (Hitotsumachi et al., 1985). This is followed by a period of infertility of 6-13 weeks, during which time mutagenised spermatogonial stem cells repopulate the testes. An estimated 1.6 mutations per megabase of DNA are transmitted to the progeny, more than 80% of which change A-T base pairs (Bull et al., in press). Where these mutations fall into protein-coding intervals, they primarily cause missense (64%), splicing (26%) and nonsense (10%) mutations (Arnold et al., 2012a). Mutations that cause detectable phenotypes almost exclusively fall into these categories (Arnold et al., 2012a), with exceptional cases in a miRNA gene and highly conserved *cis*-regulator of the Sonic hedgehog (*Shh*) gene (Masuya et al., 2007; Lewis et al., 2009). Based on comparisons of ENU-induced mutations that cause phenotype, and those which occur incidentally in the same mice, it has been estimated that 15.4% of ENU-induced missense variants are phenotypically detectable (Arnold et al., 2012a).

1.5.2. Linkage analysis

Traditional methods to isolate phenotypic mutations require the use of genetic linkage (Morgan, 1911). This involves tracking the inheritance of phenotypes and defined chromosomal markers after meiotic recombination, and searching for a significant association (Morton, 1955). The original linkage markers were themselves mutations that caused visible phenotypes (Haldane et al., 1915), and were eventually

collected for all 20 mouse chromosomes (Lyon and Searle, 1989). Following the development of restriction enzyme- (Danna and Nathans, 1971; Botstein et al., 1980) and PCR-based (Saiki et al., 1985) assays, high resolution genetic maps were assembled across the entire mouse genome (Dietrich et al., 1996). The use of inbred strains became essential for high-resolution mapping, since only markers that were polymorphic between strains were informative. Yet the more different two strains were, the more likely it was that a phenotype would be masked by strain-specific modifier alleles. As more interstrain variation was discovered, more closely-related strains could be used for mapping sensitive phenotypes (Xia et al., 2010). In addition to the C57BL/6J reference genome, sequence is now available for an additional 17 inbred strains (Keane et al., 2011).

A standard mapping cross begins by outcrossing a mutant animal to a different inbred strain (**Figure 1.1B**). F1 progeny are then either intercrossed or backcrossed to their mutant parent (if recessive), or bred again to the outcross strain (if dominant). F2 mice are scored for phenotype, and genotyped at polymorphic markers either in groups or individually. The more F2 mice that are analysed, the more likely it is that an informative meiotic recombination event will occur, and the smaller the chromosomal interval becomes.

Once a phenotype has been isolated to a small chromosomal interval, the causative mutation within it must be found. This initially required the use of positional cloning, in which genomic fragments were systematically cloned and capillary sequenced (Sanger et al., 1977) until the causative mutation was revealed (Zhang et al., 1994). This approach was drastically accelerated by the availability of the mouse genome sequence (Mouse Genome Sequencing Consortium et al., 2002), which allowed investigators to focus their efforts on defined genes within their interval.

1.5.3.Mutation isolation by whole-genome sequencing

Massively parallel sequencing has transformed how ENU-induced mutations are found. Capillary sequencing of small linkage intervals was initially replaced by targeted exome capture (Zhang et al., 2009), and later by whole exome (Fairfield et al., 2011) and whole genome (Arnold et al., 2011) approaches. These obviate the need for high-resolution fine mapping, requiring little more than linkage to a chromosome (Arnold et al., 2011).

Sequencing multiple affected genomes removes the need for outcross-based mapping altogether, since ENU-induced mutations themselves can be used for linkage analysis (Bull et al., in press). Combined with knowledge of the mutations present in G1 pedigree founders (Andrews et al., 2012), causative mutations may now be discovered within days of finding a phenotype.

1.5.4. Validation of cause and effect

When one or more candidate mutations are found, their connection to a phenotype must be validated. Multiple candidate mutations within a region may be prioritised based on their predicted detrimental effects (Adzhubei et al., 2010), or tissue-restricted expression (Su et al., 2004). In some cases an existing allele may be known to cause a similar phenotype, and where possible, can be bred to test for allelism. Where a phenotype is cell-intrinsic it may be complemented with wild-type cDNA via transfection or transduction, or where possible, by wild-type recombinant protein (Jiang et al., 2005). For cases where the affected cell type is not accessible, or where the mutation has wider systematic effects, transgene complementation may be used. The availability of gene-trap and conditional null allelic archives also provides a valuable resource for mutation validation (International Mouse Knockout Consortium et al., 2007).

1.6. Immunity and the application of germline ENU mutagenesis

The general phenomenon to be addressed in this thesis is immunity: how is it that most of us resist infection by pathogenic microbes, despite constant exposure to them? While the microbe is necessary to cause disease (Koch, 1876), it is not always sufficient, and host genetics are an important determinant of susceptibility (Sørensen et al., 1988). This is hardly surprising given the powerful selective pressure that infection confers.

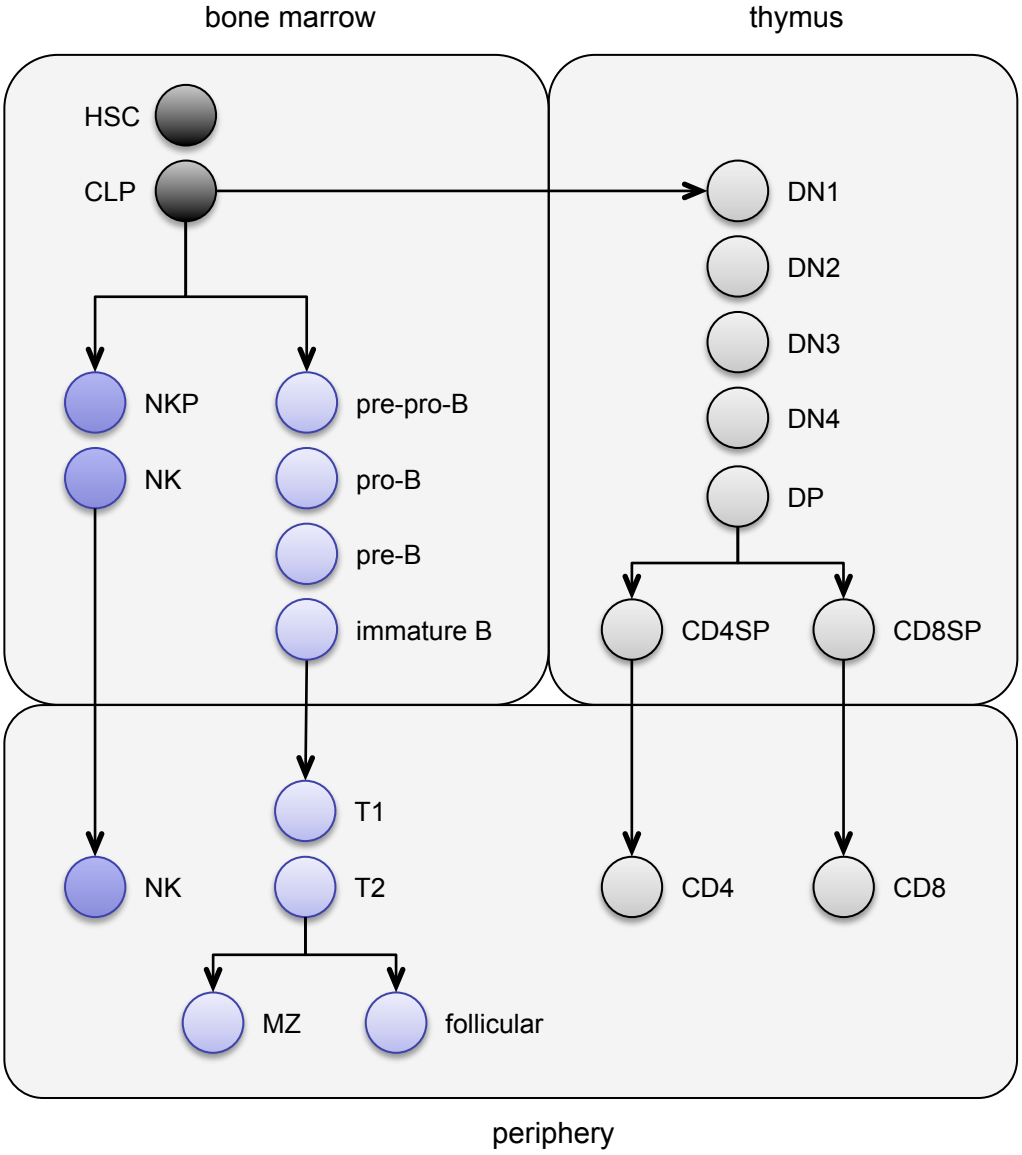
Forward and reverse genetics have revealed much about immunity, and as our understanding has increased, so too has the number of phenomena available to study. The two primary branches of immunity, and forward genetic screens to study each of them, will be described below.

1.6.1. Adaptive immunity and lymphocyte development

Following the discovery of microbes and their ability to cause disease, it became clear that organisms possessed ways to avoid them. One of these was only acquired after exposure to a pathogen, and forms the basis of vaccination. This adaptive form of immunity has evolved independently at least twice in vertebrates (Pancer et al., 2004), and forms an anticipatory arm of immunity with an enormous breadth of potential specificities (Hozumi and Tonegawa, 1976). This breadth also encompasses antigens in our own bodies, and immune cells bearing these specificities must be purged or silenced to avoid autoimmune disease (Goodnow et al., 2005). The importance of adaptive immunity is underlined by the consequences of its absence: unless patients receive a bone marrow transplant it is almost universally lethal (Gatti et al., 1968).

T and B lymphocytes are the primary effector cells of the adaptive immune system, and arise from self-renewing haematopoietic stem cells present first in the mammalian foetal liver, and later in the adult bone marrow (Becker et al., 1963)(**Figure 1.2**). B cells complete most of their development in the foetal liver or bone marrow (Osmond and Nossal, 1974; Owen et al., 1974), with further maturation in the spleen. T cell progenitors, on the other hand, migrate to and mature within the thymus (Miller, 1961) where their primary sublineage ($CD4^+$ or $CD8^+$) is defined. The most severe inherited immunodeficiencies are caused by an arrest of T cell development, which may result from failures to rearrange or transmit signals through the T cell antigen receptor, or to respond to essential cytokines (Fischer, 2007). Similarly, inherited immunodeficiencies can arise from failures in B cell development, immunoglobulin class-switching, or

Figure 1.2 | Overview of lymphocyte development.
Primary developmental stages of the three primary lymphocyte subsets (T, grey; B, light blue; NK, dark blue). Each of them arise from bone marrow progenitors, and complete their maturation in peripheral lymphoid organs. HSC, haematopoietic stem cell; CLP, common lymphoid progenitor; NKP, natural killer precursor; T1/T2, transitional 1/2; MZ, marginal zone; DN, double negative; DP, double positive; SP, single positive.



general antibody production (Conley et al., 2009). The majority of inherited immunodeficiencies fall into the latter category, collectively known as common variable immunodeficiency (CVID), for which the genetic basis of most cases is unknown.

Since adaptive immunity is unique to vertebrates, the mouse represents an ideal model organism to study it. Spontaneous mouse mutants have revealed the genetic basis of several adaptive immune phenomena, including lymphocyte death (Watanabe-Fukunaga et al., 1992), dominant tolerance (Brunkow et al., 2001), and T cell lineage commitment (He et al., 2005). Phenotypic screening of mutagenised mice continues to reveal many more molecules, largely through the study of lymphocyte development and the response to immunisation (Nelms and Goodnow, 2001; Vinuesa and Goodnow, 2004).

1.6.2.Innate immunity and Toll-like receptor signalling

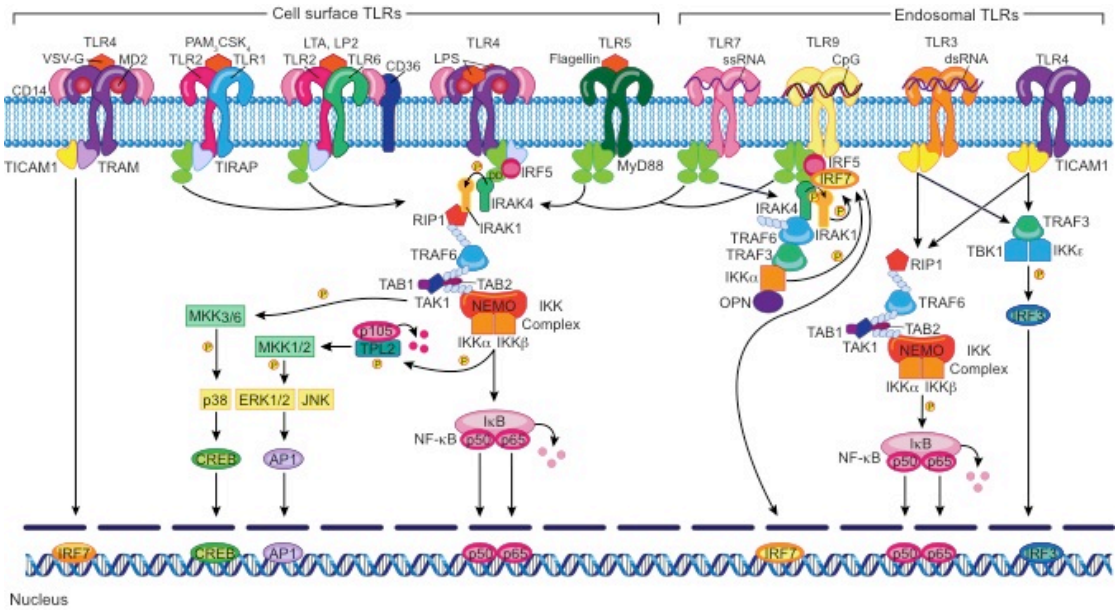
Mammals also possess more immediate pathogen-avoidance mechanisms, many of which are shared with invertebrates. Phagocytosis, first described by Ilya Mechnikov, was one such mechanism, whereby cells of the host would engulf and destroy invading microbes. Precisely how the body became aware of microbes was learned much later, starting with the observation that the gram-negative bacterial product endotoxin could induce fever and shock in guinea pigs (Pfeiffer, 1892). Many years later, two strains of mice were identified that did not respond to endotoxin challenge, yet were extremely sensitive to infection with gram-negative bacteria (Heppner and Weiss, 1965; Coutinho and Meo, 1978). This laid the foundation for a positional cloning effort, culminating in the discovery that Toll-like receptor 4 (TLR4), a homolog of the *Drosophila* protein Toll (Lemaitre et al., 1996), mediated the effects of bacterial lipopolysaccharide (Poltorak et al., 1998).

Many other mammalian TLRs have since been characterised by targeted gene deletion (Takeuchi and Akira, 2010), accounting for the effects of multiple inflammatory substances (**Table 1.2**). Some TLRs also require accessory proteins to recognise their ligand: CD14 and MD2, for example, are required for lipopolysaccharide to bind to TLR4 (Wright et al., 1990; Nagai et al., 2002), while CD36 is required for sensing diacylated lipopeptides (Hoebe et al., 2005). All TLRs signal via one or more of the cytoplasmic adapter proteins MyD88, Trif, Tram and Tirap, culminating in the expression of proinflammatory cytokines such as tumour necrosis factor alpha and type I interferon (Beutler et al., 2006)(**Figure 1.3**).

Table 1.2 | Mammalian Toll-like receptors.
There are 10 TLRs encoded by the human genome, with 12 in the mouse, for a total of 13 TLRs between the two species.

TLR	species	associated molecules	ligand(s)	adaptor
TLR1/ TLR2	human mouse	CD14, CD36, Dectin-1	triacylated lipoproteins, glycolipids	MyD88, Tirap
TLR2/ TLR6	human mouse	CD14	diacylated lipoproteins, lipotechoic acid, zymosan, peptidoglycan	MyD88, Tirap
TLR3	human mouse		poly(I:C), dsRNA	Trif
TLR4	human mouse	CD14, MD2	LPS, taxol, heparan, hyaluronate, F-prot (RSV), G-prot (VSV), Env prot (MMTV)	MyD88, Tirap, Trif, Tram
TLR5	human mouse		flagellin	MyD88
TLR7	human mouse		ssRNA, nucleoside analogues (imiquimod, loxoribine, resiquimod)	MyD88
TLR8	human mouse		ssRNA, nucleoside analogues (imiquimod, loxoribine, resiquimod)	MyD88
TLR9	human mouse		CpG DNA	MyD88
TLR10	human		?	?
TLR11	mouse		profilin	MyD88
TLR12	mouse		?	?
TLR13	mouse		23*S* rRNA	MyD88

Figure 1.3 | Overview of Toll-like receptor signalling.
TLRs signal either from the cell surface, or from within endosomal compartments. Modified from a figure produced by Diantha La Vine.



Other proinflammatory substances are recognised by additional receptor families, including the NOD-like (Martinon et al., 2006), RIG-I-like (Yoneyama et al., 2004), and C-type lectin receptors (Brown et al., 2002). Loss-of-function mutations affecting these and other innate immune pathways have since been found to cause primary immunodeficiencies in man (Casanova et al., 2011), and rare gain-of-function mutations have also been shown to cause sterile inflammatory diseases (Hoffman et al., 2001).

While their effects are usually studied at a cellular level, many conceptual leaps in innate immunity have been made with the help of inherited phenotypes in mice. These include the first description of microbial recognition by a Toll-like receptor (Poltorak et al., 1998), the identification of essential signalling adapters (Hoebe et al., 2003) and coreceptors (Hoebe et al., 2005), and molecules that traffic endosomal TLRs (Tabeta et al., 2006).

In this thesis, I have applied germline ENU mutagenesis and phenotypic screening to reveal new components of mammalian innate and adaptive immunity. In Chapter 3, I will describe mutations that affect Toll-like receptor signalling, including variants of the *Ikbkg* and *Rhbdf2* genes. Mutations affecting lymphocyte development will be described in Chapter 4, including alleles of *Atp11c*, *Zbtb1* and *Fnip1*.

2. Materials & Methods

2.1. Mice, mutagenesis and mutation identification

All animal procedures were in accordance with guidelines of the Institutional Animal Care and Use Committee of The Scripps Research Institute and University of Texas Southwestern Medical Center, or were performed under a UK Home Office License.

2.1.1. Inbred, outbred & congenic strains

- **BALB/cByJ**: Inbred strain obtained from The Scripps Research Institute breeding colony. Homozygous for the *a* allele at the *Igh* locus, which can be distinguished from the *b* allele of C57BL/6J by flow cytometry.
- **C3H/HeN**: Inbred strain obtained from Taconic. Used for outcross-based mapping.
- **C57BL/6J**: Inbred males used for ENU mutagenesis were obtained from The Jackson Laboratory, while all others were obtained from The Scripps Research Institute breeding colony.
- **B6.SJL-*Ptprc*^{a}*Pep3*^{b}/BoyJ**: Abbreviated as CD45.1. SJL congenic strain, backcrossed more than 22 generations to C57BL/6J. Homozygous for the *a* allele of *Ptprc*, which can be distinguished from the *b* allele of C57BL/6J by flow cytometry. Obtained from The Jackson Laboratory.
- **C57BL/10J**: Inbred strain obtained from The Jackson Laboratory. Used for outcross-based mapping.
- **CD-1**: Outbred strain obtained from Harlan. Mated to vasectomised CD-1 males to create pseudopregnant surrogates for ES cell-injected blastocysts.
- **FVB/NJ**: Inbred strain obtained from The Jackson Laboratory. Used as blastocyst donors for ES cell injection.

2.1.2. Transgenic strains

- **Tg(IghelMM4)**: Abbreviated as MM4. A hen egg lysozyme-specific B cell receptor transgenic, consisting of cointegrated V_H10-μ heavy chain and $V_\kappa10$-C_κ light chain segments derived from the HyHEL10 hybridoma (Brink et al., 1992). Obtained from Christopher Goodnow.
- **Tg(IgkHyHEL10)1Rbr**: Abbreviated as LC2. Transgenic for the same $V_\kappa10$-C_κ light chain transgene as MM4, and commonly known as SW_{HEL} when in conjunction with the ***Igh*^{tm1Rbr}**

knockin allele (V_H10 anti-HEL heavy chain variable region gene targeted to the *Igh* locus) (Phan et al., 2003). Obtained from Robert Brink.

- **Tg(BCL2)22Wehi**: Human *BCL2* transgene driven by the immunoglobulin heavy chain enhancer (E*μ*) (Strasser et al., 1991). Obtained from The Jackson Laboratory.

2.1.3.Mutant strains

All mutant strains were generated in the Beutler laboratory by C57BL/6J ENU mutagenesis unless otherwise specified. With the exception of *Fnip1*^{hamel}, all genotyping was performed by Terrence Robinson, Sara Kalina and Chip Ross at The Scripps Research Institute.

- ***Atp11c***^{emptyhive}: A C to T transition in exon 19 of 30 total exons, resulting in a glutamine to stop mutation at amino acid position 655 (Siggs et al., 2011a)
- ***Atp11c***^{spelling}: A T to A transversion in exon 12 of 30 total exons, leading to an isoleucine to lysine substitution at amino acid position 355 (Siggs et al., 2011a).
- ***Bcl2l11***$^{tm1.1Ast}$: Cre-mediated deletion of the BH3 domain-encoding exon, resulting in the absence of full-length Bim protein expression (Bouillet et al., 1999). Generated in W9.5 ES cells (129S1/Sv background) and backcrossed to C57BL/6J more than 13 generations. Obtained from The Jackson Laboratory.
- ***Cd19***$^{tm1(cre)Cgn}$: An in frame insertion of a cre recombinase gene into the first coding exon followed by an frt-flanked neomycin cassette (Rickert et al., 1995). Generated in E14.1 ES cells (129P2/OlaHsd) and backcrossed to C57BL/6J more than 11 generations. Obtained from The Jackson Laboratory.
- ***Cd247***^{allia}: An A to T transversion at position 255 in the second of eight total exons, resulting in an aspartic acid to valine substitution at codon 36 (D36V).
- ***Fas***^{lpr}: A spontaneous genomic rearrangement within intron 2, leading to a near-absence of mRNA expression (Watanabe-Fukunaga et al., 1992). Originally arose in the MRL/MpJ strain, and backcrossed more than 11 generations to C57BL/6J. Obtained from The Jackson Laboratory.
- ***Flt3***^{warmflash}: A G to A transition at position 33572 of the *Flt3* genomic sequence, which destroys the donor site of intron 9, and results in the use of an alternative donor site within exon 9. This

causes the in-frame deletion of 2 amino acids (YS) from exon 9 of a total of 24 exons (Eidenschenk et al., 2010).

- ***Fnip1***^{hamel}: A G to A transition within the donor splice site in intron 5, one nucleotide after exon 5.
- ***Ifnar2***$^{macro\text{-}2}$: An A to T transition in the second of nine exons, converting the methionine initiation codon to valine. (Won et al., 2012)
- ***Ikbkg***^{panr2}: A T to C transition in exon 4 of 10 total exons, resulting in a leucine to proline substitution at codon 153 (Siggs et al., 2010)
- ***Inpp5d***^{styx}: A T to A transversion in the donor splice site of intron 5, predicted to result in skipping of the 141-nucleotide exon 5 (out of 27 total exons), and in-frame splicing to exon 6. This would result in deletion of 46 amino acids from the 1191 amino acid SHIP-1 protein.
- ***Irak4***^{otiose}: A T to C transition in exon 9 of 12 total exons, leading to an isoleucine to threonine substitution at residue 327. No immunoreactive protein is detected by western blot analysis of mutant macrophages.
- ***Kdelr1***$^{daniel\ gray}$: An A to G transition in exon 4 of 5 total exons, resulting in a tyrosine to cysteine substitution at amino acid 158.
- ***Klrb1c***^{Unnatural}: An A to G transition in exon 4 of 6 total exons, resulting in an aspartic acid to glycine substitution at residue 100.
- ***Map3k14***^{lucky}: A C to T transversion in exon 6 of 16 total exons, leading to an arginine to stop conversion at amino acid 396 (Arnold et al., 2012b).
- ***Ptpn6***^{spin}: A T to A transversion in exon 5 of 16 total exons, resulting in a tyrosine to arginine substitution at amino acid 208 (Croker et al., 2008).
- ***Ptprc***^{belittle}: An A to T transversion in exon 13 of 33 total exons in isoform 1, and exon 10 of 30 total exons in isoform 2. The mutation converts lysine 422 (isoform 1) or 283 (isoform 2) of the CD45 protein to a stop.
- ***Rag1***^{maladaptive}: A C to A transversion within exon 2 of 2 total exons, resulting in a tyrosine to stop substitution at amino acid position 886.
- ***Rhbdf2***^{sinecure}: An A to T transversion in exon 10 of 19 total exons, resulting in an isoleucine to phenylalanine mutation at amino acid 387 (Siggs et al., 2012b).

- ***Rhbdf2*$^{tm1a(KOMP)Wtsi}$**: An En2-IRES-lacZ-pA gene-trap cassette in intron 3 is predicted to prevent expression of the full-length protein. Created in JM8.N4 ES cells (C57BL/6N background) and obtained from the KOMP repository at UC Davis (Skarnes et al., 2011). After expansion, ES cells were injected into FVB/NJ blastocysts and transplanted into pseudopregnant CD-1 females. Chimeric male offspring were mated to *Tyr*$^{c-2J}$ albino females to confirm germ line transmission.
- ***Ticam1*^{Lps2}**: A single nucleotide deletion of a G in exon 2 of 2 total exons, causing a frameshift deletion of 24 amino acids, and replacing them with 11 unrelated amino acids and a premature stop codon (Hoebe et al., 2003).
- ***Tlr4*^{lps3}**: An A to T transversion in exon 3 of 3 total exons, resulting in replacement of an aspartic acid with valine at amino acid position 709.
- ***Tlr4*^{Lps4}**: A G to A transition in exon 3 of 3 total exons, resulting in a glycine to aspartic acid change at amino acid 724.
- ***Tlr6*^{m2sd1}**: An A to T transversion in exon 2 of 2 total exons, resulting in conversion of an arginine to a stop codon at residue 457.
- ***Tlr6*^{m2sd2}**: A T to A transversion in exon 2 of 2 total exons, resulting in conversion of a leucine to a stop codon at residue 390.
- ***Tlr6*^{m2sd3}**: A T to C transition in exon 2 of 2 total exons, resulting in conversion of isoleucine to threonine at residue 441.
- ***Tlr7*^{rsq1}**: A C to T transition in exon 3 of 3 total exons, resulting in conversion of threonine to isoleucine at residue 68 (Iavarone et al., 2011).
- ***Tlr7*^{rsq2}**: An A to T transversion in exon 3 of 3 total exons, resulting in conversion of asparagine to tyrosine at residue 182.
- ***Tyr*$^{c-2J}$**: Albino strain used for testing germline transmission of injected ES cells. Caused by a spontaneous G to T transversion, resulting in an arginine to leucine substitution at residue 77. The mutation also disrupts the alternative 5' splice donor site at exon 1, preventing the expression of 1a and 1b transcripts (Le Fur et al., 1996). No tyrosinase activity was found in hairbulb extracts from homozygous mice. Originated on a C57BL/6J congenic background, and obtained from The Jackson Laboratory.

- ***Zap70^{trebia}***: An A to T transversion in exon 10 of 13 total exons, resulting in a tyrosine to phenylalanine substitution at amino acid 492.
- ***Zbtb1^{scanT}***: A T to C transition in exon 2 of 2 total exons, resulting in a cysteine to arginine substitution at amino acid 74 (Siggs et al., 2012a).

2.1.4.Genotyping

Mice carrying point mutations were genotyped by amplifying the region containing the mutation, followed by sequencing of the amplified region to detect the single nucleotide change. Primer and other genotyping details are listed in Appendix 7.1.

Standard PCR program (using SIGMA JumpStart REDTaq):

1) 94°C 2:00

2) 94°C 0:30

3) 56°C 0:30

4) 72°C 1:00

5) repeat steps (2-4) 29X

6) 72°C 7:00

7) 4°C ∞

2.1.5.ENU mutagenesis

Isopak ENU powder (Sigma) was reconstituted with 10 ml of 95% ethanol, followed by 90 ml of phosphate citrate buffer (0.1 M NaH_2PO_4, 0.05M sodium citrate, pH 5.0–6.0). Concentration was determined by spectrophotometer (0.72 $OD_{398\ nm}$ = 1 mg/ml of ENU). Six week-old C57BL/6J males were anesthetised with an intramuscular injection of xylazine/ketamine, and injected intraperitoneally with 100 mg/kg ENU solution. This procedure was repeated at weekly intervals for a total of three injections. After the last injection, males (G0) were housed in isolation for 12 weeks to recover fertility, then mated to C57BL/6J females to create a maximum of 20 G1' female offspring. G1' females were then mated to an unrelated G0 male, and no more than 20 G1 offspring were produced. G1 siblings were intercrossed, as were their G2

offspring. The resulting G3 progeny were then screened for phenotypes. Liz Hanley, Christine Domingo, and Elaine Pirie performed all ENU injections and G0, G1, and G2 breeding.

2.1.6.Positional cloning & targeted sequencing

Index mutant mice (C57BL/6J background) were outcrossed to C3H/HeN, C57BL/10J or C57BL/6J mice. F1 mice were then either intercrossed or backcrossed to their mutant parent (for recessive phenotypes), or outcrossed once more to the mapping strain (dominant phenotypes). Phenotypes were assayed in the resulting F2 mice, and mice were grouped into mutant and wild-type cohorts. For C3H mapping crosses, individual mice were typed at 128 microsatellite markers spaced across the genome (full list provided in Appendix 7.2). Primers were labelled with 6-carboxyfluorescein, NED or VIC dyes, and products resolved on an ABI 3730xl sequencer and analysed with GeneMapper software (ABI). For C57BL/10J outcrosses, DNA from wild-type and mutant mice was grouped into separate equimolar pools, and genotyped by PCR and capillary sequencing at up to 128 single-nucleotide variants (Xia et al., 2010). Relative allele peak heights were used to estimate genotype frequencies within wild-type and mutant DNA pools. All marker genotyping was performed by Kevin Khovananth, Pei Lin and Charles Ross.

Expected and observed genotype frequencies were used to calculate logarithm of odds (LOD) scores at each marker (LOD = $\log_{10}[P_{linkage}/P_{non\text{-}linkage}]$, where $P_{non\text{-}linkage}$ is estimated from a binomial distribution, and $P_{linkage} = 1 - P_{non\text{-}linkage}$). Synthetic LOD scores were calculated from estimated genotype frequencies. For fine mapping, individual mice with recombination events within the critical region were genotyped at additional loci. Where an obvious candidate gene within the critical region was noticed, genomic DNA was amplified from wild-type and mutant samples by PCR using primers designed by the Prime program (GCG DNA software analysis package). PCR products were purified on a Biomek FX using AMPure beads (Agencourt) and sequenced using Big Dye Terminator v3.1 (Applied Biosystems) on an ABI 3730xl capillary sequencer. Sequencing trace files were analysed with the *phred* base calling and *phrap* alignment algorithms (Ewing et al., 1998), and visualized with *consed* (Gordon et al., 1998). Where no candidate was observed and the critical region was deemed to be sufficiently small (<1000 exons), all coding exons and their flanking splice regions were sequenced by PCR and capillary sequencing.

2.1.7.Whole genome sequencing

Purified genomic DNA from a single *scanT* homozygote tail section was sheared into 60-90 bp fragments using the Covaris S2 sonicator. Sheared DNA was end-repaired and ligated to P1 and P2 adapters, and products were separated by gel electrophoresis. 150-200 bp products were excised, purified, and PCR amplified. The fragment library was clonally amplified on P1-coupled beads by emulsion PCR. Templated beads were enriched using P2-coupled polystyrene beads, and attached to the surface of a single SOLiD slide via a 3' DNA modification. The slide was subjected to SOLiD 3 sequencing (Applied Biosystems), and data were analysed with Corona Lite software (Applied Biosystems). Pei Lin performed SOLiD library preparation and sequencing, and Yu Xia performed bioinformatic analysis of SOLiD data.

Genomic DNA from three *hamel* homozygotes was prepared in barcoded libraries for sequencing on the Illumina HiSeq 2000 platform. DNA was fragmented, end-repaired, A-tailed and adapter-ligated, then size-selected and amplified. Prepared libraries were multiplexed and paired-end sequenced over one lane of a flow cell. Data were aligned to the NCBI Build 37 mouse reference sequence using Stampy (Lunter and Goodson, 2011). Discrepancies were called using the Platypus variant caller (Rimmer A, Mathieson I, Lunter G, McVean G, (2012) Platypus: An Integrated Variant Caller (www.well.ox.ac.uk/platypus)). The resulting VCF file was then filtered to remove variants previously seen more than once in 7 unrelated mouse genomes sequenced by the High-Throughput Genomics Group, followed by a filter to remove calls that were clustered within 1000 bp of another call (and therefore unlikely to have been created by ENU). All variant calls below a Phred-based quality of 20 were removed, as were calls that failed Platypus allele- or strand-bias filters, had a high local frequency of bad reads, were located within homopolymer tracts of otherwise repetitive sequence, or were annotated as indels.

Filtered VCF files were then annotated by ANNOVAR (Wang et al., 2010) according to NCBI RefSeq gene definitions (Pruitt et al., 2012). The deleterious effects of ENU-induced mutations were predicted using the HumVar-trained PolyPhen-2 server (version 2.2.2)(Adzhubei et al., 2010). Illumina HiSeq library generation and reference genome alignment was performed by the High-Throughput Genomics Group at the Wellcome Trust Centre for Human Genetics.

2.2. Macrophage isolation, stimulation and analysis

2.2.1. Peritoneal cell isolation

Mice were injected with 1.5 ml of a 4% solution of Brewer's thioglycollate (wt/vol in distilled water, autoclaved, protected from light and aged for at least 1 month; BBL Microbiology Systems). Four to five days later, peritoneal cells were recovered from isoflurane-anesthetized mice by peritoneal lavage with 5 ml PBS solution. Peritoneal cells were plated in 96-well tissue culture treated plates (Costar) at a density of 1×10^5 cells per well [in DMEM (Cellgro) plus 5% FBS (Atlanta Biosciences) and 2% penicillin/streptomycin (Gibco)]. Following overnight incubation (37 °C in 5% CO_2), supernatant was discarded, and the remaining adherent cells (primarily macrophages) were used for stimulation. After stimulation, media was replaced with a 2 mg/ml solution of MTT (3-(4,5-Dimethylthiazol-2-yl)-2,5-diphenyltetrazolium bromide, M2128; Sigma) in DMEM plus 5% FBS and 2% penicillin/streptomycin. Supernatant was then discarded and replaced with 80 µL/well lysis solution (90% (v/v) isopropanol, 0.5% (w/v) SDS, 0.04N HCl in distilled water), then incubated at room temperature for 30 minutes to allow the purple formazan precipitate to enter solution. Absorbance at 590 nm was then read, allowing adherent cell numbers to be quantified.

2.2.2. TLR stimulation

Cells were stimulated in duplicate with 100 µL/well of TLR ligand solutions [in DMEM (Cellgro) plus 5% FBS (Atlanta Biosciences) and 2% penicillin/streptomycin (Gibco)] for a period of 4 hours. Supernatant was collected and cytokines measured by bioassay or ELISA. For the induction of NO, macrophages were preactivated with 20 ng/ml IFN-γ (R&D Systems) for 24 hours, and stimulated with TLR ligands for an additional 24 hours. LPS (from *Salmonella minnesota* R595), poly(I:C), MALP-2, and R-848 were all obtained from Enzo Life Sciences. Pam_3CSK_4 was from EMC Microcollections, CpG ODN from IDT (sequence TCCATGACGTTCCTGATGCT with phosphorothioate bonds), and peptidoglycan from Sigma. Purity of all ligands was validated using cells deficient for their corresponding TLR.

2.2.3. NALP3 stimulation

Adherent peritoneal cells were stimulated with 100 µL/well LPS solution (100 ng/ml). Following overnight incubation, supernatant was discarded and replaced with 150 µL/well of a 5 nM nigericin solution (Sigma)

and incubated for a further 8 hours. Conditioned supernatant was then collected, and IL-1β measured by ELISA.

2.2.4.dsDNA stimulation

Adherent peritoneal cells were stimulated with a mixture of 0.1 µg/well dsDNA (TGTAGATCATGTACAGATCAGTCATAGATCACTAGTAGATCTGTA duplex; IDT) and 0.25 µL/well Lipofectamine (Invitrogen) in 150 µL/well of OptiMEM medium (Gibco). After overnight incubation (~16 hours) supernatant was collected for type I IFN bioassay.

2.2.5.TNF bioassay

For the detection of TNF, supernatant from TLR-stimulated macrophage cultures was subjected to a TNF bioassay (Carswell et al., 1975). On the day prior to bioassay, $5x10^4$ L-929 cells were added to tissue culture treated 96 well flat-bottomed plates in a volume of 100 µL DMEM plus 10% FBS and 2% penicillin/streptomycin, and incubated overnight (37°C in 5% CO_2). Immediately prior to bioassay, supernatant was replaced with 50 µL/well of cycloheximide solution (400 µg/ml), and incubated for at least 20 minutes. A mouse recombinant TNFα (ALX-522-009, Alexis, San Diego, CA) standard series was prepared in the interim, with 50 µL of each dilution added in duplicate to wells of an L-929 plate. 50 µL of media was added to all other wells, along with ~5 µL of conditioned supernatant. Plates were incubated for 12-16 hours, after which 25 µL/well of MTT solution (2 mg/ml) was added to the L-929 plates, which are then incubated for an additional hour. Supernatant was then discarded and replaced with 80 µL/well lysis solution (90% (v/v) isopropanol, 0.5% (w/v) SDS, 0.04N HCl in distilled water), then incubated at room temperature for 30 minutes to allow the purple formazan precipitate to enter solution. Absorbance at 590 nm is read, and bioactive TNF concentrations are inferred from the TNFα standard absorbance.

2.2.6.Type I IFN bioassay & cytokine ELISA

For type 1 IFN, L-929 mouse fibroblasts stably transfected with an IFN-sensitive luciferase element (L-929-ISRE) were incubated with supernatant or standard (IFNβ, eBioscience) for 5 hours, washed once with PBS solution, lysed with reporter lysis buffer (Promega), and incubated overnight at -80°C. After thawing, 35 µL luciferase reagent (Promega) was added to each well, and luminescence read immediately on an Lmax plate reader (Molecular Devices). IL-1β, TNFα, IL-6, IL-12p40 and MCP-1 were all measured

by ELISA according to the manufacturer's instructions (eBioscience). NO was measured by Griess assay. Concentrations of all cytokines and NO were interpolated from a standard curve.

2.2.7.Western blotting

Peritoneal macrophages (2×10^6) were stimulated in 24-well plates with LPS (1 μg/ml) or MALP-2 (100 ng/ml) for the indicated lengths of time, separated into cytoplasmic and nuclear fractions (Nuclear Extract Kit; Active Motif) or lysed directly in sample buffer (Invitrogen), separated by SDS/PAGE, and transferred to nitrocellulose membranes. Membranes were probed with antibodies to NEMO (Imgenex), phospho-IκBα (Ser32/36), phospho-IκBε (Ser18/22), IκBα, IκBβ, IκBε, phospho-p38 (Thr180/Tyr182), phospho-p105 (Ser933), p105, phospho-MEK1/2 (Ser217/221), ERK1/2, phospho-ERK1/2 (Thr202/Tyr204), p65, and β-tubulin (Cell Signalling Technology).

2.3. *In vivo* challenges

2.3.1. Infections

Mice were infected with an intraperitoneal dose of 2×10^5 PFU murine cytomegalovirus (MCMV, Smith strain) prepared from homogenised BALB/c salivary glands. *Listeria monocytogenes* strain 10403S (Xenogen) was cultured in brain-heart infusion broth at 37°C, resuspended in PBS solution, and 10^5 CFU were administered via the tail vein. Infected mice were monitored daily for signs of illness. MCMV infections were performed by Celine Eidenschenk, and *Listeria monocytogenes* infections by Philippe Krebs at The Scripps Research Institute.

2.3.2. DSS-induced colitis

Performed by Wataru Tomisato at The Scripps Research Institute. Sex- and age-matched littermates received 3% (wt/vol) dextran sulfate sodium (DSS; MP Biomedicals) in drinking water for 7 days, with weight recorded daily and normalized to day 0.

2.4. Flow cytometry

Blood from the retro-orbital plexus of isoflurane-anesthetized mice was collected in cluster tubes (Costar) containing 20 µl of 6% (wt/vol) EDTA in water. 50 µl of blood was subjected to two rounds of red blood cell lysis with ammonium chloride buffer (Sigma) before staining. Single cell suspensions from bone marrow (femurs and tibias from one hind leg), spleen, peritoneum or thymus were counted (Z2 Coulter Counter; Beckman Coulter), and stained with a combination of fluorochrome-conjugated antibodies against the following mouse antigens: FITC-conjugated anti- CD4 (GK1.5), CD23 (B3B4), CD24 (30-F1), CD25 (7D4), CD34 (RAM34), CD48 (HM48-1), F4/80 (BM8), CD127 (A7R34), IgD (11-26), IgM (a allotype; DS-1), IgM (goat polyclonal; 1020-02; SouthernBiotech), Ly6C (AL-21); PE-conjugated anti- BP-1 (BP-1), CD11b (M1/70), CD19 (1D3), CD21/35 (7G6), CD44 (IM7), CD45.2 (104), CD122 (5H4), CD135 (A2F10), CD150 (9D1), IgD (11-26), PDCA1 (927); PerCP-Cy5.5-conjugated anti- B220 (RA3-6B2), CD8α (53–6.7), CD19 (1D3), IgM (b allotype; AF6-78), NK1.1 (PK136), TCRβ (H57-597); eFluor710-conjugated anti-CD117 (2B8); APC-conjugated anti- CD3ε (145-2C11), CD8α (53-6.7), CD11b (M1/70), CD11c (HL3), CD43 (S7), CD93 (AA4.1), IgM (II/41), Ly6G (RB6-8C5), NK1.1 (PK136), SiglecH (551), TER119 (TER-119), Thy-1.2 (53-2.1); APC-Cy7-conjugated anti- Sca-1 (D7) and CD45.2 (104); PE-Cy7-conjugated anti- CD16/32 (93) and CD19 (6D5); Horizon V500-conjugated anti-CD44 (IM7); Pacific Blue-conjugated anti-CD45.1 (A20); biotin-conjugated anti- CD179b (λ5; LM34) and CD5 (53-7.3). Biotinylated antibodies were detected with FITC- or PE-conjugated streptavidin (BD). For analysis of λ5 expression, cells were first incubated for 1 h at 37 °C in DMEM, then stained with biotinylated anti-λ5 (LM34; BD) or rat IgG2a isotype-matched control antibody (R35-95; BD). Fcγ receptors were blocked prior to staining by incubating cells with a 1/1000 dilution of purified anti-CD16/32 antibody for 20 minutes (93; BioLegend).

Staining of intracellular Foxp3 was performed according to the manufacturer's protocol (eBioscience), and intracellular IgM was stained using the Foxp3 Fixation/Permeabilization Buffer kit (eBioscience). For staining of TNF on macrophages, 2×10^5 cells were stimulated with the indicated dose of LPS for 2 hours in the presence or absence of 5 µg/ml brefeldin A (Sigma), and stained with PE-conjugated anti-TNF (BD Biosciences) using the Cytofix/Cytoperm Fixation/Permeabilization solution kit (BD Biosciences). FITC-conjugated cholera toxin was from Sigma, and 7-AAD was from eBioscience. Annexin V-FITC staining was performed according to the manufacturer's instructions (BD), and EdU labelling and staining were performed according to the manufacturer's instructions (Invitrogen) 4 hours

after a single intraperitoneal injection of 100 mg/kg EdU. All samples were acquired on a FACSCalibur or LSRFortessa (BD), and all cell sorting was performed on a FACSAria II (BD) by the flow cytometry core facility of The Scripps Research Institute.

2.4.1.Ex vivo B cell culture

B cell precursors (7-AAD$^-$B220$^+$IgM$^-$IgD$^-$; Hardy fractions A–D) were sorted from bone marrow suspensions (to a purity of >90%) and cultured (or cocultured, where allotypic markers were available) for up to 4 days in Iscove's modified Dulbecco's medium with 10% (vol/vol) FBS, 200 U/ml of penicillin, 200 μg/ml of streptomycin, 50 μM β-mercaptoethanol and 2 mM L-glutamine in the presence or absence of mouse recombinant IL-7 (eBioscience). Cell size, viability (assessed by 7-AAD exclusion) and mIgM expression were measured by flow cytometry.

2.4.2.Quantitative RT-PCR

B cell precursors from Hardy fraction A (7-AAD$^-$B220$^+$IgM$^-$IgD$^-$CD19$^-$NK1.1$^-$Ly6C$^-$) were sorted from bone marrow suspensions directly into 1 ml TRIzol (Invitrogen). RNA was extracted according to the manufacturer's instructions and was purified on RNeasy columns (Qiagen). cDNA was then transcribed with oligo(dT) primers (Retroscript; Ambion) and was amplified over 40 cycles by PCR. Primers were as follows: *Actb*, 5'-GGCTGTATTCCCCTCCATCG (forward) and 5'-CCAGTTGGTAACAATGCCATGT (reverse); *Ebf1*, 5'-GCATCCAACGGAGTGGAAG (forward) and 5'-GATTTCCGCAGGTTAGAAGGC (reverse); *Igll1*, 5'-ACTCTGTTCCTGCCTTCCTTA (forward) and 5'-GAGGGTTGGGTTGTCTCTACA (reverse).

2.5. Immunisations & ELISAs

Single-round infectious recombinant Semliki forest virus (rSFV) encoding β-gal was generated and titered by Gerald McInerney at the Karolinska Institutet (Smerdou and Liljeström, 1999). Mice were injected i.p. with 200 µL of 0.9% sterile saline solution containing 2×10^6 infectious units of rSFV-β-gal on day 0. On day 14, blood was collected from the retro-orbital cavities of anesthetized mice into serum separator tubes and stored at −70°C. Other mice were injected intraperitoneally with 200 µl of 0.9% (vol/vol) sterile saline containing 50 µg NP_{28}-aminoethylcarboxymethyl–Ficoll (Biosearch Technologies), or with 50 µg Imject alum–precipitated NP_{38}-CGG (Biosearch Technologies) combined with 5 µg lipopolysaccharide (from *Salmonella minnesota* R595 (Re); Alexis). Blood was collected 7, 14 or 28 days later from the retro-orbital plexus into serum separator tubes and was stored at −70°C.

For rSFV-β-gal ELISA, polyvinylchloride microtiter 96-well round-bottom plates (Fisher Scientific) were coated overnight at 4°C with 2 µg/ml β-gal (Roche). For NP ELISA, polyvinylchloride microtiter 96-well round-bottomed plates (Fisher Scientific) were coated overnight at 4°C with NP_{23}-BSA or NP_4-BSA (5 µg/ml; Biosearch Technologies). Plates were blocked with 5% (wt/vol) milk, and serum samples were serially diluted in 1% (wt/vol) milk. Plates were incubated with horseradish peroxidase–conjugated goat antibody to mouse IgM or IgG1 (1021-05 or 1070-05; Southern Biotechnology) and developed with SureBlue TMB Microwell Peroxidase Substrate and TMB Stop Solution (KPL), and absorbance was measured at 450 nm on a MAXline EMax microplate reader (Molecular Devices). Background for assays was determined by incubation of serum pooled from immunised wild-type mice on uncoated wells. Total serum immunoglobulins in preimmune serum were measured as described (Gavin et al., 2006) by Christoph Huber at The Scripps Research Institute. Carrie Arnold and Elaine Pirie performed all rSFV-β-gal immunisations and ELISAs.

2.6. Haematopoietic stem cell assays

2.6.1. Haematopoietic chimeras and colony-forming unit assay

Recipient mice were γ-irradiated with a split dose of 11 Gy (2 × 5.5 Gy, ^{137}Cs source, Gammacell 40; Atomic Energy of Canada). The next day, mice were injected with 2 × 10^6 bone marrow cells or E16.5 foetal liver cells via the retro-orbital plexus. Mice were maintained for 4 weeks on water containing trimethroprim-sulfamethoxazole antibiotics and were killed for analysis 8 weeks after reconstitution. For colony forming unit assays, mice received 10^5 bone marrow cells and were sacrificed 8 or 12 days later. Spleens were fixed overnight in Bouin's solution (Sigma-Aldrich), and colonies were counted the next day. For unconditioned chimeras, unconditioned recipients received a single retro-orbital injection of 2 × 10^6 bone marrow cells.

2.6.2. Retroviral transductions

The open reading frame of *Zbtb1* was cloned into the *Bgl*II–*Eco*RI site of pMIG (MSCV2.2-IRES-GFP; Addgene #9044, deposited by W. Hahn [Dana-Farber Cancer Institute, Boston, MA]) to generate the pMIG-*Zbtb1* vector. Vectors were transfected into the Plat-E packaging cell line using Fugene 6 (Roche), and retrovirus-containing supernatant was collected 24 and 48 hours later. Bone marrow donor mice were primed 5 days before harvest with 150 mg/kg 5-fluorouracil (Sigma-Aldrich), and bone marrow cells were prestimulated overnight with 10 ng/ml of mouse recombinant IL-3, 10 ng/ml IL-6, 50 ng/ml SCF, 50 ng/ml TPO, and 5 ng/ml FLT3L (all from PeproTech). The next day, 3 ml/well of retroviral supernatant was centrifuged (2,000 rpm for 2 hours at 32°C) onto RetroNectin-coated 6-well plates (20 μg/ml; Takara Bio Inc.), and cells were cultured on coated plates in the presence of 4 μg/ml Polybrene (Sigma-Aldrich) for 48 hours. Recipient CD45.1$^+$ mice were γ-irradiated with a split dose of 11 Gy (^{137}Cs source) and the next day injected with ~2 × 10^6 transduced bone marrow cells via the retro-orbital plexus.

2.7. Histology

Organs were fixed in 10% neutral buffered formalin (Sigma) and embedded in paraffin wax, and 5 μm sections were stained with hematoxylin and eosin (H&E). Histology was performed at core facilities of The Scripps Research Institute or the University of California San Diego.

2.8. Data analysis

FlowJo (TreeStar) and FACSDiva (BD Biosciences) software was used to analyse all flow cytometry data. Prism software (GraphPad) was used for all statistical analyses.

3. Forward genetic analysis of innate immunity

3.1. Innate immune receptor screen

Three forward genetic screens were applied to identify new components of the innate immune system. These screens all involved the *ex vivo* stimulation of peritoneal macrophages from mutant mice, which were collected five days after a peritoneal injection of thioglycollate broth. These cells express an array of innate immune receptors including Toll-like receptors, NOD-like receptors, and RIG-I-like receptors. A summary of the screens applied is provided in **Figure 3.1**, with phenotypes detailed in **Table 3.1**.

3.1.1. Toll-like receptor screen

Cells were stimulated with a total of seven TLR ligands, which collectively stimulate a total of seven different TLRs. Since TLRs are known to be potent inducers of tumour necrosis factor alpha (TNFα), supernatant was collected and subjected to a TNF bioassay (Carswell et al., 1975). In total, 7500 G3 mutant offspring were tested. A total of 7 unique phenovariants were identified, including three alleles of *Tlr6*, two alleles of *Tlr7*, one allele of *Tlr4*, and one allele of *Ikbkg*. All of these genes had previously been implicated in innate immunity, although in one case (*Ikbkg*), the allele was a unique hypomorph. This allele will be described in more detail in section 3.2. A final phenovariant identified in the same screen by a former member of the Beutler laboratory was also carried forward for analysis. This was revealed to be caused by a mutation in *Rhbdf2*, and will be described in detail in section 3.3.

3.1.2. NALP3-inflammasome screen

In addition to TNF, TLR stimulation triggers the accumulation of cytoplasmic pro-IL-1β. The release of mature IL-1β requires the proteolytic processing and activation of caspase 1, which is activated by a multimolecular complex known as the inflammasome (Martinon et al., 2002). A variety of stimuli can activate the inflammasome, including uric acid crystals (Martinon et al., 2006), and the antibiotic nigericin (Mariathasan et al., 2006). To screen for new components of NALP3 inflammasome-induced IL-1β secretion, cells from 2500 G3 mice were prestimulated with LPS, activated with nigericin, and supernatant assayed by ELISA for the presence of interleukin-1β. Only one phenovariant was identified during the course of this screen, which also had an overlapping defect in LPS-induced TNF synthesis. Given this phenotype, the coding exons of *Tlr4* were sequenced directly, revealing a semidominant mutation.

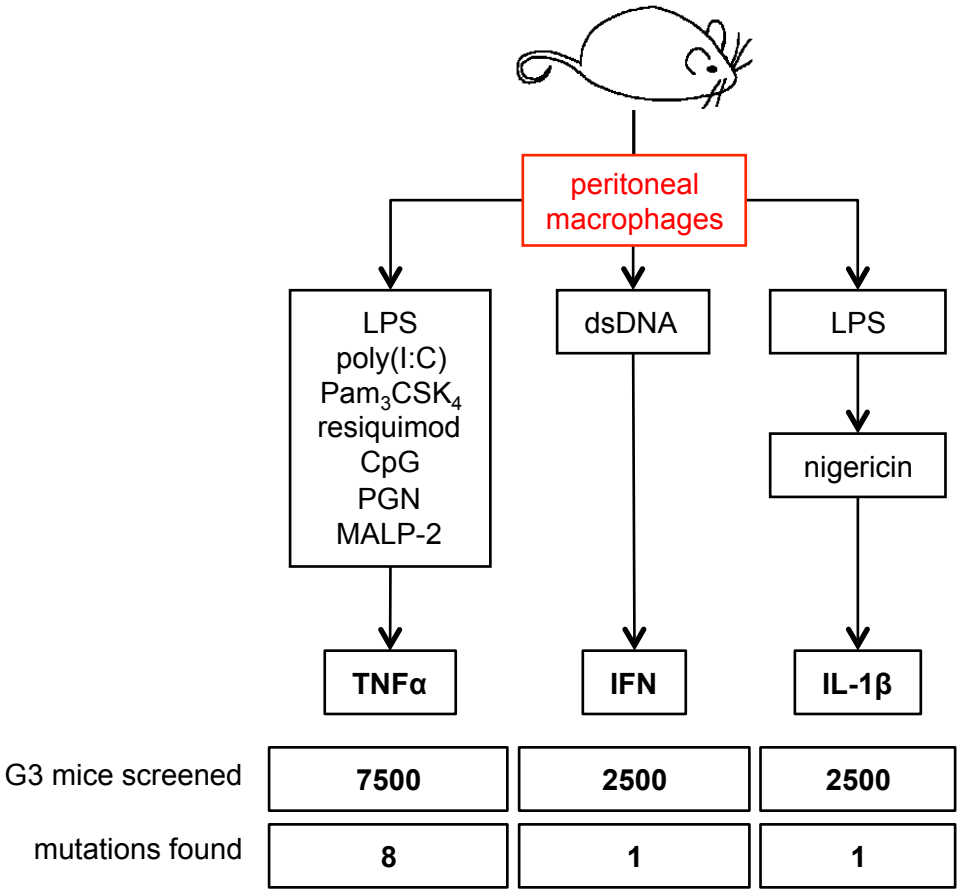


Figure 3.1 | Summary of three forward genetic screens for innate immune phenotypes.
Thioglycollate-elicited macrophages were harvested from the peritoneum of G3 mutant mice, and stimulated with the indicated substances. Following stimulation, cell supernatant was collect and cytokine concentrations measured by bioassay or ELISA.

Table 3.1 | Summary of phenotypes and mutations identified in three forward genetic screens for innate immune phenotypes.
All phenotypes are recessive, with the exception of *Lps4*, which is semidominant.

gene	allele	screen	phenotype
Ifnar2	*macro-2*	Cytoplasmic DNA	reduced dsDNA-induced type I IFN
Ikbkg	*panr2*	TLR	reduced TLR-induced TNFα
Rhbdf2	*sinecure*	TLR	reduced TLR-induced TNFα
Tlr4	*lps3*	TLR	reduced LPS-induced TNFα
Tlr4	*Lps4*	TLR/NALP3 inflammasome	reduced LPS-induced TNFα, reduced LPS/nigericin-induced IL-1β
Tlr6	*m2sd1*	TLR	reduced MALP-2-induced TNFα
Tlr6	*m2sd2*	TLR	reduced MALP-2-induced TNFα
Tlr6	*m2sd3*	TLR	reduced MALP-2-induced TNFα
Tlr7	*rsq1*	TLR	reduced resiquimod-induced TNFα
Tlr7	*rsq2*	TLR	reduced resiquimod-induced TNFα

3.1.3.Cytoplasmic DNA screen

CpG motif-containing DNA is a known ligand of TLR9 (Hemmi et al., 2000), yet transfection of double-stranded DNA can also induce a TLR9-independent type I interferon response (Ishii et al., 2006; Stetson and Medzhitov, 2006). While the receptor is yet to be identified, the downstream signalling pathway is known to require TANK-binding kinase 1 (TBK1), inhibitor of NF-κB kinase ε (IKKε), interferon regulatory factor 3 (IRF3), and the ER-associated protein STING (Ishii et al., 2006; Stetson and Medzhitov, 2006; Ishikawa and Barber, 2008). Part of the response also depends upon the high-mobility group box proteins, which bind directly to dsDNA (Yanai et al., 2009). In certain human cell lines RNA polymerase III transcribes dsDNA into 5' triphosphate-bearing RNA, which in turn activates the RNA-binding protein RIG-I (Chiu et al., 2009). RIG-I is not, however, required for dsDNA-induced IFN in mouse fibroblasts (Ishii et al., 2006).

In an effort to reveal the hypothetical dsDNA receptor, cells from 2500 mice were also transfected with double-stranded DNA (dsDNA), and type I interferon measured in the supernatant by bioassay (Jiang et al., 2005). One phenovariant was identified, and discovered to be an allele of *Ifnar2*. Although not essential for the initial dsDNA-induced synthesis of type I IFN, type I interferon receptor signalling was known to play an important role in the amplification of the type I IFN response (Marié et al., 1998).

3.2. A mutation of *Ikbkg* causes immune deficiency without impairing degradation of IκBα

The work presented in section 3.2 is a reproduction of previously published work (Siggs et al., 2010). The full publication is provided in Appendix 7.3.

3.2.1. NEMO and NF-κB signalling

NF-κB transcription factors orchestrate numerous immunological and developmental responses (Hayden and Ghosh, 2008). Among the receptors that trigger their activity are the Toll-like receptors (TLRs); the IL-1 receptor family; B and T cell antigen receptors (BCR/TCR); and TNF receptor family members, including the lymphotoxin β receptor (LTβR), CD40, and ectodysplasin-A receptor (EDAR). NF-κB activity is restrained by members of the IκB family, which prevent nuclear translocation of NF-κB subunits. IκB proteins (IκBα, IκBβ, and IκBε) are phosphorylated and degraded in response to stimulation, allowing release and nuclear translocation of NF-κB. IκB phosphorylation is mediated by the IκB kinase (IKK) complex, which consists of IKK1 (IKKα) and IKK2 (IKKβ) catalytic subunits, and the regulatory subunit NEMO (IKKγ). IKK activity is also required for phosphorylation of the NF-κB members p105 (NF-κB1) and p65 (RelA). Phosphorylated p105 is polyubiquitinated and degraded in a manner similar to the IκB proteins (Heissmeyer et al., 2001), promoting activation of the TPL2 (tumor progression locus 2) → ERK axis (Beinke et al., 2004; Waterfield et al., 2004). p65 undergoes IKK-dependent phosphorylation at serine 536 (Sakurai et al., 1999), although the significance of this is unclear.

The range of diseases caused by NEMO mutations highlights the physiological importance of NEMO and the IKK complex. Null alleles of the X-linked gene encoding NEMO, *IKBKG*, cause the inflammatory skin disease incontinentia pigmenti in heterozygous females (Smahi et al., 2000), and are lethal in hemizygous males, as they are in mice (Makris et al., 2000; Rudolph et al., 2000; Schmidt-Supprian et al., 2000). Milder hypomorphic alleles are compatible with viability in males, but cause severe immune deficiency and developmental abnormalities of the teeth, hair, and sweat glands (Zonana et al., 2000). These abnormalities of ectodermal derivatives are thought to result from disruption of EDAR signalling, yet there are reports of *IKBKG* mutations in immune-deficient patients without ectodermal dysplasia (Niehues et al., 2004; Orange et al., 2004). Other mutations appear to disrupt EDAR signalling and CD40-mediated immunoglobulin class switching but not TLR signalling (Jain et al., 2001), whereas

another mutation disrupts EDAR signalling, but leaves TLR and CD40 signalling largely intact (Salt et al., 2008).

Whatever the combination of pathways affected, immune deficiency is a unifying consequence of germline NEMO mutations. But of all of the targets of NEMO and the IKK complex, there is no consensus of which are most critical for immunity. A great deal has been learned from conditional mutations of IKKα, IKKβ, and NEMO, but a full understanding of their physiological function has been precluded by the embryonic lethality that occurs in their absence. The same may be true of the biochemical functions of NEMO, some of which may occur downstream of pathways arrested in the absence of NEMO (e.g., p65 translocation or TPL2 activation).

3.2.2.Identification of the panr2 phenotype

Among 7,500 G3 progeny of C57BL/6J males mutagenized with ENU, a heritable phenotype was observed marked by diminished secretion of soluble, bioactive TNF from macrophages stimulated with TLR ligands. This phenotype, named *panr2* (*pan-r*esistance *2*), was characterized by an impaired response to ligands for TLR3 [poly(I:C)], TLR4 (LPS), TLR7 (R-848) and TLR9 (CpG oligodeoxynucleotides) and the heterodimers TLR1/2 (Pam_3CSK_4) and TLR2/6 (MALP-2, peptidoglycan; **Figure 3.2**). Multiple cytokines were affected, including TNFα, IL-6, IL-12p40, and MCP-1, as well as the inflammatory mediator nitric oxide (NO). Secretion of type I IFN in response to TLR3 and TLR4 stimulation was not affected. *panr2* mice were also highly susceptible to an otherwise sublethal dose of murine cytomegalovirus (MCMV; **Figure 3.3A**). Death within 6 days of MCMV infection was indicative of an innate immune defect, as combined deficiency of B and T cells permits survival of a similar infection for more than 2 weeks (Welsh et al., 1991). Similarly, *panr2* mice succumbed to infection with *Listeria monocytogenes* within 4 days (**Figure 3.3B**).

3.2.3.panr2 mice have a mutation in Ikbkg

Given the broad suppression of NF-κB–dependent cytokine secretion (TNFα, IL-6, IL-12p40, MCP-1), along with normal secretion of an IRF3-dependent cytokine (type 1 IFN), the coding exons and splice junctions of five genes known to be required exclusively for TLR-induced activation of NF-κB were sequenced (*Traf6, Map3k7, Ikbkg, Chuk, Ikbkb*). Of a total of 26,246 target nucleotides, 21,056 (80.2%) were covered by high-quality reads in both wild-type and mutant samples, and a single mutation was

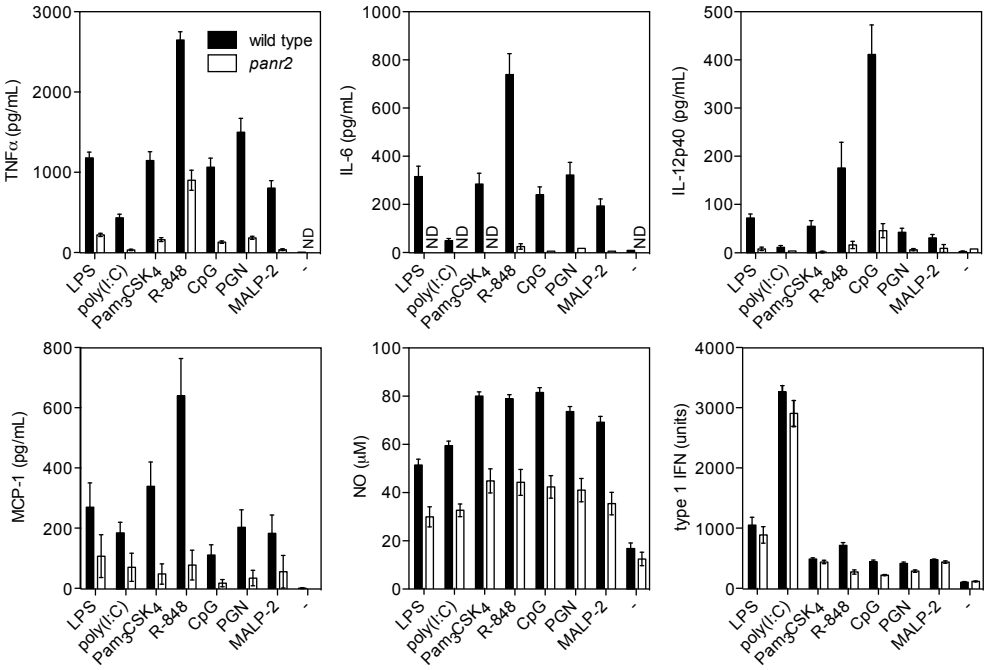


Figure 3.2 | The *panr2* mutation impairs TLR-induced cytokine secretion.
Thioglycollate-elicited peritoneal macrophages from wild-type (n=12) and *panr2* (n=6) mice were stimulated with TLR ligands, and TNFα, IL-6, IL-12p40 and MCP-1 concentrations were calculated by ELISA. Nitric oxide (NO) was measured by Griess assay, and type I IFN was measured by bioassay. Ligand concentrations were as follows: LPS (800 pg/mL), poly(I:C) (60 μg/mL), Pam_3CSK_4 (100 ng/mL), R-848 (40 ng/mL), CpG (1 μM), peptidoglycan (PGN, 2 μg/mL), MALP-2 (20 ng/mL). Bars indicate mean and standard error.

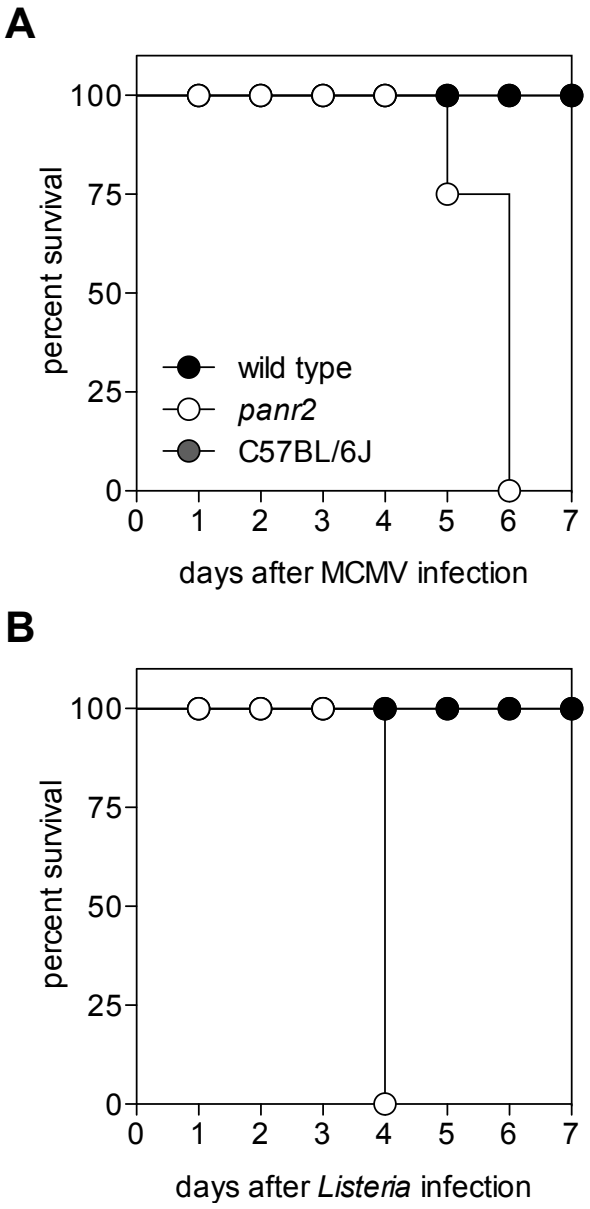


Figure 3.3 | *panr2* mice are susceptible to viral and bacterial infection.
panr2 (n=4,5), wild-type sibling (n=5,2), or age- and sex-matched C57BL/6J (n=5,5) mice were infected with $2x10^5$ PFU MCMV (A), or $1x10^5$ CFU *Listeria monocytogenes* (B) respectively and survival was monitored for seven days.

identified in *Ikbkg* (**Figure 3.4A**). The mutation was a T-to-C transition at position 473 of *Ikbkg* cDNA, in exon 4 of a total of 10, leading to a leucine to proline substitution at residue 153 (L153P). The affected amino acid lay within the first coiled-coil domain of NEMO (**Figure 3.4D**), and did not alter protein expression or electrophoretic mobility in macrophage lysates (**Figure 3.4C**). Consistent with the chromosomal location of *Ikbkg*, the *panr2* phenotype was inherited in an X-linked recessive manner.

Unlike *Ikbkg* knockout mice, *panr2* hemizygotes were viable and born at Mendelian ratios (**Figure 3.4B**). *panr2* hemizygous males were azoospermic, however, with histological analysis revealing cystic formations in the seminiferous tubules, as well as abnormal maturation of spermatids (**Figure 3.4E**), and a mean testis weight approximately 35% lower than WT siblings (**Figure 3.4F**). Conditional deletion of *Ikbkg* is known to affect a variety of other tissues, including the skin (Nenci et al., 2006), liver (Luedde et al., 2007), and intestinal epithelium (Nenci et al., 2007), yet none of these tissues showed histological abnormalities in mutant mice. Survival of T (Schmidt-Supprian et al., 2003) and B (Pasparakis et al., 2002) lymphocytes is also precluded by conditional deletion of *Ikbkg*, yet both of these populations were present in *panr2* mice (**Figure 3.5**). Inguinal lymph nodes were also absent or of diminished size in most mutant mice (**Figure 3.6**).

3.2.4.Ikbkg^{panr2} impairs adaptive immunity

While NEMO is essential for the survival of all T cells, IKKβ is specifically required for the development of memory and regulatory T cells (Schmidt-Supprian et al., 2003). Similarly, mice with an engineered mutation of p105 that cannot be phosphorylated by IKK (*Nfkb1*$^{SSAA/SSAA}$) also have fewer memory and regulatory T cells, and additionally have a reduction of NKT cells (Sriskantharajah et al., 2009). These populations were also reduced in *panr2* mutants (**Figure 3.7**), despite normal thymic development of T cells (**Figure 3.5**). IKK activity is further required for signals transduced from the BCR, and for CD40-mediated recombination of immunoglobulin heavy chains. Serum of unimmunised *panr2* mice was deficient for all immunoglobulin isotypes tested, including IgM, indicating a broad impairment of B cell activation (**Figure 3.8A**). After immunization with a recombinant Semliki Forest virus (rSFV) vector, *panr2* mice produced no specific IgG or IgM antibody (**Figure 3.8B**).

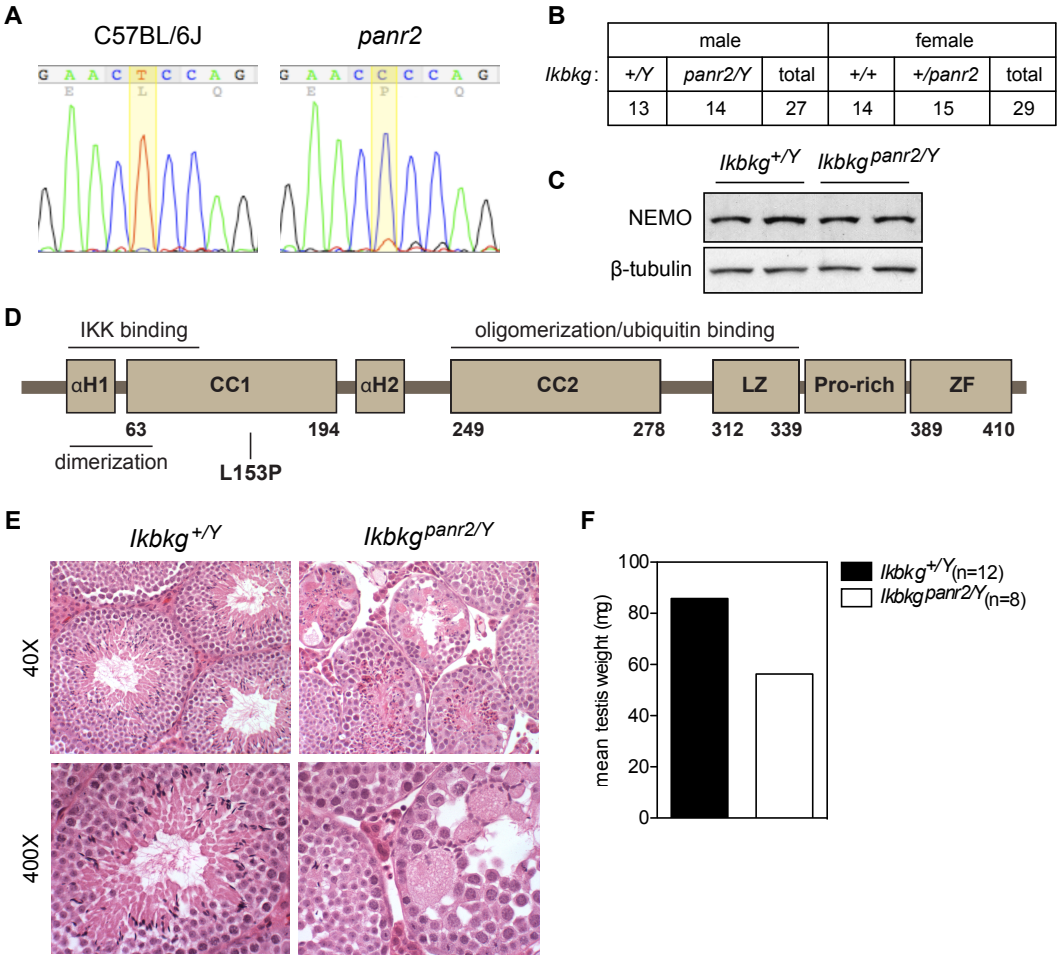


Figure 3.4 | *panr2* is a viable allele of *Ikbkg*.
(A) Representative sequence trace of the *Ikbkg* gene from C57BL/6J and *panr2* mice. (B) Genotype ratios of 4 week-old offspring from an $Ikbkg^{+/Y}$ x $Ikbkg^{+/panr2}$ cross. (C) Expression of NEMO protein in macrophage lysates. (D) Domain structure and location of the *panr2* mutation (L153P) in the NEMO protein. Hematoxylin and eosin staining (E) and mean weight (F) of pooled testes from $Ikbkg^{+/Y}$ and $Ikbkg^{panr2/Y}$ littermates.

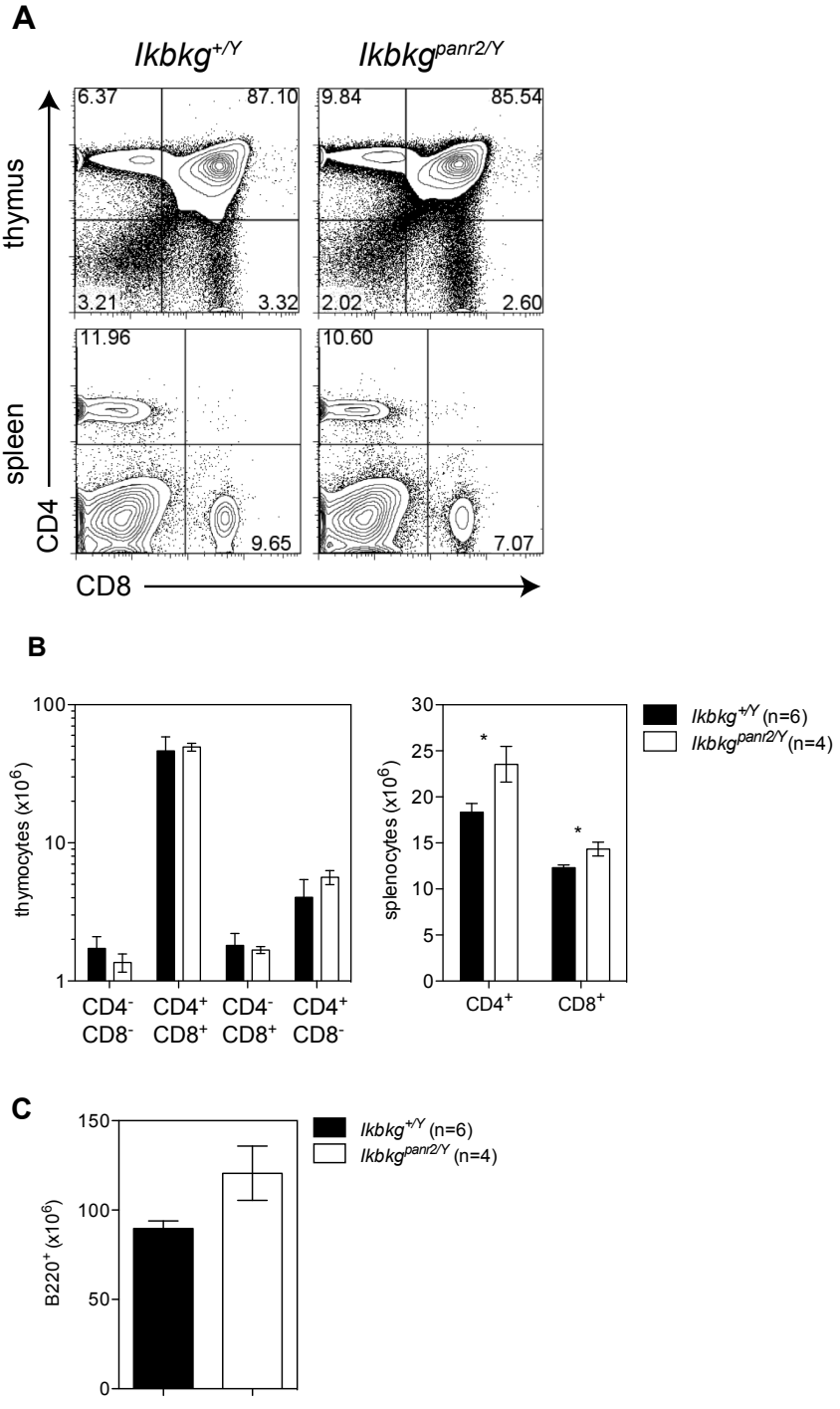


Figure 3.5 | T and B cell development is intact in *panr2* mice.
Frequencies (A) and absolute numbers (B) of T cell populations in the thymus and spleen of *Ikbkg*$^{+/Y}$ and *Ikbkg*$^{panr2/Y}$ littermates. Absolute numbers of B cells present in the spleens of *Ikbkg*$^{+/Y}$ and *Ikbkg*$^{panr2/Y}$ littermates (C). *, P<0.05 (B; Student's t-test).

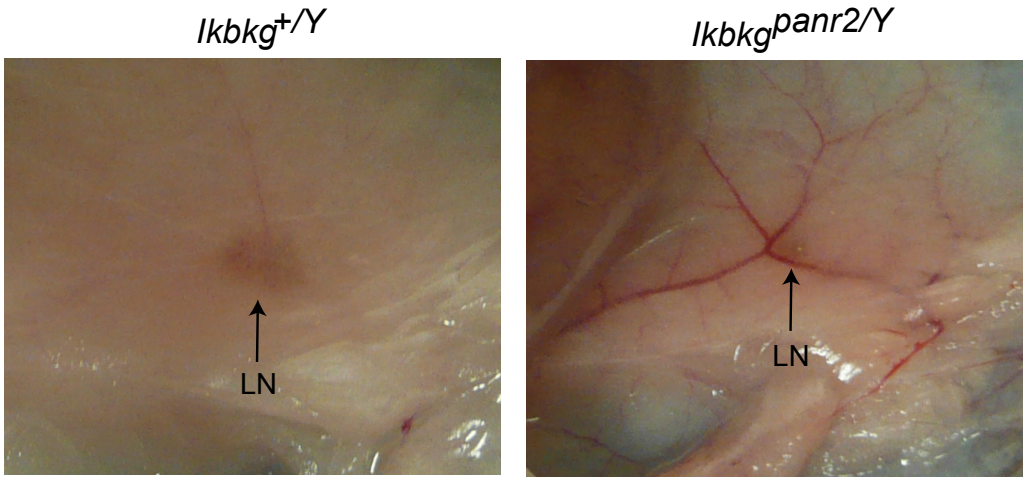


Figure 3.6 | Lymph nodes are diminished in *panr2* mice.
Ikbkg$^{+/Y}$ and *Ikbkg*$^{panr2/Y}$ inguinal lymph nodes *in situ.* LN, lymph node.

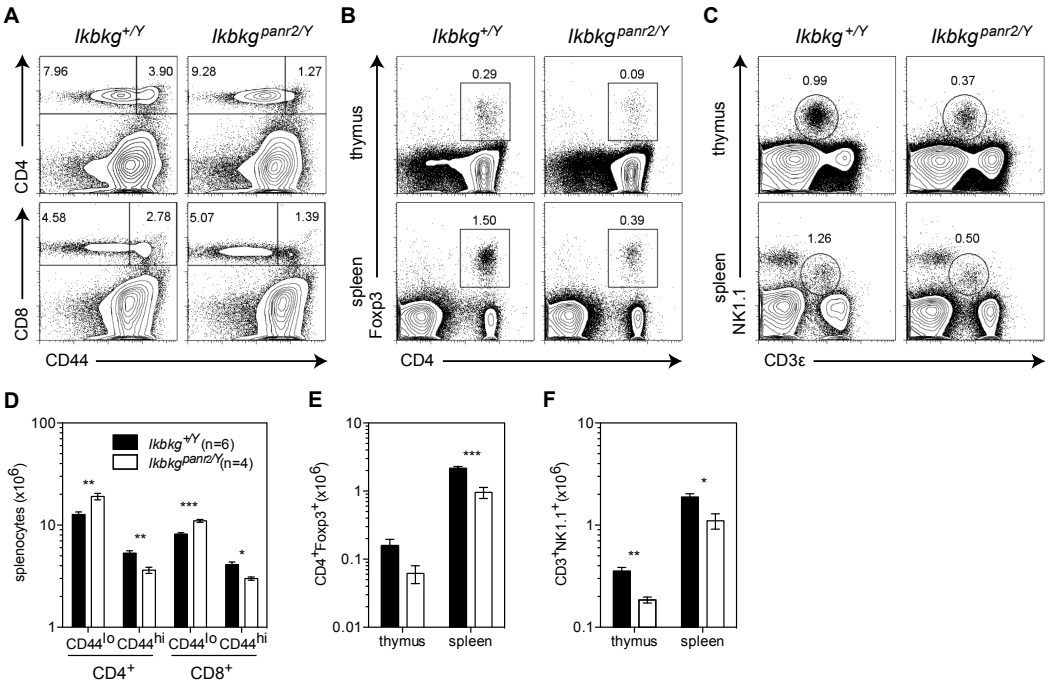


Figure 3.7 | Impaired development of memory, regulatory and natural killer T cells.

Representative flow cytometry plots and relative frequencies of $CD44^{lo}$ (naïve) and $CD44^{hi}$ (memory) T cells in spleen (A), $Foxp3^{+}$ regulatory T cells in thymus and spleen (B), and $CD3\varepsilon^{+}NK1.1^{+}$ natural killer T cells in thymus and spleen (C). Absolute numbers are represented in panels (D), (E) and (F) respectively. Numbers in each flow cytometry plot represent percentages of total lymphocytes, and bars represent mean and standard error. *, P<0.05; **, P<0.01 and ***, P<0.001 (D, E, F; Student's t-test).

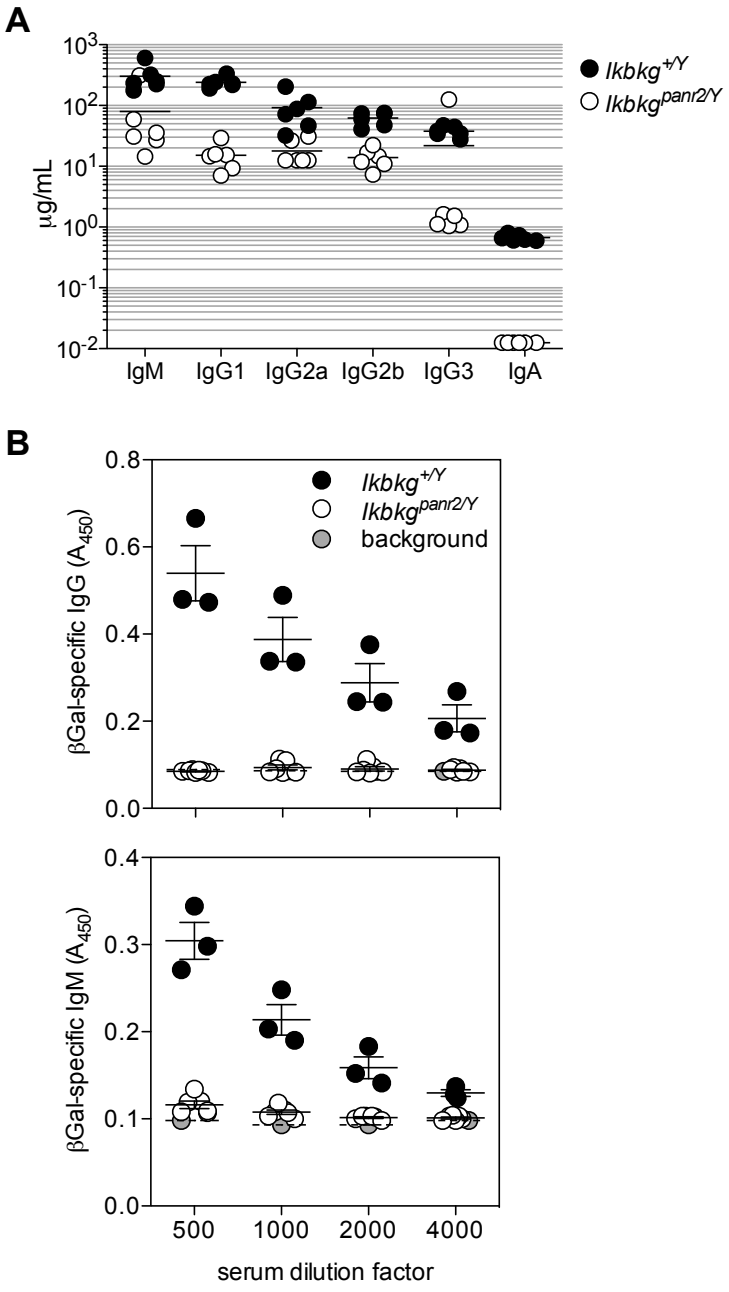


Figure 3.8 | Low serum immunoglobulin levels and impairment of antibody responses in *panr2* mice.
(A) Total immunoglobulin isotypes in the serum of naïve mice as measured by ELISA. Sample concentrations below the detection thresholds for IgG2a and IgA were given values of 12.5 μg/mL and 12.5 ng/mL respectively. (B) Mice were immunized with a recombinant Semliki Forest virus vector expressing β-galactosidase (rSFV-βGal), and βGal-specific IgG and IgM at day 14 post-immunization was measured by ELISA.

3.2.5.Impairment of p65 translocation, but not IκBα degradation

To characterize the biochemical consequences of the *panr2* mutation, NF-κB and MAPK signalling events were examined in TLR-stimulated macrophages. In response to both LPS (**Figure 3.9A**) and MALP-2 (**Figure 3.10A**), p38 MAPK phosphorylation occurred normally in *panr2* cells, yet phosphorylation of p105, MEK (MAPK or ERK kinase), and ERK was severely impaired. Despite a mild impairment of IκBα phosphorylation, IκBα degradation remained intact. Nonetheless, nuclear translocation of p65 was suppressed in *panr2* cells (**Figure 3.9B**), with accumulation occurring instead in the cytoplasmic fraction. Degradation of two other classical IκB proteins, IκBβ and IκBε, was not detected in cells of either genotype, although phosphorylation of IκBε was impaired to a similar degree as IκBα (**Figure 3.10B**). p105 was also stabilized in *panr2* cells, consistent with its reduced phosphorylation (**Figure 3.10B**).

The predominant role of the TPL2/MEK/ERK cascade is to promote the secretion of TNFα, rather than the accumulation of its 26-kDa membrane-associated precursor inside the cell (Rousseau et al., 2008). To examine the accumulation of TNFα inside *panr2* cells, macrophages were stimulated with LPS in the presence or absence of the secretory pathway inhibitor brefeldin A. Brefeldin A-treated *panr2* cells accumulated approximately 50% less intracellular TNFα than wild-type, in contrast to a 60-75% reduction of surface TNFα (**Figure 3.9B**) and an 80% reduction of TNFα in the supernatant (**Figure 3.2**). This disparity between intracellular and secreted TNF is consistent with observations in TPL2-deficient (Rousseau et al., 2008) and mutant (Xiao et al., 2009) cells, but also imply that synthesis of TNFα precursor protein is affected independently of TPL2.

3.2.6.Discussion

By separating developmental and immunological functions of NEMO, the *panr2* mutant models a rare immune deficiency of man (Niehues et al., 2004; Orange et al., 2004). This allele is likely to be hypomorphic (rather than null or hypermorphic) for a number of reasons, viability being chief among them. TLR signalling is reduced, but not abolished as it is in NEMO-deficient fibroblasts (Yamaoka et al., 1998), and survival of naive lymphocytes is also intact, in contrast to conditional knockouts of *Ikbkg* in B and T cells (Pasparakis et al., 2002; Schmidt-Supprian et al., 2003). An absence of ectodermal dysplasia, which occurs in mice with mutations of *Eda* (Srivastava et al., 1997), *Edar* (Headon and Overbeek, 1999), and

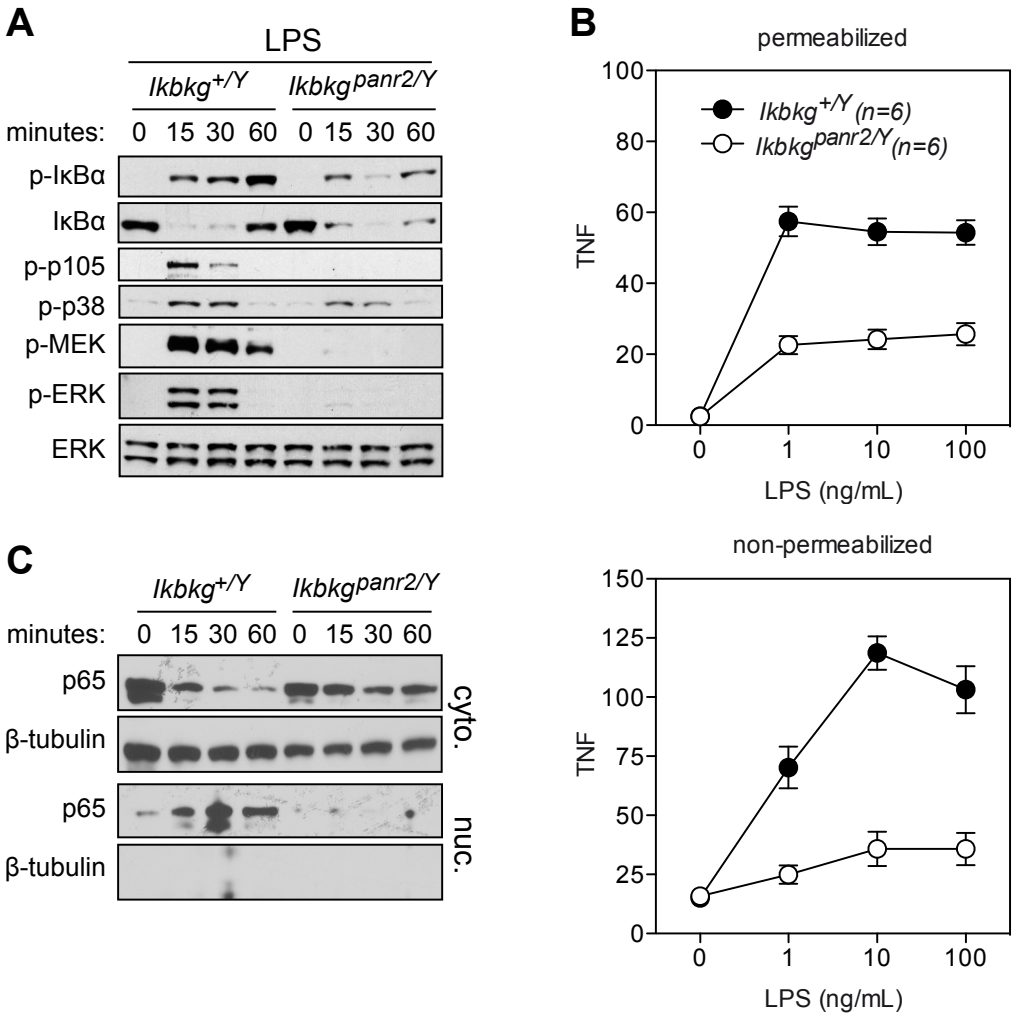


Figure 3.9 | The *panr2* mutation impairs MAPK and p105 phosphorylation, p65 translocation, and TNF production, but not IκBα degradation.
(A) Thioglycollate-elicited macrophages were stimulated with LPS (1 μg/mL) for the indicated times, and cell lysates analyzed by Western blotting. (B) Macrophages were stimulated with LPS, and intracellular (top panel) or surface (bottom panel) TNF was measured by flow cytometry (C) Cytoplasmic and nuclear fractions of LPS-stimulated macrophages stimulated with 1 μg/mL LPS were probed with antibodies against NF-κB, p65 and β-tubulin.

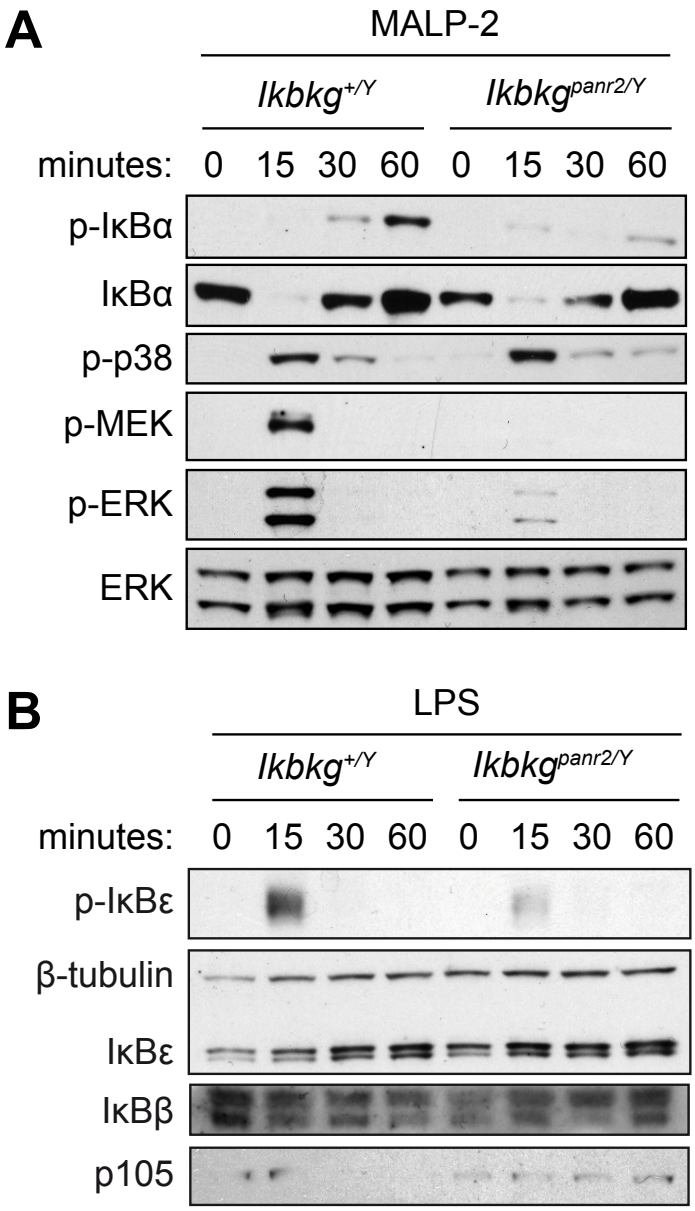


Figure 3.10 | MALP-2-induced signalling events and impaired IκBε phosphorylation and p105 degradation in *panr2* macrophages.
(A) Thioglycollate-elicited peritoneal macrophages were stimulated with MALP-2 (100 ng/mL) for the indicated times, and cell lysates analysed by Western blotting. (B) LPS-stimulated macrophage lysates were examined for the presence of phosphorylated IκBε, and total IκBε, IκBβ and p105.

Edaradd (Headon et al., 2000), suggests that the *panr2* mutation is permissive for signals transduced from EDAR, but not from the TLRs, CD40, LTβR, BCR, and/or TCR.

NEMO also appears to be important for the development of lymph nodes. IKK-mediated phosphorylation of the p50 precursor p105 is required for complete lymph node development (Sriskantharajah et al., 2009), as are the NF-κB subunits p50 and p52 (Lo et al., 2006). Activation of both subunits via signalling from LTβR is required for secondary lymphoid organogenesis, with combined p50/p52 deficiency preventing lymph node development altogether (Lo et al., 2006). Together with our observations in *panr2* mice, these data suggest that canonical NF-κB activation through the IKK complex is important for the development of lymphoid architecture. Conversely, azoospermia has not been associated with mutations of the IKK complex, and may indicate a new developmental role for NEMO. NF-κB is known to be activated during spermatogenesis (Lilienbaum et al., 2000), although the possibility of an additional X-linked mutation has not been excluded.

An L153R mutation (as opposed to L153P in *panr2*) has also been described in a patient with hypohidrotic ectodermal dysplasia and immune deficiency (Orange et al., 2002). Unlike *panr2*, L153R mutant cells do not degrade IκBα in response to TLR stimulation (Orange et al., 2002), potentially accounting for a disruption of EDAR signalling and the development of ectodermal dysplasia in this patient. Mice expressing a “superrepressive” form of IκBα also develop ectodermal dysplasia (Schmidt-Ullrich et al., 2001). These results may be consistent with the largely intact nuclear translocation of p65 in an *IKBKG* mutant patient without ectodermal dysplasia (Orange et al., 2004).

But of all of the biochemical pathways disrupted by mutations in NEMO, which are the most important for immunity? The data presented here would imply that IκBα degradation alone is insufficient for immune competence, at least in macrophages, as TLR-induced IκBα degradation proceeds normally in *panr2* cells. Nuclear translocation of p65 is severely affected, however, implying a requirement for NEMO beyond IκBα degradation. In agreement with this finding, cytoplasmic retention of most p65 can occur in the combined absence of IκBα, IκBβ, and IκBε (Tergaonkar et al., 2005). The molecule(s) that retain p65 in the cytoplasm in this context are not known, although greater quantities of p100 and p105 can be recovered by p65 immunoprecipitation. As p105 phosphorylation and degradation are impaired in TLR-stimulated *panr2* cells, this may account for p65 cytoplasmic retention in the presence of IκBα degradation.

Impairment of the TPL2/MEK/ERK pathway could also account for immune deficiency, although this cannot be entirely responsible for the phenotypes observed. TLP2 mutant mice do not exhibit reduced numbers of memory or regulatory T cells (Sriskantharajah et al., 2009), suggesting that development of these subsets depends on a TPL2-independent pathway. This pathway nevertheless requires IKK-mediated phosphorylation of p105, as *Ikbkg*$^{panr2/Y}$, p105 (*Nfkb1*$^{SSAA/SSAA}$), and IKKβ (*Ikbkb*$^{FL/-}$;*Cd4-cre*) mutant mice all show reductions in these populations. It will be of great interest to test the susceptibility of *Nfkb1*$^{SSAA/SSAA}$ mice to infection, as well as their ability to translocate p65, to determine the role of p105 phosphorylation in innate immunity.

Finally, polyubiquitination of NEMO is also necessary for complete activation of TLR-induced cytokine secretion. As revealed by mice lacking the target lysine residue (K392R) (Ni et al., 2008), TLR-induced IκBα degradation, NF-κB activation and ERK phosphorylation are all intact in the absence of NEMO polyubiquitination, whereas the cytokine response is not, suggesting that NEMO ubiquitination may regulate processes beyond IκBα degradation and ERK activation. The *panr2* mutation, in contrast, uncouples ERK phosphorylation and nuclear translocation of p65 without impairing IκBα degradation.

It has since been found that the *panr2* phenotype closely resembles that of the chronic proliferative dermatitis mutation (*cpdm)* strain (Zak et al., 2011). *cpdm* mice harbour a mutation in the gene encoding SHARPIN (SHANK-associated RH domain-interacting protein) (Seymour et al., 2007), which forms part of the linear ubiquitin chain assembly complex (LUBAC) (Gerlach et al., 2011; Ikeda et al., 2011; Tokunaga et al., 2011). LUBAC normally promotes NF-κB signalling through association with and polyubiqutination of NEMO (Tokunaga et al., 2009), yet the *panr2* mutation prevents this association (Zak et al., 2011). Since ERK phosphorylation is also disrupted by the *panr2* mutation, but not the K392R mutation (Ni et al., 2008), it appears that loss of polyubiquitination is not the only biochemical consequence of the *panr2* mutation.

In summary, the *panr2* mutation may disrupt NF-κB signalling partly by preventing LUBAC-mediated polyubiquitination, and this pathway may also influence the nuclear translocation of p65. This separation of function may offer a mechanistic explanation for rare immune deficiencies in man, and provides an animal model for their investigation.

3.3. iRhom2 is necessary for the secretion of TNFα

The work presented in section 3.3 is a reproduction of previously published work (Siggs et al., 2012b). The full publication is provided in Appendix 7.3.

3.3.1. TLR-induced TNFα secretion

TLR activation triggers a signalling pathway that culminates in the activation of NF-κB and the synthesis of proinflammatory cytokines such as TNFα. TNFα, which is synthesized as a membrane-bound precursor, is liberated from the cell surface by the TNFα converting enzyme (TACE, also known as ADAM17) (Black et al., 1997; Moss et al., 1997). TACE itself is processed by the furin protease (Borroto et al., 2003; Endres et al., 2003), and is negatively regulated at the cell surface by the TIMP3 (tissue inhibitor of metalloproteinase 3) protein (Mohammed et al., 2004). Mammalian TACE is also required for the cleavage of other membrane-bound ligands, including the EGFR ligand TGFβ (Peschon et al., 1998), whose counterpart in *Drosophila* is cleaved by the unrelated protease rhomboid-1 (Lee et al., 2001; Urban et al., 2001). The rhomboid protease family is also present in mammals, and includes members with no predicted catalytic function, known as iRhoms (Freeman, 2008). Until very recently, the physiological function of these proteins was unknown.

To reveal new regulators of TLR-induced TNFα, peritoneal macrophages from the progeny of chemically-mutagenized mice were stimulated with TLR agonists (Beutler et al., 2006). This screen has revealed mutant alleles throughout the pathway, from TLRs and the proteins that control their expression (Tabeta et al., 2006), to TNFα itself (Rutschmann et al., 2006). Here I describe a new mutation affecting TLR-induced TNFα secretion that did not affect secretion of IL-6. The causative mutation lay in the gene encoding iRhom2, a catalytically inactive member of the rhomboid protease family.

3.3.2. Mutation of Rhbdf2 reduces secretion of TNFα

During the course of a forward genetic screen for regulators of TLR-induced TNFα, an individual with a mildly impaired response was identified (**Figure 3.11A**). This phenotype, named *sinecure*, was inherited as a recessive trait most apparent after stimulation with the TLR2/6 agonist MALP-2. *sinecure* mice were otherwise healthy and fertile, with no other externally obvious phenotypes.

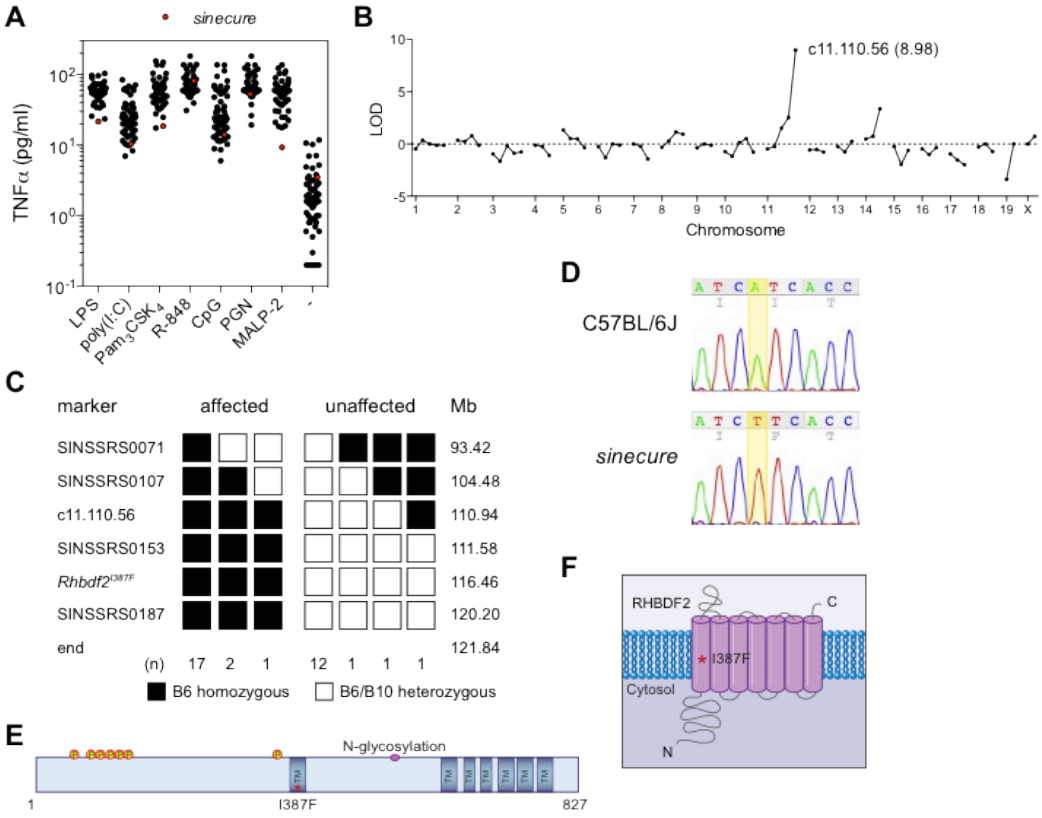


Figure 3.11 | A recessive mutation in *Rhbdf2* is associated with reduced TLR-induced TNF secretion.
(**A**) Phenotype of the index sinecure mouse. Peritoneal macrophages from G3 descendants of an ENU-mutagenized sire were stimulated with a panel of TLR ligands, and TNF production measured by L-929 bioassay. Genome-wide (**B**) and fine (**C**) mapping of the sinecure mutation to distal chromosome 11. (**D**) A homozygous transversion mutation in *Rhbdf2*, corresponding to an isoleucine to phenylalanine missense mutation (**E**) in the N-terminal transmembrane domain (TM) of iRhom2 protein. Predicted phosphorylation (P) and glycosylation sites are also indicated. (**F**) Topology of the iRhom2 protein, indicating the position of the *sinecure* missense mutation.

To isolate the causative mutation of the *sinecure* phenotype, the index *sinecure* male was outcrossed to C57BL/10J females, and backcrossed to his F1 daughters. Macrophages from progeny were stimulated with MALP-2, and grouped into wild-type or mutant cohorts based on their TNFα response. After genotyping individual mice at 70 polymorphic loci across the genome, the *sinecure* phenotype showed strong linkage to distal chromosome 11 (**Figure 3.11B**). This interval was refined to a 10.9 Mb region using additional markers (**Figure 3.11C**), encompassing an estimated 212 protein-coding genes. Among these, *Rhbdf2* was proposed as a candidate due to its strikingly high expression in mouse macrophages (Su et al., 2004)(**Figure 3.12**), and was sequenced directly. A single nonsynonymous mutation was identified: an A to T transversion at position 1680 of the *Rhbdf2* transcript, in exon 10 of 19 total exons (**Figure 3.11D**), corresponding to an isoleucine to phenylalanine substitution at amino acid 387 of the encoded iRhom2 protein (**Figure 3.11E-F**).

To establish that the missense mutation in *Rhbdf2* was responsible for the *sinecure* phenotype, mice were derived with an independent mutation of *Rhbdf2*. This allele was created by the targeted insertion of a gene trap cassette between exons 3 and 4 (Skarnes et al., 2011). Since exon 3 is the first coding exon of all coding transcripts of *Rhbdf2*, this insertion is predicted to result in a null allele, and is hereafter referred to as $Rhbdf2^{KO}$. Like $Rhbdf2^{sinecure}$ homozygotes, mice homozygous for the $Rhbdf2^{KO}$ allele were fully viable and fertile, with no externally visible phenotypes, and their peritoneal macrophages secreted less TNFα in response to both MALP-2 and LPS stimulation (**Figure 3.13A**). This response was lower than that of $Rhbdf2^{sin/sin}$ cells (indicating that the $iRhom2^{I387F}$ substitution was a probable hypomorph), but not as low as $Ticam1^{Lps2/Lps2};Irak4^{oti/oti}$ cells, suggesting that either the $Rhbdf2^{KO}$ allele was not a complete null, or that an iRhom2-independent pathway of TNFα secretion exists. iRhom2 might therefore act purely as a catalyst of TNFα secretion, or alternatively is functionally redundant with other protein(s). Mice with a compound heterozygous mutation of *Rhbdf2* ($Rhbdf2^{sin/KO}$) showed a similar reduction of TNFα secretion (**Figure 3.13A**), indicating that the *Rhbdf2* mutation in both strains was the cause of the impaired TNFα response. Unlike compound homozygosity for $Ticam1^{Lps2/Lps2}$ and $Irak4^{oti/oti}$ mutations, which blocks all known signals emanating from all TLRs, neither *Rhbdf2* mutation had any effect on IL-6 secretion (**Figure 3.13B**). The point of influence for iRhom2 therefore appears to be downstream of NF-κB activation and cytokine gene transcription.

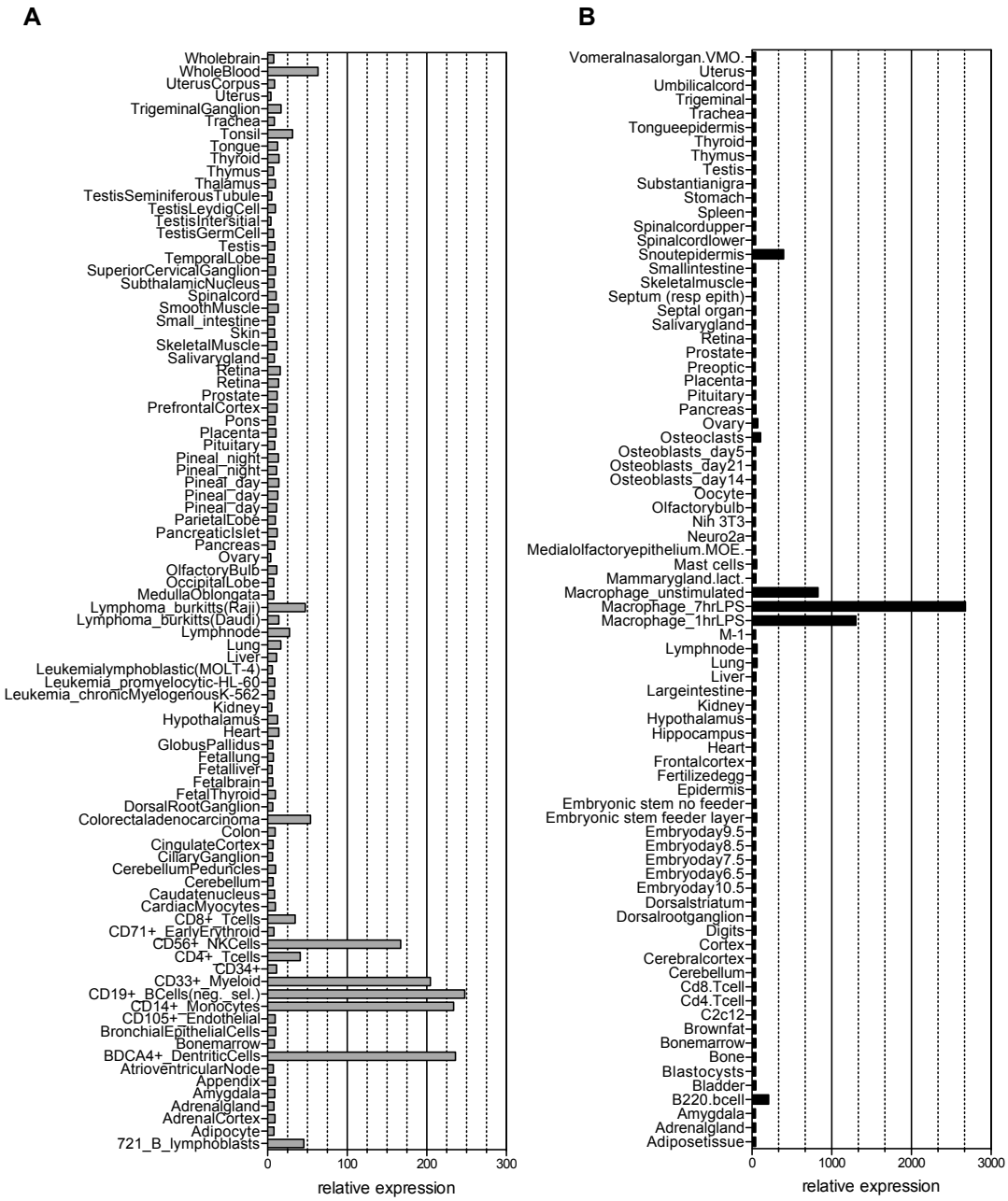


Figure 3.12 | Relative enrichment of RHBDF2-encoding transcripts in hematopoietic lineages.
(**A**) Expression of *RHBDF2* transcripts in human cells and tissues (Human U133A/ GNF1H Gene Atlas, GEO DataSets accession no. GSE1133). (**B**) Expression of mouse *Rhbdf2* (Mouse GNF1M Gene Atlas, GEO DataSets accession no. GSE1133).

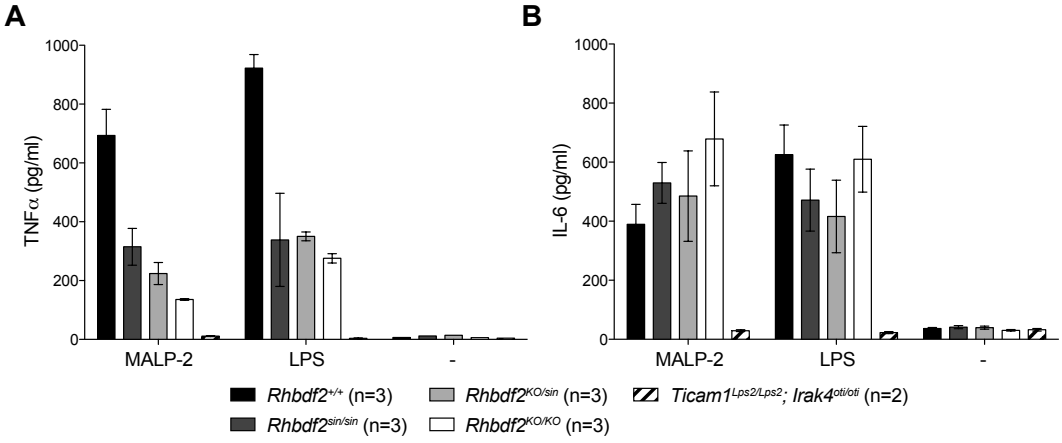


Figure 3.13 | Mutant alleles of *Rhbdf2* are non-complementary, and cause a specific block in TNFα secretion.
Thioglycollate-elicited peritoneal cells were isolated from mice of the indicated genotype, and cultured in the presence of 200 pg/ml MALP-2, 1 ng/ml LPS, or media alone (-) for four hours. TNFα (**A**) and IL-6 (**B**) was then measured in the culture supernatant.

3.3.3.Discussion

Since TACE is a key mediator of TNFα secretion, but not the secretion of other cytokines, regulation of TACE activity would seem a likely function for iRhom2, particularly given that iRhom2 is localized to the ER (Zettl et al., 2011), and both rhomboid proteins and TACE are known to play important roles during EGFR ligand processing (Peschon et al., 1998; Lee et al., 2001; Urban et al., 2001). Two groups independently reached similar conclusions, and have also revealed a specific interaction between iRhom2 and the protein precursor of TACE (Adrain et al., 2012; McIlwain et al., 2012).

It remains to be seen if iRhom2 is required for the function of proteases other than TACE (Blobel, 2005), or indeed for the processing of other proteins by TACE, such as FLT3L and EGFR ligands. To test whether iRhom2 was necessary *in vivo* for the processing of EGFR ligands, *Rhbdf2*^{sinecure} mutants were tested in a DSS-induced colitis model system. Unlike TACE and EGFR mutants (Brandl et al., 2010; Chalaris et al., 2010), the *Rhbdf2* mutation did not affect sensitivity to DSS-induced weight loss (**Figure 3.14**), implying that iRhom2 was physiologically redundant for the processing of EGFR ligands. In support of this conclusion, *Rhbdf2*^{sinecure} and *Rhbdf2*^{KO} homozygotes also did not display the epidermal phenotypes that are characteristic of EGFR and TACE mutant mice. This may in part be due to the partial functional redundancy of TACE with ADAM10, which is capable of processing EGFR ligands and TNFα in the absence of TACE (Le Gall et al., 2009).

The phenotypic effects of iRhom2 mutation could also depend upon genetic modifiers. The *curly bare* mutation, which is unidentified but maps to a region of chromosome 11 encompassing *Rhbdf2*, causes hairlessness on one genetic background and a waved coat on another (Johnson et al., 2003). This phenotypic difference can be attributed to a single modifier locus on chromosome 5, which includes genes for the EGFR ligands betacellulin, amphiregulin, epiregulin, and epigen (Johnson et al., 2003). It is therefore tempting to speculate that *curly bare* represents a new allele of *Rhbdf2*, which would reveal a new physiological function for iRhom2 in the processing of EGFR ligands.

While iRhom2 may be a valid target for the treatment of inflammatory disease, unlike most other rhomboid proteins (and indeed even TACE), iRhom2 is not an active protease, and may therefore be a challenging target for small molecule inhibition. Caution should also be taken given the potential role of iRhom2 in EGFR ligand processing.

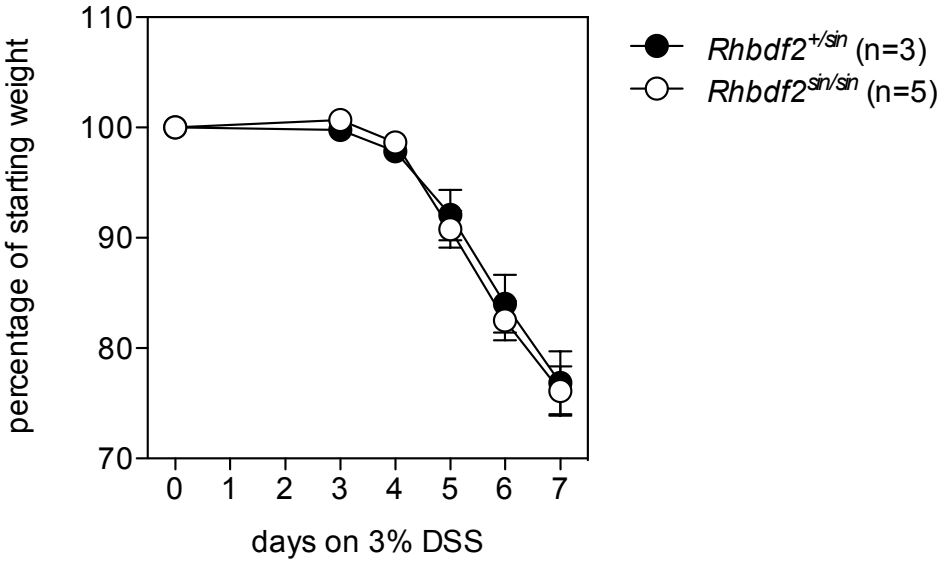


Figure 3.14 | Mutation of *Rhbdf2* does not alter sensitivity to DSS-induced weight loss.
Rhbdf2$^{sin/sin}$ mutants and *Rhbdf2*$^{+/sin}$ sex-matched littermates were treated with 3% DSS in drinking water for seven days, with weight recorded on each day.

4. Forward genetic analysis of adaptive immunity

4.1. Lymphocyte development screens

Two forward genetic screens were used to reveal new regulators of adaptive immunity. Both screens monitored the development of lymphocytes, under either homeostatic or competitive conditions (**Figure 4.1**). A summary of the phenotypes identified is provided in **Table 4.1**.

4.1.1. Blood lymphocyte screen

Frequencies of the major blood lymphocyte populations were screened in a total of 2500 G3 mice. These populations include B cells ($CD19^+$), NK cells ($NK1.1^+$), and naive ($CD44^-$) and memory/activated ($CD44^+$) $CD4^+$ and $CD8^+$ T cells. A total of 4 phenovariants were identified in genes with previously established roles in lymphocyte development (*Klrb1c*, *Map3k14*, *Ptprc*, and *Rag1*). An additional three phenotypes were caused by mutations in genes with no precedent in lymphocyte development (*Atp11c*, *Kdelr1*, and *Zbtb1*), and two of these mutations were studied in greater detail and will be presented in section 4.2 (*Atp11c*) and 4.3 (*Zbtb1*).

4.1.2. Competitive bone marrow chimera screen

Mutations with only subtle effects on lymphocyte development are often exaggerated when the cells develop in competition with wild-type cells. Since these phenotypes might be missed amongst the normal variation inherent in the standard lymphocyte screen, a sensitised competitive screen was applied. This screen involved administering a sublethal dose of irradiation to G3 mice, transplanting them with congenically marked ($CD45.1^+$) bone marrow cells, and measuring chimerism in the resulting lymphocyte populations (**Figure 4.2A**). The starting point for this screen was a dose titration of gamma irradiation, to identify a dose which would allow ~50% chimerism after reconstitution (**Figure 4.2B**). A total of 1200 G3 mice were irradiated (400R), transplanted with $CD45.1^+$ bone marrow cells, and bled four weeks later. Five unique phenovariants were identified, with mutations identified in three of them. Two of these genes have well characterised roles in T cell development (*Cd247* and *Zap70*), while the third (*Fnip1*) did not have a described role in lymphocyte development. The *Fnip1* mutation will be described in more detail in section 4.4.

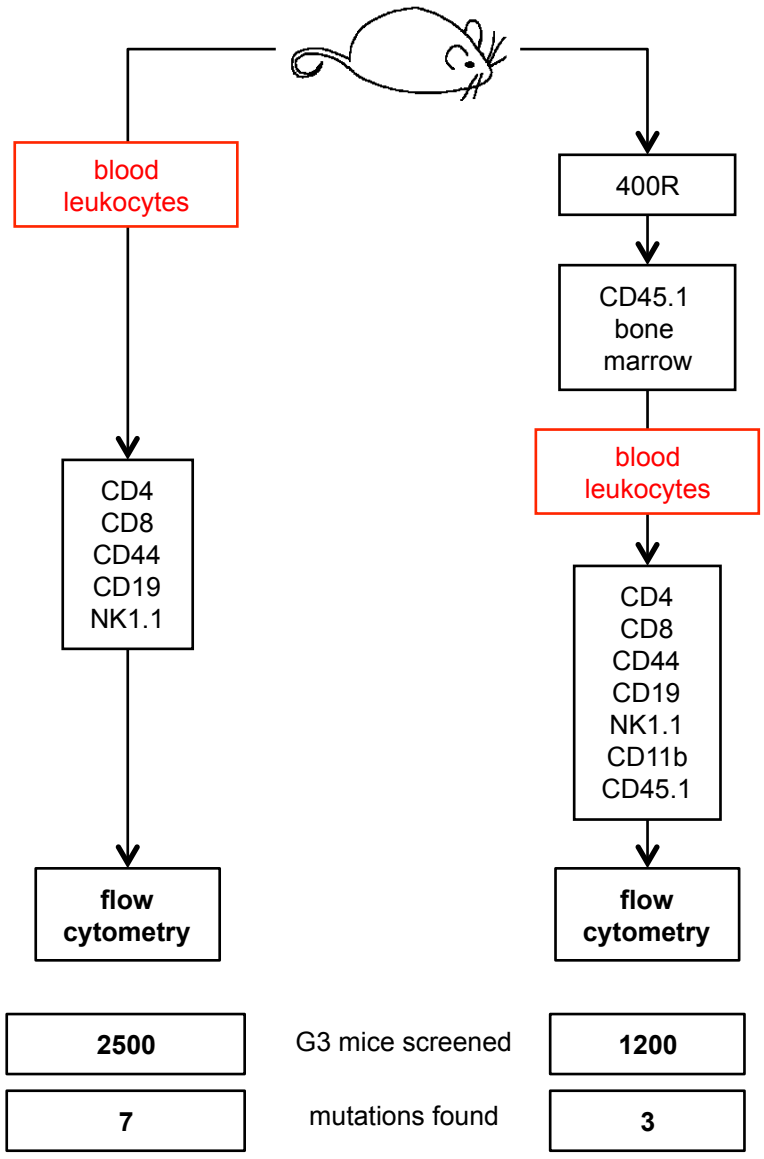


Figure 4.1 | Summary of two forward genetic screens for lymphocyte development phenotypes.
Mice were either bled directly (left) or four weeks after sublethal irradiation and transplantation with CD45.1+ bone marrow cells (right). Following red blood cell lysis, cells were labelled with a panel of fluorochrome-conjugated antibodies and analysed by flow cytometry.

Table 4.1 | Summary of phenotypes and mutations identified in two lymphocyte development screens.
All phenotypes are recessive, with the exception of *Unnatural*, which is semidominant. The genetic cause of two phenotypes (*salamis* and *saratoga*) is unknown.

gene	allele	screen	phenotype
Atp11c	*emptyhive*	blood lymphocyte screen	reduced CD19+
Cd247	*allia*	competitive chimera screen	outcompeted CD4+
Fnip1	*hamel*	competitive chimera screen	outcompeted CD19+
Kdelr1	*daniel gray*	blood lymphocyte screen	reduced CD4+ and CD8+
Klrb1c	*Unnatural*	blood lymphocyte screen	absent NK1.1+
Map3k14	*lucky*	blood lymphocyte screen	increased CD44 expression in CD4+ and CD8+
Ptprc	*belittle*	blood lymphocyte screen	absent CD4+ and CD8+, CD19+ cells are B220–
Rag1	*maladaptive*	blood lymphocyte screen	absent CD4+, CD8+ and CD19+
Zap70	*trebia*	competitive chimera screen	outcompeted CD4+ and CD8+
Zbtb1	*scanT*	blood lymphocyte screen	absent CD4+ and CD8+
?	*salamis*	competitive chimera screen	no donor cell engraftment
?	*saratoga*	competitive chimera screen	outcompeted CD19+ and CD11b+

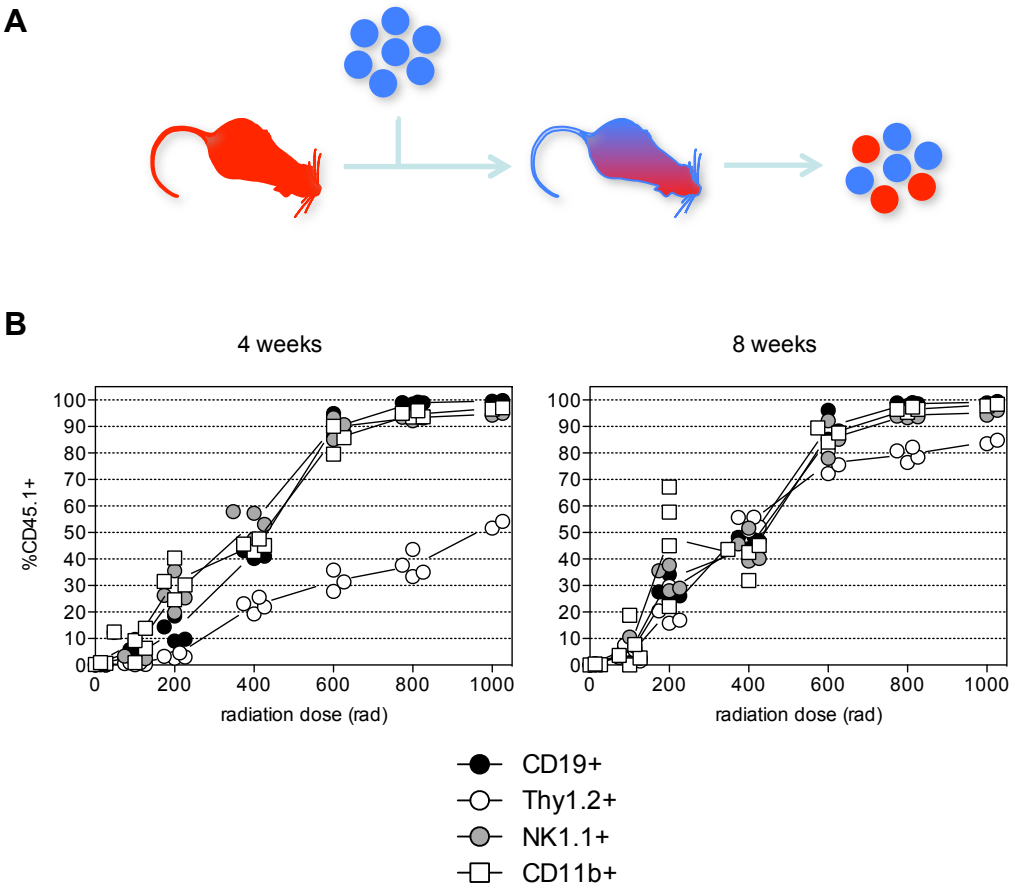


Figure 4.2 | A competitive bone marrow chimera screen.
(A) To create a competitive environment for lymphocyte development, mice can be sublethally irradiated and transplanted with competitor bone marrow cells. (B) A dose titration was performed to identify a dose at which $2x10^6$ CD45.1+ bone marrow cells gave ~50% chimerism (2-5 mice per dose). Mice were bled at four and eight weeks post-transplant, and chimerism measured in B (CD19+) T (Thy1.2+) NK (NK1.1+) and myeloid (CD11b+) compartments. 400 rad was chosen as the optimal dose, with mice bled four weeks later.

4.2. The P4-type ATPase ATP11C is essential for B lymphopoiesis in adult bone marrow

The work presented in section 4.2 is a reproduction of previously published work (Siggs et al., 2011a). The full publication is provided in Appendix 7.3.

4.2.1. B cell development

B cell progenitors arise first in foetal liver and then in bone marrow shortly after birth, and give rise to three main mature populations (Hardy and Hayakawa, 2001). Marginal zone B cells localize to the splenic marginal zone and respond to blood-borne antigens independently of T cell help (Lopes-Carvalho et al., 2005). Follicular B cells, in contrast, respond to protein antigens in a T cell–dependent manner and progressively undergo immunoglobulin isotype switching and affinity maturation. B-1 cells constitute a much smaller population that predominates in the pleural and peritoneal cavities and contributes most of the serum immunoglobulin M (IgM) during the early phases of infection (Tung and Herzenberg, 2007).

While marginal zone and B-1 B cells can self-renew, follicular B cells require constant replenishment from bone marrow, as demonstrated in mice with conditional deletion of recombinase-activating gene 2 (*Rag2*) (Hao and Rajewsky, 2001). Deletion of *Rag2* in newborn mice prevents almost all follicular B cell development but leaves marginal zone and B-1 populations largely intact. Similarly, in adult mice, deletion of *Rag2* results in a progressive decrease in follicular B cell numbers, while marginal zone and B-1 populations persist. A similar phenomenon has been reported for mice with mutation of *Il7*, which encodes the cytokine interleukin 7 (IL-7) (Carvalho et al., 2001). Although redundant with the receptor tyrosine kinase Flt3 in the foetal liver (Freeden-Jeffry et al., 1995; Sitnicka et al., 2003; Kikuchi and Kondo, 2006), IL-7 becomes essential for B cell development in the bone marrow shortly after birth (Kikuchi and Kondo, 2006). As a result, marginal zone and B-1 B cells predominate in the periphery of IL-7-mutant mice, whereas follicular B cell numbers are much lower.

In the absence of IL-7 or its receptor component IL-7Rα, B cell development is arrested in the adult bone marrow shortly after cells acquire surface expression of the B cell–associated marker B220 but before they express the coreceptor CD19 or B cell–differentiation marker CD24 (Freeden-Jeffry et al., 1995; Kikuchi et al., 2005). Expression of the transcription factor early B cell factor (EBF) via the transcription factor STAT5 seems to be important at this stage, as overexpression of EBF or constitutively

active STAT5 can overcome the developmental arrest in IL-7R-mutant progenitors (Dias et al., 2005; Kikuchi et al., 2005). Other data suggest that rather than inducing transcription of the gene encoding EBF (*Ebf1*), STAT5 signalling instead promotes the survival of B cell progenitors through induction of the antiapoptotic protein Mcl-1 (Malin et al., 2010). Whichever the mechanism, IL-7 and EBF are both key determinants of B cell differentiation (Lin and Grosschedl, 1995; Busslinger, 2004) and little else is known of the molecules and micro-environments that induce and maintain their expression in the adult. I describe below an essential role for the previously uncharacterized P4-type ATPase ATP11C in early B cell differentiation. ATP11C was redundant during B cell development in the foetal liver yet was essential in the context of adult bone marrow, where it was required for optimal responses to IL-7 and sustained expression of *Ebf1*.

4.2.2.A heritable B cell deficiency

During a forward genetic screen for nonredundant regulators of lymphopoiesis, I identified several mice from a common *N*-ethyl-*N*-nitrosourea–treated founder with low percentages of $CD19^+$ cells in blood (**Figure 4.3A**). The phenotype, named '*emptyhive*', was transmitted as an X-linked recessive trait. Affected male mice were outwardly normal in behaviour, fertility, lifespan and appearance but were notably hyperbilirubinemic. This last aspect of the phenotype, which stemmed from effects of the mutation in the liver, has been considered separately (Siggs et al., 2011b).

Among B cell progenitors in the bone marrow, *emptyhive* mutants had fewer cells beginning at the transition from pre-pro-B cell to pro-B cell (Hardy fraction A ($B220^+CD43^+BP\text{-}1^-CD24^-$) to Hardy fraction B ($B220^+CD43^+BP\text{-}1^-CD24^+$) (Hardy et al., 1991)), with a severe deficiency of immature B cells (Hardy fraction E ($B220^+CD43^-IgM^-IgD^+$); **Figure 4.3B**). In the spleen, *emptyhive* mice had one tenth the normal number of $CD19^+$ cells, largely due to a lack of follicular and transitional subsets, although the number of marginal zone B cells and Thy-1.2^+ cells was normal (**Figure 4.3C,D**). The number of B-1 cells (the predominant population of B cells in the peritoneal cavity), was three times greater in wild-type mice than in mutant mice, whereas the number of peritoneal B-2 cells was ten times greater in wild-type mice than in mutant mice (**Figure 4.3D,E**). B cells in the blood of mutant mice had also undergone normal allelic exclusion at the immunoglobulin heavy-chain locus (**Figure 4.3F**).

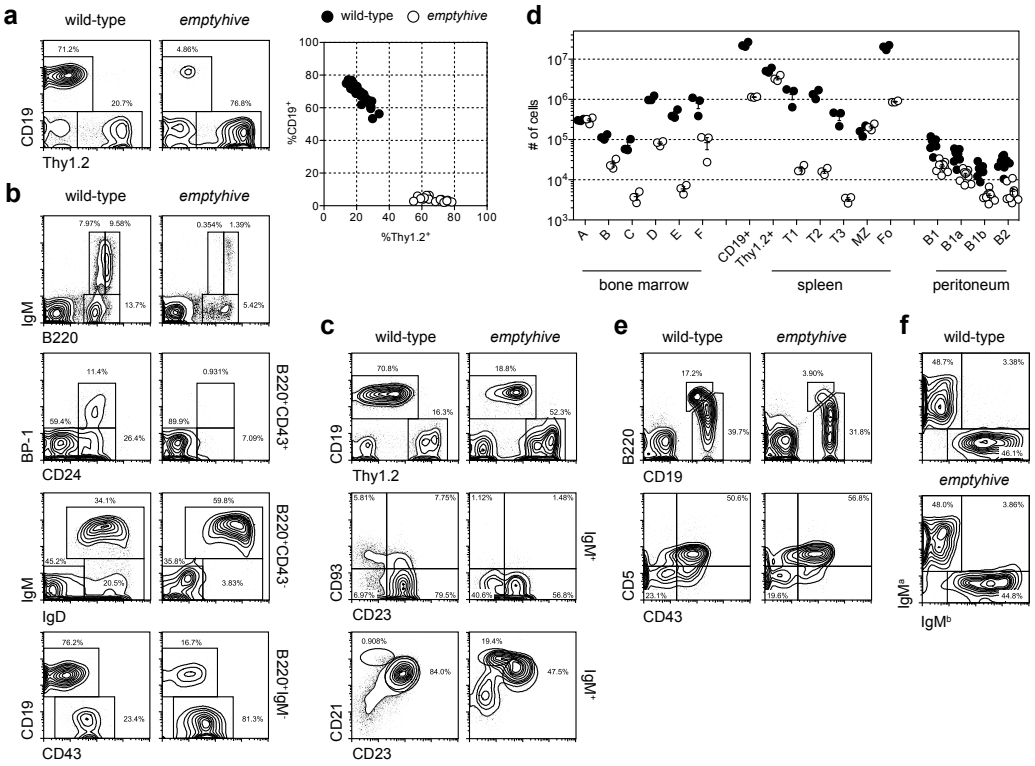


Figure 4.3 | A heritable B cell deficiency.
(**a**) Frequency of CD19$^+$ and Thy-1.2$^+$ blood lymphocytes in wild-type (WT) and *emptyhive* mice. (**b**–**e**) Frequency (**b**,**c**,**e**) and number (**d**) of B cell subsets in the bone marrow (**b**), spleen (**c**) or peritoneal cavity (**e**) or all three (**d**). Hardy fractions in bone marrow (A–F) were gated as follows: A, B220$^+$CD43$^+$BP-1$^-$CD24$^-$; B, B220$^+$CD43$^+$BP-1$^-$CD24$^+$; C, B220$^+$CD43$^+$BP-1$^+$CD24$^+$; D, B220$^+$CD43$^-$IgM$^-$IgD$^-$; E, B220$^+$CD43$^-$IgM$^-$IgD$^+$; F, B220$^+$CD43$^-$IgM$^+$IgD$^+$; the C′ fraction (B220$^+$CD43$^+$BP-1$^+$CD24^{hi}) was not resolved. Fractions A and B–D may also be gated as CD19$^-$ and CD19$^+$ populations among B220$^+$IgM$^-$ cells, respectively (**b**). IgM$^+$ splenocytes were separated into the following subsets: T1, CD93$^+$CD23$^-$; T2, CD93$^+$CD23$^+$IgM^{int}; T3, CD93$^+$CD23$^+$IgM^{hi}; marginal zone (MZ), CD93$^-$CD23$^-$IgM^{hi}CD21^{hi}; and follicular (Fo), CD93$^-$CD23$^+$. Peritoneal lymphocytes were separated into the following subsets: B-2, CD19$^+$B220^{hi}; B-1, CD19$^+$B220$^{lo–int}$; B-1a, CD5$^+$CD43$^+$; and B-1b, CD5$^-$CD43$^-$. (**f**) IgM allotype expression on CD19$^+$ blood lymphocytes from wild-type and emptyhive mice on a (C57BL/6 × BALB/c)F$_2$ background (heterozygous IgM allotype). Each symbol (**a**,**d**) represents an individual mouse; numbers adjacent to outlined areas or quadrants (**a**–**c**,**e**,**f**) indicate percent cells in each. Data are representative of three independent experiments (**a**–**e**) or one experiment (**f**) with three mice per genotype (error bars (**d**), s.e.m.).

Despite the lower number of follicular B cells, the B cells that remained in mutant mice retained the ability to produce many immunoglobulin isotypes (**Figure 4.4A**). They were also able to generate specific antibodies to T cell–independent and T cell–dependent immunogens (4-hydroxy-3-nitrophenylacetyl (NP)-conjugated Ficoll (NP-Ficoll) and NP-conjugated chicken γ-globulin (NP-CGG), respectively; **Figure 4.4B,C**). However, 50% less NP-specific IgM and high-affinity IgG1 was produced in response to immunization with NP-Ficoll and alum-precipitated NP-CGG, respectively.

4.2.3.A cell-intrinsic failure of adult B lymphopoiesis

To determine the cellular origin of the *emptyhive* phenotype, irradiated mice were reconstituted with an equal mixture of mutant and wild-type bone marrow cells. Although the Thy-1.2$^+$ compartment was reconstituted equally by wild-type and *emptyhive* cells, less than 1% of CD19$^+$ cells were of mutant origin (**Figure 4.5A**), which indicated that the defect was intrinsic to *emptyhive* B cell progenitors but did not appreciably affect T cell development. Even in the absence of competition, bone marrow cells from *emptyhive* donors were unable to repopulate any peripheral B cell compartment in irradiated recipients (**Figure 4.5B,C**), and unlike their non-chimeric counterparts (**Figure 4.4B**), recipients of mutant bone marrow also failed to produce specific antibody after immunization with NP-Ficoll (**Figure 4.5D**). These data suggested a failure of adult B cell development in *emptyhive* mice, consistent with the much lower number of immature B cells in mutant bone marrow (**Figure 4.3B**) and the age-dependent decrease in follicular but not marginal zone B cells in mutant spleens (**Figure 4.5E**). This effect was not due to an intrinsic difference between adult and foetal progenitors, as neither bone marrow nor foetal liver cells reconstituted the B cell compartment of irradiated recipients (**Figure 4.5C**). Instead, the results suggest that *emptyhive* B cell progenitors, regardless of their source, cannot develop in the microenvironment of adult bone marrow.

Immature and mature B cells were also entirely absent from the bone marrow of recipients reconstituted with *emptyhive* cells (**Figure 4.5B**), with very few progressing beyond the B220$^+$CD19$^-$ pre-pro-B stage. This developmental arrest was even more severe than that observed in nonirradiated *emptyhive* mice or mice with a mutation in *Rag1* (**Figure 4.5B**), which indicated that a failure of IgM rearrangement was not the cause of developmental arrest in *emptyhive* mutants. Few mutant progenitors were able to induce expression of cytoplasmic IgM (**Figure 4.5F**), consistent with the interpretation that

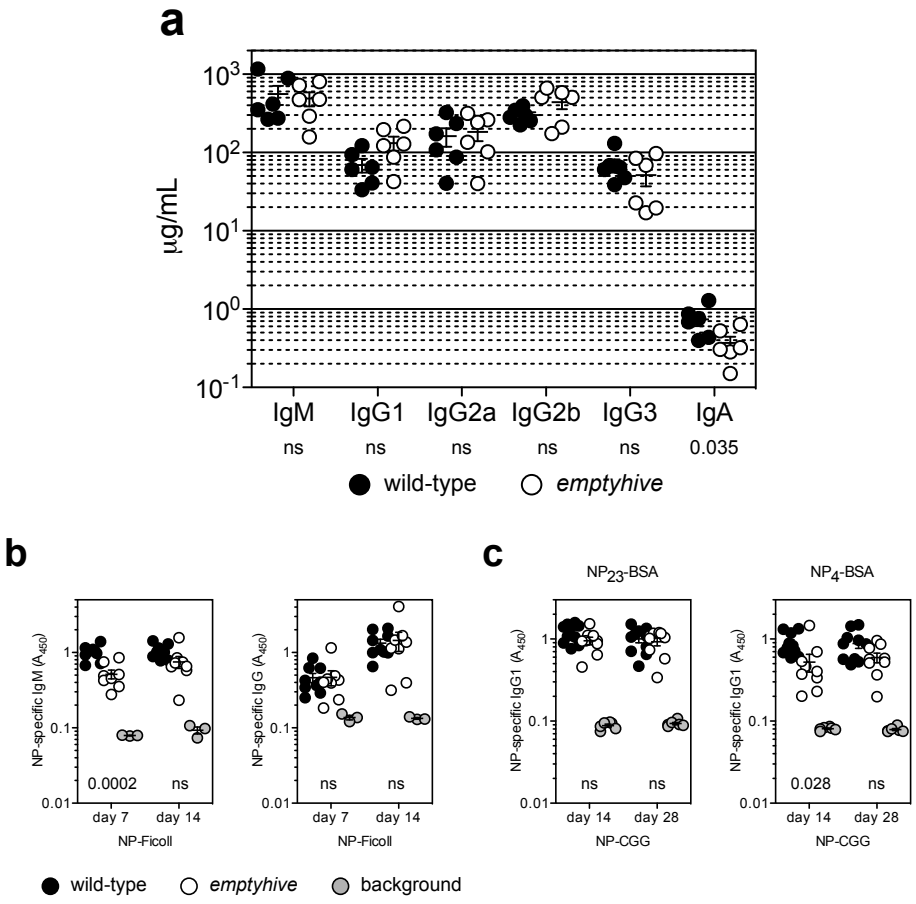


Figure 4.4 | Immunoglobulin secretion in *emptyhive* mice.
(**a**) Total immunoglobulins in the serum of 12- to 24-week-old naive mice. (**b**,**c**) NP-specific antibodies 7, 14 or 28 d after immunization of 12-week-old mice with NP-Ficoll (**b**) or alum-precipitated NP-CGG (**c**), presented as absorbance at 450 nm (A_{450}). Different capture antigens were used to discriminate between total IgG1 (NP_{23}-BSA) and high-affinity IgG1 (NP_4-BSA) in response to NP-CGG. Each symbol represents an individual mouse. NS, not significant ($P > 0.05$); *P* values, wild-type versus emptyhive (unpaired *t*-test). Data are from one experiment (error bars, s.e.m.).

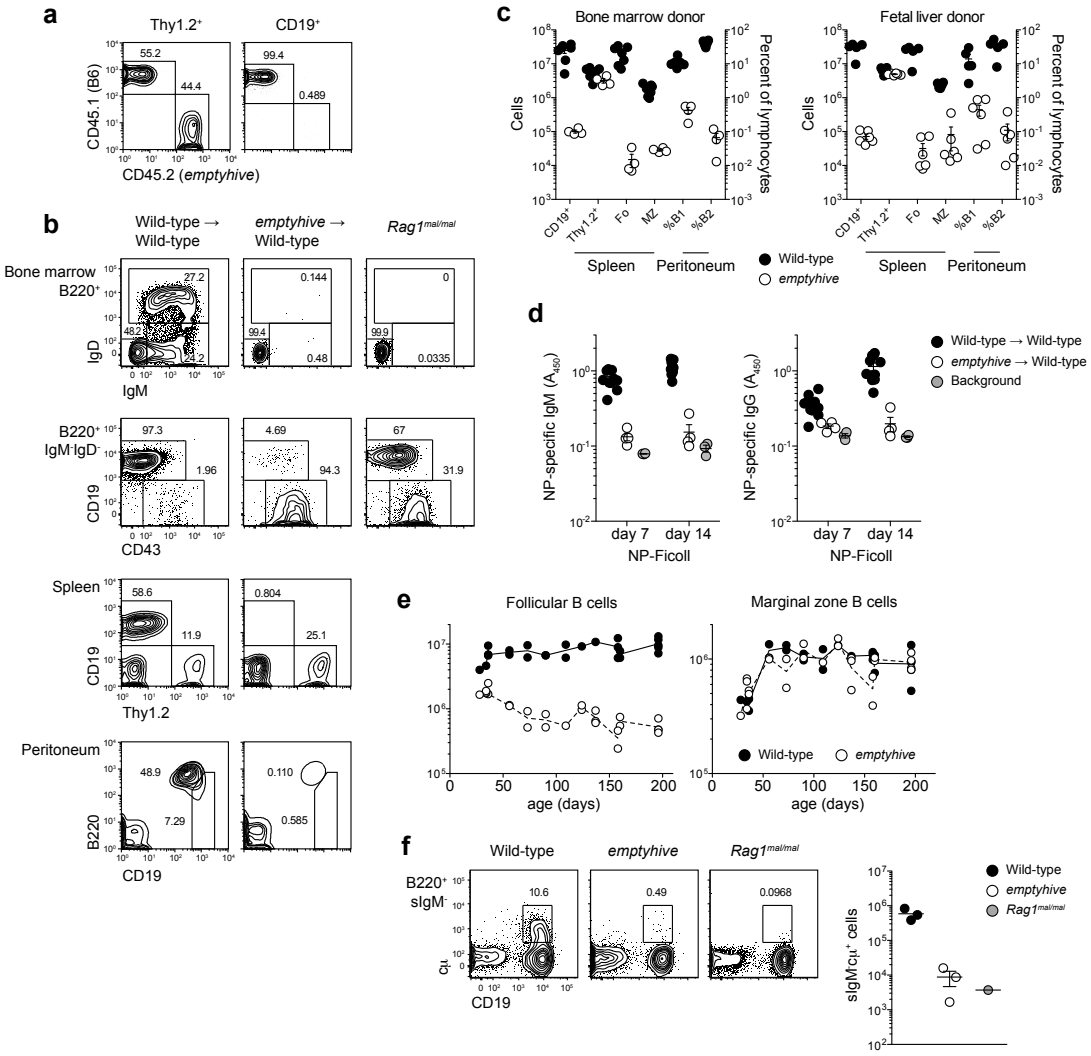


Figure 4.5 | A cell-intrinsic failure of adult B cell development.
(**a**) Lymphocyte repopulation in blood 8 weeks after reconstitution of irradiated RAG-1-mutant recipients with a 1:1 mixture of *emptyhive* (CD45.2$^+$) and wild-type (C57BL/6 (B6); CD45.1$^+$) bone marrow. (**b**,**c**) Reconstitution of bone marrow, spleen and peritoneal B cell subsets with donor-derived cells 8 weeks after reconstitution of irradiated wild-type recipients (CD45.2$^+$) with unmixed bone marrow (**b**,**c**) or fetal liver cells at embryonic day 16.5 (**c**) from either mutant or wild-type donors (CD45.1$^+$). (**d**) NP-specific immunoglobulin titers in bone marrow chimeras immunized with NP-Ficoll at 8 weeks after reconstitution, assessed 7 and 14 d later. (**e**) Absolute number of follicular and marginal zone B cells as a function of age. (**f**) Intracellular IgM (cμ) expression in B220$^+$ bone marrow cells negative for surface IgM. Each symbol (**c**,**d**,**f**) represents an individual mouse; numbers adjacent to outlined areas or quadrants (**a**,**b**,**f**) indicate percent cells in each. Data are from one (**a–e**) or two (**f**) independent experiments with six (**a**), four to seven (**b**) or three (**f**) mice per genotype (error bars (**c**,**d**,**f**), s.e.m.).

the *emptyhive* phenotype originated from a defect upstream of RAG recombinase–mediated recombination.

4.2.4.Compromised responsiveness to IL-7

Because IL-7 is known to be essential for adult B cell development but not foetal B cell development (Carvalho et al., 2001), it was hypothesized that a specific failure of IL-7R signalling in B cell progenitors could explain the *emptyhive* phenotype. To examine the competence of IL-7R signalling in mutant progenitors, precursors negative for IgM at the membrane ($mIgM^-$) were purified by flow cytometry and cultured *ex vivo* in the presence of IL-7. The *emptyhive* progenitors formed lymphoblasts with kinetics similar to those of wild-type progenitors in response to IL-7 (**Figure 4.6A**), which indicated that IL-7R-induced proliferation was largely intact. *In vitro* treatment with IL-7 also led to the differentiation of low frequencies of $mIgM^+$ cells, which unexpectedly also emerged in *emptyhive* cultures (**Figure 4.6B**). The absolute number of IL-7-induced $mIgM^+$ cells was nonetheless lower in mutant cultures, with as few as 50% of the number wild-type cells at high concentrations of IL-7 (**Figure 4.6B**).

As the data reported above suggested a qualitative or quantitative difference in the IL-7 response of *emptyhive* progenitors, the expression of *Ebf1*, whose expression is lost in the absence of IL-7R signalling (Kikuchi et al., 2005), was examined. *Ebf1* transcription was measured in sorted pre-pro-B cells by RT-PCR and was found to be much lower in *emptyhive* progenitors (**Figure 4.6C**). Transcription of *Igll1*, a target of EBF1 that encodes the λ5 component of the surrogate light chain portion of the precursor to the B cell antigen receptor (pre-BCR) (Karasuyama et al., 1994), was also measured. Neither transcription of *Igll1* (**Figure 4.6C**) nor surface expression of λ5 (**Figure 4.6D**) was compromised in *emptyhive* progenitors, which suggested that the lack of *Ebf1* transcripts was either transient (and isolated to adult pre-pro-B cells or a subset thereof) or insufficient to affect *Igll1* expression.

Consistent with their intact IL-7 responsiveness *in vitro*, *emptyhive* progenitors had surface expression of IL-7Rα equivalent to that of their wild-type counterparts (**Figure 4.6E**). Furthermore, in the absence of IL-7, Flt3 signalling is thought to account for residual B lymphopoiesis in foetal liver (Jensen et al., 2008). Although mutant mice with the compound mutations $Flt3^{-/-};Il7^{-/-}$ or $Flt3^{-/-};Il7r^{-/-}$ lack all peripheral B cells (Sitnicka et al., 2003; Jensen et al., 2008), *emptyhive* mice with a homozygous mutation of *Flt3* had numbers of $CD19^+$ splenocytes similar to those of *emptyhive* mice with wild-type *Flt3* (**Figure**

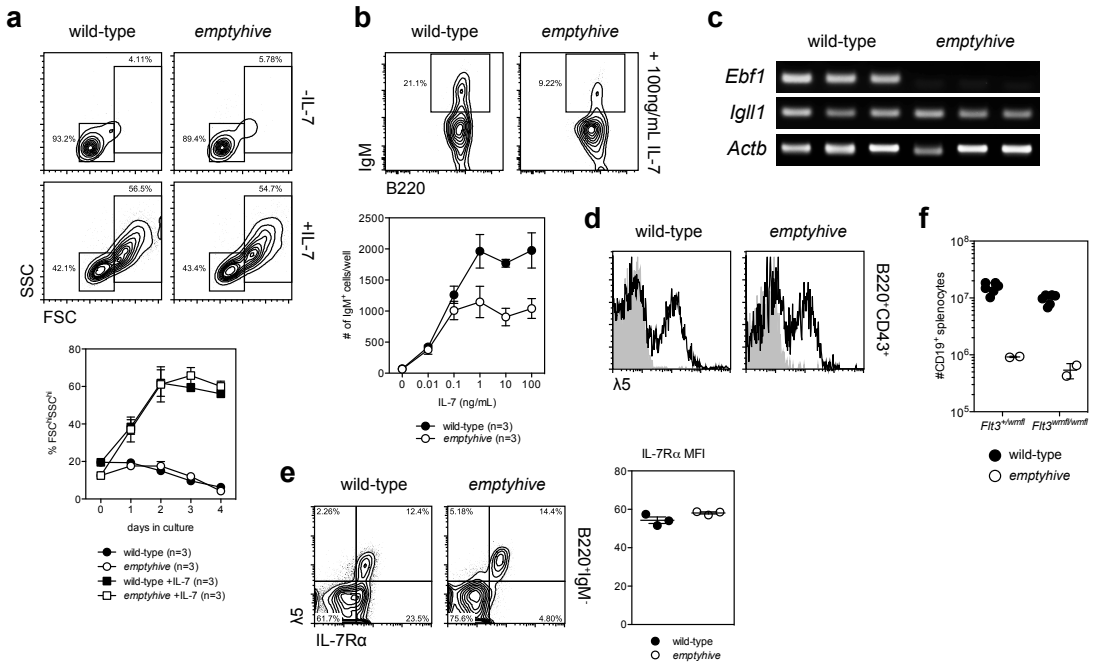


Figure 4.6 | Sensitivity to IL-7 and a failure to sustain expression of *Ebf1*.
(**a**) Frequency of 7-AAD$^-$ lymphoblasts (FSC^{hi}SSC^{hi}) among B220$^+$ surface IgM$^-$ bone marrow cells sorted by flow cytometry and cultured *ex vivo* in the presence or absence of IL-7 (100 ng/ml). FSC, forward scatter; SSC, side scatter. (**b**) Frequency (left) and number (right) of 7-AAD$^-$ surface IgM$^+$ cells among B220$^+$ surface IgM$^-$ bone marrow cells sorted from wild-type (CD45.1$^+$) mice or *emptyhive* (CD45.2$^+$) mice and cultured together for 4 d in the presence of various concentrations of IL-7. (**c**) RT-PCR analysis of cDNA from pre-pro-B cells (7-AAD$^-$B220$^+$IgM-IgD$^-$CD19$^-$ NK1.1$^-$Ly6C$^-$); each lane represents an individual mouse. (**d**) Expression of λ5 (CD179b; solid lines) on the surface of B220$^+$CD43$^+$ bone marrow lymphocytes; shaded histograms, rat IgG2a isotype-matched control antibody. (**e**) Expression of IL-7Rα (CD127) on the surface of B220$^+$IgM$^-$ bone marrow lymphocytes (left), or B220$^+$IgM$^-$λ5$^+$ cells (right; presented as mean fluorescence intensity (MFI)). (**f**) Splenic B cell numbers in emptyhive mice with an additional homozygous mutation of *Flt3* (*warmflash*, *wmfl*) . Numbers adjacent to outlined areas or in quadrants (**a**,**b**,**d**,**e**) indicate percent cells in each. Data are representative of two independent experiments, each with three mice per genotype (error bars, s.e.m.; mean ± s.e.m. of three mice per genotype in **a**,**b**).

4.6F). This result indicated that IL-7R signalling remained intact in *emptyhive* foetal liver progenitors, at least to a degree sufficient for foetal B lymphopoiesis in the absence of Flt3.

Programmed cell death was also not found to be a major cause of the *emptyhive* phenotype. Homozygosity for the Fas^{lpr} mutation (Watanabe-Fukunaga et al., 1992) or a null allele of the gene encoding the apoptosis facilitator Bim (Bouillet et al., 1999) did not correct the B cell deficiency in blood or bone marrow (**Figure 4.7A–C**), although the presence of B lineage–restricted *BCL2* transgene (Strasser et al., 1991) could partially restore B cell numbers (**Figure 4.7A–C**). Yet despite the increase in early B cell progenitor ($B220^+IgM^-IgD^-$) numbers in mutants expressing the *BCL2* transgene (**Figure 4.7B,C**), the number of mature B cells ($B220^+IgM^+IgD^+$) in the bone marrow of such mutants was as low as in the absence of the transgene (**Figure 4.7C**). In the spleen, the number of follicular and marginal zone B cells was greater (**Figure 4.7D**), probably because of a longer half-life (Strasser et al., 1991; Hao and Rajewsky, 2001), consistent with the greater frequency of recirculating B cells in the blood (**Figure 4.7A**).

4.2.5.Partial correction of B cell deficiency by a BCR transgene

Signalling through the pre-BCR is an essential step in the progression of B cell development, as it signals productive rearrangement at the immunoglobulin heavy-chain locus, triggers the proliferation and differentiation of pre-B cells, and initiates recombination of the κ-light-chain allele (Herzog et al., 2009). The presence of recombined heavy- and light-chain transgenes renders pre-BCR signalling redundant and effectively bypasses the developmental stages that surround it. The hen egg lysozyme (HEL)-specific MM4 transgene (Brink et al., 1992), for example, is expressed at the pre-pro-B cell stage, bypassing RAG-mediated recombination of endogenous heavy- and light-chain genes and diverting progenitors directly to the $mIgM^+$ stage (**Figure 4.8A**). Combining the *emptyhive* mutation with the MM4 transgene resulted in moderately greater $CD19^+$ cell frequencies in the blood (**Figure 4.8A**) as well as more IgM^+ cells in the bone marrow (**Figure 4.8B**).

As the MM4 transgene is a cointegration of heavy- and light-chain elements, this correction could have reflected the effect of either recombined chain or the effect of both in combination. These possibilities were directly tested using the 'switch-HEL' (SW_{HEL}) system (Phan et al., 2003), which consists of a HEL-specific *Igh* knock-in of the heavy-chain variable region 10 (V_H10) and the LC2 κ-light-chain transgene. Significant correction of the *emptyhive* B cell deficiency was achieved only in the presence of

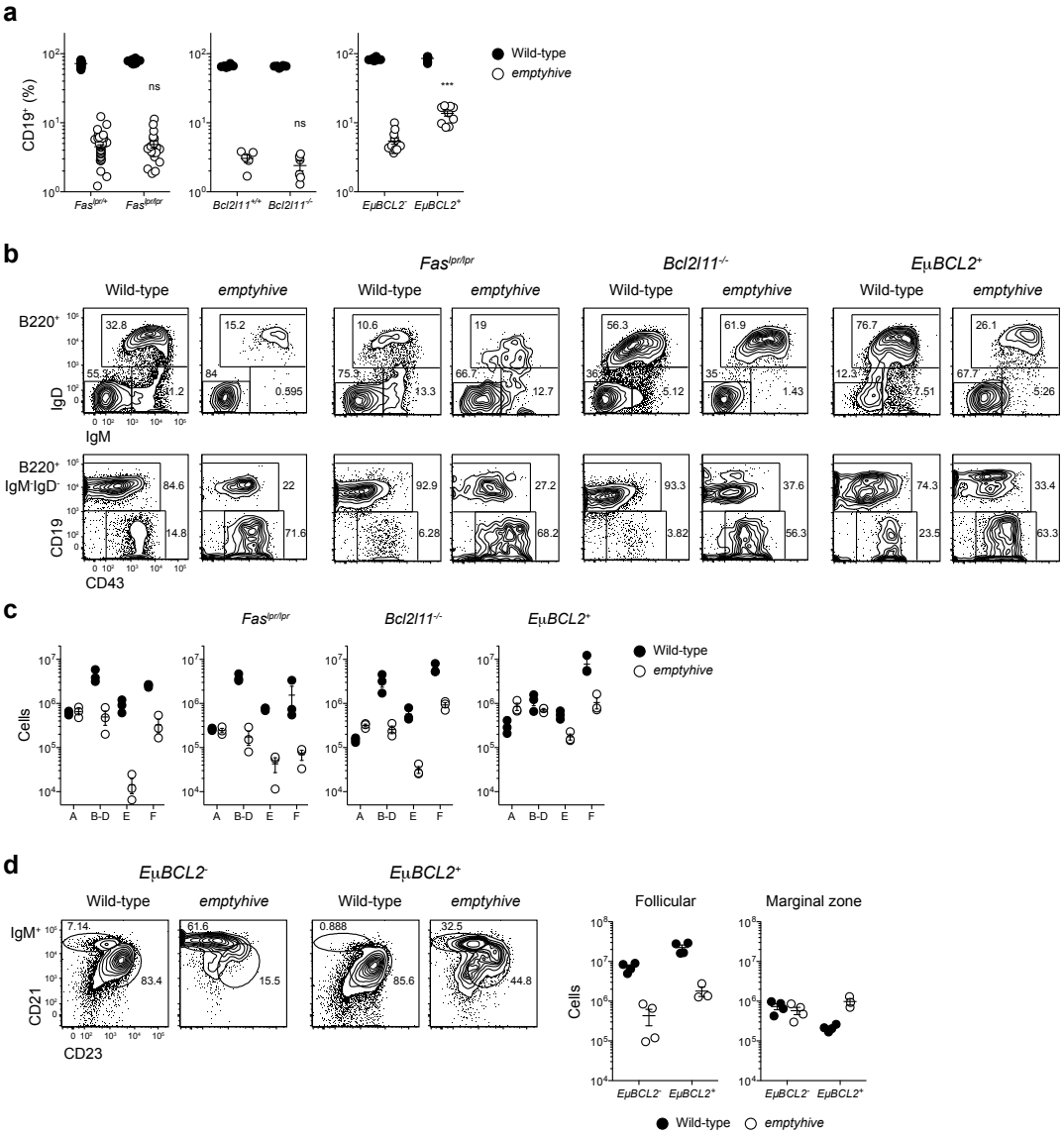


Figure 4.7 | A *Fas*- and *Bcl2l11*-independent phenotype that cannot be corrected by a *BCL2* transgene.

The *emptyhive* mutation was combined with *Fas*$^{lpr/lpr}$ or *Bcl2l11*$^{-/-}$ mutations, or with the *EμBCL2-22* transgene, and B cell frequencies were measured in the blood (**a**), bone marrow (**b**, with absolute numbers in **c**), or spleen (**d**). ***P > 0.001; ns, not significant (P > 0.05), as calculated by unpaired t-test comparing wild-type and *emptyhive* groups. Each symbol represents an individual mouse from one (**b**-**d**) or two (**a**) independent experiments.

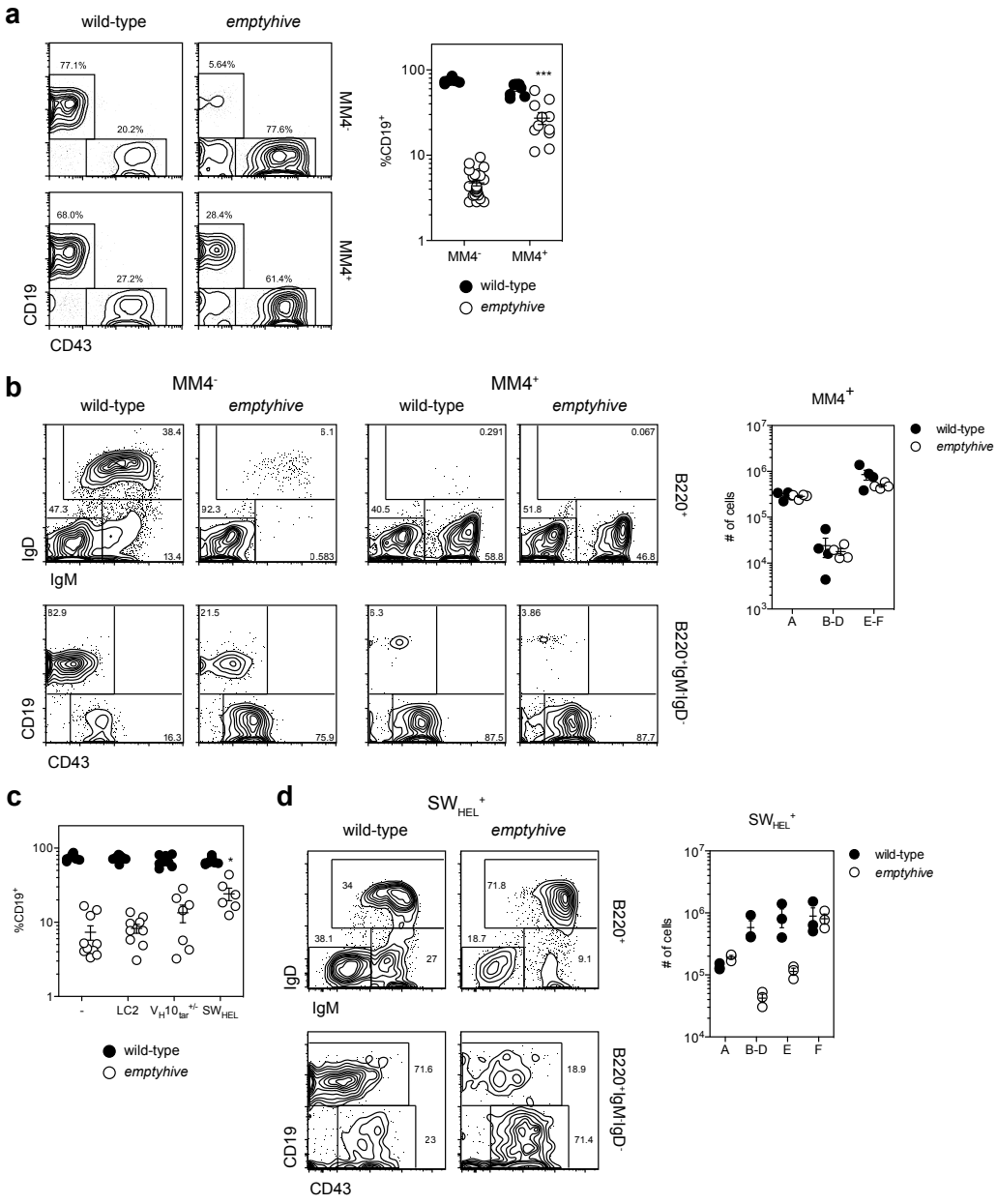


Figure 4.8 | Partial correction of the emptyhive phenotype by BCR transgenes. (**a**,**b**) Frequency of CD19$^+$ cells in the blood (**a**) and B cell subsets in the bone marrow (**b**) of mice with the *emptyhive* mutation combined with the MM4 transgene, assessed by flow cytometry. (**c**,**d**) Frequency of CD19$^+$ cells in the blood (**c**) and B cell subsets in the bone marrow (**d**) of mice with the *emptyhive* mutation combined with the LC2 light chain transgene or the knock-in allele of heavy-chain variable region 10 (V_H10) or both (SW_{HEL}), assessed by flow cytometry. Hardy fractions in (**b**) and (**d**) were gated as follows: A, B220$^+$IgM$^-$IgD$^-$CD19$^-$; B-D, B220$^+$IgM$^-$IgD$^-$CD19$^+$; E, B220$^+$IgM$^+$IgD$^-$; F, B220$^+$IgM$^+$IgD$^+$. Numbers adjacent to outlined areas indicate percent cells in each; each symbol represents an individual mouse. *P < 0.05 and **P < 0.001, versus nontransgenic emptyhive (unpaired t-test (**a**) or one-way analysis of variance followed by Bonferroni's post-test (**c**)). Data are representative of two independent experiments (error bars, s.e.m.).

both the heavy-chain knock-in allele and light-chain transgene (**Figure 4.8C,D**). This result was in contrast to mice with a mutated surrogate light-chain gene or recombinase-activating gene 1, whose respective B cell deficiencies can be fully or partially corrected by light- or heavy-chain transgenes alone (Spanopoulou et al., 1994; Pelanda et al., 1996), and showed that bypassing intermediate stages of B cell development (those in the $B220^{+}CD19^{+}IgM^{-}IgD^{-}$ subset) partially but not completely overcame the B cell deficiency in *emptyhive* mice. IL-7R and pre-BCR signalling are both important during these stages (Herzog et al., 2009), and this may therefore reflect a failure of one pathway or both pathways during the development of *emptyhive* precursor cells.

4.2.6.Mutation of Atp11c

To identify the mutation responsible for the *emptyhive* phenotype, male *emptyhive* mice were outcrossed to C3H/HeN females and then backcrossed to their F1 daughters. A total of 25 F2 males were genotyped (11 mutant and 14 wild-type) at 128 polymorphic microsatellite markers. Phenotypic linkage was detected on the X chromosome (maximum logarithm of odds score of 8.37 at DXMit68; **Figure 4.9A**), and fine mapping with a further 105 meioses confined the mutation to a 13.51-megabase interval between DXMit68 and DXMit74 (**Figure 4.9B**). After sequencing the coding exons and flanking splice junctions of the 81 annotated protein-encoding genes in the interval by capillary sequencing (85.6% high-quality coverage [*phred* score > 30] of all nucleotides (129,589 of 151,336), a single hemizygous transition mutation was identified in *Atp11c* (cytosine to thymine at position 2113, resulting in substitution of the glutamine codon CAG with the stop codon TAG at position 655 of the encoded protein; **Figure 4.9C**). As this mutation (in exon 19 of 30) occurs before the penultimate exon, the mutant transcript is most likely targeted by the nonsense-mediated decay pathway shortly after transcription (Chang et al., 2007), although this has yet to be confirmed. In addition, an independent mutant pedigree was identified ('*spelling*') that was a phenocopy of *emptyhive*. After sequencing *Atp11c* in these mice a second *Atp11c* mutant allele was identified (thymine to adenine at position 1214, resulting in the substitution of ATA with AAA and the amino acid replacement of isoleucine at position 355 with lysine) that introduced a charged residue into the fourth of ten membrane-spanning domains (**Figure 4.9C** and **Figure 4.10**). Compound heterozygosity for both alleles caused a B cell deficiency as severe as that of either parental strain (**Figure 4.9D,E**), which indicated that both the *emptyhive* and *spelling* phenotypes were caused by recessive loss of function alleles of *Atp11c* (**Figure 4.9F**).

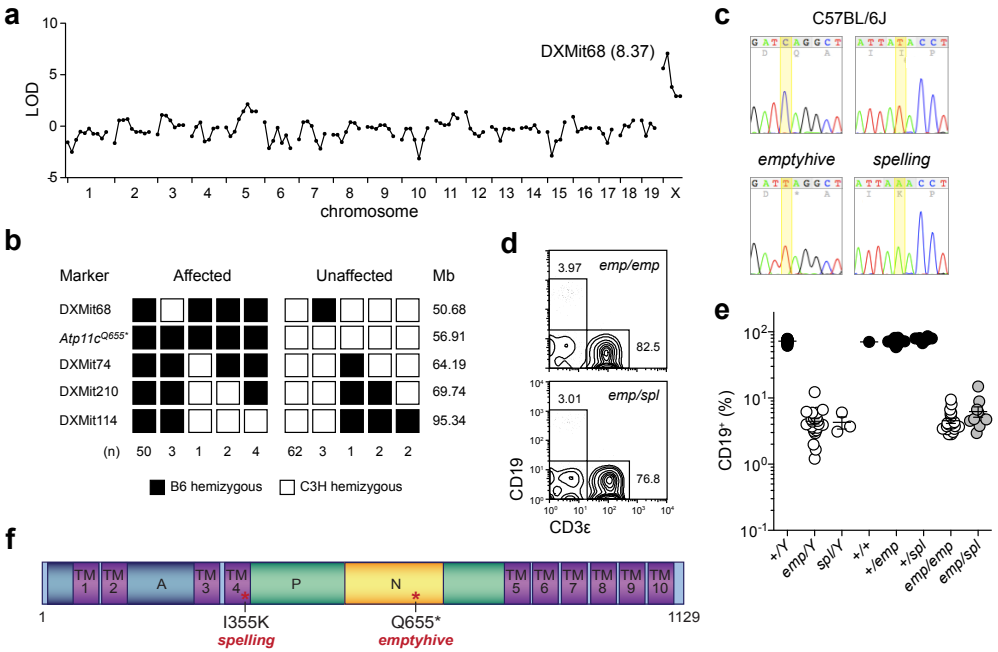


Figure 4.9 | The *emptyhive* phenotype is caused by a recessive mutation of *Atp11c*.

(**a**,**b**) Chromosomal mapping (**a**) and fine mapping (**b**) of the *emptyhive* phenotype. LOD, logarithm of odds score; Mb, megabases. (**c**) DNA sequence chromatograms of the mutated nucleotides in *Atp11c* (cytosine to thymine at position 2113, resulting in the substitution of a stop codon (*) for glutamine at position 655; and thymine to adenine at position 1214, resulting in the substitution of lysine for isoleucine at position 355) as detected in emptyhive and spelling males. (**d**,**e**) Analysis of phenotypic complementation in the progeny of a mating between a *spelling* hemizygous male (*Atp11c*$^{spl/Y}$) and a heterozygous *emptyhive* female (*Atp11c*$^{+/emp}$) (to assess allelism of *spelling* and *emptyhive* alleles), by measurement of the frequency of B cells in blood. Each symbol represents an individual mouse. (**f**) Predicted ATP11C protein domain structure: TM, transmembrane domain; P, phosphorylation domain; A, actuator domain; N, nucleotide binding domain. Data are representative of one (**a–c**), or two (**d**,**e**) experiments (error bars (**e**), s.e.m.).

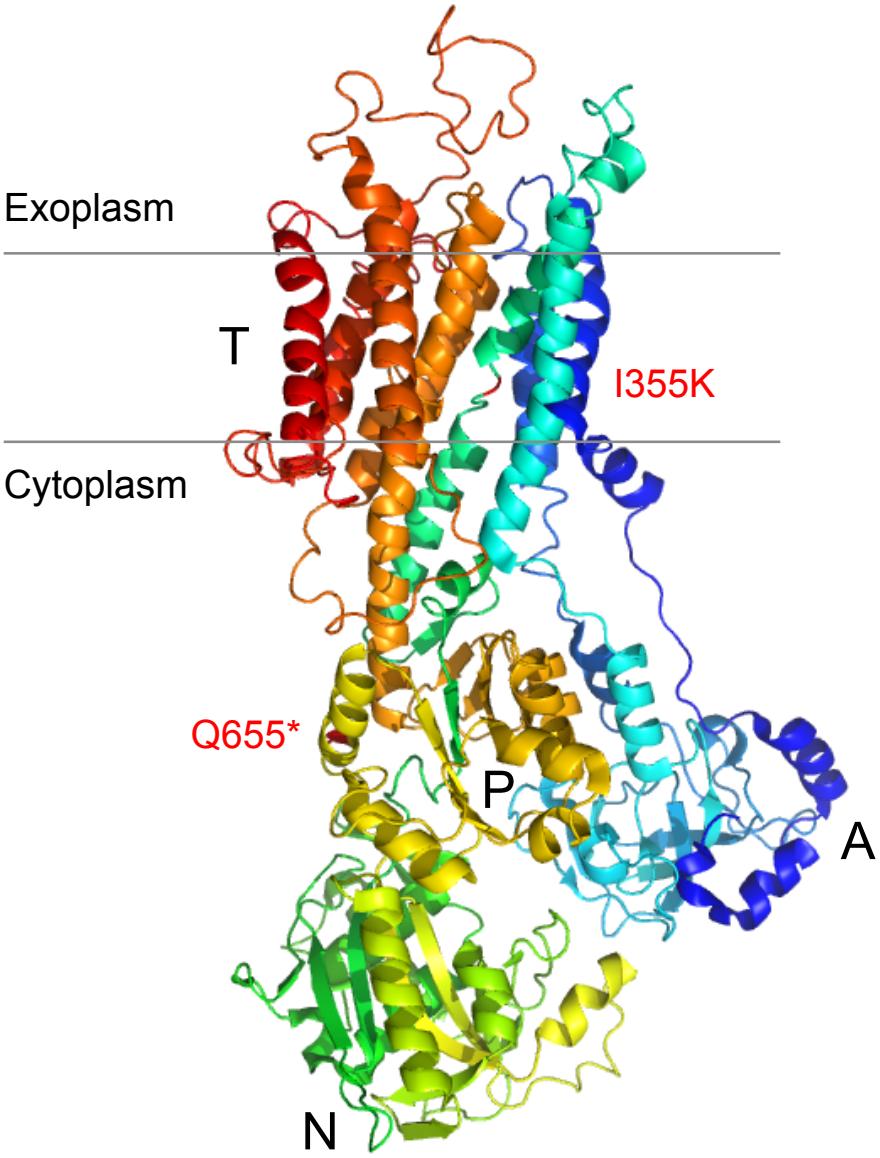


Figure 4.10 | Structural representation of *Atp11c*^{emptyhive} and *Atp11c*^{spelling} mutations.
X-ray crystal structure of the Ca^{2+} ATPase SERCA1 (ref. [1]) (PDB: 2EAR, model generated using MacPyMOL) showing residues corresponding to those mutated in *emptyhive* (Q655) and *spelling* (I355) pedigrees in red. T, transmembrane domain; P, phosphorylation domain; A, actuator domain; N, nucleotide binding domain.

Atp11c is a previously uncharacterized gene encoding a P4-type ATPase expressed most prominently in the liver but also by many other cell types (Su et al., 2004)(**Figure 4.11**). Little is known about mammalian P4-type ATPases in general, although mutation of the gene encoding one of these (ATP8B1) can cause progressive intrahepatic cholestasis in man (Bull et al., 1998). Although P-type ATPases are typically involved in cation transport (Kühlbrandt, 2004), the P4 subtype includes translocases that move aminophospholipids in an inward direction (flippases), enriching them at the cytoplasmic leaflet of lipid bilayers (Tang et al., 1996; Holthuis and Levine, 2005). Because P4-type ATPases have been linked to the asymmetry of phosphatidylserine (PS) in yeast (Tang et al., 1996), it was hypothesized that higher surface exposure of PS and consequent PS-mediated phagocytosis could account for the lower number of B cells in mice with mutated *Atp11c* (Leventis and Grinstein, 2010). PS expression was examined on λ5-expressing cells with annexin V, yet surface expression of PS was no different on *emptyhive* cells than on wild-type cells (**Figure 4.12**). Another requirement for phospholipid asymmetry could conceivably occur at the level of lipid rafts, which are membrane domains specialized in signal transduction (Dykstra et al., 2003) and are potentially important for signalling through the IL-7R or pre-BCR (Guo et al., 2000). Total surface expression of the raft-associated ganglioside GM1 (a target of the B subunit of cholera toxin) did not differ in wild-type versus mutant cells (**Figure 4.12**), although closer examination of membrane microdomains around IL-7R or the pre-BCR will be needed to assess assembly of the rafts themselves.

Although it is not an aminophospholipid, phosphatidylinositol-(3,4,5)-trisphosphate (PtdIns(3,4,5)P_3) is a phospholipid vital for signalling initiated at the IL-7R and pre-BCR (Fruman and Cantley, 2002). Mutation of the gene encoding CD19 (*Cd19*) or the catalytic p110δ subunit of phosphatidylinositol-3-OH kinase (*Pik3cd*) cripples the function of phosphatidylinositol-3-OH kinase and the generation of PtdIns(3,4,5)P_3 at the cytoplasmic leaflet of the pre-BCR signalosome, resulting in impaired development of marginal zone and B-1 B cells (Anzelon et al., 2003; Janas et al., 2008). Conversely, in the absence of the PtdIns(3,4,5)P_3 phosphatase PTEN, an excess of PtdIns(3,4,5)P_3 leads to expansion of marginal zone and B-1 subsets (Anzelon et al., 2003). As mutations of genes encoding both positive regulators (*Pik3cd*, *Pik3r1*, *Btk*, *Pik3ap1*, *Plcg2* and *Blnk*) and negative regulators (*Pten* and *Ptpn6*) of the availability of PtdIns(3,4,5)P_3 are known to affect B cell development (Miosge and Goodnow, 2005), and as phosphatidylinositol asymmetry may be disrupted in *emptyhive* progenitors, the *emptyhive*

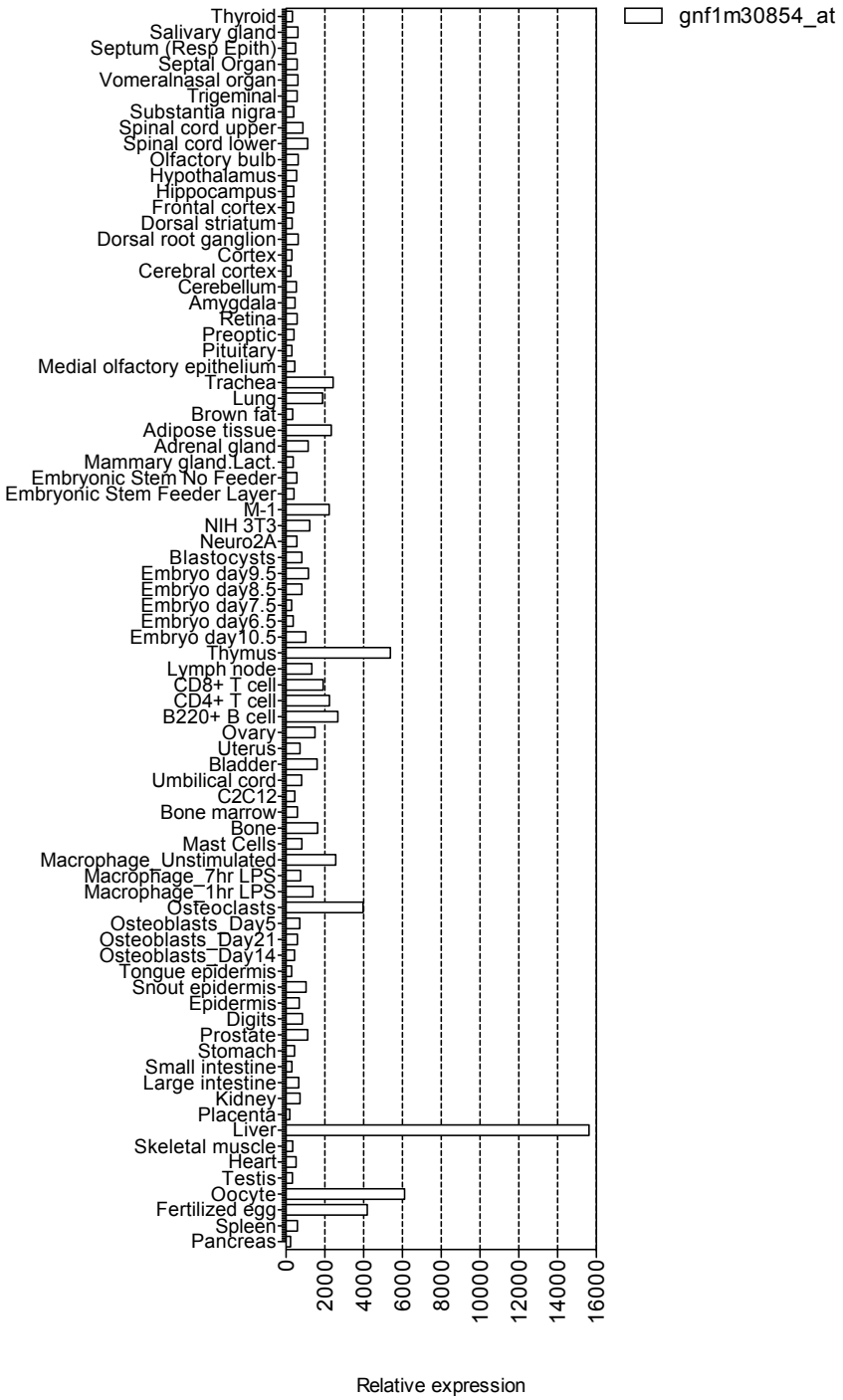


Figure 4.11 | Relative expression of the *Atp11c* transcript in multiple tissues in mouse.
Atp11c transcript data (gnf1m30854_at probeset, from mouse MOE430 Gene Atlas, GEO code GSE10246) (Lattin et al., 2008).

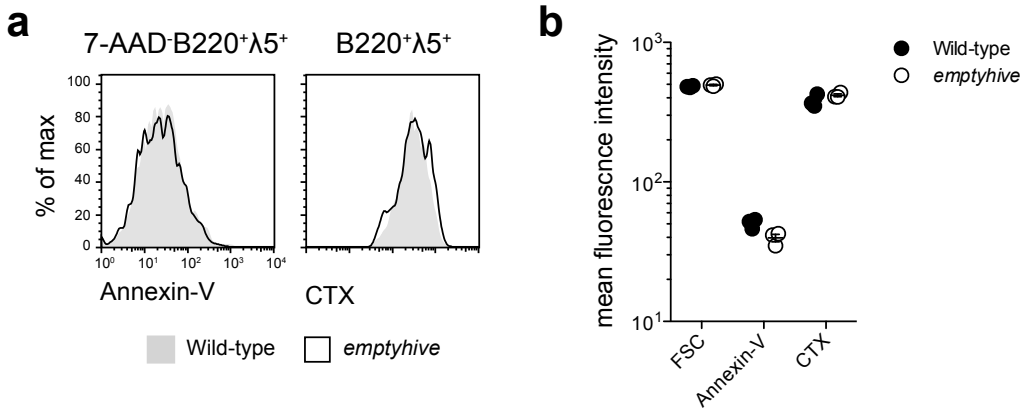


Figure 4.12 | Surface expression of phosphatidylserine and G_{M1} ganglioside. (**a**) Histograms of Annexin-V and cholera toxin (CTX) staining on the surface of 7-AAD$^-$B220$^+$λ5$^+$ (Annexin-V) and B220$^+$λ5$^+$ (CTX) bone marrow lymphocytes from wild-type (shaded, gray) or mutant (open, black) mice. (**b**) Mean fluorescence intensity values for forward scatter (FSC), Annexin-V and CTX. Data are representative of two experiments, each including three mice per genotype. Each symbol represents an individual mouse.

mutation was combined with mutant alleles of *Cd19*, *Ptprc*, *Inpp5d* (which encodes the tyrosine phosphatase SHIP-1) or *Ptpn6*. Neither genetic enhancement (mutation of *Inpp5d* or *Ptpn6*) nor genetic diminishment (mutation of *Cd19* or *Cd45*) of PtdIns(3,4,5)P_3 availability altered the *emptyhive* phenotype (**Figure 4.13**), which indicated that disruption of phosphatidylinositol asymmetry at the cytoplasmic leaflet of the pre-BCR was an unlikely cause of the B cell deficiency in mice with mutation of *Atp11c*.

4.2.7.A context-sensitive requirement for ATP11C

Having identified the causative mutation of the *emptyhive* phenotype, it was possible to directly compare foetal B lymphopoiesis *in utero* between wild-type mice and their mutant siblings. As IgM^+ cells only appear around embryonic day 16 (Raff et al., 1976) foetal liver cells were examined at embryonic day 18.5. No difference was observed in the number or frequency of $B220^+IgM^-$ or $B220^+IgM^+$ cells in *emptyhive* embryos relative to wild-type embryos (**Figure 4.14**). This finding provided further evidence that foetal B cell development was intact in *emptyhive* mice and that the residual B cells in mutant mice were of pre-adult origin. Despite this result, mutant foetal liver cells were unable to reconstitute any B cell lineage in irradiated adult recipients (**Figure 4.5C**), which indicated that the B cell deficiency was cell autonomous yet microenvironment dependent.

4.2.8.Discussion

These results define a key role for ATP11C in adult B cell development but not foetal B cell development. The marginal zone and B-1 B cell compartments were both relatively intact in mutant mice, whereas follicular B cell numbers decreased with age, closely resembling that seen after postnatal deletion of *Rag2* (Hao and Rajewsky, 2001). Most notably, B cell progenitors with mutated *Atp11c* developed normally in foetal liver but not in adult bone marrow, which indicated a cell-intrinsic but context-dependent requirement for ATP11C.

Few molecules have been reported to act in such a way (Hardy and Hayakawa, 2001), with IL-7 and IL-7R being the prototypical exceptions. IL-7, IL-7R and ATP11C are all essential for adult B cell development but not foetal B cell development, with a cell-intrinsic requirement for both IL-7R and ATP11C in sustaining *Ebf1* transcription in pre-pro-B cells ($B220^+CD43^+BP\text{-}1^-CD24^-$) and promoting their differentiation to the pro-B cell stage ($B220^+CD43^+BP\text{-}1^-CD24^+$) (Kikuchi et al., 2005). But there are many key distinctions, the most notable being that T cell development proceeds in mice with mutant ATP11C

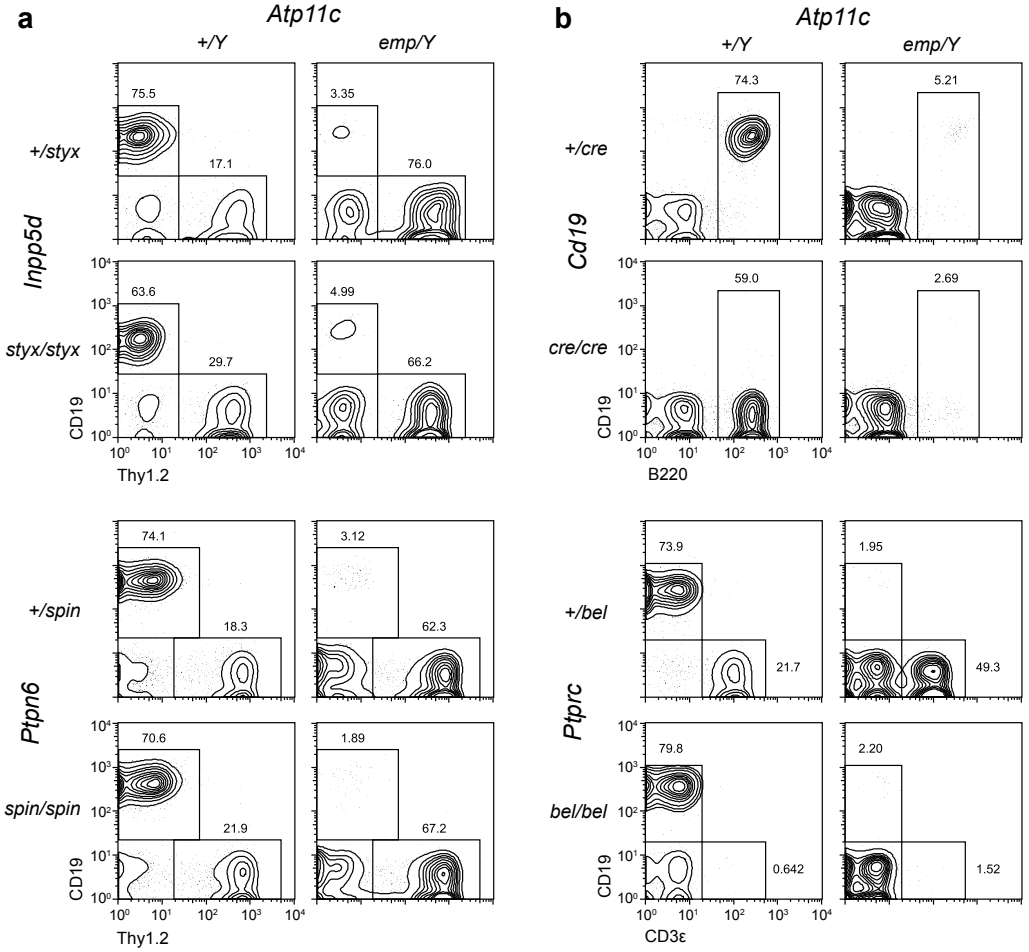


Figure 4.13 | Genetic modulation of PtdIns(3,4,5)P_3 availability does not affect B cell deficiency.
Mutations known to either increase (**a**) (*Inpp5d*^{styx}, *Ptpn6*^{spin}) or decrease (**b**) (*Cd19*^{cre}, *Ptprc*^{belittle}) PtdIns(3,4,5)P_3 signaling were combined with the *emptyhive* mutation, and B cell frequencies were measured in the blood of double mutant mice. Plots are representative of 1-3 mice per genotype from a single experiment.

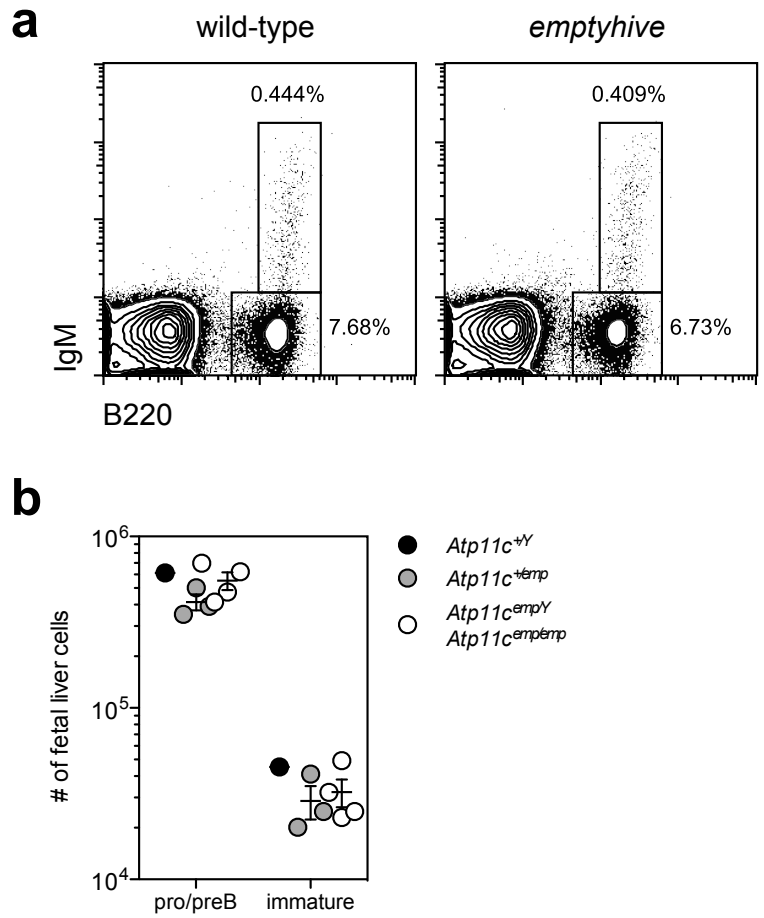


Figure 4.14 | Intact B lymphopoiesis in fetal liver.
Percentage (**a**) and absolute number (**b**) of B cells of fractions A–D ($B220^{+}IgM^{-}$) and immature B cells ($B220^{+}IgM^{+}$; fraction E) in the fetal livers of embryonic siblings from a mating between a hemizygous mutant male (*Atp11c*$^{emp/Y}$) and a heterozygous mutant female (*Atp11c*$^{+/emp}$), assessed at embryonic day 18.5. Numbers adjacent to outlined areas (**a**) indicate percent cells in each; each symbol (**b**) represents an individual embryo. Data are representative of two experiments with eight to fourteen embryos per experiment (error bars, s.e.m.).

but not in the absence of IL-7 or IL-7Rα (Grabstein et al., 1993; Peschon et al., 1994; Freeden-Jeffry et al., 1995). Even among B cell progenitors, *Igll1* transcription and λ5 expression are intact in mice with mutant ATP11C but not those with mutant IL-7R (Kikuchi et al., 2005). *Ebf1*$^{-/-}$ mice show a similar arrest in B cell development, yet they too fail to transcribe *Igll1*, and as these mice lack all peripheral IgM^{+} cells, it does not seem to be an adult-restricted defect (Lin and Grosschedl, 1995). Progenitor cells with mutant ATP11C can proliferate and differentiate *ex vivo* in the presence of IL-7, as well as during foetal development in the absence of Flt3 signalling (Sitnicka et al., 2003; Vosshenrich et al., 2003), and unlike foetal liver cells with mutant IL-7R (which can give rise to mature B cells in the bone marrow of irradiated adults (Kikuchi and Kondo, 2006)), their developmental potential is determined by their environment rather than their source.

Although ATP11C is clearly not essential for all IL-7-dependent phenotypes, it may still be quantitatively or qualitatively important, affecting only a given threshold or branch of IL-7R signalling or the migration of B cell progenitors to a stromal depot of IL-7. Another interpretation is that ATP11C has only a transiently important role in early B cell development. Temporal restriction of IL-7R expression seems to be critical, as retroviral overexpression arrests B cell development at the pre-pro-B cell stage and inhibits *Ebf1* expression (Purohit et al., 2003), which indicates that transient downregulation of IL-7R is important for the progression of B cell development.

IL-7 is also necessary for sustaining expression of *Ebf1* and the progression of B cell development beyond the pre-pro-B cell stage, but not because of IL-7R signalling in pre-pro-B cells themselves. Instead, signalling during the transition from common lymphoid precursor to pre-pro-B cell induces high and persistent expression of *Ebf1*, presumably via a series of feedback loops at the *Ebf1* promoter (Roessler et al., 2007), and allows maturation of pre-pro-B cells even in the absence of IL-7 (Dias et al., 2005; Kikuchi et al., 2005; 2008). Even though *Ebf1* seemed not to be expressed in ATP11C-mutant precursors, the EBF target gene *Igll1* was, which suggests that ATP11C may be important not for the initial induction of *Ebf1* but instead for sustaining *Ebf1* expression through a feedback loop (Roessler et al., 2007). Whatever the cause, a failure to sustain *Ebf1* expression has broad consequences for the regulation of early B cell development (Busslinger, 2004).

Beyond the transcriptional consequences, what is the substrate of ATP11C, and how might it affect IL-7 responsiveness and sustained expression of *Ebf1*? The aminophospholipids

phosphatidylserine and phosphatidylethanolamine are chief candidate substrates, on the basis of the study of ATP11C orthologs in yeast (Tang et al., 1996; Holthuis and Levine, 2005), and lipid-reconstitution experiments will be useful in determining which specific variants are trafficked by ATP11C and in which membrane compartments and/or domains they are trafficked. In an independent study, fluorescently-labelled phosphatidylserine was internalised less efficiently in *Atp11c* mutant B cell progenitors (Yabas et al., 2011), but whether this is the critical substrate remains to be seen. Further work should define if and how this translates into aberrant sensitivity to IL-7 and particularly why it does so only in the context of B cell development in the adult bone marrow. Identification of the substrate and affected pathway should determine a vital target for the specific regulation of adult B cell development, whereas ATP11C-mutant strains will provide key experimental models for the study of membrane asymmetry and the origins of B cell immunity and malignancy.

4.3. ZBTB1 is a determinant of lymphoid development

The work presented in section 4.3 is a reproduction of previously published work (Siggs et al., 2012a). The full publication is provided in Appendix 7.3.

4.3.1. Lymphocyte development

Lymphocytes arise from multipotent progenitors in the bone marrow (Kondo et al., 1997), deviating from the myeloid lineage and completing their differentiation under the influence of a suite of transcriptional regulators (Busslinger, 2004; Rothenberg and Taghon, 2005), including Ikaros, Pax5, and Notch1 (Radtke et al., 1999). The transcriptional regulators that guide this process are of special interest because many are also involved in lymphoid tumorigenesis (Weng et al., 2004; Mullighan et al., 2007; 2008), whereas others can be manipulated for directed reprogramming of cell fate (Cobaleda et al., 2007).

Among all known transcriptional regulators of lymphopoiesis, the BTB-ZF (Broad complex, Tramtrack, and Bric à brac–zinc finger) family of proteins is well represented. These proteins influence lymphoid development from the common lymphoid progenitor (CLP) stage (Kosan et al., 2010), to the T versus B fate decision (Maeda et al., 2007), to $CD4^+$ versus $CD8^+$ T cell selection (He et al., 2005), and even as late as the differentiation of Tfh (Johnston et al., 2009; Nurieva et al., 2009; Yu et al., 2009) and NKT (Kovalovsky et al., 2008; Savage et al., 2008) effector lineages.

In this study, mouse chemical mutagenesis has been used to reveal the physiological function of the BTB-ZF protein ZBTB1 (zinc finger and BTB domain containing 1). ZBTB1 was essential for T cell development and also for the development of B and NK cells under competitive conditions.

4.3.2. Severe T cell lymphopenia

While surveying the descendants of chemically mutagenized mice for lymphocyte deficiencies, a single male mouse devoid of T cells was identified. This phenotype, nicknamed *scanT* because of the low (or scant) frequency of T cells, was transmitted as a recessive trait (**Figure 4.15A,B**). *scanT* mutant mice were born at the expected Mendelian ratio, were typically fertile, and were outwardly normal in behaviour. *scanT* thymi were severely hypoplastic (**Figure 4.15C**), containing around 2% of the number of wild-type cells, and lacked cortico-medullary definition (**Figure 4.15D**). Thymocyte development was impaired from the early thymic precursor (ETP) stage and beyond (**Figure 4.15E,F**). Of the lymphocytes that were

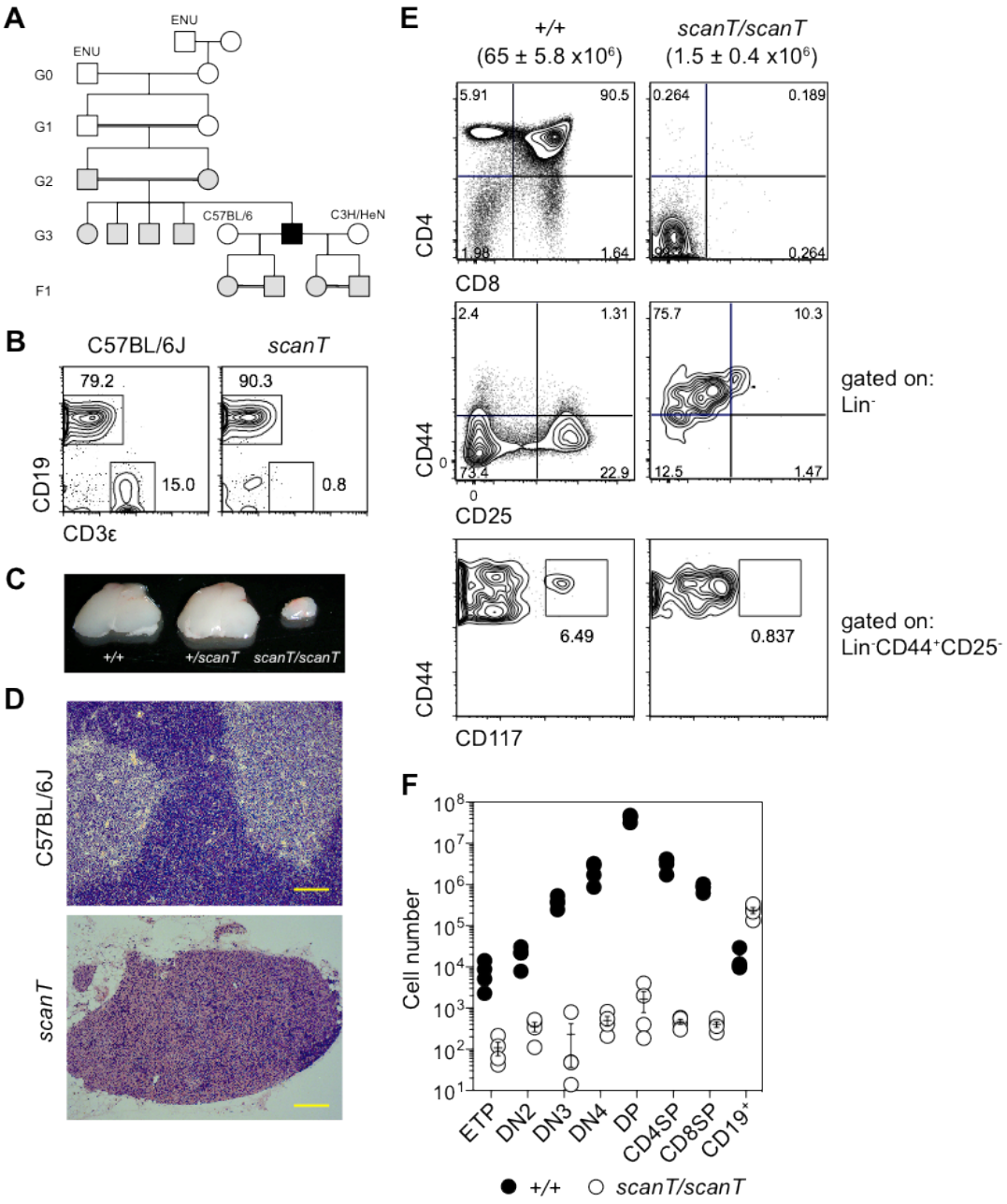


Figure 4.15 | T cell aplasia in *scanT* mice.
(A) Initial generations of the *scanT* pedigree. Black filling, T-deficient phenotype; grey filling, wild-type phenotype; no filling, not tested. ENU, *N*-ethyl-*N*-nitrosourea. (B) Percentages of B ($CD19^+$) and T ($CD3\varepsilon^+$) cells in the peripheral blood of 8 week-old mice as measured by flow cytometry. Relative size (C), histological appearance (H&E, scale bars represent 100μm) (D), and cellular composition (E-F) of the thymus of wild-type and mutant siblings at 8 weeks of age. Lineage markers in (E)-(F) were CD11b, CD3ε, B220, Ter119, Ly6G, NK1.1 and CD8α. Subsets in (F) were gated as follows: ETP ($Lin^-CD44^+CD25^-CD117^+$), DN2 ($Lin^-CD44^+CD25^+$), DN3 ($Lin^-CD44^-CD25^+$), DN4 ($Lin^-CD44^-CD25^-$), DP ($CD4^+CD8\alpha^+$), CD4SP ($CD4^+CD8\alpha^-$), CD8SP ($CD4^-CD8\alpha^+$). Data are representative of one (A, D), two to three (E-F), or more than three (B, C) independent experiments. Error bars represent standard error, and symbols (in F) represent individual mice. Numbers in parentheses in (E) represent mean thymic cellularity and standard error.

present in the thymus, almost all were B cells, representing a 20-fold increase over wild-type numbers (**Figure 4.15F**).

4.3.3.Mutation of a previously uncharacterized zinc finger protein

The *scanT* genetic lesion was mapped first by genome-wide linkage to chromosome 12 (**Figure 4.16A**) and then by fine mapping to a 5 Mb interval between markers D12Mit33 and D12Mit4 (**Figure 4.16B**). Because none of the 35 annotated protein-encoding genes in the interval had previously been implicated in T cell development, the coding exons and flanking splice junctions of three were sequenced (*Zbtb1*, *Zbtb25*, and *Ppp2r5e*) based on their predominant expression in lymphocytes (http://biogps.gnf.org/). 93.4% of all target nucleotides (6,081/6,511) were covered on both strands of wild-type and *scanT* samples with a *phred* quality score of >30, and a single missense transition was identified in *Zbtb1* (C74R; **Figure 4.16C**). PolyPhen-2 (Adzhubei et al., 2010) assigned a score of 0.954 to this mutation, predicting a deleterious effect with 93% confidence. 43.2% of the total coding critical region (59,447/137,702 nt) was also covered at least three times by SOLiD 3 sequencing, with no additional mutations found.

Zbtb1 encodes a 713 amino acid member of the POK (POZ [Poxviruses and zinc finger] and Krüppel) or BTB-ZF family of transcriptional regulators, and had no previously described function. Mouse ZBTB1 is 94% identical to its counterpart in man. Two characteristic domains are shared by BTB-ZF family members: an N-terminal BTB/POZ domain and a series of C-terminal C_2H_2 Krüppel-type zinc finger motifs. ZBTB1 itself contains an N-terminal BTB domain, eight zinc finger motifs, and two nuclear localization sequences (Matic et al., 2010). The residue mutated in the *scanT* pedigree (C74) is predicted to lie within the A3 helix of the BTB domain (**Figure 4.16D** and **Figure 4.17**; (Stogios et al., 2005)) and is highly conserved across the vertebrate lineage (**Figure 4.16E**). Two unique transcripts are predicted to arise from the *Zbtb1*/*ZBTB1* locus, both of which harbour the *scanT* mutation, yet only one of which (Ensembl release 65 accession no. ENST00000394712) is predominantly expressed in T cells and other leukocytes in mouse and man (**Figure 4.18**). The other (Ensembl release 65 accession no. ENST00000358738) is known to be transcribed in HeLa cells by the nonconventional single-polypeptide nuclear RNA polymerase IV (Kravchenko et al., 2005).

To confirm that the mutation in *Zbtb1* was responsible for the *scanT* phenotype, wild-type *Zbtb1* was retrovirally transduced into *scanT* haematopoietic progenitors (**Figure 4.16F**). GFP^+ T cells were

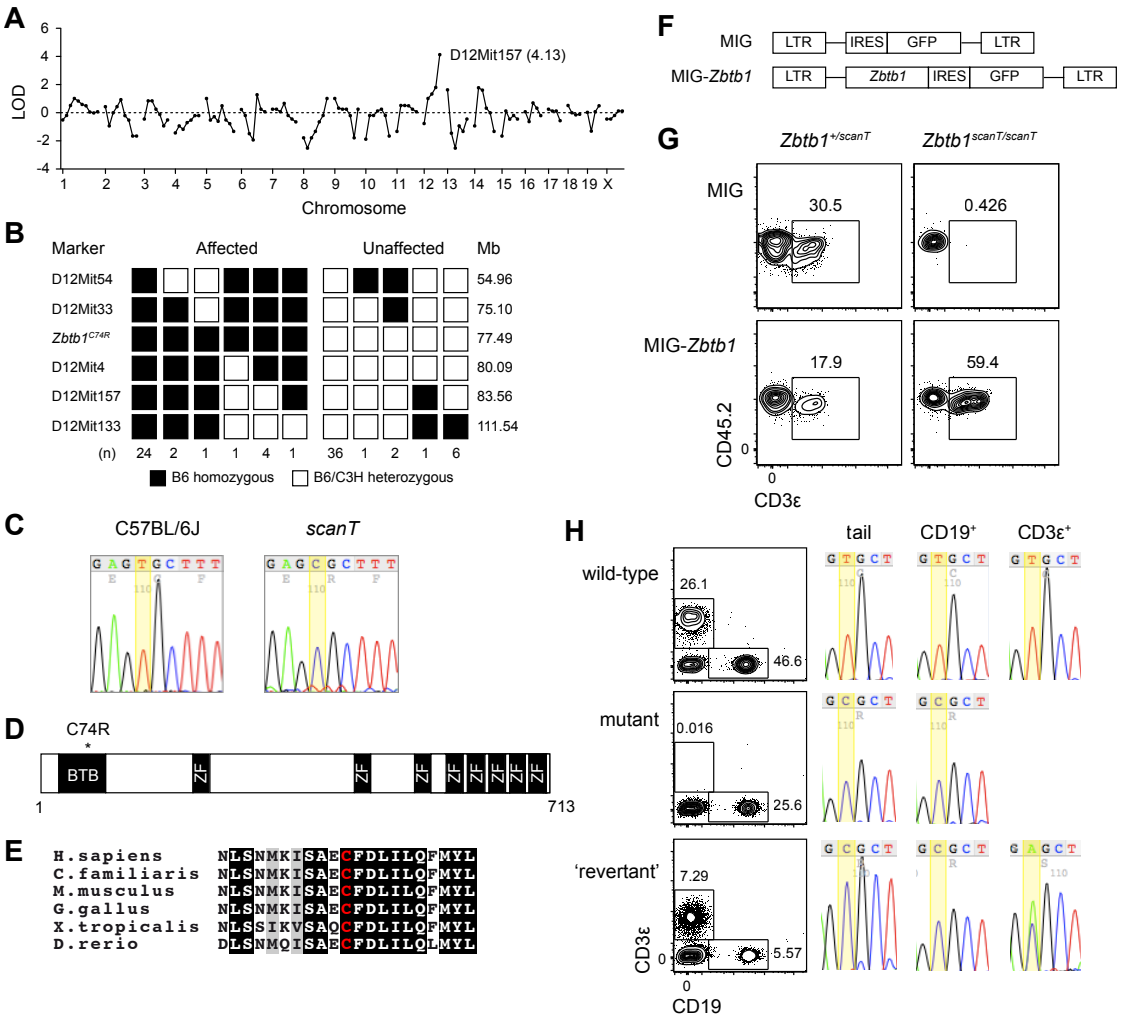


Figure 4.16 | Identification of a missense mutation in *Zbtb1*.
Chromosomal mapping (A) and fine mapping (B) of the *scanT* phenotype. LOD, logarithm of odds score. (C) DNA sequence chromatograms of the mutated nucleotide in *Zbtb1* (thymine to cytosine), resulting in the substitution of arginine for cysteine at codon 74. (D) Predicted ZBTB1 protein domain structure: BTB, Broad complex/Tramtrack and Bric à brac domain; ZF, C_2H_2 Krüppel-type zinc finger motif. (E) Conservation of ZBTB1 sequence across multiple vertebrates, with the amino acid corresponding to ZBTB1^{C74} highlighted in red. ZBTB1 orthologs were not found in non-vertebrate proteomes. (F) Schematic of the MIG-*Zbtb1* and control retroviral constructs: MIG, MSCV-IRES-GFP; LTR, long terminal repeat. (G) Bone marrow cells from *scanT* mice or heterozygous controls (CD45.2$^+$) were transduced with a retroviral construct expressing *Zbtb1* and transferred into irradiated CD45.1$^+$ recipients (~2x10^6 cells/mouse). Transduced CD3ε$^+$ cells were identified in blood 4 months after transfer by coexpression of GFP. (H) Phenotypic reversion associated with somatic mutation of *Zbtb1*. DNA was prepared from tail clippings and flow-sorted CD19$^+$ and CD3ε$^+$ lymph node cells, and sequenced at the locus mutated in the *scanT* pedigree. Contour plots were obtained from blood. Data in (G) are representative of three independent experiments.

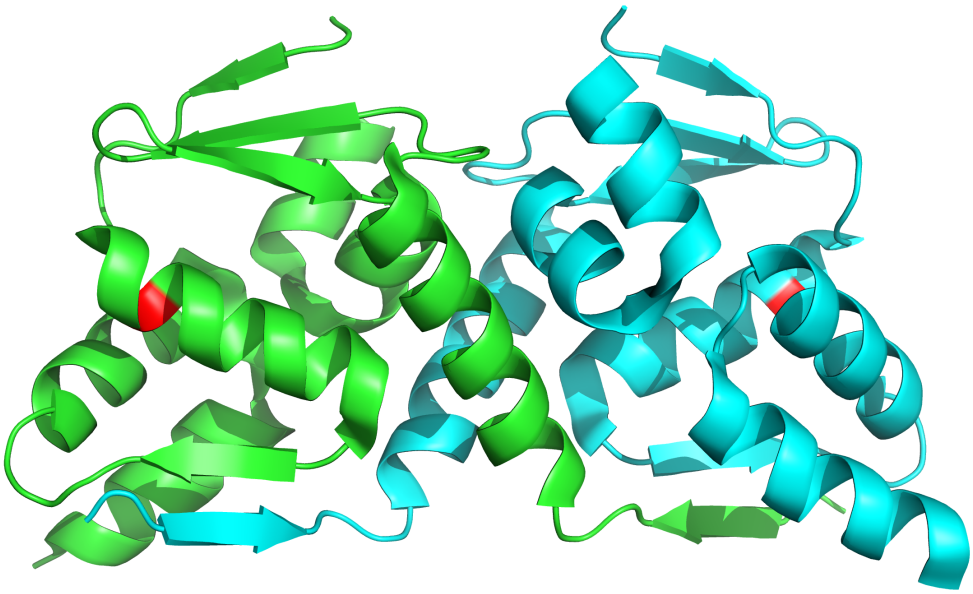


Figure 4.17 | BTB domain alignment w/ structural features.
Crystal structure representations of BCL6 BTB domain dimer (green & blue)(PDB: 1R29). The amino acid corresponding to cysteine 74 of ZBTB1 (mutated in *scanT*) is indicated in red.

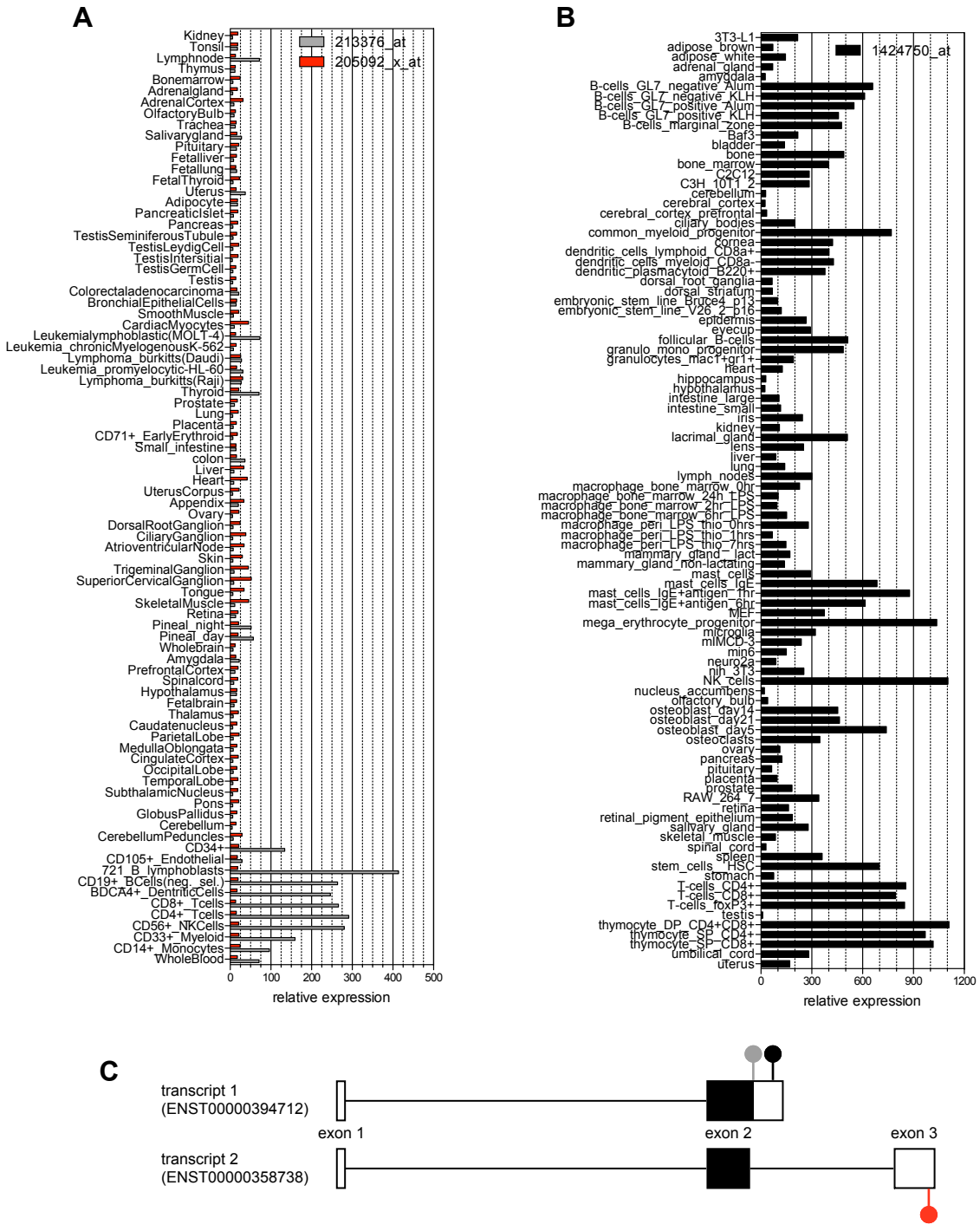


Figure 4.18 | Enrichment of *Zbtb1* expression in leukocyte lineages of mouse and man.

(A) Expression of *ZBTB1* transcripts in human cells and tissues (Human U133A/ GNF1H Gene Atlas, GEO code GSE1133) (Su et al., 2004). (B) Expression of mouse *Zbtb1* (Mouse MOE430 Gene Atlas, GEO code GSE10246) (Lattin et al., 2008). (C) Relative locations of mouse and human Affymetrix probesets (color-coded with (A) and (B)) in *Zbtb1*/*ZBTB1* transcripts. Ensembl accession numbers correspond to human transcripts.

recovered from recipients of *Zbtb1*-transduced *scanT* progenitors (**Figure 4.16G**), presumably as a consequence of restored thymic development. These data indicated that the mutation in *Zbtb1* could account for T cell deficiency in *scanT* mice.

In a minority of cases (3/16 in a 3-mo-old cohort), T cells were detected at diminished frequencies in the blood of $Zbtb1^{scanT}$ homozygotes. It was hypothesized that these cells arose from a somatic mutation that suppressed the *scanT* phenotype, considering the strong selective advantage that such a mutation would confer and given that a similar phenomenon is known to occur in human T cell–deficient SCID (Hirschhorn et al., 1996). To test for somatic suppressor mutations, DNA was isolated from sorted T and B cells. Sequencing of the mutated *Zbtb1* locus revealed a heterozygous mutation within the T cell compartment of one phenotypic revertant (but not the other two; **Figure 4.16H**), indicating that most, if not all, T cells in this mouse were clonally derived. This mutation either occurred after the CLP stage or did not confer a selective advantage in the B cell lineage because it was not observed in DNA from $CD19^{+}$ cells (**Figure 4.16H**). The mutation in question occurred at the same nucleotide as the *scanT* mutation (the first base of codon 74), yet rather than a reversion to the wild-type codon (TGC, encoding cysteine) changed the codon to serine (AGC). Given the physical similarities of serine and cysteine, I propose that $Zbtb1^{C74S}$ is permissive to T cell development and T cell clonal expansion, whereas $Zbtb1^{C74R}$ is not.

4.3.4.Defects in lymphoid but not myeloid development

The effects of *Zbtb1* mutation were not restricted to the T cell lineage. Numbers of all lymphocyte lineages (T, B, and NK) were reduced in the spleens of mutant mice, whereas numbers of myeloid cells were not (**Figure 4.19A**). An examination of B cell development in mutant bone marrow revealed an accumulation of B cell progenitors at the Hardy Fraction C stage, followed by a reduction of progenitors at each subsequent stage (**Figure 4.19B,D**). In the mutant spleen, numbers of transitional and follicular B cells were significantly reduced by an average of 72% and 44%, respectively (**Figure 4.19C,D**). The relatively minor reduction in follicular as compared with transitional B cell numbers may indicate mild compensatory expansion in the follicular compartment. Mutant B cells nevertheless responded to T-independent (but not T dependent) immunization (**Figure 4.19E**), implying a developmental rather than a functional B cell defect.

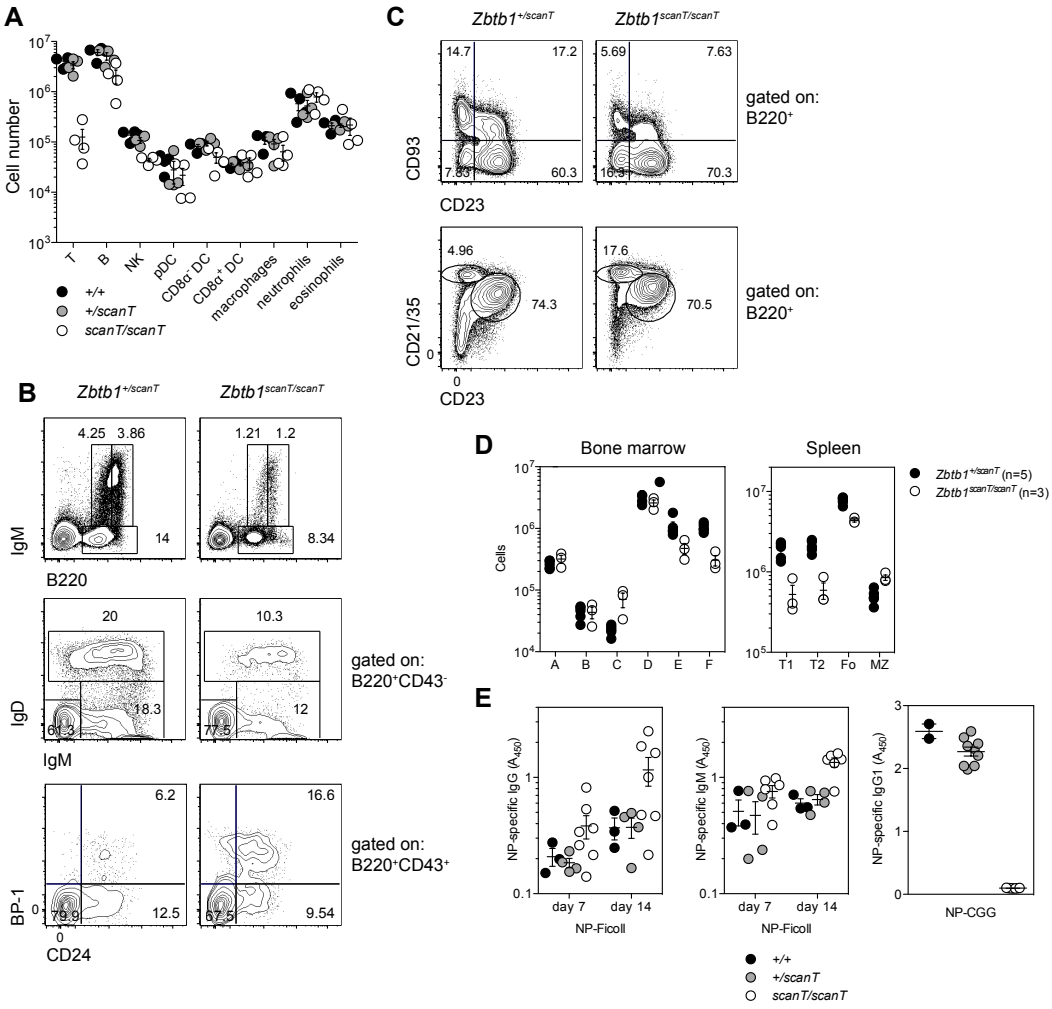


Figure 4.19 | *scanT* mice have generalized deficiencies of lymphoid, but not myeloid, cells.

(A) Total numbers of major lymphoid and myeloid cell subsets in the spleen of 8 week-old sex-matched littermates, gated as follows: T ($CD3\varepsilon^+$), B ($CD19^+$), NK ($NK1.1^+CD3\varepsilon^-$), pDC ($Lin^-PDCA1^+SiglecH^+$), CD8α⁻ DC ($Lin^-CD11c^+CD11b^+CD8\alpha^-$), CD8α⁺ DC ($Lin^-CD11c^+CD11b^-CD8\alpha^+$), macrophages ($Lin^-CD11b^+F4/80^+SSC^{lo}$), neutrophils ($Lin^-CD11b^+F4/80^-Ly6G^{hi}$), eosinophils ($Lin^-CD11b^+F4/80^+SSC^{hi}$). Lineage markers included CD19, TCRβ, NK1.1 and the viability dye 7-AAD. Frequencies (B, C) and numbers (D) or major B cell subsets in bone marrow and spleen. Subsets in bone marrow were gated as follows: A ($CD11b^-CD3\varepsilon^-Ter119^-Ly6G^-NK1.1^-IgM^-B220^+CD19^-CD24^-BP\text{-}1^-$), B ($B220^+IgM^-CD43^+CD24^+BP\text{-}1^-$), C ($B220^+IgM^-CD43^+CD24^+BP\text{-}1^+$), D ($B220^+CD43^-IgM^-IgD^-$), E ($B220^+CD43^-IgM^+IgD^-$), F ($B220^+CD43^-IgM^+IgD^+$). Subsets in spleen were gated as follows: T1 ($B220^+CD93^+CD23^-$), T2 ($B220^+CD93^+CD23^+$), Fo (follicular, $B220^+CD93^-CD23^+CD21/35^{int}$), MZ (marginal zone, $B220^+CD93^-CD23^-CD21/35^{hi}$). (E) NP-specific antibodies in the serum of mice immunized with NP-Ficoll or NP-CGG at 7 or 14 (NP-Ficoll) or 14 days (NP-CGG) after immunization, presented as absorbance at 450nm (A_{450}). Data are representative of one (E) or two (A-D) independent experiments, with four or more mice per group. Error bars represent standard error, and symbols represent individual mice.

4.3.5.A cell-intrinsic defect

Radiation chimeras were established to distinguish between potential haematopoietic and non-haematopoietic origins of the *Zbtb1* mutant phenotype. *Rag1* mutants reconstituted with *Zbtb1* mutant bone marrow developed B cells but not T cells (**Figure 4.20A**). This defect was intrinsic to *Zbtb1* mutant T cell progenitors, rather than other radiosensitive haematopoietic cells, because T cells in mixed bone marrow chimeras were exclusively derived from wild-type donors (**Figure 4.20B**). In fact, all blood lymphocytes (but not $CD11b^+$ myeloid cells) were wild-type donor derived, implying a general competitive failure of *Zbtb1* mutant lymphoid progenitors (**Figure 4.20B**). Finer phenotyping of the spleen, bone marrow, and thymus of mixed bone marrow chimeric mice confirmed this to be the case. B, T, and NK cells in the spleen were exclusively wild-type derived ($CD45.1^+$), whereas little or no competitive disadvantage was seen in the myeloid compartments (**Figure 4.20C**). Cells of wild-type origin dominated the B cell compartment from the Fraction A stage onward and similarly outcompeted *Zbtb1* mutant NK progenitors in bone marrow and T cell progenitors in the thymus (**Figure 4.20C**).

4.3.6.Uncompromised haematopoietic progenitor function

The *scanT* mutation did not appear to affect haematopoietic development before lymphoid specification. Percentages and numbers of early haematopoietic progenitors, including CLPs, were comparable in heterozygous and homozygous mutant bone marrow (**Figure 4.21A,B**) and were reconstituted at equivalent percentages in mixed bone marrow chimeras (**Figure 4.21C**). Haematopoietic stem cell (HSC) turnover, as measured by incorporation of the thymidine analogue 5-ethynyl-2'-deoxyuridine (EdU), occurred at similar rates in wild-type and mutant mice (**Figure 4.21D**). Wild-type and *Zbtb1* mutant bone marrow also generated equivalent numbers of haematopoietic colonies in the spleens of lethally irradiated recipients, both at days 8 (indicative of megakaryocyte/erythroid progenitor function) and 12 (reflective of multipotent progenitor function; **Figure 4.21E**; (Na Nakorn et al., 2002)). Myeloid engraftment did not occur in unconditioned *Zbtb1* mutant recipients of wild-type bone marrow, which is consistent with the interpretation of intact HSC function (**Figure 4.21F**).

4.3.7.Discussion

In certain aspects, *Zbtb1* mutants reflect the phenotype of mice lacking Notch1. Both *Zbtb1* and *Notch1* mutants are profoundly T cell deficient and show an accumulation of B cells in the thymic rudiment

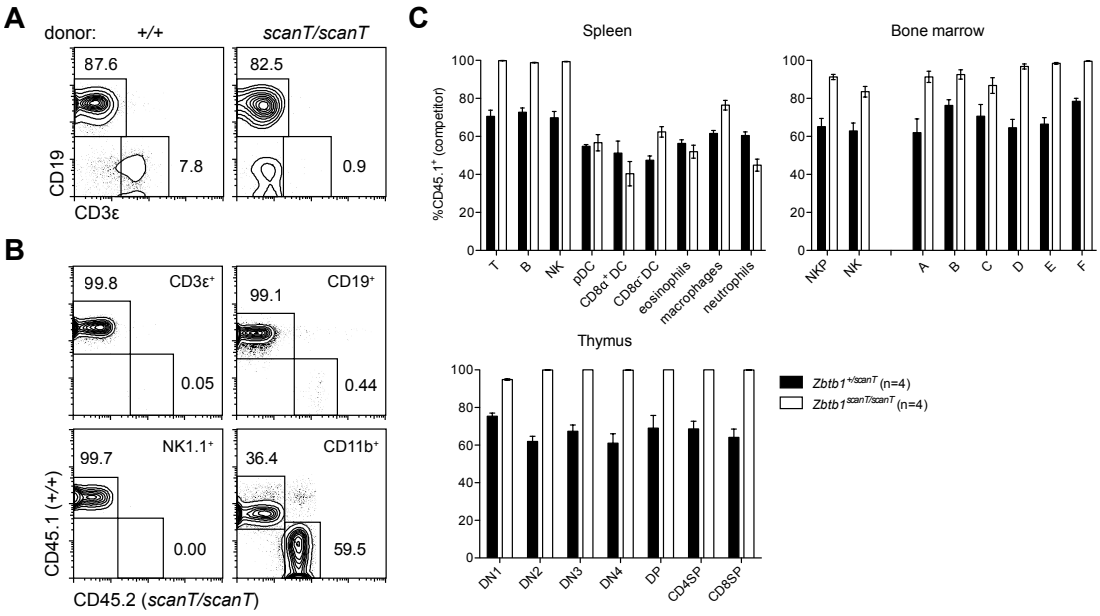


Figure 4.20 | A cell-intrinsic T cell deficiency and competitive failure of lymphoid reconstitution.

Lethally-irradiated *Rag1* mutant mice (CD45.2$^+$) were reconstituted with unmixed *scanT* or wild-type bone marrow (CD45.2$^+$) (A), or a mixture of *scanT* or wild-type marrow (CD45.2$^+$) with wild-type bone marrow (CD45.1$^+$) (B). Chimerism was measured 8 weeks after transplant. Panels in (B) have been gated on the indicated cell subset. (C) Lethally-irradiated wild-type recipients (CD45.1$^+$) were transplanted with an equal mixture of wild-type (CD45.1$^+$) and heterozygous or homozygous mutant (CD45.2$^+$) bone marrow. Wild-type donor chimerism (CD45.1$^+$) was measured 8 weeks later in the spleen, bone marrow and thymus. Subsets were gated as in Figure 3, with the addition of NK progenitors (NKP, 7-AAD$^-$CD19$^-$TCRβ$^-$CD122$^+$NK1.1$^-$). Data are representative of one (A) or three (B, C) independent experiments with at least three mice per group. Error bars represent standard error.

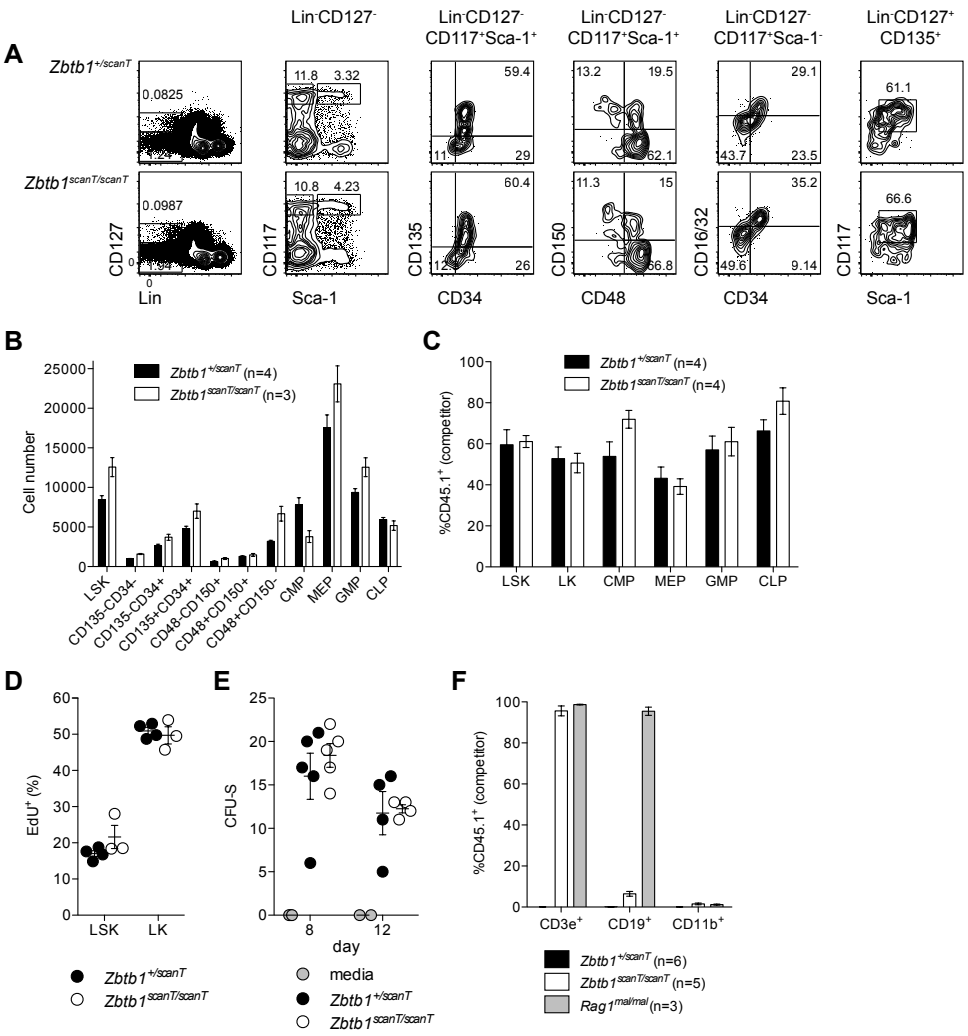


Figure 4.21 | Normal development and function of hematopoietic progenitors. Frequencies (A) and numbers (B) or hematopoietic progenitors in heterozygous and homozygous *Zbtb1* mutant bone marrow. LT-HSC (long-term HSC, $CD135^{-}CD34^{-}$ or $CD150^{+}CD48^{-}$), ST-HSC (short-term HSC, $CD135^{-}CD34^{+}$ or $CD150^{+}CD48^{+}$), MPP (multipotent progenitors, $CD135^{+}CD34^{+}$ or $CD150^{-}CD48^{+}$), CMP (common myeloid progenitors, $CD16/32^{-}CD34^{+}$), GMP (granulocyte/monocyte progenitors, $CD16/32^{+}CD34^{+}$), MEP (megakaryocyte/erythroid progenitors, $CD16/32^{-}CD34^{-}$) and CLP (common lymphoid progenitors, $CD117^{int}Sca\text{-}1^{int}$) were gated as indicated. (C) Chimerism of a subset of hematopoietic progenitors outlined in (A), 8 weeks after reconstitution of lethally-irradiated $CD45.1^{+}$ recipients with an equal mixture of $CD45.1^{+}$ and *Zbtb1*$^{+/scanT}$ ($CD45.2^{+}$) or $CD45.1^{+}$ and *Zbtb1*$^{scanT/scanT}$ ($CD45.2^{+}$) bone marrow cells. (D) Incorporation of the thymidine analogue EdU 4 hours after injection. (E) Spleen colony forming units (CFU-S) counted 8 or 12 days after transfer of $1x10^{5}$ bone marrow cells (or media alone) into lethally-irradiated recipients. (F) Engraftment of $2x10^{6}$ $CD45.1^{+}$ bone marrow cells in unconditioned recipients 8 weeks after injection. Lineage markers in (A)-(D) were CD11b, CD3ε, B220, Ter119, Ly6G, NK1.1 and CD8α. Data are representative of one (D, F), two (A, B, C) and three (E) independent experiments with at least three mice per group. Error bars represent standard error, and symbols (in D & E) represent individual mice.

(Radtke et al., 1999). Yet although *Zbtb1* mutants have a competitive disadvantage in the B and NK lineages, *Notch1* mutants do not (Radtke et al., 1999). Germline mutation of *Zbtb1* appears permissive to embryonic development, whereas mutation of *Notch1* is not (Swiatek et al., 1994), indicating a more specialized role for ZBTB1 in determining lymphoid fate. This is consistent with the conservation of *Zbtb1* only among vertebrate genomes and might implicate the human *ZBTB1* locus in genetically obscure cases of T cell–deficient SCID (Fischer, 2007).

Although there are no previous studies of a physiological role for ZBTB1, one describes some of its biochemical characteristics (Matic et al., 2010). ZBTB1, like many of its BTB-ZF counterparts, acts as a potent transcriptional repressor, as determined by the repressive activity of a Gal4-ZBTB1 fusion protein. This repressive activity, as well as the colocalization of ZBTB1 with the SMRT transcriptional repressor, is also regulated by SUMOylation (Matic et al., 2010).

These data raise several questions about the function of ZBTB1 in T cell and lymphoid specification. In particular, why is ZBTB1 critical for T cell development but only essential for B and NK development under competition? Can the reduction in ETP numbers be explained by their failure to migrate to the thymus, by a failure to proliferate within it, or a combination of both? Programmed death of T cell progenitors is unlikely to account for this because T cells also fail to develop in the absence of the proapoptotic protein Bim (which can rescue erythropoiesis in mice deficient for the BTB-ZF relative LRF; **Figure 4.22**; (Maeda et al., 2009)).

In summary, this work defines ZBTB1 as a regulator of lymphoid development, joining the ranks of other lymphoid-promoting BTB-ZF proteins. As is the case with other BTB-ZF family members, ZBTB1 presumably acts as a transcriptional suppressor, and the determination of precisely which genes it regulates will be of central importance to our understanding of lymphopoiesis.

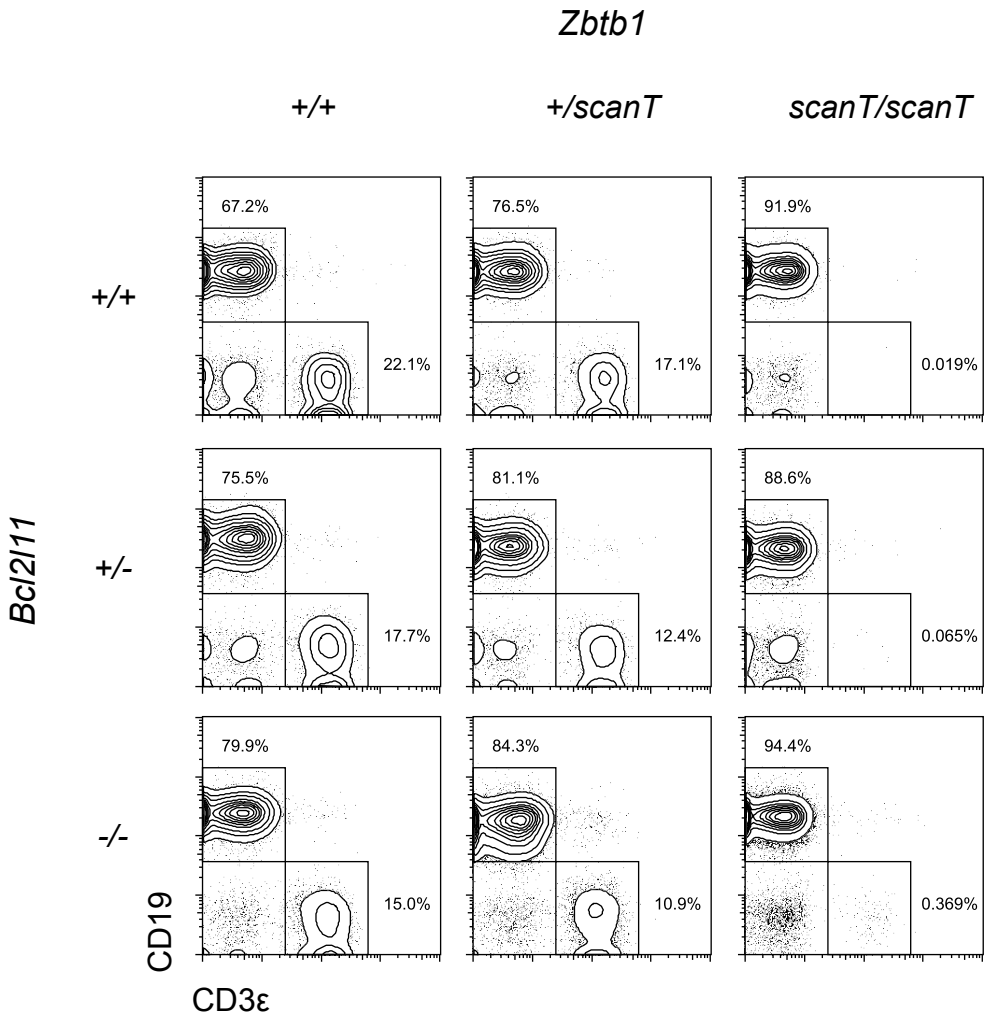


Figure 4.22 | T cell deficiency is independent of BIM.
Zbtb1$^{+/scanT}$;*Bcl2l11*$^{+/-}$ double heterozygotes were intercrossed, and frequencies of CD19^{+} and CD3ε^{+} blood lymphocytes were examined in the progeny. Data are from a single experiment, with plots representative of 1-7 mice per genotype.

4.4. Folliculin-interacting protein 1 is required for B cell development

4.4.1. Birt-Hogg-Dubé syndrome and folliculin

Birt-Hogg-Dubé syndrome (BHD) is an inherited cancer predisposition syndrome, characterised by an increased risk of hair follicle hamartomas, renal and lung cysts, and renal cell carcinoma (Birt et al., 1977). BHD patients are known to carry germline heterozygous mutations of *FLCN*, a gene encoding the protein folliculin (Nickerson et al., 2002). The second allele of *FLCN* is somatically mutated in a majority of renal tumours from BHD patients (Vocke et al., 2005), suggesting that FLCN may act as a classical tumour suppressor (Knudson, 1971). A spontaneous heterozygous mutation of *Flcn* is also known to cause inherited renal cell carcinoma in the rat (Okimoto et al., 2004), as does an engineered mutation in the mouse (Hasumi et al., 2009). FLCN itself is essential for embryogenesis, as homozygous germline deletion of mouse *Flcn* is lethal before E6.5 (Hasumi et al., 2009), while kidney-specific *Flcn* deletion leads to the development of enlarged polycystic kidneys and death at three weeks of age (Baba et al., 2008; Chen et al., 2008).

FLCN mutant tumours in both mice and humans are characterised by hyperactivation of the mammalian target of rapamycin (mTOR) pathway (Hasumi et al., 2009), and rapamycin can extend the survival of mice with FLCN-deficient kidneys (Baba et al., 2008). mTOR activation is also characteristic of other hamartoma and renal cancer syndromes, including those caused by mutation of *MET*, *PTEN*, *LKB1*, *TSC1* and *TSC2* (Linehan et al., 2010). Precisely how FLCN and mTOR are linked is still uncertain, but is suspected to involve the 5'-AMP-activated protein kinase (AMPK). FLCN binds indirectly to the gamma subunit of AMPK with the help of folliculin-interacting proteins 1 and 2 (FNIP1 and FNIP2) (Baba et al., 2006; Hasumi et al., 2008; Takagi et al., 2008), and both FLCN and FNIP1 are phosphorylated in an AMPK inhibitor-sensitive manner (Baba et al., 2006).

Despite their importance in the regulation of FLCN, the physiological function of FNIP1 and FNIP2 had not been examined. I describe below the identification and initial characterisation of one of the first *Fnip1* mutant alleles in the mouse.

4.4.2.A cell-intrinsic B cell deficiency

During the course of a sensitised screen for lymphocyte development defects, I detected a single G3 mouse in which the B cell compartment was entirely derived from the wild-type bone marrow donor (**Figure 4.23**). No competitive defect was observed in the $CD4^+$, $CD8^+$, $NK1.1^+$ or $CD11b^+$ compartments, implying that the defect was intrinsically restricted to the B cell lineage. The phenotype was not competition-specific, however, since mice from the same pedigree also showed B cell deficiency prior to irradiation. B cell-deficient mice also appeared smaller than their littermates, and were infertile.

4.4.3.Mutation of Fnip1

To identify the cause of the B cell deficiency, male siblings of the index G3 male mutant were paired with C57BL/10J and C57BL/6J females (**Figure 4.24**). Female F1 progeny were backcrossed to their father, and F2 mice were tested for an expansion of donor-derived cells in the B cell compartment. DNA from six C57BL/10J-derived F2s with the mutant phenotype was subjected to conventional bulk segregation analysis, revealing linkage to distal chromosome 11 (46027800 bp-end) (Xia et al., 2010) (**Figure 4.25**).

Three C57BL/6J-derived F2 samples were also subjected to massively parallel sequencing (to a mean coverage depth of 4X). A list of discrepancies with the mouse genome reference sequence was generated with an in-house variant caller. Variants that had previously been seen in the genomes of unrelated mice (and sequenced at the same facility and on the same platform) were subtracted, as were variants seen in only one unique read.

Since the phenotype was known to be recessive, a genome-wide plot of homozygous mutations (both coding and non-coding) was created for each mouse. This revealed discrete clusters of mutations, presumably inherited from the original ENU-treated founder. A subset of these clustered mutations was shared between all three mice, indicating linkage of the phenotype to chromosome 8 or 11 (**Figure 4.26**). Amongst the variants called as homozygous in all three mice, only two were predicted to change coding sense: a missense mutation in *Smad1* (L168P) on chromosome 8, and a critical splice donor mutation in *Fnip1* on chromosome 11. Since null mutations of *Smad1* prevent placental development and lead to early embryonic lethality (Tremblay et al., 2001), we considered this an unlikely candidate for a viable B cell deficient phenotype. Although the physiological function was not known at the time, *Fnip1* appeared to be a more probable candidate given the enriched expression of *Fnip1* in leukocytes (Baba et al., 2006). The

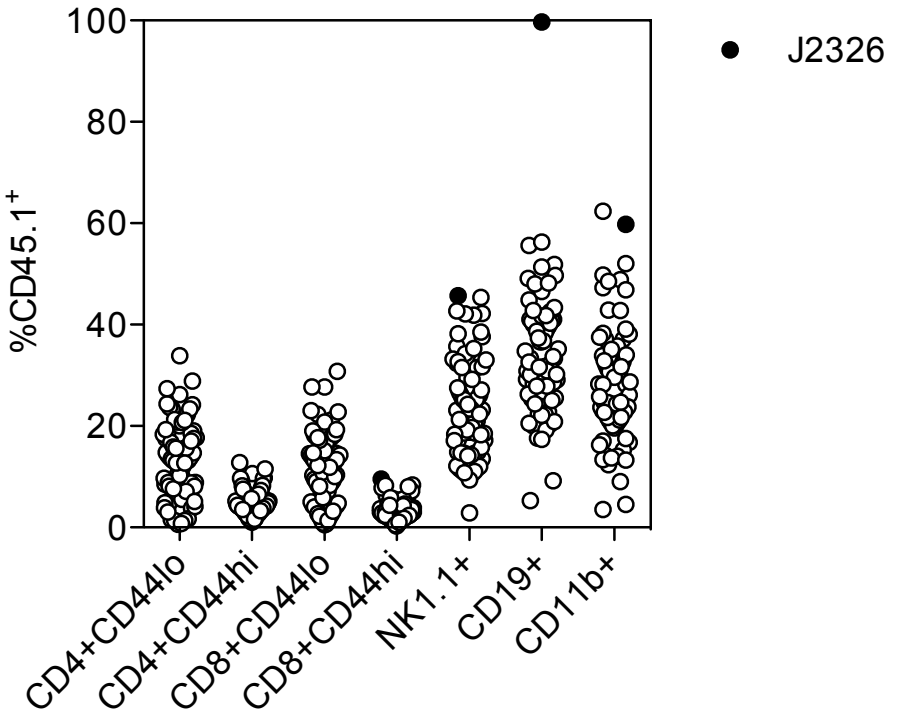


Figure 4.23 | The *hamel* phenotype.
A cohort of 82 G3 mutant progeny were irradiated (400 rad), transplanted with CD45.1$^+$ bone marrow cells, and bled four weeks later. CD45.1$^+$ chimerism in multiple blood leukocyte populations was measured by flow cytometry, revealing a single mouse in which the CD19$^+$ compartment was entirely donor-derived.

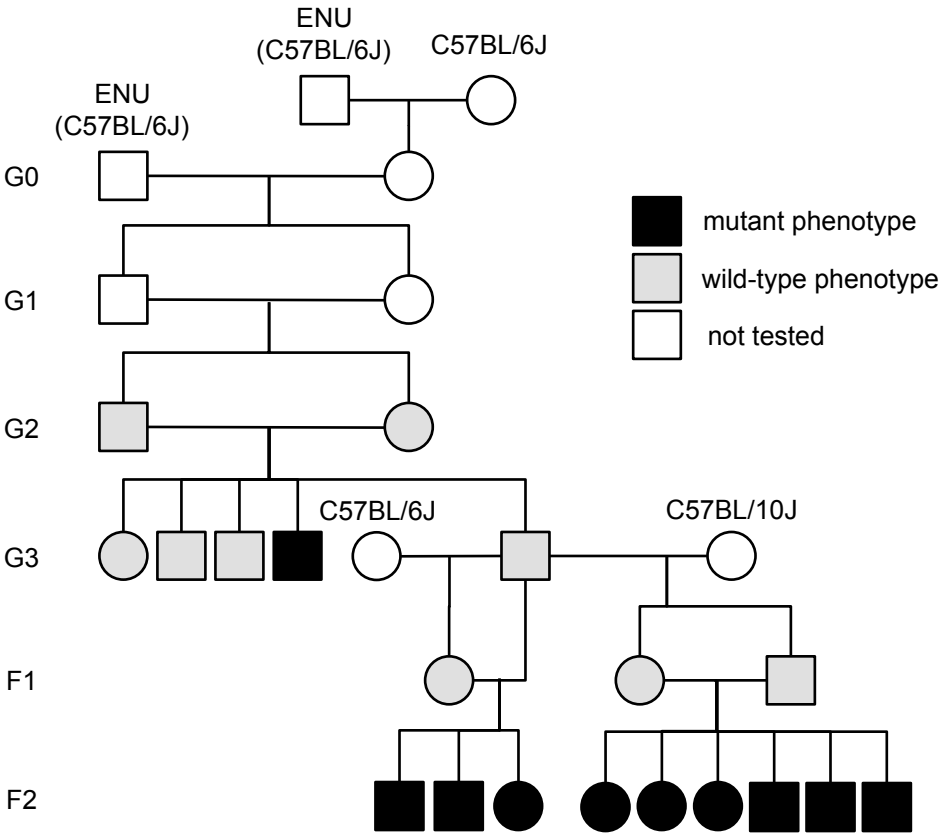


Figure 4.24 | *hamel* pedigree and initial mapping crosses.
Brothers of the index *hamel* male were outcrossed to C57BL/10J females for conventional mapping by bulk segregation analysis. The same mice were also crossed to C57BL/6J females to recover additional *hamel* homozygotes for whole genome sequencing-based mapping. For simplicity, F2 mice without phenotype are not displayed.

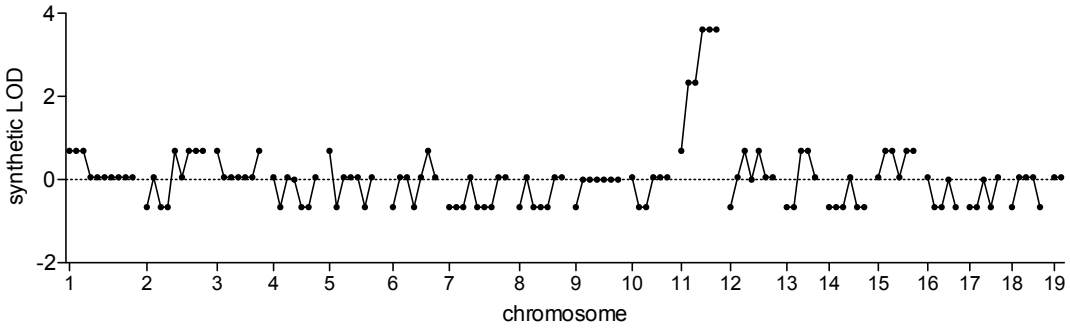


Figure 4.25 | Isolation of the *hamel* phenotype to distal chromosome 11.
Six C57BL/10J F2IC mice with the *hamel* phenotype were subjected to mapping by bulk segregation analysis. Estimated genotype frequencies were used to generate synthetic LOD scores at each of 128 markers, revealing a trio of markers on distal chromosome 11 with scores of 3.61.

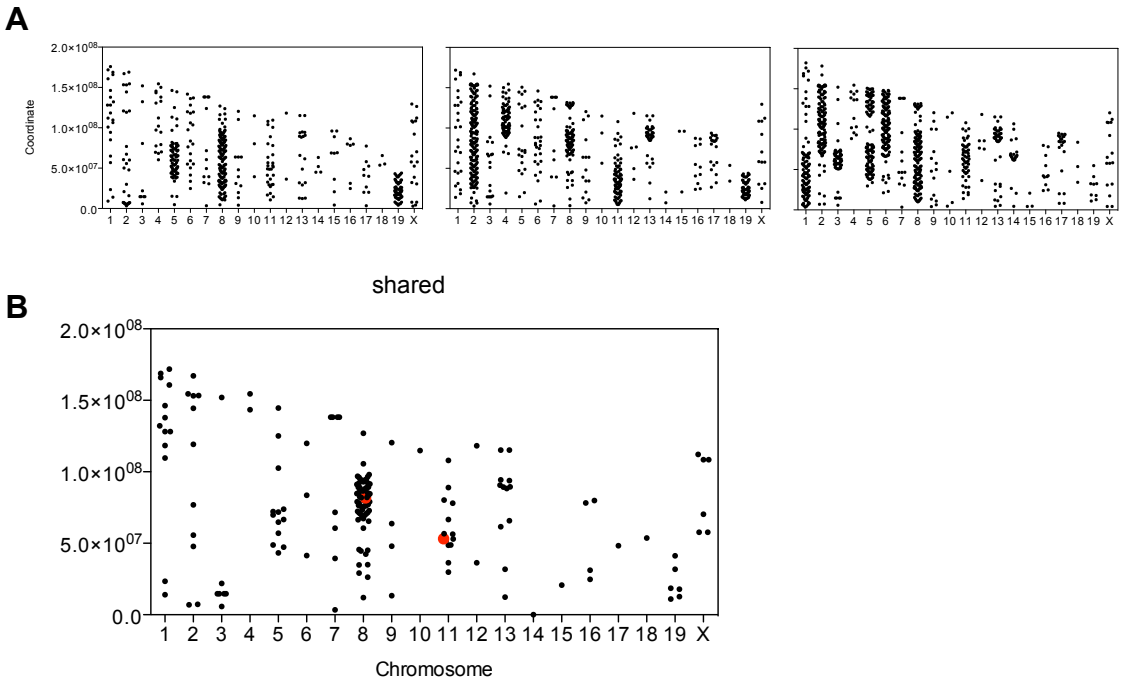


Figure 4.26 | Homozygous variants shared between three *hamel* mutants.
(A) Chromosomal distribution of homozygous mutations found in three individually sequenced *hamel* mice. (B) Homozygous mutations common to all three mutants are shown, with mutations predicted to alter coding sense labelled in red. These include a missense mutation in *Smad1* on chromosome 8, and a splice donor mutation at the *Fnip1* locus on chromosome 11.

mutation in *Fnip1* was validated by capillary sequencing, and as a polymorphic restriction enzyme site (**Figure 4.27**).

4.4.4.Discussion

While FLCN was not known to play a role in B cell development, there are many reports that mTOR dysregulation can disrupt it. mTOR is assembled in one of two multiprotein complexes in mammalian cells: mTORC1 and mTORC2. While a hypomorphic knockin allele of mTOR can disrupt both complexes and partially block early B cell development (Zhang et al., 2011), mutation of the mTORC2 component Sin1 has an even more severe effect (Lazorchak et al., 2010). Sin1 deficiency leads to increased IL-7 receptor expression and V(D)J recombination activity, and an expansion of $CD43^{+}IgM^{-}$ precursor B cells. This is associated with reduced phosphorylation of the mTORC2 target Akt and an accumulation of FoxO1, which would otherwise be degraded after Akt-mediated phosphorylation. Increased amounts of FoxO1 protein in Sin1-deficient B cells then leads to increased expression of *Il7r* and *Rag1*/*Rag2* target genes (Dengler et al., 2008). It might therefore be expected that FNIP1 deficiency could have the opposite effect: reduced suppression of mTORC2 by FLCN and FNIP1 leading to increased activation of Akt, increased phosphorylation and degradation of FoxO1, and decreased expression of *Il7r* and *Rag1*/*Rag2*. Since the expression of *Il7r* and *Rag1*/*Rag2* genes are tightly regulated during early B cell development (Herzog et al., 2009), a reduction in expression can be equally as disruptive as an increase in expression. Overexpression of *Il7r*, for instance, can block B cell development to the same degree as an *Il7r* null mutation (Peschon et al., 1994; Purohit et al., 2003).

During the course of this work, two groups independently described a role for *Fnip1* in early B cell development (Baba et al., 2012; Park et al., 2012). In the first case, a spontaneous 32 bp exonic deletion in *Fnip1* was associated with an arrest of B cell development at the pre-B cell stage (Park et al., 2012). Phosphorylation of S6 kinase and S6 ribosomal protein was enhanced in *Fnip1* mutant progenitors in response to AMPK activation, indicating that mTOR activity was increased. Phosphorylation of Akt at the mTORC2 target residue Thr473 also appeared to be increased in *Fnip1* mutant progenitors. These data are consistent with the hypothesis that *Fnip1* mutation leads to increased Akt activation and FoxO1 degradation, leading to increased silencing of *Rag1*/*Rag2* and *Il7r* expression. Expression of heavy and light chain immunoglobulin transgenes (Phan et al., 2003) did not rescue this block, indicating that impaired V(D)J recombination was not the sole cause of the deficiency.

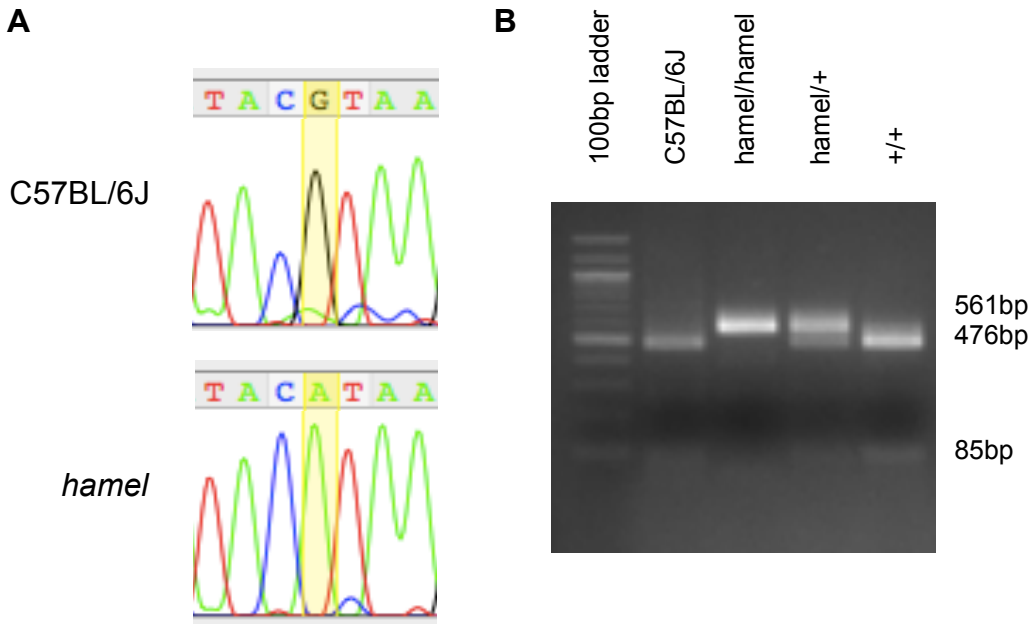


Figure 4.27 | Validation of the *Fnip1* mutation.
(A) Capillary sequencing trace of the *Fnip1* mutation in hamel. (B) Restriction fragment length polymorphism, as determined by *Bsa*A1 digest. A 561bp PCR amplicon of *Fnip1* is cleaved once by the enzyme in C57BL/6J mice, whereas the restriction site is lost in *hamel* mice.

In the second paper, *Fnip1* was inactivated by targeted deletion of exon 6, and in a separate allele, by a gene trap insertion in intron 2 (Baba et al., 2012). Both alleles recapitulated the pre-B cell arrest seen in the spontaneous *Fnip1* mutant, and a conditional allele of *Flcn* revealed that FLCN was also required for early B cell development. Overexpression of a *BCL2* transgene rescued the developmental block in *Fnip1* mutants, although similar transgenes were not sufficient to rescue B cell development in *Il7r* or *Rag2* mutant mice (Young et al., 1997; Maraskovsky et al., 1998). This counters the hypothesis that reduced FoxO1-induced expression of *Il7r* and *Rag1*/*Rag2* is responsible for the B cell deficiency in *Fnip1* mutants, although it does not exclude the possibility that a quantitative reduction could still be rescued by BCL2. Heterozygous *Il7* mutant mice also have a mild B cell deficiency, which can be corrected by deficiency of the Bcl2 family member Bim (Oliver et al., 2004). In summary, the mechanism by which *Fnip1* promotes B cell development is yet to be determined.

5. Discussion

5.1. Summary

In this thesis, I describe the application of mouse germline mutagenesis to the study of immunity. While most of the variants discovered were in genes already known to be important for immunity, some of them are entirely unexpected, and reveal new entry points into the understanding of haematopoiesis and inflammation. In at least one case, a hypomorphic allele has also revealed functions that would not have been predicted from the null allele alone.

While connecting phenotype to mutation is a critical step, it does not explain mechanism, and there is much left to explain about the phenotypes described here. In general, developmental phenotypes are more difficult to explain than cellular ones: we are much further from explaining how mutations in *Atp11c*, *Zbtb1* or *Fnip1* prevent lymphocyte development than we are from explaining how mutation of *Rhbdf2* or *Ikbkg* inhibits the secretion of TNFα in macrophages, for example. But the nature of the mutated gene can help us form testable hypotheses. ZBTB1 belongs to a family of zinc-finger transcription factors, most of which are transcriptional repressors, so a simple prediction would be that ZBTB1 represses transcription of one or more genes to promote lymphocyte development. ATP11C belongs to a family of putative phospholipid flippases, and might therefore control the localisation of a lipid important for early B cell differentiation. FNIP1 interacts with a known regulator of the mTOR pathway, so perhaps it too can influence mTOR signalling.

We might now consider using forward genetics to delve deeper into the mechanism of each phenotype. Mutations that modify another monogenic phenotype have been extremely valuable in organisms such as *C. elegans* (Hodgkin, 2005), and despite some successes in mice (Carpinelli et al., 2004) are generally so rare for most phenotypes that modifier screens are prohibitively expensive. Instead, the greatest value of mouse forward genetics appears to be in revealing new pathways, which can then be studied in further depth by other means.

5.2. The future of mouse genetics

5.2.1. Forward genetics in mouse and man

In an era of affordable whole-genome sequencing, what might we expect for the future of mouse forward genetics? It is reasonable to predict that ENU-induced phenotypes will soon be solved almost as quickly as they are found, either through knowledge of the heterozygous mutations present in G1 founders, or by directly sequencing affected mice. Phenotypes, then, will become the limiting factor for forward genetics.

So why go to the trouble of creating mutations and phenotypes in mice when they already exist in abundance in man (MacArthur et al., 2012; Tennessen et al., 2012)? The costs of revealing the underlying mutation will be largely equivalent, and a human mutation can always be studied in greater detail in the mouse. There is no question that these cases are a priority, and will be solved at an increasingly rapid rate: medical specialists are skilled at identifying inherited phenotypes in patients, and genome sequencing and interpretation services will become increasingly affordable and accessible.

The mouse might therefore linger in the shadow of human forward genetics, validating human disease mutations rather than alluding to them, for all but the most intractable of cases. These could include phenotypes that require combinations of mutations, or those that emerge only under specific circumstances. Mutations in *NPC1*, for example, cause Niemann–Pick disease in humans, yet they also confer resistance to Ebola virus infection (Carette et al., 2011). Since not every member of the population will be exposed to every pathogen, observations such as these would be unlikely in a clinical setting.

5.2.2. Systematic reverse genetics and new tools in forward genetics

An international consortium is now on track to produce null alleles of every gene in the mouse genome (Skarnes et al., 2011). While this alone is a significant scientific resource, the next priority is to bring each of these mutations to homozygosity, and study their effects in whole animals through a series of phenotypic screens (Gates et al., 2011). Analysing large numbers of mice with a common mutation will allow discovery of subtle effects, which would have otherwise been missed amongst the variation of a forward genetic screen. Yet this approach is far from comprehensive: only a limited set of phenotypes will be examined, and a third of null mutations are estimated to be lethal in homozygous form (Ayadi et al., 2012). ENU mutagenesis, on the other hand, focuses on specific phenotypes, and regularly reveals viable

hypomorphic mutations in genes that are lethal when knocked out (*Ikbkg* being one such example) (Siggs et al., 2010).

Partially haploid human cancer cell lines (Carette et al., 2009) and haploid mouse ES cells (Leeb and Wutz, 2011) have both become valuable tools for mammalian forward genetics. So long as the phenotype can be replicated *in vitro*, saturation mutagenesis screens are now well within reach. The Toll-like receptor screen described in this thesis, for example, might be better studied in macrophages differentiated from haploid ES cells.

5.2.3. The mouse as a model of human disease

With few exceptions, the mouse is still the best available model of human physiology. This is certainly the case in a genetic sense, since 99% of human genes have a direct counterpart in the mouse (Mouse Genome Sequencing Consortium et al., 2002), and in the near future we will have access to null, conditional null, and missense variant alleles of all of them (Coghill et al., 2002; Skarnes et al., 2011).

The mouse has been a driving force in understanding the mammalian immune system, propelled by thousands of spontaneous, induced and engineered mutations. For example, the mechanism by which *FOXP3* mutations caused a fatal autoimmune disease was initially a mystery (Chatila et al., 2000; Bennett et al., 2001; Wildin et al., 2001), until studies in spontaneous and engineered mouse mutants revealed that it controlled the development of regulatory T cells (Hori et al., 2003). Indeed, it was the positional cloning of a *Foxp3* mutation in mice that precipitated its discovery in man to begin with (Russell et al., 1959; Brunkow et al., 2001).

Yet mice are by no means an ideal reflection of their human counterparts (Davis, 2008). They can teach us an enormous amount about the underlying biology of a disease, yet when it comes to predicting the effectiveness of treatments they are notoriously unreliable. Part of this may be due to the sheer heterogeneity of disease, in which a single diagnosis can encompass a range of distinct molecular causes. On the other hand, studies in the mouse are almost too focussed, and rarely venture beyond the confines of the C57BL/6 genetic background and defined pathogen-free environments.

There are many experimental alternatives to the mouse. Where possible, this alternative should be the patients themselves, from whom there is much data to collect (Bendall et al., 2011). Where a patient's cells cannot be examined *ex vivo*, mutations can be engineered in human cells *in vitro* (Zou et al.,

2009; Hockemeyer et al., 2011). For experiments that cannot be performed *ex vivo* or *in vitro*, humanized mice offer an alternative: immunodeficient mice can already be used to sustain human xenografts (Shultz et al., 2007), and efforts to introduce human genes will only improve this further (Rathinam et al., 2011).

There are now dozens of human immune disorders with a known disease gene but unknown mechanism, with dozens more expected to follow. A certain amount can be learned from patients themselves, but for everything else, the mouse is often still the best way to obtain physiological insight.

5.2.4. Outstanding immunological phenomena

Beyond unsolved Mendelian diseases, immunology is full of unexplained phenomena. Why do people develop autoimmunity? Why are autoimmune diseases more prevalent further from the equator, and why is their incidence increasing (Bach, 2002)? We know that TNF inhibition is an effective treatment for inflammatory autoimmune diseases such as rheumatoid arthritis (Feldmann, 2009), but what triggers TNF production in the first place? And how on earth does alum function as an adjuvant? Many of these phenomena are clearly influenced by the environment, but this does not prevent us from applying mouse and human genetics to understand them. After all, it was a genetic approach that revealed the molecular link between infection and inflammation (Poltorak et al., 1998).

5.3. Conclusions

Mouse germline mutagenesis permits an unbiased genetic dissection of physiological phenomena. By applying this to the study of innate and adaptive immunity, I have revealed four unexpected genetic components, with an additional unexpected role for a previously characterised gene.

There is no shortage of immunological phenomena in nature, and new phenomena are constantly emerging. All of them are encoded to some extent by genes and are therefore susceptible to genetic dissection. We can then expect that forward genetics, whether practiced in humans or mice or other organisms, will be a source of many more surprises.

6. References

Adams, J.M., Harris, A.W., Pinkert, C.A., Corcoran, L.M., Alexander, W.S., Cory, S., Palmiter, R.D., and Brinster, R.L. (1985). The c-myc oncogene driven by immunoglobulin enhancers induces lymphoid malignancy in transgenic mice. Nature *318*, 533–538.

Adrain, C., Zettl, M., Christova, Y., Taylor, N., and Freeman, M. (2012). Tumor necrosis factor signaling requires iRhom2 to promote trafficking and activation of TACE. Science *335*, 225–228.

Adzhubei, I.A., Schmidt, S., Peshkin, L., Ramensky, V.E., Gerasimova, A., Bork, P., Kondrashov, A.S., and Sunyaev, S.R. (2010). A method and server for predicting damaging missense mutations. Nat Methods *7*, 248–249.

Altenburg, E. (1928). The Limit of Radiation Frequency Effective in Producing Mutations. The American Naturalist *62*, 540–545.

Andersson, B.S., Collins, V.P., Kurzrock, R., Larkin, D.W., Childs, C., Ost, A., Cork, A., Trujillo, J.M., Freireich, E.J., and Siciliano, M.J. (1995). KBM-7, a human myeloid leukemia cell line with double Philadelphia chromosomes lacking normal c-ABL and BCR transcripts. Leukemia *9*, 2100–2108.

Andrews, T.D., Whittle, B., Field, M.A., Balakishnan, B., Zhang, Y., Shao, Y., Cho, V., Kirk, M., Singh, M., Xia, Y., et al. (2012). Massively parallel sequencing of the mouse exome to accurately identify rare, induced mutations: an immediate source for thousands of new mouse models. Open Biol *2*, 120061.

Anzelon, A.N., Wu, H., and Rickert, R.C. (2003). Pten inactivation alters peripheral B lymphocyte fate and reconstitutes CD19 function. Nat Immunol *4*, 287–294.

Arber, W. (1965). Host-controlled modification of bacteriophage. Annu. Rev. Microbiol. *19*, 365–378.

Arnold, C.N., Barnes, M.J., Berger, M., Blasius, A.L., Brandl, K., Croker, B., Crozat, K., Du, X., Eidenschenk, C., Georgel, P., et al. (2012a). ENU-induced phenovariance in mice: inferences from 587 mutations. BMC Res Notes *5*, 577.

Arnold, C.N., Pirie, E., Dosenovic, P., McInerney, G.M., Xia, Y., Wang, N., Li, X., Siggs, O.M., Karlsson Hedestam, G.B., and Beutler, B. (2012b). A forward genetic screen reveals roles for Nfkbid, Zeb1, and Ruvbl2 in humoral immunity. Proc Natl Acad Sci USA *109*, 12286–12293.

Arnold, C.N., Xia, Y., Lin, P., Ross, C., Schwander, M., Smart, N.G., Müller, U., and Beutler, B. (2011). Rapid identification of a disease allele in mouse through whole genome sequencing and bulk segregation analysis. Genetics *187*, 633–641.

Auerbach, C., Robson, J.M., and Carr, J.G. (1947). The Chemical Production of Mutations. Science *105*, 243–247.

Ayadi, A., Birling, M.-C., Bottomley, J., Bussell, J., Fuchs, H., Fray, M., Gailus-Durner, V., Greenaway, S., Houghton, R., Karp, N., et al. (2012). Mouse large-scale phenotyping initiatives: overview of the European Mouse Disease Clinic (EUMODIC) and of the Wellcome Trust Sanger Institute Mouse Genetics Project. Mamm Genome.

Baba, M., Furihata, M., Hong, S.-B., Tessarollo, L., Haines, D.C., Southon, E., Patel, V., Igarashi, P., Alvord, W.G., Leighty, R., et al. (2008). Kidney-targeted Birt-Hogg-Dube gene inactivation in a mouse model: Erk1/2 and Akt-mTOR activation, cell hyperproliferation, and polycystic kidneys. J Natl Cancer Inst *100*, 140–154.

Baba, M., Hong, S.-B., Sharma, N., Warren, M.B., Nickerson, M.L., Iwamatsu, A., Esposito, D., Gillette, W.K., Hopkins, R.F., Hartley, J.L., et al. (2006). Folliculin encoded by the BHD gene interacts with a binding protein, FNIP1, and AMPK, and is involved in AMPK and mTOR signaling. Proc Natl Acad Sci USA *103*, 15552–15557.

Baba, M., Keller, J.R., Sun, H.-W., Resch, W., Kuchen, S., Suh, H.C., Hasumi, H., Hasumi, Y., Kieffer-Kwon, K.-R., Gonzalez, C.G., et al. (2012). The folliculin-FNIP1 pathway deleted in human Birt-Hogg-Dube syndrome is required for murine B-cell development. Blood *120*, 1254–1261.

Bach, J.-F. (2002). The effect of infections on susceptibility to autoimmune and allergic diseases. N Engl J Med *347*, 911–920.

Baltimore, D. (1970). RNA-dependent DNA polymerase in virions of RNA tumour viruses. Nature *226*, 1209–1211.

Becker, A.J., McCulloch, E.A., and Till, J.E. (1963). Cytological demonstration of the clonal nature of spleen colonies derived from transplanted mouse marrow cells. Nature *197*, 452–454.

Beinke, S., Robinson, M.J., Hugunin, M., and Ley, S.C. (2004). Lipopolysaccharide activation of the TPL-2/MEK/extracellular signal-regulated kinase mitogen-activated protein kinase cascade is regulated by IkappaB kinase-induced proteolysis of NF-kappaB1 p105. Mol Cell Biol *24*, 9658–9667.

Bendall, S.C., Simonds, E.F., Qiu, P., Amir, E.-A.D., Krutzik, P.O., Finck, R., Bruggner, R.V., Melamed, R., Trejo, A., Ornatsky, O.I., et al. (2011). Single-cell mass cytometry of differential immune and drug responses across a human hematopoietic continuum. Science *332*, 687–696.

Bennett, C.L., Christie, J., Ramsdell, F., Brunkow, M.E., Ferguson, P.J., Whitesell, L., Kelly, T.E., Saulsbury, F.T., Chance, P.F., and Ochs, H.D. (2001). The immune dysregulation, polyendocrinopathy, enteropathy, X-linked syndrome (IPEX) is caused by mutations of FOXP3. Nat Genet *27*, 20–21.

Berns, K., Hijmans, E.M., Mullenders, J., Brummelkamp, T.R., Velds, A., Heimerikx, M., Kerkhoven, R.M., Madiredjo, M., Nijkamp, W., Weigelt, B., et al. (2004). A large-scale RNAi screen in human cells identifies new components of the p53 pathway. Nature *428*, 431–437.

Beutler, B., Jiang, Z., Georgel, P., Crozat, K., Croker, B., Rutschmann, S., Du, X., and Hoebe, K. (2006). Genetic analysis of host resistance: Toll-like receptor signaling and immunity at large. Annu Rev Immunol *24*, 353–389.

Birt, A.R., Hogg, G.R., and Dubé, W.J. (1977). Hereditary multiple fibrofolliculomas with trichodiscomas and acrochordons. Arch Dermatol *113*, 1674–1677.

Black, R.A., Rauch, C.T., Kozlosky, C.J., Peschon, J.J., Slack, J.L., Wolfson, M.F., Castner, B.J., Stocking, K.L., Reddy, P., Srinivasan, S., et al. (1997). A metalloproteinase disintegrin that releases tumour-necrosis factor-alpha from cells. Nature *385*, 729–733.

Blobel, C.P. (2005). ADAMs: key components in EGFR signalling and development. Nat Rev Mol Cell Biol *6*, 32–43.

Boch, J., Scholze, H., Schornack, S., Landgraf, A., Hahn, S., Kay, S., Lahaye, T., Nickstadt, A., and Bonas, U. (2009). Breaking the code of DNA binding specificity of TAL-type III effectors. Science *326*, 1509–1512.

Borroto, A., Ruiz-Paz, S., la Torre, de, T.V., Borrell-Pages, M., Merlos-Suarez, A., Pandiella, A., Blobel, C.P., Baselga, J., and Arribas, J. (2003). Impaired trafficking and activation of tumor necrosis factor-alpha-converting enzyme in cell mutants defective in protein ectodomain shedding. J Biol Chem *278*, 25933–25939.

Botstein, D., White, R.L., Skolnick, M., and Davis, R.W. (1980). Construction of a genetic linkage map in

man using restriction fragment length polymorphisms. Am J Hum Genet *32*, 314–331.

Bouillet, P., Metcalf, D., Huang, D.C., Tarlinton, D.M., Kay, T.W., Köntgen, F., Adams, J.M., and Strasser, A. (1999). Proapoptotic Bcl-2 relative Bim required for certain apoptotic responses, leukocyte homeostasis, and to preclude autoimmunity. Science *286*, 1735–1738.

Bradley, A., Evans, M., Kaufman, M.H., and Robertson, E. (1984). Formation of germ-line chimaeras from embryo-derived teratocarcinoma cell lines. Nature *309*, 255–256.

Brandl, K., Sun, L., Neppl, C., Siggs, O.M., Le Gall, S.M., Tomisato, W., Li, X., Du, X., Maennel, D.N., Blobel, C.P., et al. (2010). MyD88 signaling in nonhematopoietic cells protects mice against induced colitis by regulating specific EGF receptor ligands. Proc Natl Acad Sci USA *107*, 19967–19972.

Brenner, S. (1974). The genetics of Caenorhabditis elegans. Genetics *77*, 71–94.

Brink, R., Goodnow, C.C., Crosbie, J., Adams, E., Eris, J., Mason, D.Y., Hartley, S.B., and Basten, A. (1992). Immunoglobulin M and D antigen receptors are both capable of mediating B lymphocyte activation, deletion, or anergy after interaction with specific antigen. J Exp Med *176*, 991–1005.

Brinster, R.L., Chen, H.Y., Trumbauer, M., Senear, A.W., Warren, R., and Palmiter, R.D. (1981). Somatic expression of herpes thymidine kinase in mice following injection of a fusion gene into eggs. Cell *27*, 223–231.

Brown, G.D., Taylor, P.R., Reid, D.M., Willment, J.A., Williams, D.L., Martinez-Pomares, L., Wong, S.Y.C., and Gordon, S. (2002). Dectin-1 is a major beta-glucan receptor on macrophages. J Exp Med *196*, 407–412.

Brown, M.S., and Goldstein, J.L. (1976). Receptor-mediated control of cholesterol metabolism. Science *191*, 150–154.

Brunkow, M.E., Jeffery, E.W., Hjerrild, K.A., Paeper, B., Clark, L.B., Yasayko, S.-A., Wilkinson, J.E., Galas, D., Ziegler, S.F., and Ramsdell, F. (2001). Disruption of a new forkhead/winged-helix protein, scurfin, results in the fatal lymphoproliferative disorder of the scurfy mouse. Nat Genet *27*, 68–73.

Bull, L.N., van Eijk, M.J., Pawlikowska, L., DeYoung, J.A., Juijn, J.A., Liao, M., Klomp, L.W., Lomri, N., Berger, R., Scharschmidt, B.F., et al. (1998). A gene encoding a P-type ATPase mutated in two forms of hereditary cholestasis. Nat Genet *18*, 219–224.

Busslinger, M. (2004). Transcriptional control of early B cell development. Annu Rev Immunol *22*, 55–79.

Carette, J.E., Guimaraes, C.P., Varadarajan, M., Park, A.S., Wuethrich, I., Godarova, A., Kotecki, M., Cochran, B.H., Spooner, E., Ploegh, H.L., et al. (2009). Haploid genetic screens in human cells identify host factors used by pathogens. Science *326*, 1231–1235.

Carette, J.E., Raaben, M., Wong, A.C., Herbert, A.S., Obernosterer, G., Mulherkar, N., Kuehne, A.I., Kranzusch, P.J., Griffin, A.M., Ruthel, G., et al. (2011). Ebola virus entry requires the cholesterol transporter Niemann-Pick C1. Nature *477*, 340–343.

Carmell, M.A., Zhang, L., Conklin, D.S., Hannon, G.J., and Rosenquist, T.A. (2003). Germline transmission of RNAi in mice. Nat. Struct. Biol. *10*, 91–92.

Carpinelli, M.R., Hilton, D.J., Metcalf, D., Antonchuk, J.L., Hyland, C.D., Mifsud, S.L., Di Rago, L., Hilton, A.A., Willson, T.A., Roberts, A.W., et al. (2004). Suppressor screen in Mpl-/- mice: c-Myb mutation causes supraphysiological production of platelets in the absence of thrombopoietin signaling. Proc Natl Acad Sci USA *101*, 6553–6558.

Carswell, E.A., Old, L.J., Kassel, R.L., Green, S., Fiore, N., and Williamson, B. (1975). An endotoxin-induced serum factor that causes necrosis of tumors. Proc Natl Acad Sci USA *72*, 3666–3670.

Carvalho, T.L., Mota-Santos, T., Cumano, A., Demengeot, J., and Vieira, P. (2001). Arrested B lymphopoiesis and persistence of activated B cells in adult interleukin 7(-/)- mice. J Exp Med *194*, 1141–1150.

Casanova, J.-L., Abel, L., and Quintana-Murci, L. (2011). Human TLRs and IL-1Rs in host defense: natural insights from evolutionary, epidemiological, and clinical genetics. Annu Rev Immunol *29*, 447–491.

Chalaris, A., Adam, N., Sina, C., Rosenstiel, P., Lehmann-Koch, J., Schirmacher, P., Hartmann, D., Cichy, J., Gavrilova, O., Schreiber, S., et al. (2010). Critical role of the disintegrin metalloprotease ADAM17 for intestinal inflammation and regeneration in mice. J Exp Med *207*, 1617–1624.

Chambers, I., Colby, D., Robertson, M., Nichols, J., Lee, S., Tweedie, S., and Smith, A. (2003). Functional expression cloning of Nanog, a pluripotency sustaining factor in embryonic stem cells. Cell *113*, 643–655.

Chang, Y.-F., Imam, J.S., and Wilkinson, M.F. (2007). The nonsense-mediated decay RNA surveillance pathway. Annu Rev Biochem *76*, 51–74.

Chatila, T.A., Blaeser, F., Ho, N., Lederman, H.M., Voulgaropoulos, C., Helms, C., and Bowcock, A.M. (2000). JM2, encoding a fork head-related protein, is mutated in X-linked autoimmunity-allergic disregulation syndrome. J Clin Invest *106*, R75–R81.

Chen, J., Futami, K., Petillo, D., Peng, J., Wang, P., Knol, J., Li, Y., Khoo, S.K., Huang, D., Qian, C.-N., et al. (2008). Deficiency of FLCN in mouse kidney led to development of polycystic kidneys and renal neoplasia. PLoS ONE *3*, e3581.

Chen, Y., Yee, D., Dains, K., Chatterjee, A., Cavalcoli, J., Schneider, E., Om, J., Woychik, R.P., and Magnuson, T. (2000). Genotype-based screen for ENU-induced mutations in mouse embryonic stem cells. Nat Genet *24*, 314–317.

Chiu, Y.-H., Macmillan, J.B., and Chen, Z.J. (2009). RNA polymerase III detects cytosolic DNA and induces type I interferons through the RIG-I pathway. Cell *138*, 576–591.

Christian, M., Cermak, T., Doyle, E.L., Schmidt, C., Zhang, F., Hummel, A., Bogdanove, A.J., and Voytas, D.F. (2010). Targeting DNA double-strand breaks with TAL effector nucleases. Genetics *186*, 757–761.

Churchill, G.A., Airey, D.C., Allayee, H., Angel, J.M., Attie, A.D., Beatty, J., Beavis, W.D., Belknap, J.K., Bennett, B., Berrettini, W., et al. (2004). The Collaborative Cross, a community resource for the genetic analysis of complex traits. Nat Genet *36*, 1133–1137.

Cobaleda, C., Jochum, W., and Busslinger, M. (2007). Conversion of mature B cells into T cells by dedifferentiation to uncommitted progenitors. Nature *449*, 473–477.

Coghill, E.L., Hugill, A., Parkinson, N., Davison, C., Glenister, P., Clements, S., Hunter, J., Cox, R.D., and Brown, S.D.M. (2002). A gene-driven approach to the identification of ENU mutants in the mouse. Nat Genet *30*, 255–256.

Conley, M.E., Dobbs, A.K., Farmer, D.M., Kilic, S., Paris, K., Grigoriadou, S., Coustan-Smith, E., Howard, V., and Campana, D. (2009). Primary B cell immunodeficiencies: comparisons and contrasts. Annu Rev Immunol *27*, 199–227.

Coutinho, A., and Meo, T. (1978). Genetic basis for unresponsiveness to lipopolysaccharide in C57BL/10Cr mice. Immunogenetics *7*, 17–24.

Croker, B.A., Lawson, B.R., Rutschmann, S., Berger, M., Eidenschenk, C., Blasius, A.L., Moresco, E.M.Y., Sovath, S., Cengia, L., Shultz, L.D., et al. (2008). Inflammation and autoimmunity caused by a SHP1 mutation depend on IL-1, MyD88, and a microbial trigger. Proc Natl Acad Sci USA *105*, 15028–15033.

Cuénot, L. (1902). La loi de Mendel et l'hérédité de la pigmentation chez les souris. Arch Zool Exp Gen *10*,

27–30.

Cuénot, L. (1903). L'hérédité de la pigmentation chez les souris. Arch Zool Exp Gen *1*, 33–41.

Danna, K., and Nathans, D. (1971). Specific cleavage of simian virus 40 DNA by restriction endonuclease of Hemophilus influenzae. Proc Natl Acad Sci USA *68*, 2913–2917.

Davis, M.M. (2008). A prescription for human immunology. Immunity *29*, 835–838.

Dengler, H.S., Baracho, G.V., Omori, S.A., Bruckner, S., Arden, K.C., Castrillon, D.H., DePinho, R.A., and Rickert, R.C. (2008). Distinct functions for the transcription factor Foxo1 at various stages of B cell differentiation. Nat Immunol *9*, 1388–1398.

Dias, S., Silva, H., Cumano, A., and Vieira, P. (2005). Interleukin-7 is necessary to maintain the B cell potential in common lymphoid progenitors. J Exp Med *201*, 971–979.

Dickins, R.A., McJunkin, K., Hernando, E., Premsrirut, P.K., Krizhanovsky, V., Burgess, D.J., Kim, S.Y., Cordon-Cardo, C., Zender, L., Hannon, G.J., et al. (2007). Tissue-specific and reversible RNA interference in transgenic mice. Nat Genet *39*, 914–921.

Dietrich, W.F., Miller, J., Steen, R., Merchant, M.A., Damron-Boles, D., Husain, Z., Dredge, R., Daly, M.J., Ingalls, K.A., and O'Connor, T.J. (1996). A comprehensive genetic map of the mouse genome. Nature *380*, 149–152.

Ding, S., Wu, X., Li, G., Han, M., Zhuang, Y., and Xu, T. (2005). Efficient transposition of the piggyBac (PB) transposon in mammalian cells and mice. Cell *122*, 473–483.

Doetschman, T., Gregg, R.G., Maeda, N., Hooper, M.L., Melton, D.W., Thompson, S., and Smithies, O. (1987). Targetted correction of a mutant HPRT gene in mouse embryonic stem cells. Nature *330*, 576–578.

Dupuy, A.J., Akagi, K., Largaespada, D.A., Copeland, N.G., and Jenkins, N.A. (2005). Mammalian mutagenesis using a highly mobile somatic Sleeping Beauty transposon system. Nature *436*, 221–226.

Dykstra, M., Cherukuri, A., Sohn, H.W., Tzeng, S.-J., and Pierce, S.K. (2003). Location is everything: lipid rafts and immune cell signaling. Annu Rev Immunol *21*, 457–481.

Eidenschenk, C., Crozat, K., Krebs, P., Arens, R., Popkin, D., Arnold, C.N., Blasius, A.L., Benedict, C.A., Moresco, E.M.Y., Xia, Y., et al. (2010). Flt3 permits survival during infection by rendering dendritic cells competent to activate NK cells. Proc Natl Acad Sci USA *107*, 9759–9764.

Elling, U., Taubenschmid, J., Wirnsberger, G., O'Malley, R., Demers, S.-P., Vanhaelen, Q., Shukalyuk, A.I., Schmauss, G., Schramek, D., Schnuetgen, F., et al. (2011). Forward and Reverse Genetics through Derivation of Haploid Mouse Embryonic Stem Cells. Cell Stem Cell *9*, 563–574.

Ellis, H.M., and Horvitz, H.R. (1986). Genetic control of programmed cell death in the nematode C. elegans. Cell *44*, 817–829.

Ellis, N.A., Groden, J., Ye, T.Z., Straughen, J., Lennon, D.J., Ciocci, S., Proytcheva, M., and German, J. (1995). The Bloom's syndrome gene product is homologous to RecQ helicases. Cell *83*, 655–666.

ENCODE Project Consortium, Bernstein, B.E., Birney, E., Dunham, I., Green, E.D., Gunter, C., and Snyder, M. (2012). An integrated encyclopedia of DNA elements in the human genome. Nature *489*, 57–74.

Endres, K., Anders, A., Kojro, E., Gilbert, S., Fahrenholz, F., and Postina, R. (2003). Tumor necrosis factor-alpha converting enzyme is processed by proprotein-convertases to its mature form which is degraded upon phorbol ester stimulation. Eur. J. Biochem. *270*, 2386–2393.

Evans, M.J., and Kaufman, M.H. (1981). Establishment in culture of pluripotential cells from mouse embryos. Nature *292*, 154–156.

Ewing, B., Hillier, L., Wendl, M.C., and Green, P. (1998). Base-calling of automated sequencer traces using phred. I. Accuracy assessment. Genome Res *8*, 175–185.

Fairfield, H., Gilbert, G.J., Barter, M., Corrigan, R.R., Curtain, M., Ding, Y., D'Ascenzo, M., Gerhardt, D.J., He, C., Huang, W., et al. (2011). Mutation discovery in mice by whole exome sequencing. Genome Biol *12*, R86.

Feldmann, M. (2009). Translating molecular insights in autoimmunity into effective therapy. Annu Rev Immunol *27*, 1–27.

Fire, A., Xu, S., Montgomery, M.K., Kostas, S.A., Driver, S.E., and Mello, C.C. (1998). Potent and specific genetic interference by double-stranded RNA in Caenorhabditis elegans. Nature *391*, 806–811.

Fischer, A. (2007). Human primary immunodeficiency diseases. Immunity *27*, 835–845.

Fisher, R. (1928). The Possible Modification of the Response of the Wild Type to Recurrent Mutations. American Naturalist *62*, 115–126.

Flavell, R.A., Sabo, D.L., Bandle, E.F., and Weissmann, C. (1974). Site-directed mutagenesis: generation of an extracistronic mutation in bacteriophage Q beta RNA. J Mol Biol *89*, 255–272.

Fraser, A.G., Kamath, R.S., Zipperlen, P., Martinez-Campos, M., Sohrmann, M., and Ahringer, J. (2000). Functional genomic analysis of C. elegans chromosome I by systematic RNA interference. Nature *408*, 325–330.

Freeden-Jeffry, von, U., Vieira, P., Lucian, L.A., McNeil, T., Burdach, S.E., and Murray, R. (1995). Lymphopenia in interleukin (IL)-7 gene-deleted mice identifies IL-7 as a nonredundant cytokine. J Exp Med *181*, 1519–1526.

Freeman, M. (2008). Rhomboid proteases and their biological functions. Annu Rev Genet *42*, 191–210.

Fruman, D.A., and Cantley, L.C. (2002). Phosphoinositide 3-kinase in immunological systems. Semin Immunol *14*, 7–18.

Gardner, R.L. (1968). Mouse chimeras obtained by the injection of cells into the blastocyst. Nature *220*, 596–597.

Gates, H., Mallon, A.-M., Brown, S.D.M., EUMODIC Consortium (2011). High-throughput mouse phenotyping. Methods *53*, 394–404.

Gatti, R.A., Meuwissen, H.J., Allen, H.D., Hong, R., and Good, R.A. (1968). Immunological reconstitution of sex-linked lymphopenic immunological deficiency. Lancet *2*, 1366–1369.

Gavin, A.L., Hoebe, K., Duong, B., Ota, T., Martin, C., Beutler, B., and Nemazee, D. (2006). Adjuvant-enhanced antibody responses in the absence of toll-like receptor signaling. Science *314*, 1936–1938.

Gerlach, B., Cordier, S.M., Schmukle, A.C., Emmerich, C.H., Rieser, E., Haas, T.L., Webb, A.I., Rickard, J.A., Anderton, H., Wong, W.W.-L., et al. (2011). Linear ubiquitination prevents inflammation and regulates immune signalling. Nature *471*, 591–596.

Goodnow, C.C., Sprent, J., Fazekas de St Groth, B., and Vinuesa, C.G. (2005). Cellular and genetic mechanisms of self tolerance and autoimmunity. Nature *435*, 590–597.

Gordon, D., Abajian, C., and Green, P. (1998). Consed: a graphical tool for sequence finishing. Genome Res *8*, 195–202.

Gordon, J.W., Scangos, G.A., Plotkin, D.J., Barbosa, J.A., and Ruddle, F.H. (1980). Genetic transformation of mouse embryos by microinjection of purified DNA. Proc Natl Acad Sci USA *77*, 7380–7384.

Grabstein, K.H., Waldschmidt, T.J., Finkelman, F.D., Hess, B.W., Alpert, A.R., Boiani, N.E., Namen, A.E., and Morrissey, P.J. (1993). Inhibition of murine B and T lymphopoiesis in vivo by an anti-interleukin 7 monoclonal antibody. J Exp Med *178*, 257–264.

Gu, H., Marth, J.D., Orban, P.C., Mossmann, H., and Rajewsky, K. (1994). Deletion of a DNA polymerase beta gene segment in T cells using cell type-specific gene targeting. Science *265*, 103–106.

Guo, B., Kato, R.M., Garcia-Lloret, M., Wahl, M.I., and Rawlings, D.J. (2000). Engagement of the human pre-B cell receptor generates a lipid raft-dependent calcium signaling complex. Immunity *13*, 243–253.

Guo, G., Wang, W., and Bradley, A. (2004). Mismatch repair genes identified using genetic screens in Blm-deficient embryonic stem cells. Nature *429*, 891–895.

Haldane, J.B.S., Sprunt, A.D., and Haldane, N.M. (1915). Reduplication in mice. J. Genet. *5*, 133–135.

Hao, Z., and Rajewsky, K. (2001). Homeostasis of peripheral B cells in the absence of B cell influx from the bone marrow. J Exp Med *194*, 1151–1164.

Hardy, R.R., and Hayakawa, K. (2001). B cell development pathways. Annu Rev Immunol *19*, 595–621.

Hardy, R.R., Carmack, C.E., Shinton, S.A., Kemp, J.D., and Hayakawa, K. (1991). Resolution and characterization of pro-B and pre-pro-B cell stages in normal mouse bone marrow. J Exp Med *173*, 1213–1225.

Hartwell, L.H., Culotti, J., and Reid, B. (1970). Genetic control of the cell-division cycle in yeast. I. Detection of mutants. Proc Natl Acad Sci USA *66*, 352–359.

Hartwell, L.H., Culotti, J., Pringle, J.R., and Reid, B.J. (1974). Genetic control of the cell division cycle in yeast. Science *183*, 46–51.

Hasty, P., Ramírez-Solis, R., Krumlauf, R., and Bradley, A. (1991). Introduction of a subtle mutation into the Hox-2.6 locus in embryonic stem cells. Nature *350*, 243–246.

Hasumi, H., Baba, M., Hong, S.-B., Hasumi, Y., Huang, Y., Yao, M., Valera, V.A., Linehan, W.M., and Schmidt, L.S. (2008). Identification and characterization of a novel folliculin-interacting protein FNIP2. Gene *415*, 60–67.

Hasumi, Y., Baba, M., Ajima, R., Hasumi, H., Valera, V.A., Klein, M.E., Haines, D.C., Merino, M.J., Hong, S.-B., Yamaguchi, T.P., et al. (2009). Homozygous loss of BHD causes early embryonic lethality and kidney tumor development with activation of mTORC1 and mTORC2. Proc Natl Acad Sci USA *106*, 18722–18727.

Hayden, M.S., and Ghosh, S. (2008). Shared principles in NF-kappaB signaling. Cell *132*, 344–362.

He, X., He, X., Dave, V.P., Zhang, Y., Hua, X., Nicolas, E., Xu, W., Roe, B.A., and Kappes, D.J. (2005). The zinc finger transcription factor Th-POK regulates CD4 versus CD8 T-cell lineage commitment. Nature *433*, 826–833.

Headon, D.J., and Overbeek, P.A. (1999). Involvement of a novel Tnf receptor homologue in hair follicle induction. Nat Genet *22*, 370–374.

Headon, D.J., Emmal, S.A., Ferguson, B.M., Tucker, A.S., Justice, M.J., Sharpe, P.T., Zonana, J., and Overbeek, P.A. (2000). Gene defect in ectodermal dysplasia implicates a death domain adapter in development. Nature *414*, 913–916.

Heissmeyer, V., Krappmann, D., Hatada, E.N., and Scheidereit, C. (2001). Shared pathways of IkappaB kinase-induced SCF(betaTrCP)-mediated ubiquitination and degradation for the NF-kappaB precursor p105 and IkappaBalpha. Mol Cell Biol *21*, 1024–1035.

Hemmi, H., Takeuchi, O., Kawai, T., Kaisho, T., Sato, S., Sanjo, H., Matsumoto, M., Hoshino, K., Wagner, H., Takeda, K., et al. (2000). A Toll-like receptor recognizes bacterial DNA. Nature *408*, 740–745.

Heppner, G., and Weiss, D.W. (1965). High Susceptibility of Strain A Mice to Endotoxin and Endotoxin-Red Blood Cell Mixtures. J. Bacteriol. *90*, 696–703.

Herzog, S., Reth, M., and Jumaa, H. (2009). Regulation of B-cell proliferation and differentiation by pre-B-cell receptor signalling. Nat Rev Immunol *9*, 195–205.

Hirschhorn, R., Yang, D.R., Puck, J.M., Huie, M.L., Jiang, C.K., and Kurlandsky, L.E. (1996). Spontaneous in vivo reversion to normal of an inherited mutation in a patient with adenosine deaminase deficiency. Nat Genet *13*, 290–295.

Hitotsumachi, S., Carpenter, D.A., and Russell, W.L. (1985). Dose-repetition increases the mutagenic effectiveness of N-ethyl-N-nitrosourea in mouse spermatogonia. Proc Natl Acad Sci USA *82*, 6619–6621.

Hockemeyer, D., Soldner, F., Beard, C., Gao, Q., Mitalipova, M., DeKelver, R.C., Katibah, G.E., Amora, R., Boydston, E.A., Zeitler, B., et al. (2009). Efficient targeting of expressed and silent genes in human ESCs and iPSCs using zinc-finger nucleases. Nat Biotechnol *27*, 851–857.

Hockemeyer, D., Wang, H., Kiani, S., Lai, C.S., Gao, Q., Cassady, J.P., Cost, G.J., Zhang, L., Santiago, Y., Miller, J.C., et al. (2011). Genetic engineering of human pluripotent cells using TALE nucleases. Nat Biotechnol *29*, 731–734.

Hodgkin, J. (2005). Genetic suppression. WormBook 1–13.

Hoebe, K., Du, X., Georgel, P., Janssen, E., Tabeta, K., Kim, S.O., Goode, J., Lin, P., Mann, N., Mudd, S., et al. (2003). Identification of Lps2 as a key transducer of MyD88-independent TIR signalling. Nature *424*, 743–748.

Hoebe, K., Georgel, P., Rutschmann, S., Du, X., Mudd, S., Crozat, K., Sovath, S., Shamel, L., Hartung, T., Zähringer, U., et al. (2005). CD36 is a sensor of diacylglycerides. Nature *433*, 523–527.

Hoffman, H.M., Mueller, J.L., Broide, D.H., Wanderer, A.A., and Kolodner, R.D. (2001). Mutation of a new gene encoding a putative pyrin-like protein causes familial cold autoinflammatory syndrome and Muckle-Wells syndrome. Nat Genet *29*, 301–305.

Holthuis, J.C.M., and Levine, T.P. (2005). Lipid traffic: floppy drives and a superhighway. Nat Rev Mol Cell Biol *6*, 209–220.

Hori, S., Nomura, T., and Sakaguchi, S. (2003). Control of regulatory T cell development by the transcription factor Foxp3. Science *299*, 1057–1061.

Hozumi, N., and Tonegawa, S. (1976). Evidence for somatic rearrangement of immunoglobulin genes coding for variable and constant regions. Proc Natl Acad Sci USA *73*, 3628–3632.

Iavarone, C., Ramsauer, K., Kubarenko, A.V., Debasitis, J.C., Leykin, I., Weber, A.N.R., Siggs, O.M., Beutler, B., Zhang, P., Otten, G., et al. (2011). A point mutation in the amino terminus of TLR7 abolishes signaling without affecting ligand binding. J Immunol *186*, 4213–4222.

Ikeda, F., Deribe, Y.L., Skånland, S.S., Stieglitz, B., Grabbe, C., Franz-Wachtel, M., van Wijk, S.J.L., Goswami, P., Nagy, V., Terzic, J., et al. (2011). SHARPIN forms a linear ubiquitin ligase complex regulating NF-κB activity and apoptosis. Nature *471*, 637–641.

International Cancer Genome Consortium, Hudson, T.J., Anderson, W., Artez, A., Barker, A.D., Bell, C., Bernabé, R.R., Bhan, M.K., Calvo, F., Eerola, I., et al. (2010). International network of cancer genome projects. Nature *464*, 993–998.

International Mouse Knockout Consortium, Collins, F.S., Rossant, J., and Wurst, W. (2007). A mouse for all reasons. Cell *128*, 9–13.

Ishii, K.J., Coban, C., Kato, H., Takahashi, K., Torii, Y., Takeshita, F., Ludwig, H., Sutter, G., Suzuki, K., Hemmi, H., et al. (2006). A Toll-like receptor-independent antiviral response induced by double-stranded B-form DNA. Nat Immunol *7*, 40–48.

Ishikawa, H., and Barber, G.N. (2008). STING is an endoplasmic reticulum adaptor that facilitates innate immune signalling. Nature *455*, 674–678.

Ivics, Z., Hackett, P.B., Plasterk, R.H., and Izsvák, Z. (1997). Molecular reconstruction of Sleeping Beauty, a Tc1-like transposon from fish, and its transposition in human cells. Cell *91*, 501–510.

Jaenisch, R. (1976). Germ line integration and Mendelian transmission of the exogenous Moloney leukemia virus. Proc Natl Acad Sci USA *73*, 1260–1264.

Jain, A., Ma, C.A., Liu, S., Brown, M., Cohen, J., and Strober, W. (2001). Specific missense mutations in NEMO result in hyper-IgM syndrome with hypohydrotic ectodermal dysplasia. Nat Immunol *2*, 223–228.

Janas, M.L., Hodson, D., Stamataki, Z., Hill, S., Welch, K., Gambardella, L., Trotman, L.C., Pandolfi, P.P., Vigorito, E., and Turner, M. (2008). The effect of deleting p110delta on the phenotype and function of PTEN-deficient B cells. J Immunol *180*, 739–746.

Jensen, C.T., Kharazi, S., Böiers, C., Cheng, M., Lübking, A., Sitnicka, E., and Jacobsen, S.E.W. (2008). FLT3 ligand and not TSLP is the key regulator of IL-7-independent B-1 and B-2 B lymphopoiesis. Blood *112*, 2297–2304.

Jiang, Z., Georgel, P., Du, X., Shamel, L., Sovath, S., Mudd, S., Huber, M., Kalis, C., Keck, S., Galanos, C., et al. (2005). CD14 is required for MyD88-independent LPS signaling. Nat Immunol *6*, 565–570.

Johnson, K.R., Lane, P.W., Cook, S.A., Harris, B.S., Ward-Bailey, P.F., Bronson, R.T., Lyons, B.L., Shultz, L.D., and Davisson, M.T. (2003). Curly bare (cub), a new mouse mutation on chromosome 11 causing skin and hair abnormalities, and a modifier gene (mcub) on chromosome 5. Genomics *81*, 6–14.

Johnson, R.S., Sheng, M., Greenberg, M.E., Kolodner, R.D., Papaioannou, V.E., and Spiegelman, B.M. (1989). Targeting of nonexpressed genes in embryonic stem cells via homologous recombination. Science *245*, 1234–1236.

Johnston, R.J., Poholek, A.C., DiToro, D., Yusuf, I., Eto, D., Barnett, B., Dent, A.L., Craft, J., and Crotty, S. (2009). Bcl6 and Blimp-1 are reciprocal and antagonistic regulators of T follicular helper cell differentiation. Science *325*, 1006–1010.

Joyner, A.L., Skarnes, W.C., and Rossant, J. (1989). Production of a mutation in mouse En-2 gene by homologous recombination in embryonic stem cells. Nature *338*, 153–156.

Justice, M.J., Noveroske, J.K., Weber, J.S., Zheng, B., and Bradley, A. (1999). Mouse ENU mutagenesis. Hum Mol Genet *8*, 1955–1963.

Karasuyama, H., Rolink, A., Shinkai, Y., Young, F., Alt, F.W., and Melchers, F. (1994). The expression of Vpre-B/lambda 5 surrogate light chain in early bone marrow precursor B cells of normal and B cell-deficient mutant mice. Cell *77*, 133–143.

Kaufman, M.H., Robertson, E.J., Handyside, A.H., and Evans, M.J. (1983). Establishment of pluripotential cell lines from haploid mouse embryos. J Embryol Exp Morphol *73*, 249–261.

Keane, T.M., Goodstadt, L., Danecek, P., White, M.A., Wong, K., Yalcin, B., Heger, A., Agam, A., Slater, G., Goodson, M., et al. (2011). Mouse genomic variation and its effect on phenotypes and gene regulation. Nature *477*, 289–294.

Kikuchi, K., and Kondo, M. (2006). Developmental switch of mouse hematopoietic stem cells from fetal to adult type occurs in bone marrow after birth. Proc Natl Acad Sci USA *103*, 17852–17857.

Kikuchi, K., Kasai, H., Watanabe, A., Lai, A.Y., and Kondo, M. (2008). IL-7 specifies B cell fate at the common lymphoid progenitor to pre-proB transition stage by maintaining early B cell factor expression. J Immunol *181*, 383–392.

Kikuchi, K., Lai, A.Y., Hsu, C.-L., and Kondo, M. (2005). IL-7 receptor signaling is necessary for stage transition in adult B cell development through up-regulation of EBF. J Exp Med *201*, 1197–1203.

Kile, B.T., Hentges, K.E., Clark, A.T., Nakamura, H., Salinger, A.P., Liu, B., Box, N., Stockton, D.W., Johnson, R.L., Behringer, R.R., et al. (2003). Functional genetic analysis of mouse chromosome 11. Nature *425*, 81–86.

Kim, K., Ng, K., Rugg-Gunn, P.J., Shieh, J.-H., Kirak, O., Jaenisch, R., Wakayama, T., Moore, M.A., Pedersen, R.A., and Daley, G.Q. (2007). Recombination signatures distinguish embryonic stem cells derived by parthenogenesis and somatic cell nuclear transfer. Cell Stem Cell *1*, 346–352.

Kim, Y.G., Cha, J., and Chandrasegaran, S. (1996). Hybrid restriction enzymes: zinc finger fusions to Fok I cleavage domain. Proc Natl Acad Sci USA *93*, 1156–1160.

Klug, A. (2010). The discovery of zinc fingers and their applications in gene regulation and genome manipulation. Annu Rev Biochem *79*, 213–231.

Knudson, A.G. (1971). Mutation and cancer: statistical study of retinoblastoma. Proc Natl Acad Sci USA *68*, 820–823.

Koch, R. (1876). Untersuchungen über Bakterien: V. Die Ätiologie der Milzbrand-Krankheit, begründet auf die Entwicklungsgeschichte des Bacillus anthracis. Cohns Beitrage Zur Biologie Der Pflanzen *2*, 277–310.

Koga, A., Suzuki, M., Inagaki, H., Bessho, Y., and Hori, H. (1996). Transposable element in fish. Nature *383*, 30.

Koller, B.H., and Smithies, O. (1989). Inactivating the beta 2-microglobulin locus in mouse embryonic stem cells by homologous recombination. Proc Natl Acad Sci USA *86*, 8932–8935.

Kondo, M., Weissman, I.L., and Akashi, K. (1997). Identification of clonogenic common lymphoid progenitors in mouse bone marrow. Cell *91*, 661–672.

Kono, T., Obata, Y., Wu, Q., Niwa, K., Ono, Y., Yamamoto, Y., Park, E.S., Seo, J.-S., and Ogawa, H. (2004). Birth of parthenogenetic mice that can develop to adulthood. Nature *428*, 860–864.

Kosan, C., Saba, I., Godmann, M., Herold, S., Herkert, B., Eilers, M., and Möröy, T. (2010). Transcription factor miz-1 is required to regulate interleukin-7 receptor signaling at early commitment stages of B cell differentiation. Immunity *33*, 917–928.

Kotecki, M., Reddy, P.S., and Cochran, B.H. (1999). Isolation and characterization of a near-haploid human cell line. Exp Cell Res *252*, 273–280.

Kovalovsky, D., Uche, O.U., Eladad, S., Hobbs, R.M., Yi, W., Alonzo, E., Chua, K., Eidson, M., Kim, H.-J., Im, J.S., et al. (2008). The BTB-zinc finger transcriptional regulator PLZF controls the development of invariant natural killer T cell effector functions. Nat Immunol *9*, 1055–1064.

Kravchenko, J.E., Rogozin, I.B., Koonin, E.V., and Chumakov, P.M. (2005). Transcription of mammalian

messenger RNAs by a nuclear RNA polymerase of mitochondrial origin. Nature *436*, 735–739.

Kuehn, M.R., Bradley, A., Robertson, E.J., and Evans, M.J. (1987). A potential animal model for Lesch-Nyhan syndrome through introduction of HPRT mutations into mice. Nature *326*, 295–298.

Kühlbrandt, W. (2004). Biology, structure and mechanism of P-type ATPases. Nat Rev Mol Cell Biol *5*, 282–295.

Kühn, R., Schwenk, F., Aguet, M., and Rajewsky, K. (1995). Inducible gene targeting in mice. Science *269*, 1427–1429.

Lakso, M., Sauer, B., Mosinger, B., Lee, E.J., Manning, R.W., Yu, S.H., Mulder, K.L., and Westphal, H. (1992). Targeted oncogene activation by site-specific recombination in transgenic mice. Proc Natl Acad Sci USA *89*, 6232–6236.

Lander, E.S., Linton, L.M., Birren, B., Nusbaum, C., Zody, M.C., Baldwin, J., Devon, K., Dewar, K., Doyle, M., FitzHugh, W., et al. (2001). Initial sequencing and analysis of the human genome. Nature *409*, 860–921.

Lazorchak, A.S., Liu, D., Facchinetti, V., Di Lorenzo, A., Sessa, W.C., Schatz, D.G., and Su, B. (2010). Sin1-mTORC2 suppresses rag and il7r gene expression through Akt2 in B cells. Mol Cell *39*, 433–443.

Le Fur, N., Kelsall, S.R., and Mintz, B. (1996). Base substitution at different alternative splice donor sites of the tyrosinase gene in murine albinism. Genomics *37*, 245–248.

Le Gall, S.M., Bobé, P., Reiss, K., Horiuchi, K., Niu, X.-D., Lundell, D., Gibb, D.R., Conrad, D., Saftig, P., and Blobel, C.P. (2009). ADAMs 10 and 17 represent differentially regulated components of a general shedding machinery for membrane proteins such as transforming growth factor alpha, L-selectin, and tumor necrosis factor alpha. Mol Biol Cell *20*, 1785–1794.

Lee, J.R., Urban, S., Garvey, C.F., and Freeman, M. (2001). Regulated intracellular ligand transport and proteolysis control EGF signal activation in Drosophila. Cell *107*, 161–171.

Lee, R.C., Feinbaum, R.L., and Ambros, V. (1993). The C. elegans heterochronic gene lin-4 encodes small RNAs with antisense complementarity to lin-14. Cell *75*, 843–854.

Leeb, M., and Wutz, A. (2011). Derivation of haploid embryonic stem cells from mouse embryos. Nature *479*, 131–134.

Leeb, M., Walker, R., Mansfield, B., Nichols, J., Smith, A., and Wutz, A. (2012). Germline potential of parthenogenetic haploid mouse embryonic stem cells. Development *139*, 3301–3305.

Lemaitre, B., Nicolas, E., Michaut, L., Reichhart, J.M., and Hoffmann, J.A. (1996). The dorsoventral regulatory gene cassette spätzle/Toll/cactus controls the potent antifungal response in Drosophila adults. Cell *86*, 973–983.

Leventis, P.A., and Grinstein, S. (2010). The distribution and function of phosphatidylserine in cellular membranes. Annu Rev Biophys *39*, 407–427.

Lewis, M.A., Quint, E., Glazier, A.M., Fuchs, H., de Angelis, M.H., Langford, C., van Dongen, S., Abreu-Goodger, C., Piipari, M., Redshaw, N., et al. (2009). An ENU-induced mutation of miR-96 associated with progressive hearing loss in mice. Nat Genet *41*, 614–618.

Li, F.-Y., Chaigne-Delalande, B., Kanellopoulou, C., Davis, J.C., Matthews, H.F., Douek, D.C., Cohen, J.I., Uzel, G., Su, H.C., and Lenardo, M.J. (2011a). Second messenger role for Mg2+ revealed by human T-cell immunodeficiency. Nature *475*, 471–476.

Li, M.A., Turner, D.J., Ning, Z., Yusa, K., Liang, Q., Eckert, S., Rad, L., Fitzgerald, T.W., Craig, N.L., and

Bradley, A. (2011b). Mobilization of giant piggyBac transposons in the mouse genome. Nucleic Acids Res.

Liang, Q., Kong, J., Stalker, J., and Bradley, A. (2009). Chromosomal mobilization and reintegration of Sleeping Beauty and PiggyBac transposons. Genesis *47*, 404–408.

Lilienbaum, A., Sage, J., Mémet, S., Rassoulzadegan, M., Cuzin, F., and Israël, A. (2000). NF-kappa B is developmentally regulated during spermatogenesis in mice. Dev Dyn *219*, 333–340.

Lin, H., and Grosschedl, R. (1995). Failure of B-cell differentiation in mice lacking the transcription factor EBF. Nature *376*, 263–267.

Linehan, W.M., Srinivasan, R., and Schmidt, L.S. (2010). The genetic basis of kidney cancer: a metabolic disease. Nat Rev Urol *7*, 277–285.

Lo, J.C., Basak, S., James, E.S., Quiambo, R.S., Kinsella, M.C., Alegre, M.-L., Weih, F., Franzoso, G., Hoffmann, A., and Fu, Y.-X. (2006). Coordination between NF-kappaB family members p50 and p52 is essential for mediating LTbetaR signals in the development and organization of secondary lymphoid tissues. Blood *107*, 1048–1055.

Lopes-Carvalho, T., Foote, J., and Kearney, J.F. (2005). Marginal zone B cells in lymphocyte activation and regulation. Curr Opin Immunol *17*, 244–250.

Luedde, T., Beraza, N., Kotsikoris, V., van Loo, G., Nenci, A., de Vos, R., Roskams, T., Trautwein, C., and Pasparakis, M. (2007). Deletion of NEMO/IKKgamma in liver parenchymal cells causes steatohepatitis and hepatocellular carcinoma. Cancer Cell *11*, 119–132.

Lunter, G., and Goodson, M. (2011). Stampy: a statistical algorithm for sensitive and fast mapping of Illumina sequence reads. Genome Res *21*, 936–939.

Luo, G., Santoro, I.M., McDaniel, L.D., Nishijima, I., Mills, M., Youssoufian, H., Vogel, H., Schultz, R.A., and Bradley, A. (2000). Cancer predisposition caused by elevated mitotic recombination in Bloom mice. Nat Genet *26*, 424–429.

Lupski, J.R., Reid, J.G., Gonzaga-Jauregui, C., Rio Deiros, D., Chen, D.C.Y., Nazareth, L., Bainbridge, M., Dinh, H., Jing, C., Wheeler, D.A., et al. (2010). Whole-genome sequencing in a patient with Charcot-Marie-Tooth neuropathy. N Engl J Med *362*, 1181–1191.

Lyon, M., and Searle, A. (1989). Genetic Variants and Strains of the Laboratory Mouse. Oxford University Press.

MacArthur, D.G., Balasubramanian, S., Frankish, A., Huang, N., Morris, J., Walter, K., Jostins, L., Habegger, L., Pickrell, J.K., Montgomery, S.B., et al. (2012). A systematic survey of loss-of-function variants in human protein-coding genes. Science *335*, 823–828.

Maeda, T., Ito, K., Merghoub, T., Poliseno, L., Hobbs, R.M., Wang, G., Dong, L., Maeda, M., Dore, L.C., and Zelent, A. (2009). LRF Is an Essential Downstream Target of GATA1 in Erythroid Development and Regulates BIM-Dependent Apoptosis. Dev Cell *17*, 527–540.

Maeda, T., Merghoub, T., Hobbs, R.M., Dong, L., Maeda, M., Zakrzewski, J., van den Brink, M.R.M., Zelent, A., Shigematsu, H., Akashi, K., et al. (2007). Regulation of B Versus T Lymphoid Lineage Fate Decision by the Proto-Oncogene LRF. Science *316*, 860–866.

Makris, C., Godfrey, V.L., Krähn-Senftleben, G., Takahashi, T., Roberts, J.L., Schwarz, T., Feng, L., Johnson, R.S., and Karin, M. (2000). Female mice heterozygous for IKK gamma/NEMO deficiencies develop a dermatopathy similar to the human X-linked disorder incontinentia pigmenti. Mol Cell *5*, 969–979.

Malin, S., McManus, S., Cobaleda, C., Novatchkova, M., Delogu, A., Bouillet, P., Strasser, A., and

Busslinger, M. (2010). Role of STAT5 in controlling cell survival and immunoglobulin gene recombination during pro-B cell development. Nat Immunol *11*, 171–179.

Maraskovsky, E., Peschon, J.J., McKenna, H., Teepe, M., and Strasser, A. (1998). Overexpression of Bcl-2 does not rescue impaired B lymphopoiesis in IL-7 receptor-deficient mice but can enhance survival of mature B cells. Int Immunol *10*, 1367–1375.

Mariathasan, S., Weiss, D.S., Newton, K., McBride, J., O'Rourke, K., Roose-Girma, M., Lee, W.P., Weinrauch, Y., Monack, D.M., and Dixit, V.M. (2006). Cryopyrin activates the inflammasome in response to toxins and ATP. Nature *440*, 228–232.

Marié, I., Durbin, J.E., and Levy, D.E. (1998). Differential viral induction of distinct interferon-alpha genes by positive feedback through interferon regulatory factor-7. Embo J *17*, 6660–6669.

Martinon, F., Burns, K., and Tschopp, J. (2002). The inflammasome: a molecular platform triggering activation of inflammatory caspases and processing of proIL-beta. Mol Cell *10*, 417–426.

Martinon, F., Pétrilli, V., Mayor, A., Tardivel, A., and Tschopp, J. (2006). Gout-associated uric acid crystals activate the NALP3 inflammasome. Nature *440*, 237–241.

Masuya, H., Sezutsu, H., Sakuraba, Y., Sagai, T., Hosoya, M., Kaneda, H., Miura, I., Kobayashi, K., Sumiyama, K., Shimizu, A., et al. (2007). A series of ENU-induced single-base substitutions in a long-range cis-element altering Sonic hedgehog expression in the developing mouse limb bud. Genomics *89*, 207–214.

Matic, I., Schimmel, J., Hendriks, I.A., van Santen, M.A., van de Rijke, F., van Dam, H., Gnad, F., Mann, M., and Vertegaal, A.C.O. (2010). Site-Specific Identification of SUMO-2 Targets in Cells Reveals an Inverted SUMOylation Motif and a Hydrophobic Cluster SUMOylation Motif. Mol Cell *39*, 641–652.

McClintock, B. (1950). The origin and behavior of mutable loci in maize. Proc Natl Acad Sci USA *36*, 344–355.

McIlwain, D.R., Lang, P.A., Maretzky, T., Hamada, K., Ohishi, K., Maney, S.K., Berger, T., Murthy, A., Duncan, G., Xu, H.C., et al. (2012). iRhom2 regulation of TACE controls TNF-mediated protection against Listeria and responses to LPS. Science *335*, 229–232.

McKusick, V.A. (2006). A 60-year tale of spots, maps, and genes. Annual Review of Genomics and Human Genetics *7*, 1–27.

Mendel, G. (1866). Versuche uber Pflanzen-Hybriden. Verhandlungen Des Naturforschenden Vereines in Brünn *4*, 3–47.

Miller, J., McLachlan, A.D., and Klug, A. (1985). Repetitive zinc-binding domains in the protein transcription factor IIIA from Xenopus oocytes. Embo J *4*, 1609–1614.

Miller, J.F. (1961). Immunological function of the thymus. Lancet *2*, 748–749.

Miosge, L.A., and Goodnow, C.C. (2005). Genes, pathways and checkpoints in lymphocyte development and homeostasis. Immunol Cell Biol *83*, 318–335.

Mohammed, F.F., Smookler, D.S., Taylor, S.E.M., Fingleton, B., Kassiri, Z., Sanchez, O.H., English, J.L., Matrisian, L.M., Au, B., Yeh, W.-C., et al. (2004). Abnormal TNF activity in Timp3-/- mice leads to chronic hepatic inflammation and failure of liver regeneration. Nat Genet *36*, 969–977.

Morgan, T.H. (1911). RANDOM SEGREGATION VERSUS COUPLING IN MENDELIAN INHERITANCE. Science *34*, 384.

Morton, N.E. (1955). Sequential tests for the detection of linkage. Am J Hum Genet *7*, 277–318.

Moscou, M.J., and Bogdanove, A.J. (2009). A simple cipher governs DNA recognition by TAL effectors. Science *326*, 1501.

Moser, A.R., Pitot, H.C., and Dove, W.F. (1990). A dominant mutation that predisposes to multiple intestinal neoplasia in the mouse. Science *247*, 322–324.

Moss, M.L., Jin, S.L., Milla, M.E., Bickett, D.M., Burkhart, W., Carter, H.L., Chen, W.J., Clay, W.C., Didsbury, J.R., Hassler, D., et al. (1997). Cloning of a disintegrin metalloproteinase that processes precursor tumour-necrosis factor-alpha. Nature *385*, 733–736.

Mouse Genome Sequencing Consortium, Waterston, R.H., Lindblad-Toh, K., Birney, E., Rogers, J., Abril, J.F., Agarwal, P., Agarwala, R., Ainscough, R., Alexandersson, M., et al. (2002). Initial sequencing and comparative analysis of the mouse genome. Nature *420*, 520–562.

Muller, H.J. (1918). Genetic Variability, Twin Hybrids and Constant Hybrids, in a Case of Balanced Lethal Factors. Genetics *3*, 422–499.

Muller, H.J. (1927). ARTIFICIAL TRANSMUTATION OF THE GENE. Science *66*, 84–87.

Muller, H.J. (1932). Further studies on the nature and causes of gene mutations. Proceedings of the 6th International Congress of Genetics 213–255.

Mullighan, C.G., Goorha, S., Radtke, I., Miller, C.B., Coustan-Smith, E., Dalton, J.D., Girtman, K., Mathew, S., Ma, J., Pounds, S.B., et al. (2007). Genome-wide analysis of genetic alterations in acute lymphoblastic leukaemia. Nature *446*, 758–764.

Mullighan, C.G., Miller, C.B., Radtke, I., Phillips, L.A., Dalton, J., Ma, J., White, D., Hughes, T.P., Le Beau, M.M., Pui, C.-H., et al. (2008). BCR-ABL1 lymphoblastic leukaemia is characterized by the deletion of Ikaros. Nature *453*, 110–114.

Munroe, R.J., Bergstrom, R.A., Zheng, Q.Y., Libby, B., Smith, R., John, S.W., Schimenti, K.J., Browning, V.L., and Schimenti, J.C. (2000). Mouse mutants from chemically mutagenized embryonic stem cells. Nat Genet *24*, 318–321.

Na Nakorn, T., Traver, D., Weissman, I.L., and Akashi, K. (2002). Myeloerythroid-restricted progenitors are sufficient to confer radioprotection and provide the majority of day 8 CFU-S. J Clin Invest *109*, 1579–1585.

Nagai, Y., Akashi, S., Nagafuku, M., Ogata, M., Iwakura, Y., Akira, S., Kitamura, T., Kosugi, A., Kimoto, M., and Miyake, K. (2002). Essential role of MD-2 in LPS responsiveness and TLR4 distribution. Nat Immunol *3*, 667–672.

Napoli, C., Lemieux, C., and Jorgensen, R. (1990). Introduction of a Chimeric Chalcone Synthase Gene into Petunia Results in Reversible Co-Suppression of Homologous Genes in trans. Plant Cell *2*, 279–289.

Nelms, K.A., and Goodnow, C.C. (2001). Genome-wide ENU mutagenesis to reveal immune regulators. Immunity *15*, 409–418.

Nenci, A., Becker, C., Wullaert, A., Gareus, R., van Loo, G., Danese, S., Huth, M., Nikolaev, A., Neufert, C., Madison, B., et al. (2007). Epithelial NEMO links innate immunity to chronic intestinal inflammation. Nature *446*, 557–561.

Nenci, A., Huth, M., Funteh, A., Schmidt-Supprian, M., Bloch, W., Metzger, D., Chambon, P., Rajewsky, K., Krieg, T., Haase, I., et al. (2006). Skin lesion development in a mouse model of incontinentia pigmenti is triggered by NEMO deficiency in epidermal keratinocytes and requires TNF signaling. Hum Mol Genet *15*, 531–542.

Ng, S.B., Bigham, A.W., Buckingham, K.J., Hannibal, M.C., McMillin, M.J., Gildersleeve, H.I., Beck, A.E.,

Tabor, H.K., Cooper, G.M., Mefford, H.C., et al. (2010). Exome sequencing identifies MLL2 mutations as a cause of Kabuki syndrome. Nat Genet *42*, 790–793.

Ngo, V.N., Davis, R.E., Lamy, L., Yu, X., Zhao, H., Lenz, G., Lam, L.T., Dave, S., Yang, L., Powell, J., et al. (2006). A loss-of-function RNA interference screen for molecular targets in cancer. Nature *441*, 106–110.

Ni, C.-Y., Wu, Z.-H., Florence, W.C., Parekh, V.V., Arrate, M.P., Pierce, S., Schweitzer, B., van Kaer, L., Joyce, S., Miyamoto, S., et al. (2008). Cutting edge: K63-linked polyubiquitination of NEMO modulates TLR signaling and inflammation in vivo. J Immunol *180*, 7107–7111.

Nickerson, M.L., Warren, M.B., Toro, J.R., Matrosova, V., Glenn, G., Turner, M.L., Duray, P., Merino, M., Choyke, P., Pavlovich, C.P., et al. (2002). Mutations in a novel gene lead to kidney tumors, lung wall defects, and benign tumors of the hair follicle in patients with the Birt-Hogg-Dubé syndrome. Cancer Cell *2*, 157–164.

Niehues, T., Reichenbach, J., Neubert, J., Gudowius, S., Puel, A., Horneff, G., Lainka, E., Dirksen, U., Schroten, H., Döffinger, R., et al. (2004). Nuclear factor kappaB essential modulator-deficient child with immunodeficiency yet without anhidrotic ectodermal dysplasia. J Allergy Clin Immunol *114*, 1456–1462.

Nurieva, R.I., Chung, Y., Martinez, G.J., Yang, X.O., Tanaka, S., Matskevitch, T.D., Wang, Y.-H., and Dong, C. (2009). Bcl6 mediates the development of T follicular helper cells. Science *325*, 1001–1005.

Nüsslein-Volhard, C., and Wieschaus, E. (1980). Mutations affecting segment number and polarity in Drosophila. Nature *287*, 795–801.

Okimoto, K., Kouchi, M., Matsumoto, I., Sakurai, J., Kobayashi, T., and Hino, O. (2004). Natural history of the Nihon rat model of BHD. Curr. Mol. Med. *4*, 887–893.

Oliver, P.M., Wang, M., Zhu, Y., White, J., Kappler, J., and Marrack, P. (2004). Loss of Bim allows precursor B cell survival but not precursor B cell differentiation in the absence of interleukin 7. J Exp Med *200*, 1179–1187.

Orange, J.S., Brodeur, S.R., Jain, A., Bonilla, F.A., Schneider, L.C., Kretschmer, R., Nurko, S., Rasmussen, W.L., Köhler, J.R., Gellis, S.E., et al. (2002). Deficient natural killer cell cytotoxicity in patients with IKK-gamma/NEMO mutations. J Clin Invest *109*, 1501–1509.

Orange, J.S., Levy, O., Brodeur, S.R., Krzewski, K., Roy, R.M., Niemela, J.E., Fleisher, T.A., Bonilla, F.A., and Geha, R.S. (2004). Human nuclear factor kappa B essential modulator mutation can result in immunodeficiency without ectodermal dysplasia. J Allergy Clin Immunol *114*, 650–656.

Orban, P.C., Chui, D., and Marth, J.D. (1992). Tissue- and site-specific DNA recombination in transgenic mice. Proc Natl Acad Sci USA *89*, 6861–6865.

Orr-Weaver, T.L., Szostak, J.W., and Rothstein, R.J. (1981). Yeast transformation: a model system for the study of recombination. Proc Natl Acad Sci USA *78*, 6354–6358.

Osmond, D.G., and Nossal, G.J. (1974). Differentiation of lymphocytes in mouse bone marrow. II. Kinetics of maturation and renewal of antiglobulin-binding cells studied by double labeling. Cell Immunol *13*, 132–145.

Owen, J.J., Cooper, M.D., and Raff, M.C. (1974). In vitro generation of B lymphocytes in mouse foetal liver, a mammalian 'bursa equivalent'. Nature *249*, 361–363.

Pancer, Z., Amemiya, C.T., Ehrhardt, G.R.A., Ceitlin, J., Gartland, G.L., and Cooper, M.D. (2004). Somatic diversification of variable lymphocyte receptors in the agnathan sea lamprey. Nature *430*, 174–180.

Park, H., Staehling, K., Tsang, M., Appleby, M.W., Brunkow, M.E., Margineantu, D., Hockenbery, D.M., Habib, T., Liggitt, H.D., Carlson, G., et al. (2012). Disruption of fnip1 reveals a metabolic checkpoint

controlling B lymphocyte development. Immunity *36*, 769–781.

Pasparakis, M., Schmidt-Supprian, M., and Rajewsky, K. (2002). IkappaB kinase signaling is essential for maintenance of mature B cells. J Exp Med *196*, 743–752.

Pelanda, R., Schaal, S., Torres, R.M., and Rajewsky, K. (1996). A prematurely expressed Ig(kappa) transgene, but not V(kappa)J(kappa) gene segment targeted into the Ig(kappa) locus, can rescue B cell development in lambda5-deficient mice. Immunity *5*, 229–239.

Peschon, J.J., Morrissey, P.J., Grabstein, K.H., Ramsdell, F.J., Maraskovsky, E., Gliniak, B.C., Park, L.S., Ziegler, S.F., Williams, D.E., Ware, C.B., et al. (1994). Early lymphocyte expansion is severely impaired in interleukin 7 receptor-deficient mice. J Exp Med *180*, 1955–1960.

Peschon, J.J., Slack, J.L., Reddy, P., Stocking, K.L., Sunnarborg, S.W., Lee, D.C., Russell, W.E., Castner, B.J., Johnson, R.S., Fitzner, J.N., et al. (1998). An essential role for ectodomain shedding in mammalian development. Science *282*, 1281–1284.

Pfeiffer, R. (1892). Untersuchungen über das Choleragift. Zeitschr. F. Hygiene. *11*, 393–412.

Phan, T.G., Amesbury, M., Gardam, S., Crosbie, J., Hasbold, J., Hodgkin, P.D., Basten, A., and Brink, R. (2003). B cell receptor-independent stimuli trigger immunoglobulin (Ig) class switch recombination and production of IgG autoantibodies by anergic self-reactive B cells. J Exp Med *197*, 845–860.

Poltorak, A., He, X., Smirnova, I., Liu, M.Y., van Huffel, C., Du, X., Birdwell, D., Alejos, E., Silva, M., Galanos, C., et al. (1998). Defective LPS signaling in C3H/HeJ and C57BL/10ScCr mice: mutations in Tlr4 gene. Science *282*, 2085–2088.

Pruitt, K.D., Tatusova, T., Brown, G.R., and Maglott, D.R. (2012). NCBI Reference Sequences (RefSeq): current status, new features and genome annotation policy. Nucleic Acids Res *40*, D130–D135.

Purohit, S.J., Stephan, R.P., Kim, H.-G., Herrin, B.R., Gartland, L., and Klug, C.A. (2003). Determination of lymphoid cell fate is dependent on the expression status of the IL-7 receptor. Embo J *22*, 5511–5521.

Radtke, F., Wilson, A., Stark, G., Bauer, M., van Meerwijk, J., MacDonald, H.R., and Aguet, M. (1999). Deficient T cell fate specification in mice with an induced inactivation of Notch1. Immunity *10*, 547–558.

Raff, M.C., Megson, M., Owen, J.J., and Cooper, M.D. (1976). Early production of intracellular IgM by B-lymphocyte precursors in mouse. Nature *259*, 224–226.

Rathinam, C., Poueymirou, W.T., Rojas, J., Murphy, A.J., Valenzuela, D.M., Yancopoulos, G.D., Rongvaux, A., Eynon, E.E., Manz, M.G., and Flavell, R.A. (2011). Efficient differentiation and function of human macrophages in humanized CSF-1 mice. Blood *118*, 3119–3128.

Revazova, E.S., Turovets, N.A., Kochetkova, O.D., Kindarova, L.B., Kuzmichev, L.N., Janus, J.D., and Pryzhkova, M.V. (2007). Patient-specific stem cell lines derived from human parthenogenetic blastocysts. Cloning Stem Cells *9*, 432–449.

Rickert, R.C., Rajewsky, K., and Roes, J. (1995). Impairment of T-cell-dependent B-cell responses and B-1 cell development in CD19-deficient mice. Nature *376*, 352–355.

Robertson, E., Bradley, A., Kuehn, M., and Evans, M. (1986). Germ-line transmission of genes introduced into cultured pluripotential cells by retroviral vector. Nature *323*, 445–448.

Roessler, S., Györy, I., Imhof, S., Spivakov, M., Williams, R.R., Busslinger, M., Fisher, A.G., and Grosschedl, R. (2007). Distinct promoters mediate the regulation of Ebf1 gene expression by interleukin-7 and Pax5. Mol Cell Biol *27*, 579–594.

Rothenberg, E.V., and Taghon, T. (2005). Molecular genetics of T cell development. Annu Rev Immunol

23, 601–649.

Rous, P. (1911). A SARCOMA OF THE FOWL TRANSMISSIBLE BY AN AGENT SEPARABLE FROM THE TUMOR CELLS. J Exp Med *13*, 397–411.

Rousseau, S., Papoutsopoulou, M., Symons, A., Cook, D., Lucocq, J.M., Prescott, A.R., O'Garra, A., Ley, S.C., and Cohen, P. (2008). TPL2-mediated activation of ERK1 and ERK2 regulates the processing of pre-TNF alpha in LPS-stimulated macrophages. J Cell Sci *121*, 149–154.

Römer, P., Hahn, S., Jordan, T., Strauss, T., Bonas, U., and Lahaye, T. (2007). Plant pathogen recognition mediated by promoter activation of the pepper Bs3 resistance gene. Science *318*, 645–648.

Rudolph, D., Yeh, W.C., Wakeham, A., Rudolph, B., Nallainathan, D., Potter, J., Elia, A.J., and Mak, T.W. (2000). Severe liver degeneration and lack of NF-kappaB activation in NEMO/IKKgamma-deficient mice. Genes Dev *14*, 854–862.

Russell, W.L. (1951). X-ray-induced mutations in mice. Cold Spring Harb Symp Quant Biol *16*, 327–336.

Russell, W.L. (1962). An augmenting effect of dose fractionation on radiation-induced mutation rate in mice. Proc Natl Acad Sci USA *48*, 1724–1727.

Russell, W.L., Kelly, E.M., Hunsicker, P.R., Bangham, J.W., Maddux, S.C., and Phipps, E.L. (1979). Specific-locus test shows ethylnitrosourea to be the most potent mutagen in the mouse. Proc Natl Acad Sci USA *76*, 5818–5819.

Russell, W.L., Russell, L.B., and Gower, J.S. (1959). EXCEPTIONAL INHERITANCE OF A SEX-LINKED GENE IN THE MOUSE EXPLAINED ON THE BASIS THAT THE X/O SEX-CHROMOSOME CONSTITUTION IS FEMALE. Proc Natl Acad Sci USA *45*, 554–560.

Rutschmann, S., Hoebe, K., Zalevsky, J., Du, X., Mann, N., Dahiyat, B.I., Steed, P., and Beutler, B. (2006). PanR1, a dominant negative missense allele of the gene encoding TNF-alpha (Tnf), does not impair lymphoid development. J Immunol *176*, 7525–7532.

Saiki, R.K., Scharf, S., Faloona, F., Mullis, K.B., Horn, G.T., Erlich, H.A., and Arnheim, N. (1985). Enzymatic amplification of beta-globin genomic sequences and restriction site analysis for diagnosis of sickle cell anemia. Science *230*, 1350–1354.

Sakurai, H., Chiba, H., Miyoshi, H., Sugita, T., and Toriumi, W. (1999). IkappaB kinases phosphorylate NF-kappaB p65 subunit on serine 536 in the transactivation domain. J Biol Chem *274*, 30353–30356.

Salt, B., Niemela, J., Pandey, R., Hanson, E., Deering, R., Quinones, R., Jain, A., Orange, J., and Gelfand, E. (2008). IKBKG (nuclear factor-kappaB essential modulator) mutation can be associated with opportunistic infection without impairing Toll-like receptor function. J Allergy Clin Immunol.

Sanger, F., Nicklen, S., and Coulson, A.R. (1977). DNA sequencing with chain-terminating inhibitors. Proc Natl Acad Sci USA *74*, 5463–5467.

Sauer, B., and Henderson, N. (1988). Site-specific DNA recombination in mammalian cells by the Cre recombinase of bacteriophage P1. Proc Natl Acad Sci USA *85*, 5166–5170.

Savage, A.K., Constantinides, M.G., Han, J., Picard, D., Martin, E., Li, B., Lantz, O., and Bendelac, A. (2008). The transcription factor PLZF directs the effector program of the NKT cell lineage. Immunity *29*, 391–403.

Schmidt-Supprian, M., Bloch, W., Courtois, G., Addicks, K., Israël, A., Rajewsky, K., and Pasparakis, M. (2000). NEMO/IKK gamma-deficient mice model incontinentia pigmenti. Mol Cell *5*, 981–992.

Schmidt-Supprian, M., Courtois, G., Tian, J., Coyle, A.J., Israël, A., Rajewsky, K., and Pasparakis, M.

(2003). Mature T cells depend on signaling through the IKK complex. Immunity *19*, 377–389.

Schmidt-Ullrich, R., Aebischer, T., Hülsken, J., Birchmeier, W., Klemm, U., and Scheidereit, C. (2001). Requirement of NF-kappaB/Rel for the development of hair follicles and other epidermal appendices. Development *128*, 3843–3853.

Schwartzberg, P.L., Goff, S.P., and Robertson, E.J. (1989). Germ-line transmission of a c-abl mutation produced by targeted gene disruption in ES cells. Science *246*, 799–803.

Seymour, R.E., Hasham, M.G., Cox, G.A., Shultz, L.D., Hogenesch, H., Roopenian, D.C., and Sundberg, J.P. (2007). Spontaneous mutations in the mouse Sharpin gene result in multiorgan inflammation, immune system dysregulation and dermatitis. Genes Immun *8*, 416–421.

Shultz, L.D., Ishikawa, F., and Greiner, D.L. (2007). Humanized mice in translational biomedical research. Nat Rev Immunol *7*, 118–130.

Siggs, O.M., Arnold, C.N., Huber, C., Pirie, E., Xia, Y., Lin, P., Nemazee, D., and Beutler, B. (2011a). The P4-type ATPase ATP11C is essential for B lymphopoiesis in adult bone marrow. Nat Immunol *12*, 434–440.

Siggs, O.M., Berger, M., Krebs, P., Arnold, C.N., Eidenschenk, C., Huber, C., Pirie, E., Smart, N.G., Khovananth, K., Xia, Y., et al. (2010). A mutation of Ikbkg causes immune deficiency without impairing degradation of IkappaB alpha. Proc Natl Acad Sci USA *107*, 3046–3051.

Siggs, O.M., Li, X., Xia, Y., and Beutler, B. (2012a). ZBTB1 is a determinant of lymphoid development. J Exp Med *209*, 19–27.

Siggs, O.M., Schnabl, B., Webb, B., and Beutler, B. (2011b). X-linked cholestasis in mouse due to mutations of the P4-ATPase ATP11C. Proc Natl Acad Sci USA *108*, 7890–7895.

Siggs, O.M., Xiao, N., Wang, Y., Shi, H., Tomisato, W., Li, X., Xia, Y., and Beutler, B. (2012b). iRhom2 is required for the secretion of mouse TNFα. Blood *119*, 5769–5771.

Silver, L.M. (1995). Mouse genetics: concepts and applications.

Siminovitch, L. (1976). On the nature of hereditable variation in cultured somatic cells. Cell *7*, 1–11.

Sitnicka, E., Brakebusch, C., Mårtensson, I.-L., Svensson, M., Agace, W.W., Sigvardsson, M., Buza-Vidas, N., Bryder, D., Cilio, C.M., Ahlenius, H., et al. (2003). Complementary signaling through flt3 and interleukin-7 receptor alpha is indispensable for fetal and adult B cell genesis. J Exp Med *198*, 1495–1506.

Skarnes, W.C., Rosen, B., West, A.P., Koutsourakis, M., Bushell, W., Iyer, V., Mujica, A.O., Thomas, M., Harrow, J., Cox, T., et al. (2011). A conditional knockout resource for the genome-wide study of mouse gene function. Nature *474*, 337–342.

Smahi, A., Courtois, G., Vabres, P., Yamaoka, S., Heuertz, S., Munnich, A., Israël, A., Heiss, N.S., Klauck, S.M., Kioschis, P., et al. (2000). Genomic rearrangement in NEMO impairs NF-kappaB activation and is a cause of incontinentia pigmenti. The International Incontinentia Pigmenti (IP) Consortium. Nature *405*, 466–472.

Smerdou, C., and Liljeström, P. (1999). Two-helper RNA system for production of recombinant Semliki forest virus particles. J Virol *73*, 1092–1098.

Smith, H.O., and Wilcox, K.W. (1970). A restriction enzyme from Hemophilus influenzae. I. Purification and general properties. J Mol Biol *51*, 379–391.

Smithies, O., Gregg, R.G., Boggs, S.S., Koralewski, M.A., and Kucherlapati, R.S. (1985). Insertion of DNA sequences into the human chromosomal beta-globin locus by homologous recombination. Nature *317*,

230–234.

Snell, G.D. (1935). The Induction by X-Rays of Hereditary Changes in Mice. Genetics *20*, 545–567.

Snell, G.D. (1948). Methods for the study of histocompatibility genes. J. Genet. *49*, 87–108.

Spanopoulou, E., Roman, C.A., Corcoran, L.M., Schlissel, M.S., Silver, D.P., Nemazee, D., Nussenzweig, M.C., Shinton, S.A., Hardy, R.R., and Baltimore, D. (1994). Functional immunoglobulin transgenes guide ordered B-cell differentiation in Rag-1-deficient mice. Genes Dev *8*, 1030–1042.

Sriskantharajah, S., Belich, M.P., Papoutsopoulou, S., Janzen, J., Tybulewicz, V., Seddon, B., and Ley, S.C. (2009). Proteolysis of NF-kappaB1 p105 is essential for T cell antigen receptor-induced proliferation. Nat Immunol *10*, 38–47.

Srivastava, A.K., Pispa, J., Hartung, A.J., Du, Y., Ezer, S., Jenks, T., Shimada, T., Pekkanen, M., Mikkola, M.L., Ko, M.S., et al. (1997). The Tabby phenotype is caused by mutation in a mouse homologue of the EDA gene that reveals novel mouse and human exons and encodes a protein (ectodysplasin-A) with collagenous domains. Proc Natl Acad Sci USA *94*, 13069–13074.

Stadler, L.J. (1928). MUTATIONS IN BARLEY INDUCED BY X-RAYS AND RADIUM. Science *68*, 186–187.

Stehelin, D., Varmus, H.E., Bishop, J.M., and Vogt, P.K. (1976). DNA related to the transforming gene(s) of avian sarcoma viruses is present in normal avian DNA. Nature *260*, 170–173.

Sternberg, N., and Hamilton, D. (1981). Bacteriophage P1 site-specific recombination. I. Recombination between loxP sites. J Mol Biol *150*, 467–486.

Stetson, D.B., and Medzhitov, R. (2006). Recognition of cytosolic DNA activates an IRF3-dependent innate immune response. Immunity *24*, 93–103.

Stogios, P.J., Downs, G.S., Jauhal, J.J.S., Nandra, S.K., and Privé, G.G. (2005). Sequence and structural analysis of BTB domain proteins. Genome Biol *6*, R82.

Strain, L., Warner, J.P., Johnston, T., and Bonthron, D.T. (1995). A human parthenogenetic chimaera. Nat Genet *11*, 164–169.

Strasser, A., Whittingham, S., Vaux, D.L., Bath, M.L., Adams, J.M., Cory, S., and Harris, A.W. (1991). Enforced BCL2 expression in B-lymphoid cells prolongs antibody responses and elicits autoimmune disease. Proc Natl Acad Sci USA *88*, 8661–8665.

Streisinger, G., Walker, C., Dower, N., Knauber, D., and Singer, F. (1981). Production of clones of homozygous diploid zebra fish (Brachydanio rerio). Nature *291*, 293–296.

Su, A.I., Wiltshire, T., Batalov, S., Lapp, H., Ching, K.A., Block, D., Zhang, J., Soden, R., Hayakawa, M., Kreiman, G., et al. (2004). A gene atlas of the mouse and human protein-encoding transcriptomes. Proc Natl Acad Sci USA *101*, 6062–6067.

Swiatek, P.J., Lindsell, C.E., del Amo, F.F., Weinmaster, G., and Gridley, T. (1994). Notch1 is essential for postimplantation development in mice. Genes Dev *8*, 707–719.

Sørensen, T.I., Nielsen, G.G., Andersen, P.K., and Teasdale, T.W. (1988). Genetic and environmental influences on premature death in adult adoptees. N Engl J Med *318*, 727–732.

Tabeta, K., Hoebe, K., Janssen, E.M., Du, X., Georgel, P., Crozat, K., Mudd, S., Mann, N., Sovath, S., Goode, J., et al. (2006). The Unc93b1 mutation 3d disrupts exogenous antigen presentation and signaling via Toll-like receptors 3, 7 and 9. Nat Immunol *7*, 156–164.

Takagi, Y., Kobayashi, T., Shiono, M., Wang, L., Piao, X., Sun, G., Zhang, D., Abe, M., Hagiwara, Y., Takahashi, K., et al. (2008). Interaction of folliculin (Birt-Hogg-Dubé gene product) with a novel Fnip1-like (FnipL/Fnip2) protein. Oncogene *27*, 5339–5347.

Takahashi, K., and Yamanaka, S. (2006). Induction of pluripotent stem cells from mouse embryonic and adult fibroblast cultures by defined factors. Cell *126*, 663–676.

Takahashi, K., Tanabe, K., Ohnuki, M., Narita, M., Ichisaka, T., Tomoda, K., and Yamanaka, S. (2007). Induction of pluripotent stem cells from adult human fibroblasts by defined factors. Cell *131*, 861–872.

Takeuchi, O., and Akira, S. (2010). Pattern recognition receptors and inflammation. Cell *140*, 805–820.

Tang, X., Halleck, M.S., Schlegel, R.A., and Williamson, P. (1996). A subfamily of P-type ATPases with aminophospholipid transporting activity. Science *272*, 1495–1497.

Temin, H.M., and Mizutani, S. (1970). RNA-dependent DNA polymerase in virions of Rous sarcoma virus. Nature *226*, 1211–1213.

Tennessen, J.A., Bigham, A.W., O'Connor, T.D., Fu, W., Kenny, E.E., Gravel, S., McGee, S., Do, R., Liu, X., Jun, G., et al. (2012). Evolution and functional impact of rare coding variation from deep sequencing of human exomes. Science *337*, 64–69.

Tergaonkar, V., Correa, R.G., Ikawa, M., and Verma, I.M. (2005). Distinct roles of IkappaB proteins in regulating constitutive NF-kappaB activity. Nat Cell Biol *7*, 921–923.

Thomas, K.R., and Capecchi, M.R. (1987). Site-directed mutagenesis by gene targeting in mouse embryo-derived stem cells. Cell *51*, 503–512.

Tjio, J.H., and Puck, T.T. (1958). Genetics of somatic mammalian cells. II. Chromosomal constitution of cells in tissue culture. J Exp Med *108*, 259–268.

Tokunaga, F., Nakagawa, T., Nakahara, M., Saeki, Y., Taniguchi, M., Sakata, S.-I., Tanaka, K., Nakano, H., and Iwai, K. (2011). SHARPIN is a component of the NF-κB-activating linear ubiquitin chain assembly complex. Nature *471*, 633–636.

Tokunaga, F., Sakata, S.-I., Saeki, Y., Satomi, Y., Kirisako, T., Kamei, K., Nakagawa, T., Kato, M., Murata, S., Yamaoka, S., et al. (2009). Involvement of linear polyubiquitylation of NEMO in NF-kappaB activation. Nat Cell Biol *11*, 123–132.

Tremblay, K.D., Dunn, N.R., and Robertson, E.J. (2001). Mouse embryos lacking Smad1 signals display defects in extra-embryonic tissues and germ cell formation. Development *128*, 3609–3621.

Tung, J.W., and Herzenberg, L.A. (2007). Unraveling B-1 progenitors. Curr Opin Immunol *19*, 150–155.

Urban, S., Lee, J.R., and Freeman, M. (2001). Drosophila rhomboid-1 defines a family of putative intramembrane serine proteases. Cell *107*, 173–182.

Uren, A.G., Mikkers, H., Kool, J., van der Weyden, L., Lund, A.H., Wilson, C.H., Rance, R., Jonkers, J., van Lohuizen, M., Berns, A., et al. (2009). A high-throughput splinkerette-PCR method for the isolation and sequencing of retroviral insertion sites. Nat Protoc *4*, 789–798.

van der Weyden, L., and Bradley, A. (2006). Mouse chromosome engineering for modeling human disease. Annual Review of Genomics and Human Genetics *7*, 247–276.

Venter, J.C., Adams, M.D., Myers, E.W., Li, P.W., Mural, R.J., Sutton, G.G., Smith, H.O., Yandell, M., Evans, C.A., Holt, R.A., et al. (2001). The sequence of the human genome. Science *291*, 1304–1351.

Vinuesa, C.G., and Goodnow, C.C. (2004). Illuminating autoimmune regulators through controlled

variation of the mouse genome sequence. Immunity *20*, 669–679.

Vitaterna, M.H., King, D.P., Chang, A.M., Kornhauser, J.M., Lowrey, P.L., McDonald, J.D., Dove, W.F., Pinto, L.H., Turek, F.W., and Takahashi, J.S. (1994). Mutagenesis and mapping of a mouse gene, Clock, essential for circadian behavior. Science *264*, 719–725.

Vocke, C.D., Yang, Y., Pavlovich, C.P., Schmidt, L.S., Nickerson, M.L., Torres-Cabala, C.A., Merino, M.J., Walther, M.M., Zbar, B., and Linehan, W.M. (2005). High frequency of somatic frameshift BHD gene mutations in Birt-Hogg-Dubé-associated renal tumors. J Natl Cancer Inst *97*, 931–935.

Vosshenrich, C.A.J., Cumano, A., Müller, W., Di Santo, J.P., and Vieira, P. (2003). Thymic stromal-derived lymphopoietin distinguishes fetal from adult B cell development. Nat Immunol *4*, 773–779.

Wang, K., Li, M., and Hakonarson, H. (2010). ANNOVAR: functional annotation of genetic variants from high-throughput sequencing data. Nucleic Acids Res *38*, e164.

Wang, W., Lin, C., Lu, D., Ning, Z., Cox, T., Melvin, D., Wang, X., Bradley, A., and Liu, P. (2008). Chromosomal transposition of PiggyBac in mouse embryonic stem cells. Proc Natl Acad Sci USA *105*, 9290–9295.

Watanabe-Fukunaga, R., Brannan, C.I., Copeland, N.G., Jenkins, N.A., and Nagata, S. (1992). Lymphoproliferation disorder in mice explained by defects in Fas antigen that mediates apoptosis. Nature *356*, 314–317.

Waterfield, M., Jin, W., Reiley, W., Zhang, M., and Sun, S.-C. (2004). IkappaB kinase is an essential component of the Tpl2 signaling pathway. Mol Cell Biol *24*, 6040–6048.

Watts, P.C., Buley, K.R., Sanderson, S., Boardman, W., Ciofi, C., and Gibson, R. (2006). Parthenogenesis in Komodo dragons. Nature *444*, 1021–1022.

Wellcome Trust Case Control Consortium (2007). Genome-wide association study of 14,000 cases of seven common diseases and 3,000 shared controls. Nature *447*, 661–678.

Welsh, R.M., Brubaker, J.O., Vargas-Cortes, M., and O'Donnell, C.L. (1991). Natural killer (NK) cell response to virus infections in mice with severe combined immunodeficiency. The stimulation of NK cells and the NK cell-dependent control of virus infections occur independently of T and B cell function. J Exp Med *173*, 1053–1063.

Weng, A.P., Ferrando, A.A., Lee, W., Morris, J.P., Silverman, L.B., Sanchez-Irizarry, C., Blacklow, S.C., Look, A.T., and Aster, J.C. (2004). Activating mutations of NOTCH1 in human T cell acute lymphoblastic leukemia. Science *306*, 269–271.

Wildin, R.S., Ramsdell, F., Peake, J., Faravelli, F., Casanova, J.L., Buist, N., Levy-Lahad, E., Mazzella, M., Goulet, O., Perroni, L., et al. (2001). X-linked neonatal diabetes mellitus, enteropathy and endocrinopathy syndrome is the human equivalent of mouse scurfy. Nat Genet *27*, 18–20.

Wilkie, A.O. (1994). The molecular basis of genetic dominance. J Med Genet *31*, 89–98.

Williams, L.A., Davis-Dusenbery, B.N., and Eggan, K.C. (2012). SnapShot: Directed Differentiation of Pluripotent Stem Cells. Cell *149*, 1174–1174.e1.

Won, S., Eidenschenk, C., Arnold, C.N., Siggs, O.M., Sun, L., Brandl, K., Mullen, T.-M., Nemerow, G.R., Moresco, E.M.Y., and Beutler, B. (2012). Increased Susceptibility to DNA Virus Infection in Mice with a GCN2 Mutation. J Virol *86*, 1802–1808.

Wright, S.D., Ramos, R.A., Tobias, P.S., Ulevitch, R.J., and Mathison, J.C. (1990). CD14, a receptor for complexes of lipopolysaccharide (LPS) and LPS binding protein. Science *249*, 1431–1433.

Xia, Y., Won, S., Du, X., Lin, P., Ross, C., La Vine, D., Wiltshire, S., Leiva, G., Vidal, S.M., Whittle, B., et al. (2010). Bulk segregation mapping of mutations in closely related strains of mice. Genetics *186*, 1139–1146.

Xiao, N., Eidenschenk, C., Krebs, P., Brandl, K., Blasius, A.L., Xia, Y., Khovananth, K., Smart, N.G., and Beutler, B. (2009). The Tpl2 mutation Sluggish impairs type I IFN production and increases susceptibility to group B streptococcal disease. J Immunol *183*, 7975–7983.

Yabas, M., Teh, C.E., Frankenreiter, S., Lal, D., Roots, C.M., Whittle, B., Andrews, D.T., Zhang, Y., Teoh, N.C., Sprent, J., et al. (2011). ATP11C is critical for the internalization of phosphatidylserine and differentiation of B lymphocytes. Nat Immunol.

Yamaoka, S., Courtois, G., Bessia, C., Whiteside, S.T., Weil, R., Agou, F., Kirk, H.E., Kay, R.J., and Israël, A. (1998). Complementation cloning of NEMO, a component of the IkappaB kinase complex essential for NF-kappaB activation. Cell *93*, 1231–1240.

Yanai, H., Ban, T., Wang, Z., Choi, M.K., Kawamura, T., Negishi, H., Nakasato, M., Lu, Y., Hangai, S., Koshiba, R., et al. (2009). HMGB proteins function as universal sentinels for nucleic-acid-mediated innate immune responses. Nature *462*, 99–103.

Yang, H., Shi, L., Wang, B.-A., Liang, D., Zhong, C., Liu, W., Nie, Y., Liu, J., Zhao, J., Gao, X., et al. (2012). Generation of genetically modified mice by oocyte injection of androgenetic haploid embryonic stem cells. Cell *149*, 605–617.

Yi, M., Hong, N., and Hong, Y. (2009). Generation of medaka fish haploid embryonic stem cells. Science *326*, 430–433.

Ying, Q.-L., Wray, J., Nichols, J., Batlle-Morera, L., Doble, B., Woodgett, J., Cohen, P., and Smith, A. (2008). The ground state of embryonic stem cell self-renewal. Nature *453*, 519–523.

Yoneyama, M., Kikuchi, M., Natsukawa, T., Shinobu, N., Imaizumi, T., Miyagishi, M., Taira, K., Akira, S., and Fujita, T. (2004). The RNA helicase RIG-I has an essential function in double-stranded RNA-induced innate antiviral responses. Nat Immunol *5*, 730–737.

Young, F., Mizoguchi, E., Bhan, A.K., and Alt, F.W. (1997). Constitutive Bcl-2 expression during immunoglobulin heavy chain-promoted B cell differentiation expands novel precursor B cells. Immunity *6*, 23–33.

Yu, D., Rao, S., Tsai, L.M., Lee, S.K., He, Y., Sutcliffe, E.L., Srivastava, M., Linterman, M., Zheng, L., Simpson, N., et al. (2009). The transcriptional repressor Bcl-6 directs T follicular helper cell lineage commitment. Immunity *31*, 457–468.

Yu, J., Vodyanik, M.A., Smuga-Otto, K., Antosiewicz-Bourget, J., Frane, J.L., Tian, S., Nie, J., Jonsdottir, G.A., Ruotti, V., Stewart, R., et al. (2007). Induced pluripotent stem cell lines derived from human somatic cells. Science *318*, 1917–1920.

Yusa, K., Horie, K., Kondoh, G., Kouno, M., Maeda, Y., Kinoshita, T., and Takeda, J. (2004). Genome-wide phenotype analysis in ES cells by regulated disruption of Bloom's syndrome gene. Nature *429*, 896–899.

Zak, D.E., Schmitz, F., Gold, E.S., Diercks, A.H., Peschon, J.J., Valvo, J.S., Niemistö, A., Podolsky, I., Fallen, S.G., Suen, R., et al. (2011). Systems analysis identifies an essential role for SHANK-associated RH domain-interacting protein (SHARPIN) in macrophage Toll-like receptor 2 (TLR2) responses. Proc Natl Acad Sci USA *108*, 11536–11541.

Zettl, M., Adrain, C., Strisovsky, K., Lastun, V., and Freeman, M. (2011). Rhomboid Family Pseudoproteases Use the ER Quality Control Machinery to Regulate Intercellular Signaling. Cell *145*, 79–91.

Zhang, S., Readinger, J.A., DuBois, W., Janka-Junttila, M., Robinson, R., Pruitt, M., Bliskovsky, V., Wu, J.Z., Sakakibara, K., Patel, J., et al. (2011). Constitutive reductions in mTOR alter cell size, immune cell development, and antibody production. Blood *117*, 1228–1238.

Zhang, Y., Proenca, R., Maffei, M., Barone, M., Leopold, L., and Friedman, J.M. (1994). Positional cloning of the mouse obese gene and its human homologue. Nature *372*, 425–432.

Zhang, Z., Alpert, D., Francis, R., Chatterjee, B., Yu, Q., Tansey, T., Sabol, S.L., Cui, C., Bai, Y., Koriabine, M., et al. (2009). Massively parallel sequencing identifies the gene Megf8 with ENU-induced mutation causing heterotaxy. Proc Natl Acad Sci USA *106*, 3219–3224.

Zheng, B., Sage, M., Cai, W.W., Thompson, D.M., Tavsanli, B.C., Cheah, Y.C., and Bradley, A. (1999). Engineering a mouse balancer chromosome. Nat Genet *22*, 375–378.

Zonana, J., Elder, M.E., Schneider, L.C., Orlow, S.J., Moss, C., Golabi, M., Shapira, S.K., Farndon, P.A., Wara, D.W., Emmal, S.A., et al. (2000). A novel X-linked disorder of immune deficiency and hypohidrotic ectodermal dysplasia is allelic to incontinentia pigmenti and due to mutations in IKK-gamma (NEMO). Am J Hum Genet *67*, 1555–1562.

Zou, J., Maeder, M.L., Mali, P., Pruett-Miller, S.M., Thibodeau-Beganny, S., Chou, B.-K., Chen, G., Ye, Z., Park, I.-H., Daley, G.Q., et al. (2009). Gene targeting of a disease-related gene in human induced pluripotent stem and embryonic stem cells. Cell Stem Cell *5*, 97–110.

7. Appendices

7.1. Genotyping conditions

7.2. Whole-genome mapping panel markers

7.2.1. C57BL/6J vs C3H/HeN

7.2.2. C57BL/6J vs C57BL/10J

7.3. Publications

gene	allele	P1	P2	amplicon size	sequencing primer	RFLP	wild-type	mutant	transgene
Atp11c	emptyhive	TCTGAAAGGAAGCCAAAGAAAGTGTCATTA	AGGTTCGATTTACAGCACTGCCAA	982	CCCTATAGAGACCATGTTAGCTTCAG				
Atp11c	spelling	GGCAAAGTTCCCCATACAATGATGAACC	GTTCAATGTCATAAGAAATGCACCCCAG	1166	TGTGATTAGACTAGCCTTCACTG				
Bcl2l11	tm1.1Ast	CTCAGTCCATTCATCAACAG	CATTCTCGTAAGTCCGAGTCT					540	
	wild-type	GTGCTAACTGAAACCAGATTAG	CATTCTCGTAAGTCCGAGTCT				400		
Cd19	tm1(cre)Cgn	GCGGTCTGGCAGTAAAAACTATC	GTGAAACAGCATTGCTGTCACTT					102	
	wild-type	CCTCTCCCTGTCTCCTTCCT	TGGTCTGAGACATTGACAATCA				481		
Cd247	allia	ATGTCACCAGAGCAGAAGTTCTGTG	GCCCTAAGAAGAGGCTGTCTTGTC	1042	TCTGTCACAGAATTGACCTGG				
Fas	lpr	TAGAAAGGTGCACGGGTGTG	GTAAATAATTGTGCTTCGTCAG					217	
	wild-type	CAAATCTAGGCATTAACAGTG	GTAAATAATTGTGCTTCGTCAG				179		
Flt3	warmflash	GCCCAAACCACAGCTCAACTTTGTCTATGC	AAGGAAAAGTGGCTCTCCTCACAGGTGC	753	CCTGGTCTACAAAGGAGGTTC				
Fnip1	hamel	CTTTCATAGCTCGCCTCCAC	CTTAGGAGGCCCAACCTTGT	561	CTTTCATAGCTCGCCTCCAC	*Bsa*AI	476+85	561	
Ifnar2	macro-2	TTGATACCACAGCGGAAGGTGAGC	AACCATAGGCGGGACACATTAACTG	1002	CCTCTCTGCTTAGAGGACAGATG				
Ikbkg	panr2	TGATGAGCCTTCTTGATGGTTCAGC	CCCCTTGGCAAAAGAGAGTGAGTG	1424	CTACCACTTGAGAGTCAAGGTTG				
Inpp5d	styx	ATTCCGACTTTTTGAAGACGGGCTCCAG	ACCCCTCTCTCAGGGCTCTCGGTT	108		*Bst*EII	82+26	108	
Irak4	otiose	CTTGCTGTCATCTGAATAATTGACTGATTTG	GCTGTAGATGTCAGATTTGGGTGTTATTTCTC	404	GATATCCTAGGCAAGAAGCATG				
Kdelr1	daniel gray	TTCTGTGATGCTGACAGTGCCTC	GAAGTCAGGAAAGGAAGCCCCATTC	420	GCTGACAGTGCCTCATCCTG				
Klrb1c	Unnatural	TACCAGGGATTACGGTCAGCCAAG	GATAACAAGCTTCCATCGGGAGGTC	1465	TGAGATCGCAATCACTTGGC				
Map3k14	lucky	TGAGTGAAAATGTCCCGTGAGCAG	TGCATACCAAGGGCAGCAATCAG	1140	GCACCAGATCTCATTATACGTGG				
Ptpn6	spin	ACGCTGGAGCTTCAGTGGAC	TGAGGTGAGGGAGGACGA	300		*Hinc*II	300	192+108	
Ptprc	belittle	TGTCTTCTCTACGCACAATTAAAGCCC	AGTCACAGATTCCACCTTACTCCAGG	1039	TACACACACCTGAAGATTTGGAG				
Rag1	maladaptive	TCTTCAGGGGCACTGGATACGATG	TCAATGCCCAAAGGGTCCCCTAAG	985	AAGCTTCTGGCTCAGTCTAC				
Rhbdf2	sinecure	GGTTGACAGTGTGACCTGATAGGC	CGAGAACTTTGCTCCCAGGTGAATG	1160	TCTTCACACAGTAGGCAGTG				
Rhbdf2	tm1a(KOMP)Wtsi	GAGATGGCGCAACGCAATTAAT	TACATGTGTTAAAGGAGGAGGCAGGG					389	
Ticam1	Lps2	ACAGTCCCAATCCTTTCCATCAGC	AGGATTCAGATTGGAGTCCCACAGTC	476/475	ACAGTCCCAATCCTTTCCATCAGC				
Tlr4	lps3	AGCACCTGGATTTTCAGCACTCTAC	AAGGCCCAGTGAAGACTGGTTCTC	1528	GGGGTATTTGACACCCTCCATAG				
Tlr4	Lps4	TCTTGGCTTGACCAGTCTCAACAC	TTGTCCTCCCATTCCAGGTAGGTG	999	GGGGTATTTGACACCCTCCATAG				
Tlr6	m2sd1	GGAGACAGCACTGAAGTCACTGATG	TGGCACCACTCACTCTGGATGAAG	1239	TGGCACCACTCACTCTGGATGAAG				
Tlr6	m2sd2	GGAGACAGCACTGAAGTCACTGATG	TGGCACCACTCACTCTGGATGAAG	1239	TTTCAAAGGAGGCGCTATACTCG				
Tlr6	m2sd3	GTTGCAAAACATCTCTTGCTGCCC	TGCTACATTGAGTTCCTGCAAAGCC	1111	TTACTTACTCGGAGACAGCACTG				
Tlr7	rsq1	AGCACTCTTCGCAGCAACTAATATGTAA	CCAACTCAACAAGGTTGGGAAGAAAATG	1911	TACTTGTGGACAAGACTGATGACC				
Tlr7	rsq2	AGCACTCTTCGCAGCAACTAATATGTAA	CCAACTCAACAAGGTTGGGAAGAAAATG	1911	GTGGACTCTCTGACTTAAAAGCC				
Tyr	c-2J	-	-						
Zap70	trebia	ACTCTGACGCTCACACTCATGC	TCATTTTCTGCTCAGGCCAGGGAC	761	GCTCACACTCATGCTATAAAGAAGAG				
Zbtb1	scanT	TACAGAGGCTCAGGCATGTGACTG	AGGTAAAGCTCCGTCCAAAGCG	1397	GCTGTATCGCTATCGACGAC				
	Tg(IghelMM4)	GCGACTCCATCACCAGCGAT	ACCACAGACCAGCAGGCAGA						430
	Tg(IgkHyHEL10)1Rbr	CAGGGCCAGCCAAAGTATTG	TCCAACCTCTTGTGGGACAGTT						405
Igh	tm1Rbr	GTCTCTGCAGGTGAGTCCTAACTTCT	CAACTATCCCTCCAGCCATAGGAT				865	302	
	Tg(BCL2)22Wehi	TGGATCCAGGATAACGGAGG	TGTTGACTTCACTTGTGGCC						167

Panel	Chr	ChrLength(Mb)	Marker	ChrLoc(Mb)	Predicted Length	B6 Length	C3H Length	Forward Primer	Reverse Primer	Vendor	Color	Row	Column
A1	1	197	d1mit242	4.19	84	83.82	147	TGTCAATCAGTAAGGCACAAGG	CATGTGATTTGTTTATTCAATCACC	Sigma	6fam	E	1
A1	1		D1Mit169.1	24.07	220	218	221	CIDR	CIDR	ABI-Cidr	ned	D	1
A1	1		d1mit243	35.13	145	146	132.72	CCAGGGCAATTGGATACAAT	GTTGTGCCAAAATGGAGGAC	ABI	ned	A	2
A1	1		d1mit161	59.28	112	112.97	115.08	ACCAGCCCTCCTTTTTTGTT	CTTGCCTCTTCAGGCACCT	Sigma	6fam	C	1
A1	1		D1Mit380.1	72.98	117	115.71	148.52	CIDR	CIDR	ABI-Cidr	vic	B	2
A1	1		d1mit10	92.58	139	135.1	141.45	AAACCATGCAGGTACTGATATGG	GAAGAAATTAACTGAGAGCAAGGC	Sigma	6fam	A	1
E1	1		d1mit136	103.89	103	105	111	TAGCCCTACACACTGTAGAAATGC	TGAACACAAAGTAGTAAATGCGTG	ABI	ned	H	9
A1	1		D1Mit495.1	129.52	144	145.56	139.48	CIDR	CIDR	ABI-Cidr	ned	H	1
A1	1		D1Mit159.1	161.59	206	206.6	187.54	CIDR	CIDR	ABI-Cidr	vic	B	1
C1	1		d1mit115	179.61	147	151.24	146.99	AAGGGAATGGAATTAGGGTCA	TAACGGACACCCATTTTAAACA	ABI	ned	E	5
A1	1		D1Mit292.1	193.23	212	210.33	208.26	CIDR	CIDR	ABI-Cidr	6fam	G	1
C1	2	182	d2mit1	3.8	123	130.73	126.49	CTTTTTCGTATGTGGTGGGG	AACATTGGGCCTCTATGCAC	ABI	ned	F	5
A1	2		d2mit365	27.66	100	108.2	112.37	GAGATCCCACTGATGATACAAGC	AGATGTGCCCAAGGGTCC	ABI	vic	F	2
B1	2		d2mit237	40.85	123	126.6	112.04	TTCCAAGTCACCTATTATCAAAAGG	TTGATACGGACACCAGCAAA	ABI	ned	H	4
A1	2		d2mit242	57.2	136	138	142	TTCCACACTCATGCCTATATGC	AAATGAACCTCTCAGGATCATATACC	ABI	6fam	E	2
A1	2		d2mit75	80.42	113	114.46	108.75	TCAGCATGTGGATGAATACACA	AACTTTTTAAAAACTACGAGCGTG	ABI	6fam	G	2
B1	2		d2mit100	106.38	112	114	129	GTGTTCCTAAGGTTGTATTTTGGC	GAAATTTGACAATTGCTAGGTGC	ABI	6fam	C	3
C1	2		d2mit277	123.26	277	279	126.24?	ATTCTGCATTCAAGCAAATTCA	CTTGAAAGTAGTTGGTTGGTTGG	ABI	vic	G	5
C1	2		D2Mit285.1	152.68	151	151.57	162.13	CIDR	CIDR	ABI-Cidr	ned	A	5
B1	2		D2Mit148.1	178.54	116	115.15	118.7	CIDR	CIDR	ABI-Cidr	6fam	G	4
D1	3	160	d3mit221	7.89	146	146.39	158.59	ATATAAGGACATAAACAGGCATTTCT	AAAATGTAGATCCCTTCATACATGC	Sigma	6fam	C	7
B1	3		D3Mit203.1	26.84	263	261	247	CIDR	CIDR	ABI-Cidr	6fam	D	3
G1	3		d3mit182	50.39	151	162	166?	TTATCTTGTTGGGGAGGTGG	AGAGAACTGATTCCTTTAAGTTGTCC	ABI	vic	F	14
C1	3		d3mit154	68.61	145	145.99	141.24	TGGAGGTTTGGAAGTGGC	AGAGTGTTTCTAGATGCCTGCC	Sigma	6fam	B	5
A1	3		D3Mit98.1	85.99	95	92.59	106.26	CIDR	CIDR	ABI-Cidr	ned	C	2
B1	3		d3mit57	115.53	157	163	161	TCCAGTTACTTGGTGAACTCCA	ATATGTGTACATGTTCATGGTGTG	ABI	vic	A	3
A1	3		d3mit116	154.2	259	268.09	282	TCACTGCCCATCTTTGTAACC	CCCAGAGACCCGGAATAGAA	ABI	vic	H	2
F1	4	156	d4mit235	8.26	116	118	101	AGGCCAAAGGTTGGATTTCT	GAGACTTGAAATTGAAGCATTTAGG	ABI	ned	G	11
D1	4		d4mit268	20.54	148	150.88	152.96	TAATCTGATCCAAACACTAAATCAGA	GCAGCCTTATGGAAACTTTCA	ABI	6fam	E	8
B1	4		d4mit236	39.06	202	201	183.97	TCTTAGCATGCTTACCGCCT	GGCCCGTAGGATGACTGTC	Sigma	6fam	F	3
B1	4		d4mit178	66.84	147	156.22	174.4	GCCCTGAAGGTAAATCAGTAACT	GCTCAGGAGGTACATTGCCT	ABI	ned	E	3
H1	4		d4mit301	88.75	104	103.55	111.81	CATTCTAAAATATGCTCCAAGTGTG	CGAGAATGTGGTTATTAAACTATTCC	Sigma	6fam	B	15
C1	4		d4mit176	101.16	138	140.7	147.32	AGATAATCCTCCAGACAGACATCC	GTAAGGATATACCTATGAAGGGTTCG	ABI	vic	C	6
E1	4		D4Mit203.1	129.25	98	96.28	105.86	CIDR	CIDR	ABI-Cidr	6fam	A	10
E1	4		d4mit253	152.38	147	144.58	140.23	ATGATTCCCTCTTCTGGCCT	AATGACTACAACAGGACATTCATTT	Sigma	6fam	B	10
B1	5	153	d5mit193	4.23	136	138.15	148.99	TGTCTTTAAAGTGGCCCAGG	TGTTTTCTATGTGTTTTATATGCTTCA	ABI	vic	B	4
B1	5		d5mit348	24.43	123	125.67	131.53?	CTGACCAGAACACAGCATAGTACA	TTTAAAATAGGAAAAGCATTCTTTCC	ABI	ned	C	4
B1	5		d5mit352	35.96	110	117	125	CCCAGAGCCCACATCAAG	TAGGTGGGTGTGTCTCTCCC	ABI	ned	D	4
D1	5		d5mit81	50.72	210	206.89	193.04	GGGAGTTCCAGGTTCATTGA	ATGTGCATTATGGCATGTAAATG	ABI	6fam	A	8
E1	5		D5Mit309.1	79.93	141	137.98	146.57	CIDR	CIDR	ABI-Cidr	6fam	E	10
C1	5		d5mit239	107.84	146	155.41	134.87	ATTGCAGACATAAAGGATATTTTGG	GCCAGCCTGGCTTACATAAG	ABI	vic	A	6
D1	5		d5mit425	120.33	124	126	129	TCGCCTTTCTTTCCCTCC	AAAATTACATTTGCATCTGGGG	ABI	6fam	F	8
B1	5		d5mit98	138.66	156	164	171	TCCTTCATTTTATCTTCTGCCC	TGAATTCACTCTCGCACCTG	ABI	ned	A	4
C1	6	150	d6mit166	5.32	100	100.24	110.49	CATTTTATTTTATTGATGGATGTGTG	GTTGTCTTATGGCTGCCATG	Sigma	6fam	D	6
E1	6		d6mit307	29.07	99	98.66	91.88	TTTTAATCTTTTGCCTCTTTCTCG	TGGGCTCAGGCACTTCTTAT	Sigma	6fam	F	10
D1	6		D6Mit274.1	48.68	111	108.85	89.57	CIDR	CIDR	ABI-Cidr	6fam	G	8
H1	6		d6mit209	75.49	134	142.79	147.21	CTCCCCCTCTGTGTGATTGT	TTATTACACCAGACCCATGTGG	ABI	ned	F	16
H1	6		D6Mit284.1	92.56	206	206.45	195.12	CIDR	CIDR	ABI-Cidr	ned	G	16
H1	6		d6mit328	112.73	125	122.55	129	ACCTGGGTAAACAGGGAAGC	ACATCTTTGTCTGGATTTTGGG	ABI	6fam	H	16
C1	6		d6mit59	138.93	169	165.55	175.02	GCCATCCTTTGTAATAACAAACA	CGTCTGGGAAAACCTCAAAA	Sigma	6fam	B	6
F1	7	153	d7mit152	4.65	129	122.3	118.48	GCCTAGCACACGCCAAAG	CCTTGTGCATGGTTGCTATG	Sigma	6fam	H	11
D1	7		d7mit76	19.58	224	224	255	CATGAGCACGTGGAGAAAGA	CGTGGAAACCTGATAAACTGA	Sigma	6fam	B	8
F1	7		d7mit27	51.22	246	252	260	TGAACTGGGGAGGAAAGTTG	AACATGAAAAGACATTCCCCC	ABI	6fam	E	11
F1	7		d7mit317	79.64	102	96.88	90	ATGTCTCCTTGACATTGGGC	TCTTGTAATCTCACATCTAAGTGTGTG	Sigma	6fam	E	12

F1	7		D7Mit350.1	90.73	223	220	226	CIDR	CIDR	ABI-Cidr	ned	A	12
C1	7		D7Mit98.1	122.06	186	186.13	180.17	CIDR	CIDR	ABI-Cidr	6fam	E	6
E1	7		d7mit71	138.17	117	118.3	114.21	CCACCTGGAATACATGTAACCC	TAAGATCCAAGAGATGGGTTAAGC	Sigma	6fam	G	10
H1	8	132	d8mit124	14.72	129	124.33	130.14	CAACTGTGTATCATAAACTGGGAA	GAAGAATCACTCAGCAGTGTATGG	Sigma	6fam	A	16
E1	8		d8mit3	25.72	172	174.27	180.41	TCCCATTCTCGCATAAGTCC	GATGGGAAGACAGGGTAGCA	Sigma	6fam	C	10
H1	8		d8mit339	41.39	123	125	107	ACCTATGGTACACACACATCGC	CAAACATTTTTAGGCATTTAGATCC	ABI	ned	D	16
H1	8		d8mit25	67.12	117	124	134	TCAGACTAATGTCCAGTAGCAAGC	ATTGCATGTCCATGTCTGGA	ABI	ned	B	16
B1	8		D8Mit45.1	89.83	95	96.2	102.58	CIDR	CIDR	ABI-Cidr	vic	E	4
F1	8		d8mit183	103.57	149	158	165	TCTCAAATAACTATCAACTCTTAGGGG	TCTTTGAACTGGCTATAATCACTCA	ABI	ned	F	12
G1	8		D8Mit88.1	117.36	131	129.57	142.95	CIDR	CIDR	ABI-Cidr	6fam	D	14
H1	9	124	d9_14.1	14.13	288	288	284.6	GGCCATGAAAGTGAATGATGATAGGTG	GCTGTGAACATAAAGGCAAGCGTTC	Sigma	6fam	E	16
C1	9		D9Mit2.1	37.2	191	190.27	194.37	CIDR	CIDR	ABI-Cidr	ned	F	6
F1	9		d9mit4	51.93	122	126	136	TGCTGAGCAAGCTATGAGGA	GACAGCCCATCACAGCTACA	ABI	vic	G	12
F1	9		D9Mit336.1	65.43	175	175.43	158.76	CIDR	CIDR	ABI-Cidr	ned	C	12
F1	9		d9mit196	85.79	143	152	162	GCCTTCTGTTCAGAACTTTCTG	TCTGTATTTAAGCATGCATGTGC	ABI	6fam	B	12
F1	9		D9Mit355.1	98.72	117	116.38	126.94	CIDR	CIDR	ABI-Cidr	ned	D	12
E1	9		d9mit151	121.39	114	123	119	TGGTCAAGGTGTGGTATCGA	AAAACTCAGCATCCAATGGG	ABI	vic	D	10
C1	10	130	d10mit298	8.51	150	151.84	162.51	TCCTGTTCACTGACTGTCTTCC	AAACAACCAGGCTCCCAAG	Sigma	6fam	C	5
F1	10		D10Mit213.1	20.13	260	258.01	244.95	CIDR	CIDR	ABI-Cidr	ned	C	11
G1	10		d10mit194	46.56	81	79.76	90.89	GATTGTTTGTAAAGACATGATCACG	AGATGTGGAATAGGAAGTATGATCG	Sigma	6fam	H	13
F1	10		D10Mit31.1	67.72	138	135	139	CIDR	CIDR	ABI-Cidr	ned	F	11
F1	10		d10mit230	89.66	115	119.25	116	AGATAGCCTAGGGGGTGCAT	ATCAGTTTCCAATCGCTGCT	ABI	6fam	B	11
D1	10		D10Mit233.1	113.82	136	132.95	111.91	CIDR	CIDR	ABI-Cidr	ned	H	8
D1	10		d10mit271	123.78	117	119	106	ACAACCAAAGGTCTTTGTAGAAGA	AATATATAGGCACACCTTAATAGCCA	ABI	vic	D	7
C1	11	122	D11Mit2.1	12.22	104	102.03	117.1?	CIDR	CIDR	ABI-Cidr	6fam	H	5
B1	11		d11mit205	33.09	104	108	111	GGCAGAGTCTAGTCTGATATCTTGG	CAGTGCACAGCCAGGTTG	ABI	vic	G	3
E1	11		d11mit235	44.19	180	185	200	GAGAGGGCAGTAGCAGCAAC	ATTTATGAGAAGGTCTGAAGGGC	ABI	ned	A	9
B1	11		D11Mit4.1	68.42	176	176.35	170.26	CIDR	CIDR	ABI-Cidr	vic	H	3
C1	11		d11mit284	88.99	86	87.99	101.97	GCTCGACCTAGGGGAAGAAG	AGAATGCTGTGCAACTGGTG	ABI	ned	G	6
D1	11		D11Mit333.1	108.58	99	99.56	79.87	CIDR	CIDR	ABI-Cidr	ned	E	7
C1	12	121	d12mit269	16.76	118	120	126	TCCCACAATCTATTCTTGGACC	ATACGTTTCCCAGAGGACATG	ABI	vic	H	6
D1	12		D12Mit60.1	35.47	121	118.48	112.75	CIDR	CIDR	ABI-Cidr	ned	F	7
G1	12		d12mit54	54.96	150	151.49	144.39	TGGTGAAATTCACTCCTTTGG	CCCTGTGCTGGTAGGTGTG	Sigma	6fam	H	14
H1	12		d12mit158	83.72	150	159	141	CATTGGGCAATGGAATTTG	ATGAGAGAAAACCAGAAACAAAGG	ABI	6fam	C	15
C1	12		d12mit133	111.54	113	121	115	TGAGCAAAAGTTATTGGGTGG	GGAGATATTGCTTATGTCTCCCC	ABI	vic	D	5
H1	13	120	d13mit57	17.09	140	135.74	144.16	GATATACTTGTTTGCACACTTGGG	AGAGAGTATGTGCCACCATGG	Sigma	6fam	E	15
D1	13		d13mit245	45.16	137	139	147.52	TGATGAGTCCCAGACCAACA	ATTCCAGTGGTTAGGCATGG	ABI	ned	G	7
B1	13		d13mit281	68.86	99	101	97	TGTCTAAGTGCACGTGGAGC	ATGTGAATTGATTTTGTGGGC	ABI	vic	F	4
H1	13		d13mit314	86.07	113	115.14	119.22	AGACTGAGCAGGTTGTATTTAGGC	CTTATTTTTAAATTGGTTTTACACACA	Sigma	6fam	D	15
D1	13		D13Mit144.1	96.87	138	136.28	140.77	CIDR	CIDR	ABI-Cidr	vic	A	7
G1	13		D13Mit260.1	113.16	206	205.81	195.02	CIDR	CIDR	ABI-Cidr	6fam	A	13
E1	14	125	d14mit49	14.72	250	245	205.03	TTCACTGAATAAAAAGACTCCTCG	TCCTTTACTTGGTGTACGTCTGC	Sigma	6fam	E	9
D1	14		d14mit174	32.46	146	148.91	153.04	ACTGCAGAGTCCACACAAGTG	TCTGAGCCACTATGCCTGG	ABI	ned	B	7
E1	14		D14Mit5.1	60.34	194	193.28	180.83	CIDR	CIDR	ABI-Cidr	6fam	F	9
H1	14		d14mit92	91.51	89	95	116.37?	CTGCTGCAGAATTAATTGATTTT	GGATATATGGATTTATACAGACACACA	ABI	ned	F	15
G1	14		d14mit197	105.72	101	97.49	93.5	TCCCATAGCAAATCTCTAGGTAGG	CATTCTGCAATAGATTTCTTGGG	Sigma	6fam	E	13
D1	14		d14mit135	121.21	172	168.51	172.44	TTTATTTTATGTGTGATTGTGCACA	TGTGTGCGTGTCACACTGAT	Sigma	6fam	H	7
E1	15	103	d15mit176	12.33	150	159	157	GCTTTCTCCTGGATAACAGGC	CTCTCCTTTTGACTACCCTAGCC	ABI	ned	C	9
H1	15		d15mit201	29.44	99	98.94	92.35	TTTTGGAGTCTTTCAGTTTTCTCC	TTGAGTGGTATAATTTTGATTTACACA	Sigma	6fam	G	15
E1	15		D15Mit143.1	51.99	135	123?	131.85	CIDR	CIDR	ABI-Cidr	vic	B	9
B1	15		D15Mit67.1	70.03	182	180.89	179.05	CIDR	CIDR	ABI-Cidr	vic	B	3
G1	15		D15Mit242.1	90.22	100	97.71	99.74	CIDR	CIDR	ABI-Cidr	6fam	B	13
G1	16	98	d16mit181	6.32	109	110.56	120.83	CTGTGTGAACGTGTTAGTATGTATGC	CATGGTTGACAATTGGCTTG	Sigma	6fam	E	14
G1	16		d16mit101	23.74	150	147.59	143.22	TTATGAAATGTTTTATCTTTTGGGG	CTCCAGATGTAGAAATTAAAATCTTGG	Sigma	6fam	F	13

G1	16		d16mit125	42.38	150	154	146	CAGAGATTACAAGCATACATCTTAGC	CAAACAACAAAACACATTCAACTC	ABI	ned	G	13
G1	16		D16Mit139.1	65.67	155	154.25	181.41	CIDR	CIDR	ABI-Cidr	6fam	C	13
D1	16		D16Mit153.1	87.58	153	151.56	155.66	CIDR	CIDR	ABI-Cidr	vic	D	8
E1	17	95	d17mit57	10.06	300	301.99	319.5	GCTGATAAACGTGGTGGCTT	GTTTAGTGGCTTCAAGTCACCC	Sigma	6fam	G	9
A1	17		phmx17.1	31.84	330	334.23	326.42	GATACAATGGGTCAGGTGGG	GTAGTCCTGGCTGGCTTCAG	ABI	vic	D	2
G1	17		d17mit181	57.39	124	130	124	TTTCCGAGGATTGGAAAAAA	GAGACCACACGCACTCACAC	ABI	6fam	D	13
G1	17		d17mit76	86.03	124	126	93	CTCCTCACCCAGATTCTTGTAA	TTTCGCAAGTTATTTTAACCCG	ABI	ned	A	14
G1	18	91	d18mit146	12.56	143	151	142	ATGTCCCTCTGCTCTTTAGTTACC	GGACCACAGAGTCATTCCGT	Sigma	6fam	B	14
G1	18		d18mit225	30.78	116	114.86	117.08	AGGACAAATAAATAAAAAGAGTGTGTG	CTTCCATATTGCTGTAACTTAAATGG	ABI	6fam	C	14
H1	18		d18mit238	57.18	122	124	128	TGTATCCTTTGTACTTAGAGACACAGC	ACATGCCTGACAAATTTATTTGG	ABI	vic	A	15
A1	18		D18Mit186.1	72.18	93	92.64	72.81	CIDR	CIDR	ABI-Cidr	6fam	F	1
H1	19	61	d19mit59	5.32	199	194.24	136.46	CTCTAACTATCCTCTGACCTTCACA	TTTTAAGCAGAACATTGAGGACC	Sigma	6fam	H	15
H1	19		d19mit96	21.92	119	126.84	118.45	CTTAACTGCAGTTTTAAAAGACATTTG	CATTTGAGAGAATGTTTGAACATACA	ABI	vic	C	16
F1	19		D19Mit17.1	45.63	107	103.48	97.71	CIDR	CIDR	ABI-Cidr	6fam	D	11
E1	19		d19mit33	56.27	262	259	322	CCTTTTCAAGAGCATCCTTAAA	GGTGGGACTTGAGAGATGCA	ABI	6fam	D	9
G1	x	167	dxmit81	33.74	200	211.66	213.78	GAGGAGCATCAACCTTCTCG	GAGGTGGGGAGAAACAGAGG	ABI	vic	G	14
F1	x		DXMit68.1	50.68	147	147.78	138.32	CIDR	CIDR	ABI-Cidr	ned	A	11
F1	x		dxmit114	95.34	146	155.28	161.71	ATGGCATCCACAGTACCACA	GTAAAATCAATTTGTGAATAAGGAAGC	ABI	vic	H	12
D1	x		DXMit172.1	119.2	219	218.72	200.09	CIDR	CIDR	ABI-Cidr	vic	C	8
E1	x		DXMit121.1	157.87	127	123.2	121.32	CIDR	CIDR	ABI-Cidr	ned	H	10

Notes:

1. Based on NCBI Build v37.1
2. Dyes- VIC (Applied Biosystems) excitation λ=488 nm, emission λ= 552 nm (green)
   NED excitation λ=_ nm, emission λ=_ nm (yellow)
   6FAM excitation λ=_ nm, emission λ=_ nm (blue)
3. CIDR markers are proprietary, and primer sequences are not publicly available.

Chr	AssemblyCoord	B6Allele	B10Allele	AmpliconId*	CoordAtAmp	PCRSize	PCR_F	PCR_R	Seq_F	Seq_R
1	4905893	C	A	B10SNP2G0001	229	568	TGTCCGTGGCACAGAATACAGTG	TCAGCCCCAGGTTTCAAAGCTC	GTGAGACACCTGCTACTTCTGAG	CCTGATGCCTGTGGATACTAAAAAG
1	24618794	A	G	B10SNPS0003	214	557	AGCTTCAACATGGGCTTTTGGTAGT	GCCTAACACTTCTATGACAAACCGACGA	TTGGTAGTCATAGGTGAACTCC	TTAACAGCCTGATTACTGCCAC
1	43063842	T	A	B10SNPS0005	299	502	TTTTGCCCACAAGGTCGAGGACAG	TGCTCAAGGCCACGTTTCCCTAAC	GTAAAGTGCCTACTGTGCAAAC	GCCACGTTTCCCTAACTTGAAG
1	61228463	T	C	B10SNPSG0001	152	494	ACTCTGGATTTGCCTATCATTGTGACTC	GCAAACCTGTGTAATGAGCACCAAG	GACTCTAAAGTCACCACTTTGTG	CTGTGTAATGAGCACCAAGTATACC
1	75483331	G	A	B10SNP2G0002	305	496	CAACCTTGAGTGTGATCTCTCCCG	GTGCGTGTCCTTATTAAGCCCCTG	CATAGGTATAGCTCGGCACTG	ATTAAGCCCCTGTCCCCC
1	95571814	T	C	B10SNP2G0015	207	983	TGAGTTTTCAAACCAGAACACAAAGCAG	GCCCAGCTTCTATTCACCAAAATGC	GCAGGAAGGAGCCTGTG	TCTGATAGCAGCCTTCAGATG
1	118565405	C	A	B10SNP2G0019	247	635	GCATAGGTGGTTCTGAATCTGGTCC	CAACATCATGTTCCCTGCTGAGTCC	ACACTGAAGTTCTGTACTGGC	GAGTCCAACTCTGCATTATTCTG
1	131470919	C	T	B10SNPS0014	186	650	TTTTAAGCATGAGGTAGTCAGGGCAC	ACAAGCACACCTGTCATCTGGTTC	CATTTAATGGAAGAGCAAGACTCC	TTGCAGGCTCAATGACAAGC
1	152988092	C	T	B10SNPSG0013	203	435	ACCATGACACCTGGGACTCTGAAC	TCCCTGTCAAGGCTTGCTGAAAG	CCTGGGACTCTGAACCAAGATG	AGTCTCAAATTTCAGCCCCC
1	173342737	T	A	B10SNPSG0020	241	412	TCCGAGGCGCATTATCCGCTAAAC	CCAGTGCCCAAGTGCATCATGTTC	GCGCATTATCCGCTAAACTAAGG	CAAGTGCATCATGTTCAAGGC
1	188081175	A	G	B10SNPS0019	189	668	AAGCCAGCATCTGTCACCTTGACC	TCTGTCCTGGAAGAAGAAGCCAGAG	TTGACCCCGTGGAAGGTG	GGTGACAGCAAAATTCCCAGTTC
2	3582646	A	G	B10SNPS0021	154	437	ACCGATTTACTGTGACTGACTGCAC	GGGCTTTCTAAATGGCACCAGACC	TGACTGCACAGGTGCTCAAG	AAGCTAACCTTCTTGACGTGG
2	25034194	C	G	B10SNPS0024	156	446	AGCCGGGAATCCTGTAACCATCAC	AGCAGAGCCTTACTTTCATCAAGCC	CATCACCTAAGAAGTTCTGTGGGTAG	TCTGAGATGCTTGCCCAGAAC
2	50942492	C	T	B10SNPS0026	232	491	ATGTGCTTCTTCTGATGTGACCCTG	TGCAGTCTAGCTTCTCCCTAGTGG	TGATGTGACCCTGTCCTTTG	TTTCCTGAGGTCAGCACAG
2	67362739	G	A	B10SNPS0028	213	534	CTCAGAGGTCATGGTGTTGCACAG	TGGGTGGGTAGTAAGATCCCCAAG	CATGGTGTTGCACAGTTTTGG	GCTCTCCGCTGGGAATAAAATC
2	84313007	A	G	B10SNPS0030	313	759	ACAAACACATGGCTCCTGGCTC	GAAGTTGTGGTCCAGATATGCCCTC	GGTTCATCATCTTCCTGAGAGACTG	TCCCCAAGTGCTGGGATTAA
2	103735349	C	A	B10SNPS0032	403	589	TGTTCACTGAACGCCATAGCCC	CCAACTTTGCACAGGTTCACGC	GTTATCACCATGCTCTAGATGAGG	ACAGGTTCACGCCTGATCC
2	122094116	T	G	B10SNPSG0021	491	651	GCTCTACATAAGGCGGAAGGCAG	GCATCCTGAAGAAGCCCACAGC	GAGAGTGGTTCTAGTACATTTTCTTC	CTGAGGCCCTGGATAGCAAG
2	146096051	C	T	B10SNPS0036	325	539	ACTGATGCCATGAACCTCAAGAAGG	GGAAACATGTCCATCCCCGTTACAC	AAAAGGCAGGTGTTTACATCTTGG	CCGTTACACGAGTGCAGAATG
2	164025160	A	G	B10SNPS0037	304	559	AGGAGAACTGAGCTGTGCCATCTG	CCCTGGACAACCTTGACTTGAAGTG	AGCTGTGCCATCTGTCAAAG	ACTTGAAGTGAGTGGCCC
3	4365615	T	C	B10SNPS0041	208	546	TCCTCACGGTGAAGATAGGACAGG	TGCATCAGTGTCCACCTTCAACAG	TGAAGATAGGACAGGTTTGATCCTAC	TGTCCACCTTCAACAGAAGGC
3	25440271	C	G	B10SNPS0044	227	750	CCATTGTGCCCTTAGTAGCTGTGTG	GGGCGGCCATGACTTAATGTAATGC	GTCATTGAACCTTCCAGAAAAAAAAC	CCCCATGCCTAGAAGAGGTTATG
3	51646346	T	C	B10SNPS0046	193	435	TTATCCACTGCCAAGTCTGCTGCG	TCAGCCAGTTCACACAACAAGGTTC	GCTGCGTGCTCATATTGAAC	GTTCACACAACAAGGTTCTAGATGG
3	67807084	G	A	B10SNPSG0029	157	702	TGTCTCCTGAAAGGACTTGAGGCAG	AGCCGTAGCACTCCCTCATAAGTAG	TTGAGCATGTCAACCGCAGT	GAGAGAACAAGTGTTTCTCCTCAG
3	84907155	T	C	B10SNPS0050	157	452	ATCAGGAGACAGCCAGCCCATTTC	TGTCAAAGACGCCCACAAGTGAG	GCCAGCCCATTTCTCTAGAAAC	GCCTTAGAACTTGGAAGCATC
3	107273295	A	G	B10SNPS0051	376	558	TGTATCTCCCTTGGAGCCTAAGACC	TGAAATGAATCCACAGCCAGCTCG	AAAGGTTCCCAAGGTGTCTC	CAGCTCGTGGAGCCTTTAAATG
3	122116882	C	T	B10SNPSG0034	238	407	ATGAGGACAAGTCCTGAAGCGACC	CCGGAGAAGCCCCTGAAGTTAATG	AGCGACCGGGTCAAATAC	GTACAATAAATCAGTGGTCCAGGC
3	146593495	C	T	B10SNPS0056	227	686	CCCAGCCTGGTGTGAACCTTTTAAC	TCTGCTAAACCCTCATGTGGCAATG	AGTTTCAACTGCATGACCTAGC	CTCATGTGGCAATGTCAGGC
4	7149610	C	T	B10SNPSG0036	213	643	GCTCCAGAAGTACCATCAGCGG	GTGGCTGAGACAGCCTCAAGTAAC	GTACCTAGACACATCCAGAAATTATC	CAAGTAACTGAGATATGTGCTGCC
4	28249560	T	C	B10SNPS0060	380	693	TTCTTACTAGAGAACCCAGTGGAGAGC	GGCTGCTGCATTTAGTATCCCATGAC	TGGGATGTGAAAGGCTCTAGC	CCCATGACTGGTAGATGGATTCTAAC
4	45462131	T	G	B10SNPS0062	188	488	CTGGCGACACTGTAACTCCTTACTG	TGGAAATAGATGCTCCCTCCCTGC	ACTGAATGAATTGATAGGTCCTCTGG	GCCTATCAGTGGGACTCATTACG
4	66040938	A	G	B10SNPS0064	224	575	CCTTCAGGGAGTGAAAGTTGGGAAC	AGTGCCCACCCAGACCTTGTAATC	TTGGGAACAGGCACAGC	TGTCACTCAGGAATACACATGG
4	87804727	C	A	B10SNPS0065	370	549	AGGACCCCAGAAGGTTTACCAGAG	GCCAGGAAGTTCAAGAAGGATGCTC	TGTCGGCCATCTACAATGGAG	TTCAAGAAGGATGCTCTAGAAGG
4	112653568	G	T	B10SNPS0067	340	564	GCACATGAGAGACCAATGAGTCCATC	TGCGACTTTTGGAGAGTGACACAATAG	ACTGACTTGAGATTGGATGCTC	TTGGAGAGTGACACAATAGTAAATTC
4	126253529	G	C	B10SNPS0069	208	401	TGCCCACATTGCTAAATAGAGTGCG	TGGCTCTGAGTGTCATCTTCCAAAC	TTGCTAAATAGAGTGCGTCCCAG	GTGTCATCTTCCAAACAGAACTGG
4	142217407	T	C	B10SNP2G0026	183	650	TCAAACCTAGAGCCAGAAGGGACTC	TGCCCAACAAATGCTTGACTGAATG	GAAGGGACTCATTAAACTCACTTAC	TGACTGAATGTCAAGTCCCAG
5	23345000	A	G	B10SNPSG0050	444	692	CAGTCGGAGCTACTCAGCAAGATTC	CTGGGACTAATAGATGAGGTTCAAGCG	TAGCCAGATATGGTGGTACACTC	GAACAGAAAATCTATGTGTGTGCTTG
5	44059873	A	G	B10SNPS0077	299	530	GTCTCAGCTCTCTGCTCATTGGAAG	ACCTGCCACTGTCTGATTGTGC	GACAGAAATGGTCCTTTGCATTC	AGTTATCTGGAGCATTGCTTTTTTTG
5	67382789	A	G	B10SNPS0079	328	479	TTGAAGTTCAGATCCATCCCGAAGC	CTGTTGGAATGGACAAAAGCAAGCC	ATAAGCTCCGAGTTCCGAGTTG	AGCCAACCAAAGGACTGTG
5	88988451	G	A	B10SNPS0081	262	719	TGCCAAGTATGTTAGGCCAAAAGCAA	TCTCCATGCACTACACACTGTTACAGA	GAGGGGTTAAATCACACATACAC	GCTGGCCTTGAAATTACGC
5	109001097	C	A	B10SNP2G0043	153	459	GTGAGACCTTAGCTGTTCAGAGGC	TCTGTGAGGCAGAGTCCACACAAG	TGGGACGATTTGCCTGC	CCTGGACCATTCAGCAGATG
5	129799057	T	C	B10SNPS0086	380	741	ACCTTCTGTGAAAACCGCCTCC	GCACCAAGTGACCAGATGTCATCTC	AGGGGAACCATTTCTGCGAC	TGACCAGATGTCATCTCACATGC
5	148405352	C	T	B10SNPS0087	248	576	TGTCAATGGAGCAAGCACTACGAG	ATGATGTTGTCAAGCCCCACCC	CTACGAGAGTTTGGACACCTC	TCTAGTCATAGACTACTAGGTGGAG
6	4944845	C	A	B10SNPS0089	220	749	AGCTGAGGTCATCCTACAGTAATGAGC	CTTTCACGCAGCTAGGCAAAGC	CTCGGAGAACAGGACAGC	CCTTCTGGGATGAAACTCAGGTC
6	23322761	T	A	B10SNPS0091	291	444	TGATTCACCCAGTCCATGCTAATCAAG	TGGAATGAATCCTGCCAGCACTC	CTCAGGATAAGCTTTTTTAAGGGTG	TGCCAGCACTCATCCTTTG
6	42395982	C	T	B10SNPSG0054	210	427	AGCTTGGCTATGTCCTTGGGCAAC	AGGCAGTCCCAGCACTTTGAAAATG	ATGTCCTTGGGCAACATGAC	CCAGCACTTTGAAAATGTAGAGC
6	67742189	C	A	B10SNPSG0061	211	405	TGCAGGCAGGAGGCAATTTGAGTC	AGACAGTCTTCCAGAATGGGGAGC	GAGGCAATTTGAGTCTTATCTCC	TCCAGAATGGGGAGCCAGAG
6	84280591	C	T	B10SNPS0097	241	703	CAGATAGGTGTGGATGGATCATGGC	TCCCATGTTCAGGATGGAGGAAGG	GATGGATCATGGCTTAAGATCCC	TTTCACAGCCAGGAATGTGAC
6	104875242	A	C	B10SNPS0099	315	656	GCAGCTTTTAGAGCAGAGCATTCAC	TGAATCCATCAACAGGAAGGAAGCC	TTTAAAGCCTGTGACGACCAAAG	GGCATGACCCTACTTATGCTAC
6	125060262	A	G	B10SNPSG0065	236	400	AGGAAGCCCCTAAGATGCCTAATGG	CAAATTGACTGCCTGGAGAAAAGACAC	ATGATGGCAGTGCCCTAATC	CTGGAGAAAAGACACTCTTCTCTTAC
6	147720182	A	G	B10SNPS0104	230	493	TTCTCTCAGTTCAAAGTGCAGAGCC	CCCGAGATGTTTTCTTGACTCCCAG	AGAGCCATCTGGTGCAAC	GTGATACTCTGAGGCTTAACATTAGC
7	7014667	T	C	B10SNPS0105	469	691	GGAAGCTGTCTCATGGAAATCCACG	TGCATTTCCTGGGCTCCAGAAAG	TGAAACCTGCTTGCTCAGGG	CTGGGCTCCAGAAAGTTCATATTC
7	28467081	T	A	B10SNP2G0049	228	748	TGTAAGCAGCCCAGACCTGCAT	TGAGCTTCTCACAGTCCACCCA	CAGACCTGCATCTCAGCG	CCAAGGGTGACTTTGAACTTC
7	38216957	A	C	B10SNP2G0052	162	496	GTGTCACTTGAAGCAGCCAGAGAG	TTGCCCAGAAAGAATAGTCGCCC	GCAGCCAGAGAGTTTCTTTTATTACG	ATCCCAGAGAGATTTGTGCC
7	54410823	C	T	B10SNP2G0058	280	674	CGTGTGTCAAGTCTAGTGATGAGCC	TGACTTAGTGAACCTGCAAATATCACCC	AAGGCCCTACTCCTACATGA	TACTTCTGAAGGCTGAAGACACTG
7	71519895	G	T	B10SNP2G0060	347	644	GCACATACAAGAGCCTGGTATAGCAA	AAATACGCCAACATTTTCCCCTTTGTC	CTAACACCTTAAAGTGTGGGGAG	ATTTGCTCCGGCCCAAAG
7	87465557	G	A	B10SNPS0113	424	709	ATCCAAGAGAGCCTCTCCTTGAGC	CAGCCACCATTCAGTGTACAGTCC	TTCTGGGGTCACATAGGCAC	CATGCCAGTGATGATATTTGCC
7	104565567	A	G	B10SNPS0115	239	410	TTCTGTCCTCTGTAGGAGGTCACG	TGAGAACGACGCTGCTGAAACG	TTCTCAATACTGGGTGAGAAGGC	CTGCTGAAACGGAGGAGG
7	130492865	A	G	B10SNPS0118	175	690	TTATGCCTGGAGCCAACTTCAGC	CTCCTGGAGATGACCTTTTGGTCAC	GCCACCAACAAAGACCTGAG	AGTGTTTCTGCAAGTCAGCC
7	141188625	A	G	B10SNP2G0065	253	599	ACGAACATTGGCTCCTGTACACC	CTGGGGAGAACGAGACACACATTAC	TGTGTCAGAATGCATCGCC	CGATGGAATCCCATTGAGCTTC
8	4235918	C	T	B10SNPS0122	163	541	TCACAACAAGCTGGAGACTCTGCC	TGTCTGAGCTGCACAAAACCGAC	TGGAGACTCTGCCCACCC	GCAGTCCCTCATAAAGGGTG
8	24145986	C	T	B10SNPS0123	496	651	TTTGTAGGACAGCACAGGTTCCG	CCCTCAGGTGAGCAGCAGAAATTC	AGCGTCAAGGCTGTCACTAC	GTGAGCAGCAGAAATTCAAAATCTAC
8	48705306	G	A	B10SNPS0126	607	778	TTGAATCCATGACAATCACCTCCCG	ACTTCCCTCCCTGACTGTGAAACG	GGGAAATGCCTCCATGAGATCC	CCTGACTGTGAAACGAGAAATAAC
8	64124535	G	A	B10SNPS0127	213	470	TGAAAACATCTCTCCTTACACAGCCTG	GTCAAGGTAACTCAGCCACTTCCTC	TCCACTGTATAAAGTACCTAAGAGG	AGCTCAGTCTCTGTGAAACG
8	86611947	C	T	B10SNPS0130	382	573	CAAGGTGGTGACCATTGCTTCCTG	TGGCTGAGCAACACCTAAGGCAAC	GCAGGCACCAGCTACTATGAG	TAAGGCAACACCACAGATGAG
8	106217064	C	A	B10SNPS0132	216	520	TGTAACCAACATGGCTGCGTTCTC	TATGTGGAAAGCCAACCAGGCCAG	TGCGTTCTCTGGAAGCAC	GTGTTTATCAACAGAAGGCTCAAG

8	126154896 A	G	B10SNPS0133	173	590	TGGTAAAACCCATCCCAAGCGG	AGTCGGGGCACATTCACAACTAC	CGGCAGAGCTGTAAGTCTGG	AACAGGCAGTGTTCCTGAC
9	8307298 T	C	B10SNP2G0067	178	531	GATCATTTACCAAGGTCCGTGCTAGG	TCAGGCAGTATAAGGCTCCCATTCTC	CAAGGTCCGTGCTAGGGATAATC	TCCTTCCCAAGGTGATTTGATAG
9	25697557 A	G	B10SNPSG0092	379	595	AGGAGAAACTGCCTGTTCAAACCC	TCAAGACCTGGTCCTAAAGACCCTG	CCCATACAAAGTCATTTCTGGACTG	TGAAATAGCCCTGGTATCCCG
9	44891469 G	A	B10SNPS0139	301	540	CAAGCGGTTAGAGTTTGGGGTCAC	CCTCCGGCTGAATTGGAATTGCAC	TATGGCAGTAGGTCTGACCC	GGAATTGCACCTTGAAACATGC
9	65069297 A	T	B10SNPS0141	191	720	CTGTCTTCCAGTCACAAGCTCTCAG	GAACGCACATGGCACCCATTTTC	AGTCACAAGCTCTCAGCTCTG	TGGGCTATGCAGTAAACTCC
9	87513872 T	G	B10SNPS0144	244	433	TGGCTGTGACGCTGTAGGTAAAAG	GTAGACTTGGAGGGCAAACCACTC	AAAGCTACGGCTTTTCAGCTTG	GGCAAACCACTCTCTCTTTGTTG
9	106375830 T	C	B10SNPS0145	192	554	TGGCATACGCTTGACCTGGAAAC	AGACAAGGTCCAGTGCCCGTTATC	CCTGGAAACTGGTCAAGGTTG	TCCGAGTACAAGGTGAACTCTG
9	122496139 A	T	B10SNPS0147	229	632	GCCTGCACAGGGATTTATATCTGCC	TGTACCCCAAAGCATTAGCCTGC	GCCTCAATTAGATGTTCCAGAAGC	TTGACAGGGTCATTCCACAG
10	25103948 A	T	B10SNPS0152	159	517	CATAATTTGTTCTTCCCAGGCCACTGA	AGGACATGGATAAACCAAGCCACATTT	CCACTGATTCAGTTTGGAGCC	CTGTCTACCCAGAGGTGTAGAAAC
10	43717117 C	T	B10SNPS0153	148	403	TTCAGAATACCTTCCACGCCATCG	GGCTAGAAAACAGCACGCTTTTCTC	CATCGCTGTTCTTCAGTTTGG	TCTGCCACAAGACAAAGTCTTTTC
10	62547650 C	T	B10SNPSG0099	450	619	TGTTTAGGCCACCTCAATGGCTC	GGCTGATGAAATTCACAAACTGCCC	AGCTCTATAAGCAGTCTGGC	TGCCCATCGTACCTTAAAATAAC
10	83411614 C	T	B10SNPS0157	183	443	TGCCGTCTAAGAGTGTCCAGCTATC	TGTCATGTCCACAGCATTAACTCCC	AAGAGTGTCCAGCTATCATCTTC	CATGCAGCTAAGGTTAGGTACTC
10	104474937 A	C	B10SNPS0159	227	766	GTGAAGTCAAATATTGCCAACAGAGCC	TCACATGGGTCGAATCAGAAATCGTC	ATCATGTACCACACTTTCAGTTTGG	CAGACTGTGGTATAATGGACTCTC
10	126774961 C	A	B10SNPS0162	459	689	TTGATGAAAGCCACCAGGGAGC	GCCAACTTTATGTCAGGGTCCCAG	GCCGTTCCTTCAAAGAATCTGAG	TCCCAGGGTTATGGAGCAG
11	5927550 A	G	B10SNPS0163	367	553	ACCCTCTGTGGAAGACAAAGCAGC	GCATTCTCTGAACCTGATGGGGAC	ATATGAACTGTCCTCACACTGG	ACCTGATGGGGACCTTCAAG
11	24352635 T	C	B10SNPS0165	339	562	GGAATTGGCTCGGAAATCTGCAATG	TGGCTTCTAGGTACTAGACGGCAAG	AAATCTGCAATGGGCTTGCTTC	CCTCTGAACTCGATCTATTAGGGC
11	46027800 G	T	B10SNPS0168	175	447	GGAACAGGCCAGAAATCAGGCTTC	TTCACCCCGCAGGTTCCCACAC	AGAAATCAGGCTTCCCACAC	ACATTGCTTTGTAGGCCACG
11	65237281 A	G	B10SNPS0170	178	634	TCAGATCCCATGAACTTCAATGAGCTG	TGGAGCCAGAGTCACACCATTAGG	TGAACTTCAATGAGCTGTTAGAAGG	CAACAGTTCCTCAGCTAGTGATG
11	83361835 C	T	B10SNPS0171	297	452	AAAGGGCAGACCCTCATTCCAGAG	AAAGCTTGCAGCCCAGAGTCTAC	ACACACAGCTTTAAGTCTGTGC	GCCCAGAGTCTACTGCAAAAAG
11	105208941 A	C	B10SNPS0173	273	487	TGTGTGAGAGCCGAAATGCCAG	GAAGACGTAGCCCGAACATCTTCC	AACACCACTGTGGATCGG	TCTTCCCAGAACCACCTGC
12	4035991 C	T	B10SNPS0175	391	622	GTAATCTGTGACCCTTTGGGAGCC	GCTGCCTTTGTCTGATAGGAGACC	CCCTTTGGGAGCCATTTAAGAAC	TCTTTCTCGGAGGGCACAG
12	25626291 A	G	B10SNPS0178	153	465	AGACCTGAACTTCTCAGTGTTCCCC	TTGTCTCAGAGGCCAGGCAGAATC	CTCAGTGTTCCCCAGGTG	GATCCCTGGACCCAATGTAG
12	33783681 T	G	B10SNPS0179	541	729	GCCATCCAGTCAGCTTGCTAACATTTC	TGGCAGAGAATCACAAGACTCTCCAG	GAACCTTGCTCAATGGCTCAG	AAGACTCTCCAGGCCGC
12	55293511 C	G	B10SNPSG0101	196	690	CCAAGGCTTCGACCCAGATGTTAG	CCATTACAATCAGGGACGTGGTCAG	GCAGTTGTTGCTTCCTAAAACC	TGAGGCACTACAGGTGAAGT
12	69022193 T	C	B10SNP2G0069	480	666	TGAGAGACACGCAGATTCCCACAG	ACGTGGTAATGGGTCCTTGTAGCC	CCTTGACCAAGGTATCATTGAGAAG	ATGGGTCCTTGTAGCCATTTAAC
12	85893620 T	C	B10SNPS0184	222	434	CTTACCACATAGCTCATTGGCACCC	GTACCTATTTCCCCAAGCCAGCAG	ATTGGCACCCACCACTGG	GCTGTTGGAATTTAAGAAAGAAGTCC
12	106196191 G	C	B10SNPS0185	181	499	GCCCCTGAGAACAAGTGTTAGTCC	TGCCTCAGTGCATACAAGTTCCC	GAGAACAAGTGTTAGTCCTTCCTG	TGTCCATACACACTTGTGGTAG
13	23458896 T	A	B10SNPS0190	231	607	GACATCACAACTGCTCTCAGTAGCC	CCAGATGCACATTGGAGACCCAAG	CTGCTCTCAGTAGCCAAGAAATTATG	TTCAGTCTGAGACTTGGCTAC
13	44605368 G	A	B10SNPS0192	242	482	GGTCAGCACTTTCAAGGTAGGAAGC	GACTCTAGTGAGTGGGCATTTGAGC	AGCTCAGAAGAACAGTGTCC	AGCTCTGGGTATGCTGAGAC
13	60294898 T	C	B10SNP2G0077	196	444	AAGCTGGCAGCCAACTTCTGAC	ACATGCCCACGAGAGACTAGGTAG	CCAACTTCTGACAGGGGC	GAAGAACGTGTCCGAGTTTTAG
13	83826961 T	G	B10SNPSG0116	201	467	ACCCAAAGTGAGGCAATGCTGG	ACTCCGTCTACATATGAGGAGCAGG	CAATGCTGGAGATAGAAAACCTTG	GTTGACTTGACTGACTCATATTCG
13	107699046 G	A	B10SNPS0198	190	409	TGGAAAAGGCTGCTTCAGACCAC	ATTGACAGACCTGAGCCCATCCAG	GCTGCTTCAGACCACATGTTAAG	ATCCAAACTCTTTCAGGGATGGC
14	13021464 C	T	B10SNPS0200	325	657	GGAATCCCATATGCTAACTGCTTCCTG	TGCCTGACATAAGCGATAGAAACGG	TGGAGACTCGTCTCACACTG	GAAACGGGACTTTATTACTGGC
14	30518255 C	T	B10SNPS0202	155	504	ACTGCAATCAGGTGTGAATGCTGAC	AGTGCCGTTGAAGTAGCCACTCTC	TGTGAATGCTGACACTGCC	TCTTCCCAAATAGGTTGCAGG
14	55673056 T	G	B10SNPSG0125	199	535	TACCAGTCACTGCGTTGCTGTG	AGCAGAGGTAACTCCTTCCTTCTCC	GCTGTGTGTCTGCCACC	AGTTGTGATGCCAACAGCTC
14	77195309 C	T	B10SNPSG0131	196	416	ATGCAACTCTGCCCTGATTACTCG	GAAAGCGGCGTCAAAATGTTCCTC	CCCTGATTACTCGTGGTCTTG	GCGTCAAAATGTTCCTCTGTTATG
14	96734196 C	A	B10SNP2G0083	303	518	GACCCTACCCATGTAAACATAAGTGCAG	CACCCTCCAAGACCCATTGTCATATC	TTAATCCCAGCACTTGGGAG	TTGTCATATCTTCCAAAATTTGTGTC
14	116124073 A	G	B10SNPSG0139	694	851	GACCGACTGGGACCTTTTACATGATTT	TTCATTCTTCATGCACAGAGGGGAC	ATTGAATCTCCTCAGGCTCAAGG	GGACTTCGGACATAGACATTCTTC
15	7117980 A	G	B10SNPS0212	318	493	TGAAAAGGTCATTCGGGCATCCAG	TCTTCAGCAAACAAGTGGGGAAGC	GAATGTCCCTCTGGGAATCAC	GGGAAGCCCTCCACACTC
15	25941148 C	T	B10SNPS0214	161	826	AATGGCTTTACCCTTTTGGCTTATGGAT	GCGGAAACCTTTCCTTCTGGTGAC	TATTCAAGCAGTACCTCTAACTGAC	AGTAAGCCTTACAGATGGGTCTC
15	42051029 A	G	B10SNPSG0142	150	966	AAAGGCTTGCTCACGTCCCCTG	CCCAAGGCTGCACAACTAAATGAGA	CCTGCTGCTTTCCAAGGTTAG	TTGTCCCAAGAGCTGTAACG
15	63931032 G	A	B10SNPS0218	165	797	TAGCAGCGTGTCTTCTGAGAAGGG	AGTAGTTCTCCATCTGGACCAGACAAC	GGGTCATTTTCTCAAGGAAACTACAG	CTACATAGTGAGTTCCAGGCCAG
15	83618701 G	A	B10SNPS0219	234	440	CAAGACTTAAGCCAGTCCCCAAGTG	GTTTTCAGACAGTAGCCTGCCTCC	TAGGCCCAGAACTGTCAAACTTG	TGCCTCCAGAAAACAGAGCTTAG
15	100309099 G	A	B10SNP2G0093	174	457	CCAAGAACAGTGCAGCTTACTCTGG	TGGCTTAGTGCAACACAGTGGAGG	CGGCAGTGGTTTTTCTTATGCC	CCCATGATAGTGACGAGGAGAA
16	4972820 A	G	B10SNPSG0155	302	538	TGCAAGCACATCTGAGCTGAAGAG	GCTGGCACAGCACTTGCTCATTAG	AGCAAAGTCAGGGCCTATTC	GTCTTCAACAGGATTGTCAAGCG
16	29856457 A	G	B10SNPS0225	466	651	AGCAACCACAGCGTGAGTTTCC	CACCCTTGAGTTTTCAAGACCCACC	CATGAGAGCCATTGCATGGTG	GAGTTTTCAAGACCCACCTTCAAC
16	44261352 A	G	B10SNPS0227	183	414	AGATGCTTCCCTGCTGTAAGGTCC	ATGTCACGGTAAGATGCAGTGTCAG	TGTAAGGTCCTCCAGGACAC	TAAGCAGCACTGCCTTTCAG
16	54901204 G	A	B10SNP2G0097	727	950	GCATTCCCCTTAATTCAGTTCAACCACA	ACTCAGAGATTTACTTGCCTCTGTCTCC	TCTGAGACTAGAGTAGCAGCCTC	CTCTGTCTCCTGAGACTAAAGG
16	87736505 C	T	B10SNPS0232	315	479	GCTTGCCATTTAGCCAGACACAAC	TCCTTGCGCCTTAGAGAATGCC	ACCATAGGTAGTAGATTCTGCG	GCCTTAGAGAATGCCGTTTTGATAC
17	3690688 G	A	B10SNPS0234	207	544	TTATCACAGGCAGGCAAGCAGG	TGTGGTTTCCAGCCCGACAAAG	GCAAGAAGAAGGGCTCCTG	GGTGGAAAGGAAACTCTTTACCTTG
17	24310623 T	A	B10SNPS0236	306	472	ACAGAATCTGTCTTGCTCTGCTTGG	GGGCACACATCCCTTTATCTAGCAAAC	GGCTCCTCGATAAGTTTGAATATCAC	ATCTAGCAAACCCATTTCTGGC
17	47451200 G	A	B10SNPS0237	387	587	GGCTCTGCTGATGACCTGTTCAAG	CGCTGGCCTGGGAATAAGTGTATTG	TGTGGCTGAACACTCATAAGC	AAGTGTATTGGTAGCCATCAGC
17	66263080 G	A	B10SNPS0239	484	693	ACAGAATCAGACTTCCTGCTTGCC	CCTGTCCAACTGTTACCCACATGG	ATTGCCAGGCTCTGTAGCAAG	GGTAGAATCCAATCCAGTGTCATC
17	84624403 A	G	B10SNPSG0168	254	478	AGTTACGCAAGTACCCCTGTGCTC	ACATGGCTCACTAGGCCCTTTCTG	GTGCTCTTCATCCTCCAAGG	TACTGCCTCATCATCTGCTG
18	15408257 C	T	B10SNPSG0174	385	638	GTTCAGACCAGAGAGCTTGGCTTG	GTCCTCAAATAGCACTGCCTGACAC	ACCCTAATTTTATCAGGGGTGC	TGCCTGACACAAGTCCTG
18	35366160 A	T	B10SNPSG0180	241	722	CTGGGAAGATCAAGGCCAAGTACTG	AGGTTACCAAAGCTCCAAGTTGCTC	CAAGGCCAAGTACTGTTTCATTG	GTGGCCTTAAATCTCAGTACTCAGG
18	46803584 T	C	B10SNPS0247	196	483	CTCCAGGATCTCAGTTGTATCTGTTGC	GGATGCTCGGTGAAGTCTGACTTAC	GTATCTGTTGCATGGCTCAC	GGGCATTATAGATCCCGGTATACAC
18	65425288 C	T	B10SNPS0249	155	440	GCACTGATTCCAATGGGCACATGAC	ACAATGGCATGGCTCTTCCAGAC	GACTATGAAGGCATACGCACTTTAC	CTTCCAGACTAGCCTTGTAGAGAG
18	83497271 G	A	B10SNPS0251	176	426	GGCAAGTTTCCGAGGAAAATCTGC	TGATGGTGCCTTTGTACCACAGTG	CAATTGCAGAGAAGTGGCAGG	AGGACATCTTGTCCGATACTG
19	23378788 T	G	B10SNPS0255	358	615	ACACAACTGTGTTGACCAGGGGAC	TTGCCCACATCTCATTAGGCTATGC	ACCAGGGGACGATCTTTGTAG	ACATCTCATTAGGCTATGCCTTTGG
19	46875560 A	G	B10SNPS0258	402	563	GATTTGTACCCTGTGGATGGAAGCC	TGCTGCTGTCACTCTGTGAAGAGC	TGAGCACACAGTTGGTCGTC	GAGCTTTTGTCTTTGTAACTCCAG
X	55120804 A	G	B10SNP2G0120	169	621	GCTTTTGCTTGGCCTTCAGCAGAC	AACCCTCGGCACTGTGAAGCATTG	TTGGCCTTCAGCAGACAAAAAG	CTTACCAGGAACACGTCTGTTAG
X	147904667 A	G	B10SNP2G0150	151	502	TGTACCTACTGAAGTCCAGTGAGGC	GCAGAGAGTGAACTGCACCATAGC	CCAGTGAGGCAGTAACTGTCAG	GGAAAAATCTGCCCAGTACTTTTCG
X	158414344 G	T	B10SNPSG0223	180	692	ACTGCCATTCCTGAAATCCCAACTG	TGGACAACAGGCATTCCTGGAGAC	TCCCAACTGAATTATTGATCTTCAC	ACACACATCTCCTTGGAATTGG

* Please click here to see DNA sequencing traces for all markers.

A mutation of *Ikbkg* causes immune deficiency without impairing degradation of IκBα

Owen M. Siggs[a], Michael Berger[a], Philippe Krebs[a], Carrie N. Arnold[a], Celine Eidenschenk[a], Christoph Huber[b], Elaine Pirie[a], Nora G. Smart[a], Kevin Khovananth[a], Yu Xia[a], Gerald McInerney[c], Gunilla B. Karlsson Hedestam[c], David Nemazee[b], and Bruce Beutler[a,1]

Departments of [a]Genetics and [b]Immunology, The Scripps Research Institute, La Jolla, CA 92037; and [c]Department of Microbiology, Tumor and Cell Biology, Karolinska Institutet, SE-171 77 Stockholm, Sweden

Contributed by Bruce Beutler, December 30, 2009 (sent for review December 17, 2009)

Null alleles of the gene encoding NEMO (NF-κB essential modulator) are lethal in hemizygous mice and men, whereas hypomorphic alleles typically cause a syndrome of immune deficiency and ectodermal dysplasia. Here we describe an allele of *Ikbkg* in mice that impaired Toll-like receptor signaling, lymph node formation, development of memory and regulatory T cells, and Ig production, but did not cause ectodermal dysplasia. Degradation of IκBα, which is considered a primary requirement for NEMO-mediated immune signaling, occurred normally in response to Toll-like receptor stimulation, yet ERK phosphorylation and NF-κB p65 nuclear translocation were severely impaired. This selective loss of function highlights the immunological importance of NEMO-regulated pathways beyond IκBα degradation, and offers a biochemical explanation for rare immune deficiencies in man.

mutagenesis | N-ethyl-nitrosourea | nuclear factor–κB essential modulator | p65 | Toll-like receptor

NF-κB transcription factors orchestrate numerous immunological and developmental responses (1). Among the receptors that trigger their activity are the Toll-like receptors (TLRs), the IL-1 receptor family, B and T cell antigen receptors (BCR/TCR), and TNF receptor family members, including the lymphotoxin β receptor (LTβR), CD40, and ectodysplasin-A receptor (EDAR). NF-κB activity is restrained by members of the IκB family, which prevent nuclear translocation of NF-κB subunits. IκB proteins (IκBα, IκBβ, and IκBε) are phosphorylated and degraded in response to stimulation, allowing release and nuclear translocation of NF-κB. IκB phosphorylation is mediated by the IκB kinase (IKK) complex, which consists of IKK1 (IKKα) and IKK2 (IKKβ) catalytic subunits, and the regulatory subunit NEMO (IKKγ).

IKK activity is also required for phosphorylation of the NF-κB members p105 (NF-κB1) and p65 (RelA). Phosphorylated p105 is polyubiquitinated and degraded in a manner similar to the IκB proteins (2), promoting activation of the TPL2 (tumor progression locus 2) → ERK axis (3, 4). p65 undergoes IKK-dependent phosphorylation at serine 536 (5), although the significance of this is unclear (1).

The range of diseases caused by NEMO mutations highlights the physiological importance of NEMO and the IKK complex. Null alleles of the X-linked gene encoding NEMO, *IKBKG*, cause the inflammatory skin disease incontinentia pigmenti in heterozygous females (6), and are lethal in hemizygous males, as they are in mice (7–9). Milder hypomorphic alleles are compatible with viability in males, but cause severe immune deficiency and developmental abnormalities of the teeth, hair, or sweat glands (10). These abnormalities of ectodermal derivatives are thought to result from disruption of EDAR signaling, yet there are reports of *IKBKG* mutations in immune-deficient patients without ectodermal dysplasia (11, 12). Other mutations appear to disrupt EDAR signaling and CD40-mediated Ig class switching but not TLR signaling (13), whereas another mutation disrupts EDAR signaling, but leaves TLR and CD40 signaling largely intact (14).

Whatever the combination of pathways affected, immune deficiency is a unifying consequence of germline NEMO mutations. But of all of the targets of NEMO and the IKK complex, there is no consensus of which are most critical for immunity. A great deal has been learned from conditional mutations of IKKα, IKKβ, and NEMO, but a full understanding of their physiological function has been precluded by the embryonic lethality that occurs in their absence. The same may be true of the biochemical functions of NEMO, some of which may occur downstream of pathways arrested in the absence of NEMO (e.g., p65 translocation or TPL2 activation).

Here we describe an *N*-ethyl-*N*-nitrosourea (ENU)–induced mutation of *Ikbkg* in mice that disrupted TLR signaling and conferred susceptibility to viral and bacterial infection. Hemizygous males were fully viable, yet azoospermic, and most lacked inguinal lymph nodes. Serum Ig concentrations were reduced, whereas memory, regulatory, and natural killer (NK) T cells were fewer in number. In response to TLR stimulation, IκBα degradation and phosphorylation of the MAPK homologue p38 were intact, yet phosphorylation of ERK and nuclear translocation of p65 were severely diminished. These data indicate that broad suppression of NEMO-mediated immune signaling can occur despite IκBα degradation.

Results

The panr2 Mutation Impairs TLR Signaling and Resistance to Infection. Among more than 30,000 third generation (G3) progeny of C57BL/6J males mutagenized with ENU, we observed a heritable phenotype marked by diminished secretion of soluble, bioactive TNF by macrophages stimulated with TLR ligands. This phenotype, designated *panr2* (*pan-r*esistance 2), was characterized by an impaired response to ligands for TLR3 [poly(I:C)], TLR4 (LPS), TLR7 (R-848) and TLR9 (CpG oligodeoxynucleotides) and the heterodimers TLR1/2 (Pam_3CSK_4) and TLR2/6 (MALP-2, peptidoglycan; Fig. 1). Multiple cytokines were affected, including TNFα, IL-6, IL-12p40, and MCP-1, as well as the inflammatory mediator NO. Secretion of type 1 IFN in response to TLR3 and TLR4 stimulation was not affected. *panr2* mice were also highly susceptible to an otherwise sublethal dose of murine cytomegalovirus (MCMV; Fig. S1*A*). Death within 6 d of MCMV infection was indicative of an innate immune defect, as combined deficiency of B and T cells permits survival of a similar infection for more than 2 weeks (15). Similarly, *panr2* mice succumbed to infection with *Listeria monocytogenes* within 4 d (Fig. S1*B*).

Author contributions: O.M.S. and B.B. designed research; O.M.S., M.B., P.K., C.A., C.E., C. H., E.P., K.K., and Y.X. performed research; G.M., G.B.K.H., and D.N. contributed new reagents/analytic tools; O.M.S. and B.B. analyzed data; and O.M.S., N.G.S., and B.B. wrote the paper.

The authors declare no conflict of interest.

[1]To whom correspondence should be addressed. E-mail: bruce@scripps.edu.

This article contains supporting information online at www.pnas.org/cgi/content/full/0915098107/DCSupplemental.

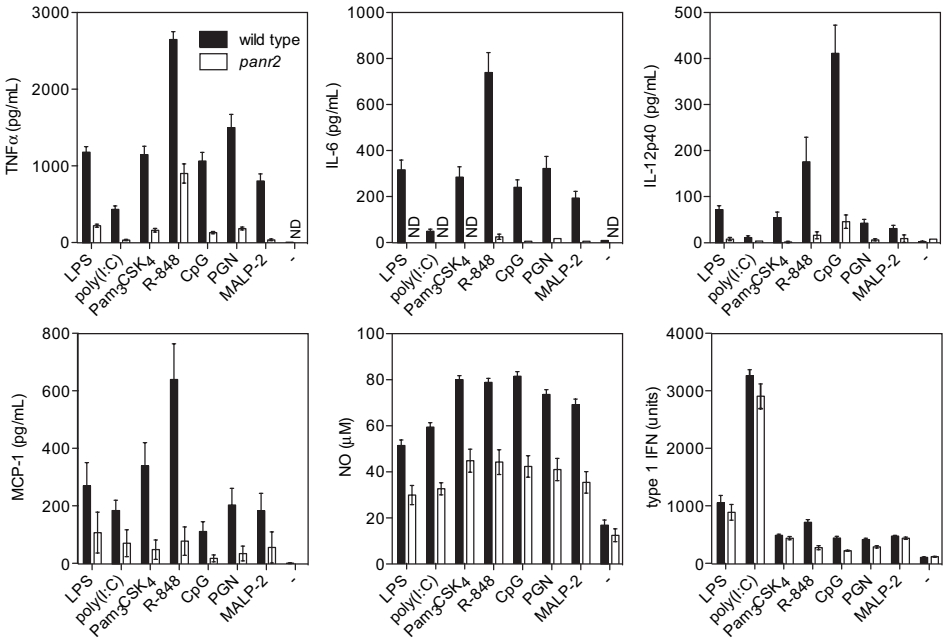


Fig. 1. The *panr2* mutation impairs TLR-induced cytokine secretion. Thioglycollate-elicited peritoneal macrophages from WT (n = 12) and *panr2* (n = 6) mice were stimulated with TLR ligands, and TNFα, IL-6, IL-12p40, and MCP-1 concentrations were calculated by ELISA. NO was measured by Griess assay, and type I IFN was measured by bioassay. Ligand concentrations were as follows: LPS (800 pg/mL), poly(I:C) (60 μg/mL), Pam_3CSK_4 (100 ng/mL), R-848 (40 ng/mL), CpG (1 μM), peptidoglycan (*PGN*, 2 μg/mL), MALP-2 (20 ng/mL). ND, not detected. Bars indicate mean and SE.

panr2 Mice Have a Mutation in Ikbkg. Given the broad suppression of NF-κB–dependent cytokine secretion (TNFα, IL-6, IL-12p40, MCP-1), along with normal secretion of an IRF3-dependent cytokine (type 1 IFN), we sequenced the coding exons and splice junction of five genes known to be required exclusively for TLR-induced activation of NF-κB (*Traf6*, *Tak1*, *Ikbkg*, *Chuk*, *Ikbkb*). Of a total of 26,246 target nucleotides, 21,056 (80.2%) were covered by high-quality reads in both wild type and mutant templates, and a single mutation was identified in *Ikbkg* (Fig. 2*A*). The mutation was a T-to-C transition at position 473 of *Ikbkg* cDNA, in exon 4 of a total of 10, leading to a leucine to proline substitution at residue 153 (L153P). The affected amino acid lay within the first coiled-coil domain of NEMO (Fig. 2*D*), and did not alter protein expression or electrophoretic mobility in macrophage lysates (Fig. 2*C*). Consistent with the chromosomal location of *Ikbkg*, the *panr2* phenotype was inherited in an X-linked recessive manner.

Unlike *Ikbkg* knockout mice, *panr2* hemizygotes were viable and born at Mendelian ratios (Fig. 2*B*). Conditional deletion of *Ikbkg* is

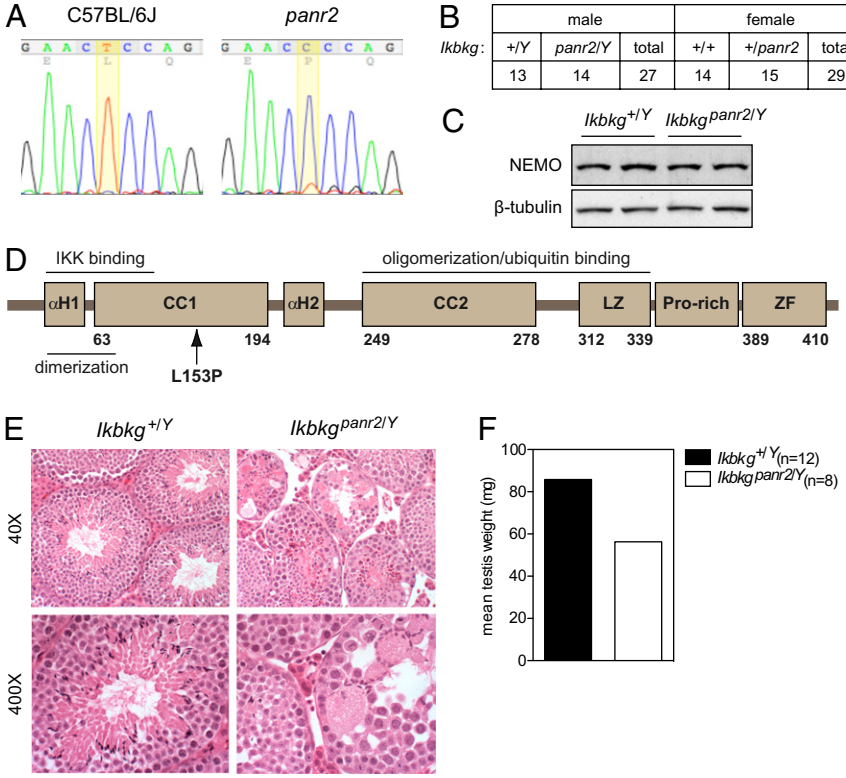


Fig. 2. *panr2* is a viable allele of *Ikbkg*. (*A*) Representative sequence trace of the *Ikbkg* gene from C57BL/6J and *panr2* mice. (*B*) Genotype ratios of 4-week-old offspring from an $Ikbkg^{+/Y}$ x $Ikbkg^{+/panr2}$ cross. (*C*) Expression of NEMO protein in macrophage lysates. (*D*) Domain structure and location of the *panr2* mutation (L153P) in the NEMO protein. H&E staining (*E*) and mean weight (*F*) of pooled testes from $Ikbkg^{+/Y}$ and $Ikbkg^{panr2/Y}$ littermates.

known to affect a variety of tissues, including the skin (16), liver (17), and intestinal epithelium (18), yet none of these tissues showed histological abnormalities in mutant mice. Survival of T (19) and B (20) lymphocytes is also precluded by conditional deletion of *Ikbkg*, yet both of these populations were present in *panr2* mice (Fig. S2). *panr2* hemizygous males were azoospermic, however, with histological analysis revealing cystic formations in the seminiferous tubules, as well as abnormal maturation of spermatids (Fig. 2*E*), and a mean testis weight approximately 35% lower than WT siblings (Fig. 2*F*). Inguinal lymph nodes were also absent or of diminished size in most mutant mice (Fig. S3).

Ikbkg^{panr2} Impairs Adaptive Immunity. Although NEMO is essential for survival of all T cells, IKKβ is not, and is known to be required specifically for the development of memory and regulatory T cells (19). Similarly, mice with an engineered mutation of p105 that cannot be phosphorylated by IKK (*Nfkb1*$^{SSAA/SSAA}$) also have fewer memory and regulatory T cells, and additionally have a reduction of NKT cells (21). These populations were also reduced in *panr2* mutants (Fig. 3), despite normal development of naive T cells (Fig. S2).

IKK activity is further required for signals transduced from the BCR, and for CD40-mediated recombination of Ig heavy chains. Serum of unimmunized *panr2* mice was deficient for all Ig isotypes tested, including IgM, indicating a broad impairment of B cell activation (Fig. 4*A*). After immunization with a recombinant Semliki Forest virus (rSFV) expressing β-gal vector, a strong inducer of antibody responses in WT mice, *panr2* mice produced no specific IgG or IgM antibody (Fig. 4*B*).

Impairment of MAPK Phosphorylation and p65 Translocation, but Not IκBα Degradation. To characterize the biochemical consequences of the *panr2* mutation, NF-κB and MAPK signaling events were examined in TLR-stimulated macrophages. In response to both LPS (Fig. 5*A*) and MALP-2 (Fig. S4*A*), p38 MAPK phosphorylation occurred normally in *panr2* cells, yet phosphorylation of p105, MEK (MAPK or ERK kinase), and ERK was severely impaired. Despite a mild impairment of IκBα phosphorylation, IκBα degradation remained intact. Nonetheless, nuclear translocation of p65 was suppressed in *panr2* cells (Fig. 5*C*), with accumulation occurring instead in the cytoplasmic fraction. Degradation of two other classical IκB proteins, IκBβ and IκBε, was not detected in cells of either genotype, although phosphorylation of IκBε was impaired to a similar degree as IκBα (Fig. S4*B*). And combined with its reduced phosphorylation, p105 was stabilized in *panr2* cells (Fig. S4*B*).

With respect to TNFα, the predominant role of the TPL2/MEK/ERK cascade is to promote its secretion, rather than accumulation of the 26-kDa membrane-associated precursor protein inside the cell (22). To examine the accumulation of TNFα inside *panr2* cells, macrophages were stimulated with LPS in the presence or absence of the secretory pathway inhibitor brefeldin A. Brefeldin A–treated *panr2* cells accumulated approximately twofold less intracellular TNFα, in contrast to a three- to fourfold reduction of surface TNFα (Fig. 5*B*) and a fivefold reduction of TNFα in the supernatant (Fig. 1). This disparity between intracellular and secreted TNF is consistent with observations in TPL2-deficient (22) and mutant (23) cells, but also imply that synthesis of TNFα precursor protein is affected independently of TPL2.

Discussion

By separating developmental and immunological functions of NEMO, the *panr2* mutant models a rare immune deficiency of man (11, 12). This allele is likely to be hypomorphic (rather than null or hypermorphic) for a number of reasons, viability being chief among them. TLR signaling is reduced, but not abolished as it is in NEMO-deficient fibroblasts (24), and survival of naive lymphocytes is also intact, in contrast to conditional knockouts of *Ikbkg* in B and T cells (19, 20). An absence of ectodermal dysplasia, which develops in mice with mutations of *Eda* (25), *Edar* (26), and *Edaradd* (27), suggests

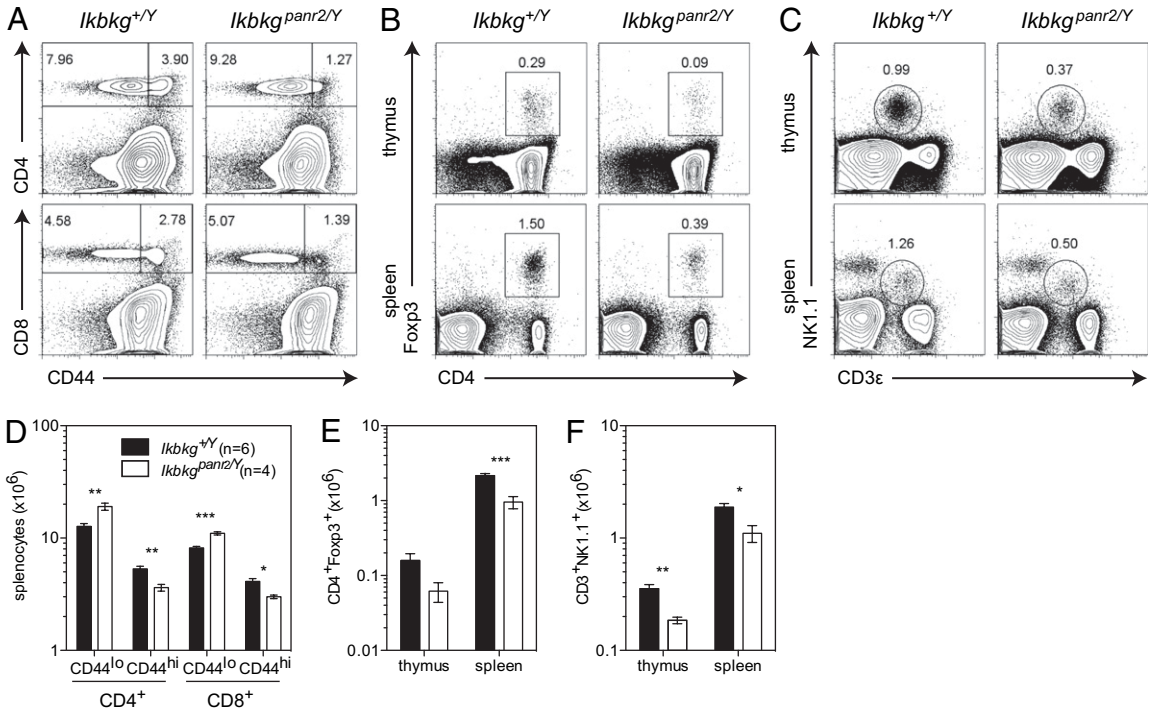


Fig. 3. Impaired development of memory, regulatory and NKT cells. Representative flow cytometry plots and relative frequencies of CD44^{lo} (naive) and CD44^{hi} (memory) T cells in spleen (*A*), Foxp3^{+} regulatory T cells in thymus and spleen (*B*), and CD3ε^{+}NK1.1^{+} NKT cells in thymus and spleen (*C*). Absolute numbers are represented in panels *D–F*. Numbers in each flow cytometry plot represents percentages of total lymphocytes, and bars represent mean and SE. (*$P < 0.05$; **$P < 0.01$; ***$P < 0.001$; Student's *t* test in *D–F*.)

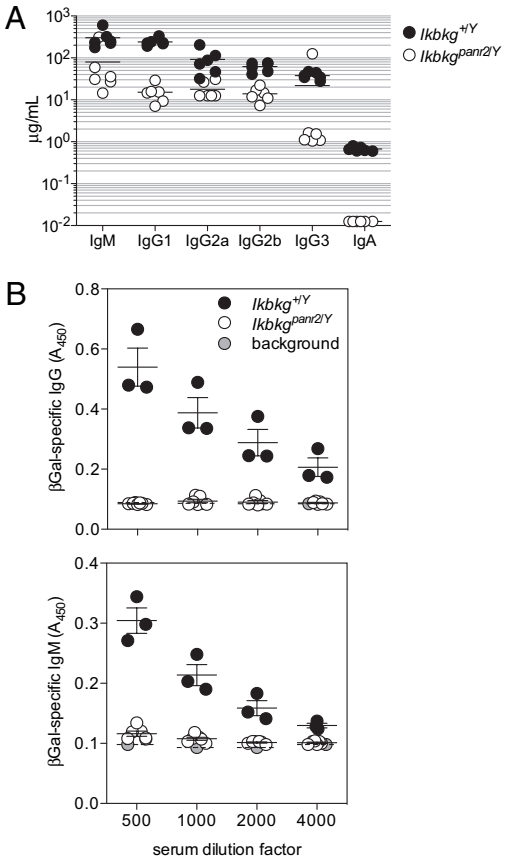


Fig. 4. Low serum Ig levels and impairment of antibody responses in *panr2* mice. (*A*) Total Ig isotypes in the serum of naive mice as measured by ELISA. Sample concentrations below the detection thresholds for IgG2a and IgA were given values of 12.5 µg/mL and 12.5 ng/mL, respectively. (*B*) Mice were immunized with a recombinant rSFV-β-gal, and β-gal–specific IgG and IgM at d 14 postimmunization was measured by ELISA.

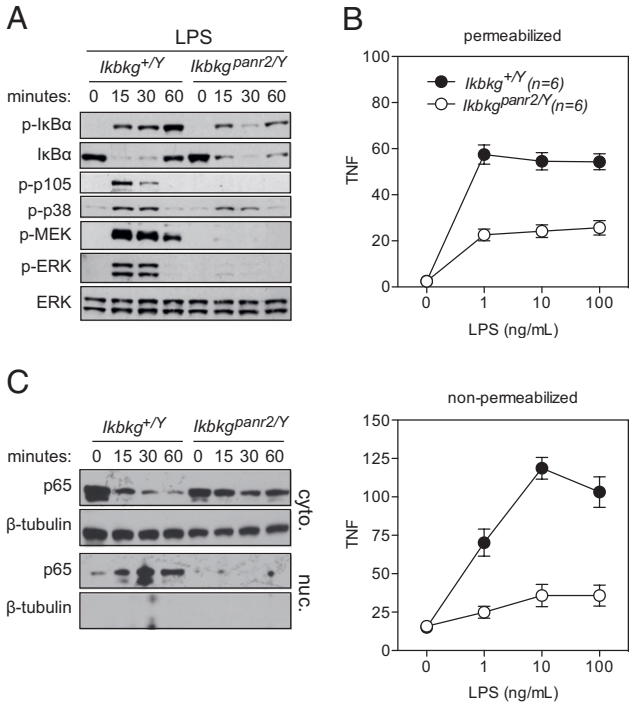


Fig. 5. The *panr2* mutation impairs MAPK and p105 phosphorylation, p65 translocation, and TNF production, but not IκBα degradation. (*A*) Thioglycollate-elicited macrophages were stimulated with LPS (1 µg/mL) for the indicated times, and cell lysates analyzed by Western blotting. (*B*) Macrophages were stimulated with LPS, and intracellular (*Upper*) or surface (*Lower*) TNF was measured by flow cytometry. (*C*) Cytoplasmic and nuclear fractions of LPS-stimulated macrophages stimulated with 1 µg/mL LPS were probed with antibodies against NF-κB p65 and β-tubulin.

that the *panr2* mutation is permissive to signals transduced from EDAR, but not from the TLRs, CD40, LTβR, BCR, and/or TCR.

Our data reveal that NEMO is important for the development of lymph nodes. IKK-mediated phosphorylation of the p50 precursor p105 is required for complete lymph node development (21), as are the NF-κB subunits p50 and p52 (28). Activation of both subunits via signaling from LTβR is required for secondary lymphoid organogenesis, with combined p50/p52 deficiency preventing lymph node development altogether (28). Together with our observations in *panr2* mice, these data suggest that canonical NF-κB activation through the IKK complex is important for the development of lymphoid architecture. Conversely, azoospermia has never, to our knowledge, been associated with mutations of the IKK complex, and may indicate a new developmental role for NEMO. Yet although the phenotypes of immune deficiency and sterility are linked, we have not excluded the possibility that an additional X-linked mutation is responsible for azoospermia.

An L153R mutation (as opposed to L153P in *panr2*) has also been described in a patient with hypohidrotic ectodermal dysplasia and immune deficiency (29). Unlike *panr2*, L153R mutant cells do not degrade IκBα in response to TLR stimulation (29), potentially accounting for a disruption of EDAR signaling and the development of ectodermal dysplasia in this patient. Mice expressing a "superrepressive" form of IκBα also develop ectodermal dysplasia (30). These results may be consistent with the largely intact nuclear translocation of p65 in an *IKBKG* mutant patient without ectodermal dysplasia (12).

But of all of the biochemical pathways disrupted by mutations in NEMO, which are the most important for immunity? The data presented here would imply that IκBα degradation alone is insufficient for immune competence, at least in macrophages, as TLR-induced IκBα degradation proceeds normally in *panr2* cells. Nuclear translocation of p65 is severely affected, however, implying a requirement for NEMO beyond IκBα degradation. In agreement with this finding, cytoplasmic retention of most p65 can occur in the combined absence of IκBα, IκBβ, and IκBε (31). The molecule(s) that retain p65 in the cytoplasm in this context are not known, although greater quantities of p100 and p105 can be recovered by p65 immunoprecipitation. As p105 phosphorylation and degradation are impaired in TLR-stimulated *panr2* cells, this may account for p65 cytoplasmic retention in the presence of IκBα degradation.

Impairment of the TPL2/MEK/ERK pathway could also account for immune deficiency, although this cannot be entirely responsible for the phenotypes observed. TLP2 mutant mice do not exhibit reduced numbers of memory or regulatory T cells (21), suggesting that development of these subsets depends on a TPL2-independent pathway. This pathway nevertheless requires IKK-mediated phosphorylation of p105, as *Ikbkg*$^{panr2/Y}$, p105 (*Nfkb1*$^{SSAA/SSAA}$), and IKKβ (*Ikbkb*$^{FL/Y}$;CD4-cre) mutant mice all show reductions in these populations. And with respect to the role of p105 phosphorylation in innate immunity, examination of the susceptibility of *Nfkb1*$^{SSAA/SSAA}$ mice to infection, as well as p65 nuclear translocation, will be of great interest.

Finally, TRAF6-mediated ubiquitination of NEMO is also necessary for complete activation of TLR-induced cytokine secretion. As revealed by mice lacking the target lysine residue (32), TLR-induced IκBα degradation, NF-κB activation and ERK phosphorylation are all intact in the absence of NEMO ubiquiti-

nation, whereas the cytokine response is not, suggesting that NEMO ubiquitination may regulate processes beyond IκBα degradation and ERK activation. The *panr2* mutation, in contrast, uncouples ERK phosphorylation and nuclear translocation of p65 without impairing IκBα degradation. We suggest that this is caused by alteration of the scaffolding function of NEMO, disrupting some but not all functions of NEMO and the IKK complex. This separation of function may offer a mechanistic explanation for rare immune deficiencies in man, and provides an animal model for their investigation.

Materials and Methods

Mice. *Ikbkg*^{panr2} (MGI:3808877, MMRRC:030659-UCD) was generated on a pure C57BL/6J background by ENU mutagenesis as previously described (33). The *panr2* strain was maintained by breeding heterozygous females with C57BL/6J males. All experiments were performed using age-matched male littermates between 5 and 10 weeks of age, and were in accordance with institutional animal care guidelines.

Macrophage Isolation and TLR Stimulation. Mice were injected with 1.5 mL of a 4% solution of Brewer's thioglycollate (wt/vol in distilled H_2O, autoclaved and aged for at least 1 month; BBL Microbiology Systems). Four days later, peritoneal cells were recovered from isofluorane-anesthetized mice by peritoneal lavage with 5 mL PBS solution. Peritoneal macrophages were plated in 96-well tissue culture treated plates (Costar) at a density of 1×10^5 cells per well. Following overnight incubation (37 °C in 5% CO_2), supernatant was discarded and replaced with 100 μL/well of TLR ligand solutions [in DMEM (Cellgro) plus 5% FBS (Atlanta Biosciences) and 2% penicillin/streptomycin (Gibco)], and incubated for 4 h. Supernatant was harvested to assay for the presence of cytokines, and replaced with a 2 mg/mL solution of MTT (M2128; Sigma) in DMEM plus 5% FBS and 2% penicillin/streptomycin to confirm macrophage viability. For the induction of NO, macrophages were preactivated with 20 ng/mL IFN-γ (R&D Systems) for 24 h, and stimulated with TLR ligands for an additional 24 h. LPS (from *Salmonella minnesota* R595), poly(I:C), MALP-2, and R-848 were all obtained from Enzo Life Sciences. Pam_3CSK_4 was from EMC Microcollections, CpG ODN from IDT (sequence TCCATGACGTTCCTGATGCT with phosphorothioate bonds), and peptidoglycan from Sigma. Purity of all ligands was validated using cells deficient for their corresponding TLR.

Detection of Cytokines and NO. TNFα, IL-6, IL-12p40 and MCP-1 were measured by ELISA according to the manufacturer's instructions (eBioscience). For type 1 IFN, L929 mouse fibroblasts stably transfected with an IFN-sensitive luciferase element (L929-ISRE) were incubated with supernatant for 5 h, washed once with PBS solution, lysed with reporter lysis buffer (Promega), and incubated overnight at −80°C. After thawing, 35 μL luciferase reagent (Promega) was added to each well, and luminescence read immediately on an Lmax plate reader (Molecular Devices). NO was measured by Griess assay. Concentrations of all cytokines and NO were interpolated from a standard curve.

Histology. Organs were fixed in 10% buffered formalin (Sigma), embedded in paraffin, sectioned, and stained with H&E.

Flow Cytometry. Lymphoid organ suspensions or macrophages were stained with antibodies against CD4, CD8, CD44, NK1.1, CD3ε, and B220 (eBioscience). Intracellular staining of Foxp3 was performed according to the manufacturer's protocol (eBioscience). For staining of TNF on macrophages, 2×10^5 cells were stimulated with the indicated dose of LPS for 2 h in the presence or absence of 5 μg/mL brefeldin A (Sigma), and stained with PE-conjugated anti-TNF (BD Biosciences). Intracellular staining of brefeldin A–treated cells was performed using the Cytofix/Cytoperm Fixation/Permeabilization solution kit (BD Biosciences).

Western Blotting. Peritoneal macrophages (2×10^6) were stimulated in 24-well plates with LPS (1 μg/mL) or MALP-2 (100 ng/mL) for the indicated lengths of time, separated into cytoplasmic and nuclear fractions (Nuclear Extract Kit; Active Motif) or lysed directly in sample buffer (Invitrogen), separated by SDS/PAGE, and transferred to nitrocellulose membranes. Membranes were probed with antibodies to NEMO (Imgenex), phospho-IκBα (Ser32/36), phospho-IκBε (Ser18/22), IκBα, IκBβ, IκBε, phospho-p38 (Thr180/Tyr182), phospho-p105 (Ser933), p105, phospho-MEK1/2 (Ser217/221), ERK1/2, phospho-ERK1/2 (Thr202/Tyr204), p65, and β-tubulin (Cell Signaling Technology).

Immunizations and Serum Antibodies. Single-round infectious rSFV encoding β-gal was generated and titered as previously described (34). Mice were injected i.p. with 200 μL of 0.9% sterile saline solution containing 2×10^6 infectious units of rSFV-β-gal on d 0. On d 14, blood was collected from the retro-orbital cavities of anesthetized mice into serum separator tubes and stored at −80°C. For antibody ELISA, polyvinyl chloride microtiter 96-well round-bottom plates (Fisher Scientific) were coated overnight at 4°C with 2 μg/mL β-gal (Roche). The plates were blocked with 5% milk, and serum samples were serially diluted in 1% milk. The plates were incubated with HRP-conjugated goat anti-mouse IgM or IgG (Southern Biotechnology), developed with SureBlue TMB Microwell Peroxidase Substrate and TMB Stop Solution (KPL), and read at 450 nm on a MAXline Emax Microplate Reader (Molecular Devices). Background for the assay was determined by incubating sera pooled from immunized WT mice on uncoated wells. Total serum immunoglobulins in preimmune sera were measured as previously described (35).

Viral and Bacterial Infections. Mice were infected with an i.p. dose of 2×10^5 PFU MCMV (Smith strain) prepared from BALB/c salivary glands. *L. monocytogenes* strain 10403S (Xenogen) was cultured in brain–heart infusion broth at 37°C, resuspended in PBS solution, and 10^5 CFU were administered via the tail vein. Infected mice were monitored daily for signs of illness.

ACKNOWLEDGMENTS. We thank Jordan Orange for valuable discussions; Liz Hanley, Christine Domingo, and Mercedes Gutierrez for mutagenesis and animal care; and the University of California San Diego histology core facility. This work was supported by National Institutes of Health Grants AI070167 (to B.B.) and RO1GM44809 (to D.N.), National Institute of Allergy and Infectious Diseases Broad Agency Announcement Contract HHSN272200700038C (to B.B.), the Bill and Melissa Gates Foundation (to B.B.), and a fellowship from the Swiss National Science Foundation (P.K.).

1. Hayden MS, Ghosh S (2008) Shared principles in NF-kappaB signaling. *Cell* 132: 344–362.
2. Heissmeyer V, Krappmann D, Hatada EN, Scheidereit C (2001) Shared pathways of IkappaB kinase-induced SCF(betaTrCP)-mediated ubiquitination and degradation for the NF-kappaB precursor p105 and IkappaBalpha. *Mol Cell Biol* 21:1024–1035.
3. Beinke S, Robinson MJ, Hugunin M, Ley SC (2004) Lipopolysaccharide activation of the TPL-2/MEK/extracellular signal-regulated kinase mitogen-activated protein kinase cascade is regulated by IkappaB kinase-induced proteolysis of NF-kappaB1 p105. *Mol Cell Biol* 24:9658–9667.
4. Waterfield M, Jin W, Reiley W, Zhang M, Sun SC (2004) IkappaB kinase is an essential component of the Tpl2 signaling pathway. *Mol Cell Biol* 24:6040–6048.
5. Sakurai H, Chiba H, Miyoshi H, Sugita T, Toriumi W (1999) IkappaB kinases phosphorylate NF-kappaB p65 subunit on serine 536 in the transactivation domain. *J Biol Chem* 274:30353–30356.
6. Smahi A, et al.; The International Incontinentia Pigmenti (IP) Consortium (2000) Genomic rearrangement in NEMO impairs NF-kappaB activation and is a cause of incontinentia pigmenti. *Nature* 405:466–472.
7. Makris C, et al. (2000) Female mice heterozygous for IKK gamma/NEMO deficiencies develop a dermatopathy similar to the human X-linked disorder incontinentia pigmenti. *Mol Cell* 5:969–979.
8. Rudolph D, et al. (2000) Severe liver degeneration and lack of NF-kappaB activation in NEMO/IKKgamma-deficient mice. *Genes Dev* 14:854–862.
9. Schmidt-Supprian M, et al. (2000) NEMO/IKK gamma-deficient mice model incontinentia pigmenti. *Mol Cell* 5:981–992.
10. Zonana J, et al. (2000) A novel X-linked disorder of immune deficiency and hypohidrotic ectodermal dysplasia is allelic to incontinentia pigmenti and due to mutations in IKK-gamma (NEMO). *Am J Hum Genet* 67:1555–1562.
11. Niehues T, et al. (2004) Nuclear factor kappaB essential modulator-deficient child with immunodeficiency yet without anhidrotic ectodermal dysplasia. *J Allergy Clin Immunol* 114:1456–1462.
12. Orange JS, et al. (2004) Human nuclear factor kappa B essential modulator mutation can result in immunodeficiency without ectodermal dysplasia. *J Allergy Clin Immunol* 114:650–656.
13. Jain A, et al. (2001) Specific missense mutations in NEMO result in hyper-IgM syndrome with hypohydrotic ectodermal dysplasia. *Nat Immunol* 2:223–228.
14. Salt BH, et al. (2008) IKBKG (nuclear factor-kappaB essential modulator) mutation can be associated with opportunistic infection without impairing Toll-like receptor function. *J Allergy Clin Immunol* 121:976–982.
15. Welsh RM, Brubaker JO, Vargas-Cortes M, O'Donnell CL (1991) Natural killer (NK) cell response to virus infections in mice with severe combined immunodeficiency. The stimulation of NK cells and the NK cell-dependent control of virus infections occur independently of T and B cell function. *J Exp Med* 173:1053–1063.
16. Nenci A, et al. (2006) Skin lesion development in a mouse model of incontinentia pigmenti is triggered by NEMO deficiency in epidermal keratinocytes and requires TNF signaling. *Hum Mol Genet* 15:531–542.
17. Luedde T, et al. (2007) Deletion of NEMO/IKKgamma in liver parenchymal cells causes steatohepatitis and hepatocellular carcinoma. *Cancer Cell* 11:119–132.
18. Nenci A, et al. (2007) Epithelial NEMO links innate immunity to chronic intestinal inflammation. *Nature* 446:557–561.

19. Schmidt-Supprian M, et al. (2003) Mature T cells depend on signaling through the IKK complex. *Immunity* 19:377–389.
20. Pasparakis M, Schmidt-Supprian M, Rajewsky K (2002) IkappaB kinase signaling is essential for maintenance of mature B cells. *J Exp Med* 196:743–752.
21. Sriskantharajah S, et al. (2009) Proteolysis of NF-kappaB1 p105 is essential for T cell antigen receptor-induced proliferation. *Nat Immunol* 10:38–47.
22. Rousseau S, et al. (2008) TPL2-mediated activation of ERK1 and ERK2 regulates the processing of pre-TNF alpha in LPS-stimulated macrophages. *J Cell Sci* 121:149–154.
23. Xiao N, et al. (2009) The Tpl2 mutation sluggish impairs type I IFN production and increases susceptibility to group B Streptococcal disease. *J Immunol* 183:7975–7983.
24. Yamaoka S, et al. (1998) Complementation cloning of NEMO, a component of the IkappaB kinase complex essential for NF-kappaB activation. *Cell* 93:1231–1240.
25. Srivastava AK, et al. (1997) The Tabby phenotype is caused by mutation in a mouse homologue of the EDA gene that reveals novel mouse and human exons and encodes a protein (ectodysplasin-A) with collagenous domains. *Proc Natl Acad Sci USA* 94: 13069–13074.
26. Headon DJ, Overbeek PA (1999) Involvement of a novel Tnf receptor homologue in hair follicle induction. *Nat Genet* 22:370–374.
27. Headon DJ, et al. (2001) Gene defect in ectodermal dysplasia implicates a death domain adapter in development. *Nature* 414:913–916.
28. Lo JC, et al. (2006) Coordination between NF-kappaB family members p50 and p52 is essential for mediating LTbetaR signals in the development and organization of secondary lymphoid tissues. *Blood* 107:1048–1055.
29. Orange JS, et al. (2002) Deficient natural killer cell cytotoxicity in patients with IKK-gamma/NEMO mutations. *J Clin Invest* 109:1501–1509.
30. Schmidt-Ullrich R, et al. (2001) Requirement of NF-kappaB/Rel for the development of hair follicles and other epidermal appendices. *Development* 128:3843–3853.
31. Tergaonkar V, Correa RG, Ikawa M, Verma IM (2005) Distinct roles of IkappaB proteins in regulating constitutive NF-kappaB activity. *Nat Cell Biol* 7:921–923.
32. Ni CY, et al. (2008) Cutting edge: K63-linked polyubiquitination of NEMO modulates TLR signaling and inflammation in vivo. *J Immunol* 180:7107–7111.
33. Georgel P, Du X, Hoebe K, Beutler BA (2008) ENU mutagenesis in mice. *Methods Mol Biol* 415:1–16.
34. Smerdou C, Liljeström P (1999) Two-helper RNA system for production of recombinant Semliki forest virus particles. *J Virol* 73:1092–1098.
35. Gavin AL, et al. (2006) Adjuvant-enhanced antibody responses in the absence of toll-like receptor signaling. *Science* 314:1936–1938.

Supporting Information

Siggs et al. 10.1073/pnas.0915098107

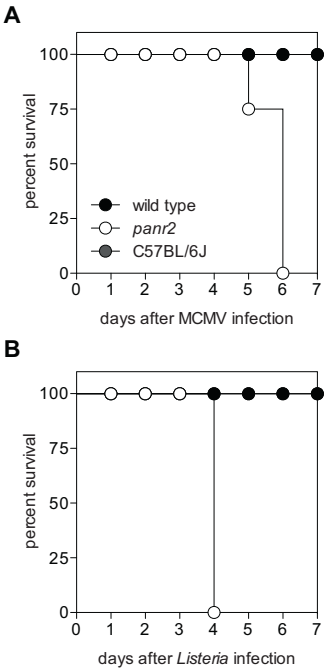


Fig. S1. *panr2* mice are susceptible to viral and bacterial infection. *panr2* (n = 4, 5), WT sibling (n = 5, 2), or age- and sex-matched C57BL/6J (n = 5, 5) mice were infected with 2×10^5 PFU MCMV (*A*), or 1×10^5 CFU *L. monocytogenes* (*B*), respectively, and survival was monitored for 7 d.

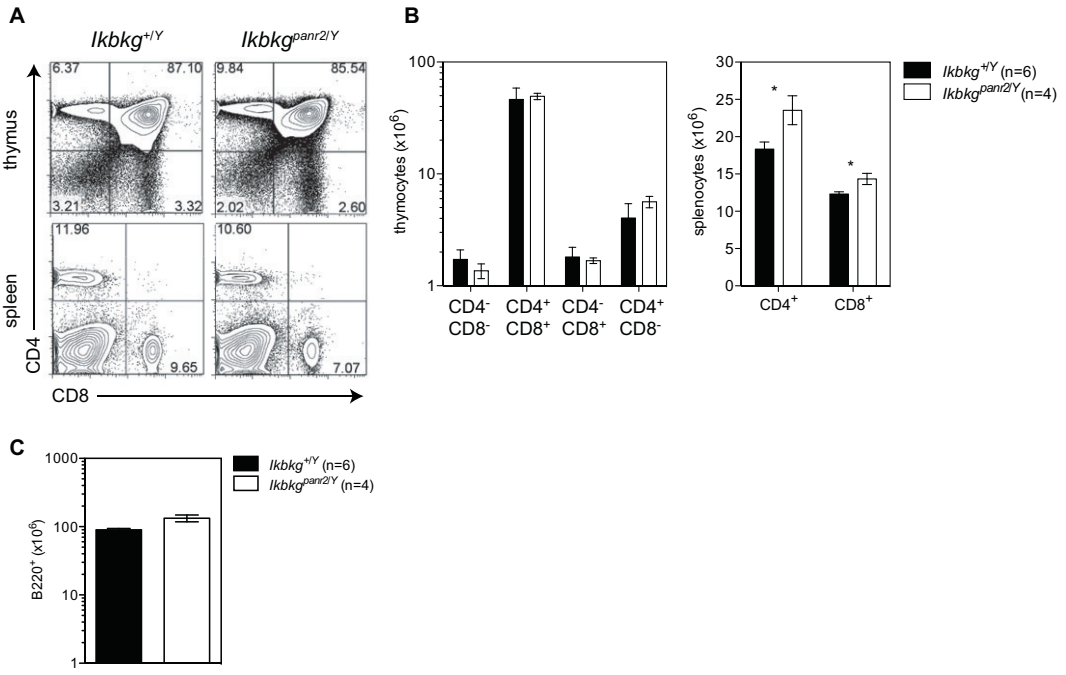


Fig. S2. T and B cell development is intact in *panr2* mice. Frequencies (*A*) and absolute numbers (*B*) of T cell populations in the thymus and spleen of *Ikbkg*$^{+/Y}$ and *Ikbkg*$^{panr2/Y}$ littermates. Absolute numbers of B cells present in the spleens of *Ikbkg*$^{+/Y}$ and *Ikbkg*$^{panr2/Y}$ littermates (*C*). (*$P < 0.05$ in *B*, Student's *t* test.)

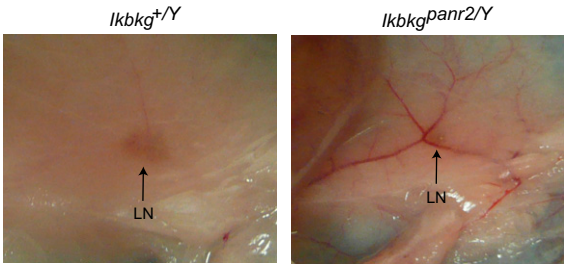


Fig. S3. Lymph nodes (*LN*) are diminished in *panr2* mice. *Ikbkg*$^{+/Y}$ and *Ikbkg*$^{panr2/Y}$ inguinal lymph nodes in situ.

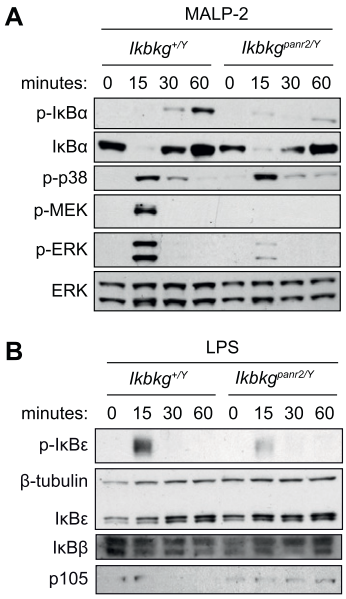


Fig. S4. MALP-2–induced signaling events and impaired IκBε phosphorylation and p105 degradation in *panr2* macrophages. (*A*) Thioglycollate-elicited peritoneal macrophages were stimulated with MALP-2 (100 ng/mL) for the indicated times, and cell lysates analyzed by Western blotting. (*B*) LPS-stimulated macrophage lysates were examined for the presence of phosphorylated IκBε, and total IκBε, IκBβ, and p105.

NIH Public Access
Author Manuscript
Nat Immunol. Author manuscript; available in PMC 2011 November 1.

Published in final edited form as:
Nat Immunol. 2011 May ; 12(5): 434–440. doi:10.1038/ni.2012.

The P4-type ATPase ATP11C is essential for B lymphopoiesis in adult bone marrow

Owen M. Siggs[1], **Carrie N. Arnold**[1], **Christoph Huber**[2], **Elaine Pirie**[1], **Yu Xia**[1], **Pei Lin**[1], **David Nemazee**[2], and **Bruce Beutler**[1]

[1] Department of Genetics, The Scripps Research Institute, 10550 North Torrey Pines Road, La Jolla, CA 92037

[2] Department of Immunology, The Scripps Research Institute, 10550 North Torrey Pines Road, La Jolla, CA 92037

Abstract

B lymphopoiesis begins in fetal liver, switching to bone marrow after birth where it persists for life. The unique developmental outcomes of each phase are well documented, yet their molecular requirements are not. Here we describe two allelic X-linked mutations in mice that caused a cell-intrinsic arrest of adult B lymphopoiesis. Mutant fetal liver progenitors generated B cells *in situ*, but not in irradiated adult bone marrow, highlighting a necessity for the affected pathway only in the context of adult bone marrow. The causative mutation was ascribed to *Atp11c*, which encodes a P4-type ATPase with no previously described function. Our data establish an essential, cell-autonomous and context-sensitive function for ATP11C, a putative aminophospholipid flippase, in B cell development.

Keywords

B cell development; fetal liver; IL-7; flippase

Introduction

B cell progenitors first arise in fetal liver, then in bone marrow shortly after birth, and give rise to three major mature populations[1]. Marginal zone (MZ) B cells localize to the splenic marginal zone and respond to blood-borne antigens independently of T cell help[2]. Follicular B cells, by contrast, respond to protein antigens in a T cell-dependent manner, and progressively undergo immunoglobulin (Ig) isotype switching and affinity maturation. B-1 B cells comprise a much smaller population, which predominates in the pleural and peritoneal cavities and contributes most of the serum IgM during the early phases of infection[3].

Users may view, print, copy, download and text and data- mine the content in such documents, for the purposes of academic research, subject always to the full Conditions of use: http://www.nature.com/authors/editorial_policies/license.html#terms

Correspondence should be addressed to: Bruce Beutler, M.D., Professor and Chairman, Department of Genetics, The Scripps Research Institute, 10550 N. Torrey Pines Road, SP293, La Jolla, CA 92037, telephone: 858-784-8610, fax: 858-784-8444, bruce@scripps.edu.

Author Contributions

O.M.S. designed and performed experiments, analyzed data and wrote the paper under the guidance of B.B.; C.N.A. and E.P. identified the *spelling* phenotype, and assisted with immunization experiments; Y.X. and P.L. assisted with positional cloning and mutation identification, and C.H. measured immunoglobulin isotypes with reagents contributed by D.N..

NIH-PA Author Manuscript
NIH-PA Author Manuscript
NIH-PA Author Manuscript

NIH-PA Author Manuscript

NIH-PA Author Manuscript

NIH-PA Author Manuscript

Whereas MZ and B-1 B cells are predominantly self-renewing, follicular B cells require constant replenishment from bone marrow, as demonstrated in mice with a conditional deletion of *Rag2* (ref. [4]). Briefly, deletion of *Rag2* in newborn mice prevents almost all follicular B cell development, but leaves MZ and B-1 populations largely intact. Similarly in adult mice, *Rag2* deletion causes a progressive decline in follicular B cell numbers, yet MZ and B-1 populations persist. A similar phenomenon has been reported for mice with a mutation of *Il7* (ref. [5]). While redundant with FLT3 in the fetal liver[6–8], interleukin 7 (IL-7) becomes essential for B cell development in the bone marrow shortly after birth[7]. As a result, MZ and B-1 B cells predominate in the periphery of *Il7* mutant mice, while follicular B cell numbers are severely reduced.

In the absence of IL-7 or its common gamma chain (γ_c)-associated receptor component IL-7R α, B cell development is arrested in the adult bone marrow shortly after cells acquiresurface B220, yet before they express CD19 or CD24 (refs. [8,9]). Expression of the transcription factor early B cell factor (EBF) via STAT5 signaling appears to be important at this stage, since overexpression of EBF or constitutively active STAT5 can overcome the developmental arrest in *Il7r* mutant progenitors[9,10]. Other data suggests that rather than inducing transcription of *Ebf1*, STAT5 signaling instead promotes B cell progenitor survival through induction of *Mcl1* (ref. [11]). Whichever the mechanism, IL-7 and EBF are both key determinants of B cell differentiation[12,13], and little else is known of the molecules and microenvironments that induce and maintain their expression in the adult.

We (and our colleagues[14]) describe here an essential role for the previously uncharacterized P4-type ATPase ATP11C in early B cell differentiation. ATP11C was redundant during B cell development in the fetal liver, yet essential in the context of adult bone marrow, where it was required for optimal responses to IL-7 and sustained expression of *Ebf1*.

Results

A heritable B cell deficiency

During a forward genetic screen for non-redundant regulators of lymphopoiesis (adapted from [15]), we identified several mice from common *N*-ethyl-*N*-nitrosourea- (ENU) treated founders with low percentages of $CD19^+$ cells in blood (Fig. 1a). The phenotype, named *emptyhive*, was transmitted as an X-linked recessive trait. Affected male mice were outwardly normal in behavior, fertility, lifespan and appearance, but were notably hyperbilirubinemic. This aspect of the phenotype, which stems from effects of the mutation in the liver, has been considered separately (O.M.S., B. Schnabl, B. Webb & B.B., submitted).

Among B cell progenitors in the bone marrow, *emptyhive* mutants had reduced numbers of cells beginning at the pre-pro-B to pro-B transition (Hardy fraction A [$B220^+CD43^+BP\text{-}1^-CD24^-$] to B [$B220^+CD43^+BP\text{-}1^-CD24^+$][16]) (Fig. 1b), with a severe deficiency of immature B cells (Hardy fraction E [$B220^+CD43^-IgM^-IgD^+$]). In the spleen, *emptyhive* mice had one-tenth the normal number of $CD19^+$ cells, largely due to a lack of follicular and transitional subsets (Fig. 1c,d), although numbers of MZ B cells and $Thy1.2^+$ cells and were normal. Numbers of B-1 cells, the predominant population of B cells in the peritoneal cavity, were reduced by a factor of three in mutant mice (Fig. 1d,e), while numbers of peritoneal B-2 cells were reduced by a factor of ten. B cells in the blood of mutant mice had undergone normal allelic exclusion at the *Igh* locus (Fig. 1f).

Despite a reduction in follicular B cell numbers, the B cells that remained appeared largely functional, and retained the capacity to produce all major immunoglobulin isotypes (Fig. 2a), as well as the ability to generate specific antibodies to T-independent and T-dependent

NIH-PA Author Manuscript

NIH-PA Author Manuscript

NIH-PA Author Manuscript

immunogens (here, 4-hydroxy-3-nitrophenylacetyl (NP)-conjugated Ficoll and NP-chicken gamma globulin, NP-CGG, Fig. 2b,c, respectively). However, 50% less NP-specific IgM and high-affinity IgG1 was produced in response to NP-Ficoll and alum-precipitated NP-CGG immunization, respectively.

Cell-intrinsic failure of adult B lymphopoiesis

To determine the cellular origin of the *emptyhive* phenotype, irradiated *Rag1* mutant mice were reconstituted with an equal mix of mutant and wild-type bone marrow. Although the Thy1.2$^+$ compartment was reconstituted equally, less than 1% of CD19$^+$ cells were of mutant origin (Fig. 3a), indicating that the defect was intrinsic to *emptyhive* B cell progenitors but did not appreciably affect T cell development. Even in the absence of competition, bone marrow cells from *emptyhive* donors were unable to repopulate any peripheral B cell compartment in irradiated recipients (Fig. 3b,c), and unlike their non-irradiated counterparts (Fig. 2b), recipients of mutant bone marrow also failed to produce specific antibody after immunization with NP-Ficoll (Fig. 3d). These data suggested a failure of adult B cell development in *emptyhive* mice, consistent with the severe reduction of immature B cells in mutant bone marrow (Fig. 1b) and the age-dependent decline of follicular, but not MZ, B cells in mutant spleens (Fig. 3e). This effect was not due to an intrinsic difference between adult and fetal progenitors, since neither bone marrow nor fetal liver cells could reconstitute the B cell compartment in irradiated recipients (Fig. 3c). Rather, the results suggest that *emptyhive* B cell progenitors, irrespective of their source, cannot develop in the microenvironment of adult bone marrow.

Immature and mature B cells were also entirely absent from the bone marrow of *emptyhive*-reconstituted recipients (Fig. 3b), with very few progressing beyond the B220$^+$CD19$^-$ pre-pro-B stage. This developmental arrest was even more severe than that observed in non-irradiated *emptyhive* or *Rag1* mutant mice, implying that a failure of IgM rearrangement was not the cause of developmental arrest in *emptyhive* mutants (Fig. 3b). Few mutant progenitors were capable of inducing expression of cytoplasmic IgM (cμ, Fig. 3f), consistent with the interpretation that the *emptyhive* phenotype originated from a defect upstream of *Rag*-mediated recombination.

Compromised responsiveness to IL-7

Because IL-7 is known to be essential for adult, but not fetal B cell development[5], we hypothesized that a specific failure of IL-7R signaling in B cell progenitors could explain the *emptyhive* phenotype. To examine the competence of IL-7R signaling in mutant progenitors, surface IgM$^-$ precursors were purified by flow cytometry and cultured *ex vivo* in the presence of IL-7. *emptyhive* progenitors formed lymphoblasts with similar kinetics to wild-type in response to IL-7, indicating that IL-7R-induced proliferation was largely intact (Fig. 4a). *In vitro* IL-7 treatment also leads to the differentiation of low frequencies of surface IgM$^+$ cells, which unexpectedly also emerged in *emptyhive* mutant cultures (Fig. 4b). Absolute numbers of IL-7-induced IgM$^+$ cells were nonetheless lower than wild-type: a deficiency exaggerated by as much as two-fold at high IL-7 concentrations (Fig. 4b).

Since these data suggested a qualitative or quantitative difference in the IL-7 response of *emptyhive* progenitors, we examined expression of EBF: an early transcriptional regulator of B cell differentiation[12] whose expression is lost in the absence of IL-7R signaling[9]. We measured *Ebf1* transcription in sorted pre-pro-B cells by RT-PCR, and found it to be severely reduced in *emptyhive* mutant progenitors (Fig. 4c). We also measured transcription of *Igll1*: a target of EBF[12] encoding the λ5 component of the surrogate light chain (SLC) portion of the pre-BCR[17]. Neither transcription of *Igll1* (Fig. 4c), nor surface expression of λ5 (Fig. 4d) was compromised in *emptyhive* mutant progenitors, suggesting that the lack of

NIH-PA Author Manuscript

NIH-PA Author Manuscript

NIH-PA Author Manuscript

Ebf1 transcript was either transient (and isolated to adult pre-pro-B cells or a subset thereof), or insufficient to affect *Igll1* expression.

Consistent with their intact IL-7 responsiveness *in vitro*, IL-7Rα was expressed in equivalent amounts on the surface of *emptyhive* mutant progenitors (Fig. 4e). Furthermore, in the absence of IL-7, FLT3 signaling is thought to account for residual B lymphopoiesis in fetal liver[18]. While *Flt3*$^{-/-}$*Il7*$^{-/-}$and *Flt3*$^{-/-}$*Il7r*$^{-/-}$double mutants lack all peripheral B cells[6,18], *emptyhive Flt3*$^{-/-}$double mutant mice had similar numbers of CD19^{+} splenocytes as *emptyhive* single mutants (Fig. 4e). This result implied that IL-7R signaling remained intact in *emptyhive* fetal liver progenitors, at least to a degree sufficient for fetal B lymphopoiesis in the absence of FLT3.

We also found no major role for programmed cell death as the cause of the *emptyhive* phenotype. Homozygosity for the *Fas*^{lpr} mutation[19] or a null allele of *Bcl2l11* (ref. [20]) could not correct the B cell deficiency in blood or bone marrow (Supplementary Fig. 1a-c), although partial rescue was observed in the presence of the B lineage-restricted *EμBCL2-22* transgene[21] (Supplementary Fig. 1a-c). Despite a relative increase of early B cell progenitors (B220^{+}IgM^{-}IgD^{-}, Supplementary Fig. 1b,c), numbers of mature B cells (B220^{+}IgM^{+}IgD^{+}) in the bone marrow of *EμBCL2* transgenic mutants were nevertheless reduced as severely as they were in the absence of the transgene (Supplementary Fig. 1c). In the spleen, numbers of follicular and marginal zone B cells were increased (Supplementary Fig. 1d), likely due to an increased half-life[4,21], which was consistent with the increased frequency of recirculating B cells observed in blood (Supplementary Fig. 1a).

Partial correction of B cell deficiency by a BCR transgene

pre-BCR signaling is an essential step in the progression of B cell development, signaling productive rearrangement at the *Igh* locus, triggering proliferation and differentiation of preB cells, and initiating recombination of the kappa light chain allele[22]. The presence of recombined heavy and light chain transgenes renders pre-BCR signaling redundant, and effectively bypasses the developmental stages that surround it. The hen egg lysozyme (HEL)-specific MM4 transgene[23], for example, is induced at the pre-pro-B stage, bypassing *Rag*-mediated recombination and expression of endogenous heavy and light chain genes and diverting progenitors directly to the surface IgM^{+} stage (Fig. 5a). Combining the *emptyhive* mutation with the MM4 transgene partially increased CD19^{+} cell frequencies in the blood (Fig. 5a) as well as numbers of IgM^{+} cells in the bone marrow (Fig. 5b). Since the MM4 transgene is a co-integration of heavy and light chain elements, this correction could reflect the effect of either recombined chain, or both in combination. We directly tested whether recombined heavy or light chains could rescue the *emptyhive* B cell defect in isolation using the 'switch- HEL' (SW_{HEL}) system[24], which consists of a HEL-specific V_H10 heavy chain knockin and the LC2 light chain transgene. Significant correction of the *emptyhive* B cell deficiency was achieved only in the presence of both a heavy chain knockin allele and light chain transgene (Fig. 5c). This result is in contrast with SLC or *Rag1*-deficient mutants, whose respective B cell deficiencies can be fully or partially corrected by light or heavy chain transgenes alone[25,26], and reveals that bypassing intermediate stages of B cell development (namely those within the B220^{+}CD19^{+}IgM^{-}IgD^{-} subset) could partially, but not completely, overcome the B cell deficiency in *emptyhive* mutant mice. IL-7R and pre-BCR signaling are both important during these stages[22], and this may therefore reflect a failure of one or both pathways during the development of *emptyhive* mutant precursors.

Mutation of an uncharacterized P4-type ATPase

To identify the mutation responsible for the *emptyhive* phenotype, mutant males were outcrossed to C3H/HeN females and backcrossed to their F1 daughters. A total of 25 F2

NIH-PA Author Manuscript

NIH-PA Author Manuscript

NIH-PA Author Manuscript

males (11 mutant and 14 wild-type phenotype) were typed at 128 polymorphic microsatellite markers. Phenotypic linkage to the X chromosome was detected (maximum LOD score of 8.37 at DXMit68) (Fig. 6a), and fine mapping with a further 105 meioses confined the mutation to a 13.51Mb interval between DXMit68 and DXMit74 (Fig. 6b). Coding exons and flanking splice junctions of the 81 annotated protein-encoding genes in the mutant interval were sequenced by capillary sequencing, with 85.6% high-quality coverage (Phred score>30) of all nucleotides (129589/151336). A single hemizygous transition mutation was identified in *Atp11c* (C2113T, CAG→TAG, Q655*) (Fig. 6c). Since this mutation (in exon 19 of 30) occurs before the penultimate exon, the mutant transcript is most likely targeted by the nonsense-mediated decay pathway shortly after transcription[27], although this has yet to be confirmed. In addition, we subsequently identified a mutant pedigree which phenocopied *emptyhive* (named *spelling*), and after sequencing *Atp11c* in these mice identified a second mutant allele (T1214A, ATA→AAA, I355K), which introduced a charged residue into the fourth of ten membrane-spanning domains (Fig. 6c, Supplementary Fig. 2). Compound heterozygosity for both alleles caused a B cell deficiency as severe as either parental strain (Fig. 6d,e), indicating that both *emptyhive* and *spelling* phenotypes were caused by X-linked recessive loss of function alleles of *Atp11c* (see Fig. 6f for protein schematic).

Atp11c is a previously uncharacterized gene encoding a P4-type ATPase, expressed most prominently in the liver, but also by many other cell types[28] (Supplementary Fig. 3). Little is known about mammalian P4-type ATPases in general, although mutation of one (ATP8B1) can cause progressive intrahepatic cholestasis in man[29]. While P-type ATPases are typically involved in cation transport[30], the P4 subtype includes inwardly-translocating lipid flippases thought to enrich aminophospholipids at the cytoplasmic leaflet of lipid bilayers[31,32]. Because P4-type ATPases have previously been implicated in phosphatidylserine (PS) asymmetry in yeast[31], we hypothesized that increased surface PS exposure and consequent PS-mediated phagocytosis could account for diminished numbers of B cells in *Atp11c* mutant mice[33]. PS expression on λ5-expressing cells was examined using Annexin V, yet no increase in surface expression was observed (Supplementary Fig. 4). Another requirement for phospholipid asymmetry could conceivably occur at the level of lipid rafts: membrane domains specialized in signal transduction[34] and potentially important for IL-7R or pre-BCR[35] signaling. Total surface expression of the raft-associated ganglioside G_{M1} (a target of the B subunit of cholera toxin) did not differ between wild-type and mutant cells (Supplementary Fig. 4), although closer examination of membrane microdomains around the IL-7R or pre-BCR will be needed to assess assembly of the rafts themselves.

Although not an aminophospholipid, phosphatidylinositol (3,4,5)-trisphosphate (PtdIns(3,4,5)P_3) is a phospholipid vital for signaling initiated at the IL-7R and pre-BCR[36]. Mutation of *Cd19* or *Pik3cd* cripples the function of phosphatidylinositol-3-kinase (PI3K) and generation of PtdIns(3,4,5)P_3 at the cytoplasmic leaflet of the pre-BCR signalosome, resulting in an impairment of MZ and B-1 B cell development[37,38]. Conversely, in the absence of the PtdIns(3,4,5)P_3 phosphatase PTEN, an excess of PtdIns(3,4,5)P_3 leads to an expansion of MZ and B-1 subsets[37]. Since mutations of both positive (*Pik3cd*, *Pik3r1*, *Btk*, *Pik3ap1*, *Plcg2* and *Blnk*) and negative (*Pten* and *Ptpn6*) regulators of PtdIns(3,4,5)P_3 availability are known to affect B cell development[39], and since phosphatidylinositol asymmetry may be disrupted in *emptyhive* progenitors, we combined the *emptyhive* mutation with mutations of *Cd19*, *Cd45*, *Inpp5d* and *Ptpn6*. Neither genetic enhancement (*Inpp5d*, *Ptpn6* mutation) nor diminishment (*Cd19*, *Cd45* mutation) of PtdIns(3,4,5)P_3 availability altered the *emptyhive* phenotype (Supplementary Fig. 5), implying that a disruption of phosphatidylinositol asymmetry at the cytoplasmic leaflet of the pre-BCR was an unlikely cause of B cell deficiency in *Atp11c* mutant mice.

NIH-PA Author Manuscript

NIH-PA Author Manuscript

NIH-PA Author Manuscript

A context-sensitive requirement for ATP11C

Having identified the causative mutation of the *emptyhive* phenotype, we were able to directly compare fetal B lymphopoiesis among wild-type and *Atp11c* mutant siblings *in utero*. Since IgM^+ cells only appear after ~E16 (ref. [40]), we examined E18.5 fetal liver cells, and found no difference in the number or frequency of $B220^+IgM^-$ or $B220^+IgM^+$ cells in *emptyhive* embryos (Fig. 7a,b). This finding provided further evidence that fetal B cell development was intact in *emptyhive* mice, and that residual B cells in mutant mice were of pre-adult origin. Despite this result, mutant fetal liver cells were unable to reconstitute any B cell lineage in irradiated adult recipients (Fig. 3c), indicating that the B cell deficiency was cell-autonomous, yet microenvironment-dependent.

Discussion

Our results define a key role for *Atp11c* in adult, but not fetal B cell development. MZ and B-1 B cell compartments were both relatively intact in mutant mice, whereas follicular B cell numbers declined with age, closely resembling that seen after postnatal deletion of *Rag2* (ref. [4]). Most strikingly, fetal liver B cell progenitors developed normally in *Atp11c* mutant fetal liver, but not in the adult bone marrow, revealing a cell-intrinsic, but context-dependent requirement for ATP11C.

Few genes have been reported to act in such a way[1], with *Il7* and *Il7r* being the prototypical examples[7]. *Il7*, *Il7r* and *Atp11c* are all essential for adult, but not fetal B cell development, with a cell-intrinsic requirement for both *Il7r* and *Atp11c* to sustain *Ebf1* transcription in pre-pro-B ($B220^+CD43^+BP\text{-}1^-CD24^-$) cells, and promote their differentiation to the pro-B ($B220^+CD43^+BP\text{-}1^-CD24^+$) stage[9]. But there are many key distinctions, the most notable being that T cell development proceeds in *Atp11c* mutants, but not in the absence of IL-7 or IL-7Rα[8,41,42]. Even among B cell progenitors, *Igll1* transcription and λ5 expression are intact in *Atp11c*, but not *Il7r* mutants[9]. *Ebf1*$^{-/-}$ mice show a similar arrest in B cell development, yet they too fail to transcribe *Igll1*, and since these mice lack all peripheral IgM^+ cells it does not appear to be an adult-restricted defect[12]. *Atp11c* mutant progenitors can clearly proliferate and differentiate *ex vivo* in the presence of IL-7, as well as during fetal development in the absence of FLT3 signaling[6,43], and unlike *Il7r* mutant fetal liver cells (which can give rise to mature B cells in the bone marrow of irradiated adults[7]), have their developmental potential determined by their environment, rather than their source.

While ATP11C is clearly not essential for all IL-7-dependent phenotypes, it may still be quantitatively or qualitatively important, affecting only a given threshold or branch of IL-7R signaling, or migration of B cell progenitors to a stromal depot of IL-7. Another interpretation is that ATP11C has only a transiently important role in early B cell development. Temporal restriction of IL-7R expression appears to be critical, since retroviral overexpression arrests B cell development at the pre-pro-B stage and inhibits *Ebf1* expression[44], implying that transient downregulation of IL-7R is important for the progression of B cell development.

IL-7 is also necessary for sustaining expression of EBF and the progression of B cell development beyond the pre-pro-B stage, but not because of IL-7R signaling in pre-pro-B cells themselves. Instead, signaling during the common lymphoid precursor to pre-pro-B transition induces high and persistent expression of *Ebf1*, presumably via a series of feedback loops at the *Ebf1* promoter[45], and allows maturation of pre-pro-B cells even in the absence of IL-7 (refs. [9,10,46]). Even though *Ebf1* appears not to be expressed in *Atp11c* mutant precursors, an EBF target gene is (*Igll1*), suggesting that ATP11C may be important not for the initial induction of *Ebf1*, but instead to sustain *Ebf1* expression through a

NIH-PA Author Manuscript

NIH-PA Author Manuscript

NIH-PA Author Manuscript

feedback loop[45]. Whatever the cause, a failure to sustain *Ebf1* expression has broad consequences for the regulation of early B cell development[13].

Beyond the transcriptional consequences, what is the substrate of ATP11C, and how might it affect IL-7 responsiveness and the sustained expression of *Ebf1*? The aminophospholipids (phosphatidylserine and phosphatidylethanolamine) are primary candidate substrates based upon the study of ATP11C orthologs in yeast[31,32], and lipid reconstitution experiments will be important to determine which specific variants are trafficked by ATP11C, and in which membrane compartments and/or domains. Further work will follow to define how this translates into an aberrant sensitivity to IL-7, and particularly why it does so only in the context of B cell development in the adult bone marrow. Presumably this outcome is related to phospholipid asymmetry during IL-7R signal transduction, or perhaps because of impaired migration to an IL-7-rich stromal niche. Identification of the substrate and affected pathway should expose a vital target for the specific regulation of adult B cell development, while *Atp11c* mutant strains will provide key experimental models to study membrane asymmetry and the origins of B cell immunity and malignancy.

Supplementary Material

Refer to Web version on PubMed Central for supplementary material.

Acknowledgments

We thank M. Gutierrez for animal care; T. Robinson, S. Kalina & C. Ross for genotyping; C. Goodnow (John Curtin School of Medical Research) & R. Brink (Garvan Institute) for mice; A. Feeney for discussions; D. La Vine for panel 5E; and reviewers for their valuable critiques. Supported by the Bill & Melinda Gates Foundation and National Institute of Allergy and Infectious Diseases Broad Agency Announcement Contract HHSN272200700038C (to B.B.), a General Sir John Monash Award (to O.M.S.), and an Irvington Institute Fellowship of the Cancer Research Institute (to C.N.A.).

References

1. Hardy RR, Hayakawa K. B cell development pathways. Annu Rev Immunol. 2001; 19:595–621. [PubMed: 11244048]
2. Lopes-Carvalho T, Foote J, Kearney JF. Marginal zone B cells in lymphocyte activation and regulation. Curr Opin Immunol. 2005; 17:244–250. [PubMed: 15886113]
3. Tung JW, Herzenberg LA. Unraveling B-1 progenitors. Curr Opin Immunol. 2007; 19:150–155. [PubMed: 17303402]
4. Hao Z, Rajewsky K. Homeostasis of peripheral B cells in the absence of B cell influx from the bone marrow. J Exp Med. 2001; 194:1151–1164. [PubMed: 11602643]
5. Carvalho TL, Mota-Santos T, Cumano A, Demengeot J, Vieira P. Arrested B lymphopoiesis and persistence of activated B cells in adult interleukin 7(-/)- mice. J Exp Med. 2001; 194:1141–1150. [PubMed: 11602642]
6. Sitnicka E, et al. Complementary signaling through flt3 and interleukin-7 receptor alpha is indispensable for fetal and adult B cell genesis. J Exp Med. 2003; 198:1495–1506. [PubMed: 14610045]
7. Kikuchi K, Kondo M. Developmental switch of mouse hematopoietic stem cells from fetal to adult type occurs in bone marrow after birth. Proc Natl Acad Sci USA. 2006; 103:17852–17857. [PubMed: 17090683]
8. von Freeden-Jeffry U, et al. Lymphopenia in interleukin (IL)-7 gene-deleted mice identifies IL-7 as a nonredundant cytokine. J Exp Med. 1995; 181:1519–1526. [PubMed: 7699333]
9. Kikuchi K, Lai AY, Hsu CL, Kondo M. IL-7 receptor signaling is necessary for stage transition in adult B cell development through up-regulation of EBF. J Exp Med. 2005; 201:1197–1203. [PubMed: 15837809]

NIH-PA Author Manuscript

NIH-PA Author Manuscript

NIH-PA Author Manuscript

10. Dias S, Silva H, Cumano A, Vieira P. Interleukin-7 is necessary to maintain the B cell potential in common lymphoid progenitors. J Exp Med. 2005; 201:971–979. [PubMed: 15767371]
11. Malin S, et al. Role of STAT5 in controlling cell survival and immunoglobulin gene recombination during pro-B cell development. Nat Immunol. 2010; 11:171–179. [PubMed: 19946273]
12. Lin H, Grosschedl R. Failure of B-cell differentiation in mice lacking the transcription factor EBF. Nature. 1995; 376:263–267. [PubMed: 7542362]
13. Busslinger M. Transcriptional control of early B cell development. Annu Rev Immunol. 2004; 22:55–79. [PubMed: 15032574]
14. Yabas M, et al. ATP11c is critical for phosphatidylserine internalization and B lymphocyte differentiation. Nat Immunol. 2011 this issue.
15. Nelms KA, Goodnow CC. Genome-wide ENU mutagenesis to reveal immune regulators. Immunity. 2001; 15 :409–418. [PubMed: 11567631]
16. Hardy RR, Carmack CE, Shinton SA, Kemp JD, Hayakawa K. Resolution and characterization of pro-B and pre-pro-B cell stages in normal mouse bone marrow. J Exp Med. 1991; 173:1213–1225. [PubMed: 1827140]
17. Karasuyama H, et al. The expression of Vpre-B/lambda 5 surrogate light chain in early bone marrow precursor B cells of normal and B cell-deficient mutant mice. Cell. 1994; 77:133–143. [PubMed: 8156589]
18. Jensen CT, et al. FLT3 ligand and not TSLP is the key regulator of IL-7-independent B-1 and B-2 B lymphopoiesis. Blood. 2008; 112:2297–2304. [PubMed: 18566323]
19. Watanabe-Fukunaga R, Brannan CI, Copeland NG, Jenkins NA, Nagata S. Lymphoproliferation disorder in mice explained by defects in Fas antigen that mediates apoptosis. Nature. 1992; 356:314–317. [PubMed: 1372394]
20. Bouillet P, et al. Proapoptotic Bcl-2 relative Bim required for certain apoptotic responses, leukocyte homeostasis, and to preclude autoimmunity. Science. 1999; 286:1735–1738. [PubMed: 10576740]
21. Strasser A, et al. Enforced BCL2 expression in B-lymphoid cells prolongs antibody responses and elicits autoimmune disease. Proc Natl Acad Sci USA. 1991; 88:8661–8665. [PubMed: 1924327]
22. Herzog S, Reth M, Jumaa H. Regulation of B-cell proliferation and differentiation by pre-B-cell receptor signalling. Nat Rev Immunol. 2009; 9:195–205. [PubMed: 19240758]
23. Brink RA, et al. Immunoglobulin M and D antigen receptors are both capable of mediating B lymphocyte activation, deletion, or anergy after interaction with specific antigen. J Exp Med. 1992; 176:991–1005. [PubMed: 1402669]
24. Phan TG, et al. B cell receptor-independent stimuli trigger immunoglobulin (Ig) class switch recombination and production of IgG autoantibodies by anergic self-reactive B cells. J Exp Med. 2003; 197:845–860. [PubMed: 12668643]
25. Pelanda R, Schaal S, Torres RM, Rajewsky K. A prematurely expressed Ig(kappa) transgene, but not V(kappa)J(kappa) gene segment targeted into the Ig(kappa) locus, can rescue B cell development in lambda5-deficient mice. Immunity. 1996; 5:229–239. [PubMed: 8808678]
26. Spanopoulou E, et al. Functional immunoglobulin transgenes guide ordered B-cell differentiation in Rag-1- deficient mice. Genes Dev. 1994; 8:1030–1042. [PubMed: 7926785]
27. Chang YF, Imam JS, Wilkinson MF. The nonsense-mediated decay RNA surveillance pathway. Annu Rev Biochem. 2007; 76:51–74. [PubMed: 17352659]
28. Su AI, et al. A gene atlas of the mouse and human protein-encoding transcriptomes. Proc Natl Acad Sci USA. 2004; 101:6062–6067. [PubMed: 15075390]
29. Bull LN, et al. A gene encoding a P-type ATPase mutated in two forms of hereditary cholestasis. Nat Genet. 1998; 18:219–224. [PubMed: 9500542]
30. Kühlbrandt W. Biology, structure and mechanism of P-type ATPases. Nat Rev Mol Cell Biol. 2004; 5:282–295. [PubMed: 15071553]
31. Tang X, Halleck MS, Schlegel RA, Williamson P. A subfamily of P-type ATPases with aminophospholipid transporting activity. Science. 1996; 272:1495–1497. [PubMed: 8633245]
32. Holthuis JC, Levine TP. Lipid traffic: floppy drives and a superhighway. Nat Rev Mol Cell Biol. 2005; 6:209–220. [PubMed: 15738987]

NIH-PA Author Manuscript

NIH-PA Author Manuscript

NIH-PA Author Manuscript

33. Leventis PA, Grinstein S. The distribution and function of phosphatidylserine in cellular membranes. Annu Rev Biophys. 2010; 39:407–427. [PubMed: 20192774]
34. Dykstra M, Cherukuri A, Sohn HW, Tzeng SJ, Pierce SK. Location is everything: lipid rafts and immune cell signaling. Annu Rev Immunol. 2003; 21:457–481. [PubMed: 12615889]
35. Guo B, Kato RM, Garcia-Lloret M, Wahl MI, Rawlings DJ. Engagement of the human pre-B cell receptor generates a lipid raft-dependent calcium signaling complex. Immunity. 2000; 13:243–253. [PubMed: 10981967]
36. Fruman DA, Cantley LC. Phosphoinositide 3-kinase in immunological systems. Semin Immunol. 2002; 14:7–18. [PubMed: 11884226]
37. Anzelon AN, Wu H, Rickert RC. Pten inactivation alters peripheral B lymphocyte fate and reconstitutes CD19 function. Nat Immunol. 2003; 4:287–294. [PubMed: 12563260]
38. Janas ML, et al. The effect of deleting p110delta on the phenotype and function of PTEN-deficient B cells. J Immunol. 2008; 180:739–746. [PubMed: 18178811]
39. Miosge LA, Goodnow CC. Genes, pathways and checkpoints in lymphocyte development and homeostasis. Immunol Cell Biol. 2005; 83:318–335. [PubMed: 16033527]
40. Raff MC, Megson M, Owen JJ, Cooper MD. Early production of intracellular IgM by B-lymphocyte precursors in mouse. Nature. 1976; 259:224–226. [PubMed: 814466]
41. Peschon JJ, et al. Early lymphocyte expansion is severely impaired in interleukin 7 receptor-deficient mice. J Exp Med. 1994; 180:1955–1960. [PubMed: 7964471]
42. Grabstein KH, et al. Inhibition of murine B and T lymphopoiesis in vivo by an anti-interleukin 7 monoclonal antibody. J Exp Med. 1993; 178:257–264. [PubMed: 8315381]
43. Vosshenrich CA, Cumano A, Müller W, Di Santo JP, Vieira P. Thymic stromal-derived lymphopoietin distinguishes fetal from adult B cell development. Nat Immunol. 2003; 4:773–779. [PubMed: 12872121]
44. Purohit SJ, et al. Determination of lymphoid cell fate is dependent on the expression status of the IL-7 receptor. EMBO J. 2003; 22:5511–5521. [PubMed: 14532123]
45. Roessler S, et al. Distinct promoters mediate the regulation of Ebf1 gene expression by interleukin-7 and Pax5. Mol Cell Biol. 2007; 27:579–594. [PubMed: 17101802]
46. Kikuchi K, Kasai H, Watanabe A, Lai AY, Kondo M. IL-7 specifies B cell fate at the common lymphoid progenitor to pre-proB transition stage by maintaining early B cell factor expression. J Immunol. 2008; 181:383–392. [PubMed: 18566404]

NIH-PA Author Manuscript
NIH-PA Author Manuscript
NIH-PA Author Manuscript

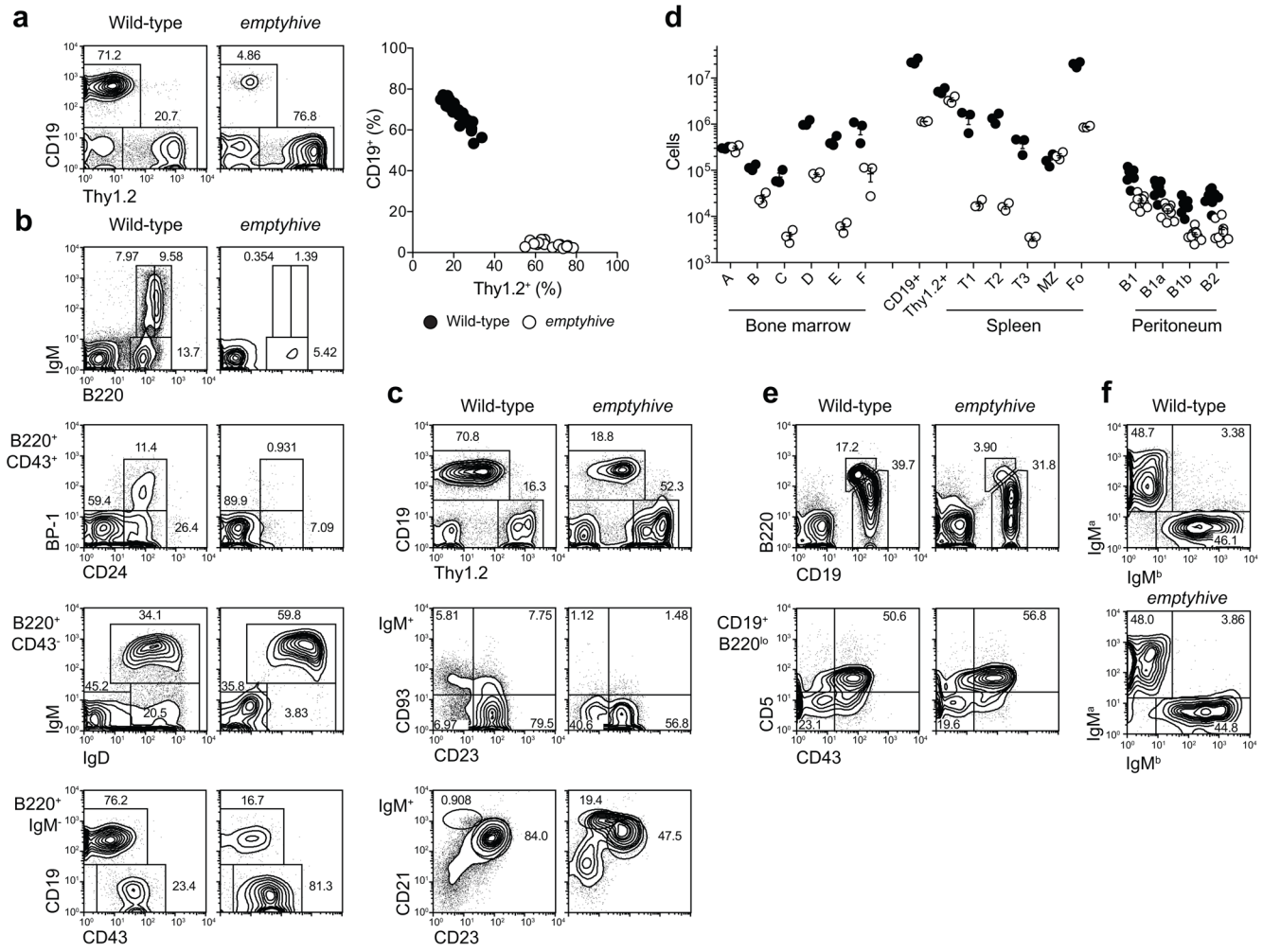


Figure 1.

A heritable B cell deficiency. (**a**) Frequencies of $CD19^+$ and $Thy1.2^+$ blood lymphocytes in the *emptyhive* pedigree. Percentages (**b**, **c, e**) and numbers (**d**) of B cell subsets in bone marrow (**b**), spleen (**c**) and peritoneal cavity (**e**). Hardy fractions in bone marrow (A-F) were gated as follows: A ($B220^+CD43^+BP\text{-}1^-CD24^-$); B ($B220^+CD43^+BP\text{-}1^-CD24^+$); C ($B220^+CD43^+BP\text{-}1^+CD24^+$); D ($B220^+CD43^-IgM^-IgD^-$); E ($B220^+CD43^-IgM^-IgD^+$); F ($B220^+CD43^-IgM^+IgD^+$). The C' fraction ($B220^+CD43^+BP^-1^+CD24^{hi}$) was not resolved. Fractions A and B-D may also be gated as $CD19^-$ and $CD19^+$ populations among $B220^+IgM^-$cells, respectively (**b**). IgM^+ splenocytes were divided into the following subsets: T1 ($CD93^+CD23^-$); T2 ($CD93^+CD23^+IgM^{int}$); T3 ($CD93^+CD23^+IgM^{hi}$); MZ ($CD93^-CD23^-IgM^{hi}CD21^{hi}$); Fo ($CD93^-CD23^+$). Peritoneal lymphocytes were divided into B-2 ($CD19^+B220^{hi}$), B-1 ($CD19^+B220^{lo-int}$), B-1a ($CD5^+CD43^+$) and B-1b ($CD5^-CD43^-$) subsets. (**f**) IgM allotype expression on $CD19^+$ blood lymphocytes from wild-type and *emptyhive* mice on a (C57BL/6 × BALB/c)F2 ($IgM^{a/b}$) background. Data are representative of three (**a** to **e**), or one (**f**) independent experiments using three mice per genotype. Each symbol represents an individual mouse.

NIH-PA Author Manuscript

NIH-PA Author Manuscript

NIH-PA Author Manuscript

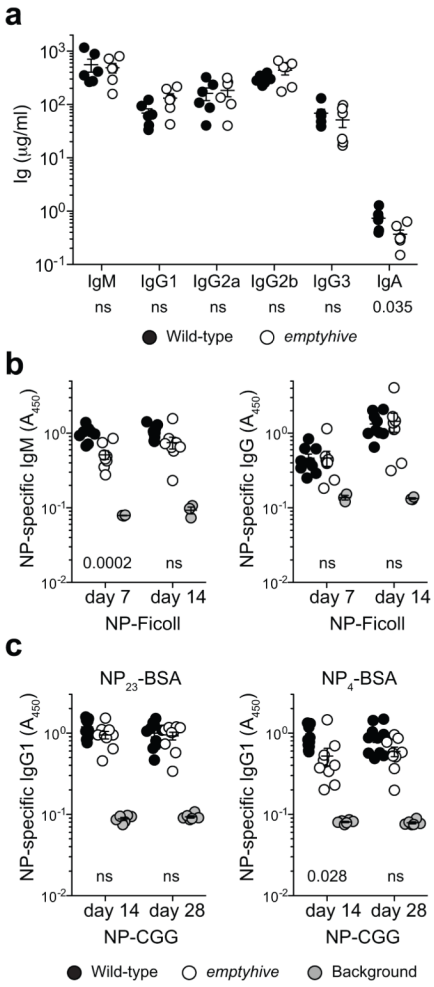


Figure 2.

Immunoglobulin secretion in *emptyhive* mice. (**a**) Total immunoglobulins as measured in the serum of 12–24 week-old naive mice. NP-specific antibodies were measured 7, 14 or 28 days after immunization of 12 week-old mice with NP-Ficoll (**b**) or alum-precipitated NP-CGG (**c**). Different capture antigens were used to discriminate between total (NP_{23}-BSA) and high-affinity (NP_4-BSA) IgG1 in response to NP-CGG. Each symbol represents an individual mouse from one experiment. *P* values indicated under plots were calculated by unpaired *t*-tests comparing wild-type and *emptyhive* groups. ns, not significant ($P > 0.05$).

NIH-PA Author Manuscript
NIH-PA Author Manuscript
NIH-PA Author Manuscript

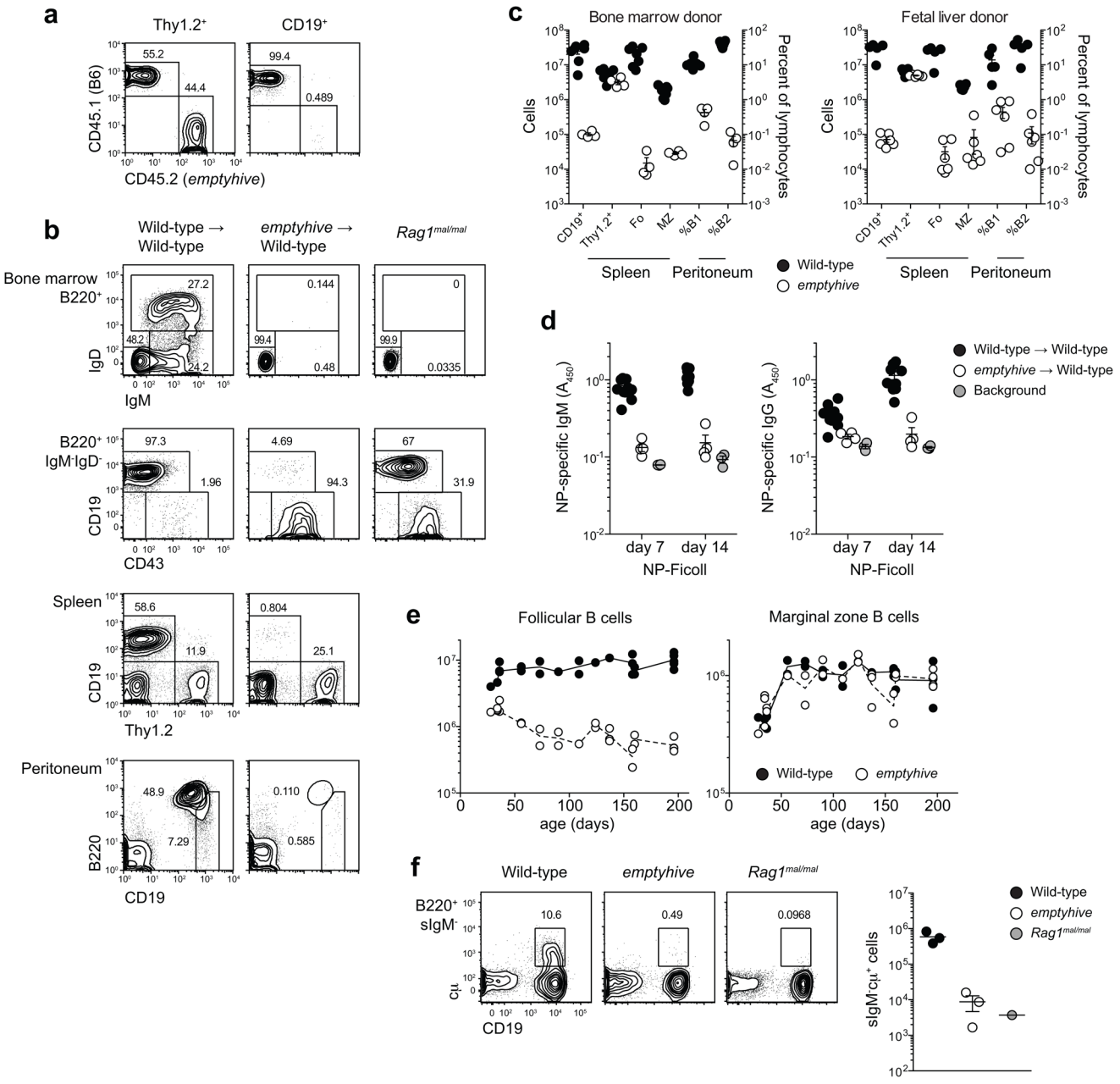


Figure 3.

A cell-intrinsic failure of adult B cell development. (**a**) A 1:1 mix of *emptyhive* (CD45.2) and wild-type (CD45.1) bone marrow was used to reconstitute irradiated *Rag1* mutant recipients, and lymphocyte repopulation was measured eight weeks later in blood. Unmixed bone marrow (**b**, **c**) or E16.5 fetal liver cells (**c**) from either mutant or wild-type donors (CD45.1) was used to reconstitute irradiated wild-type recipients (CD45.2), and donor-derived reconstitution of bone marrow, spleen and peritoneal B cell subsets was analyzed eight weeks later. (**d**) Bone marrow chimeras were immunized with NP-Ficoll 8 weeks after reconstitution, and NP-specific immunoglobulin titers measured 7 and 14 days later. (**e**) Absolute numbers of follicular and marginal zone B cells as a function of age. (**f**) Intracellular IgM (cμ) expression in $B220^+$ bone marrow cells negative for surface IgM.

Plots are representative of 6 (**a**), 4–7 (**b**), or 3 (**f**) mice per genotype, from one (**a**-**e**) or two (**f**) independent experiments. Each symbol represents an individual mouse.

NIH-PA Author Manuscript
NIH-PA Author Manuscript
NIH-PA Author Manuscript

NIH-PA Author Manuscript
NIH-PA Author Manuscript
NIH-PA Author Manuscript

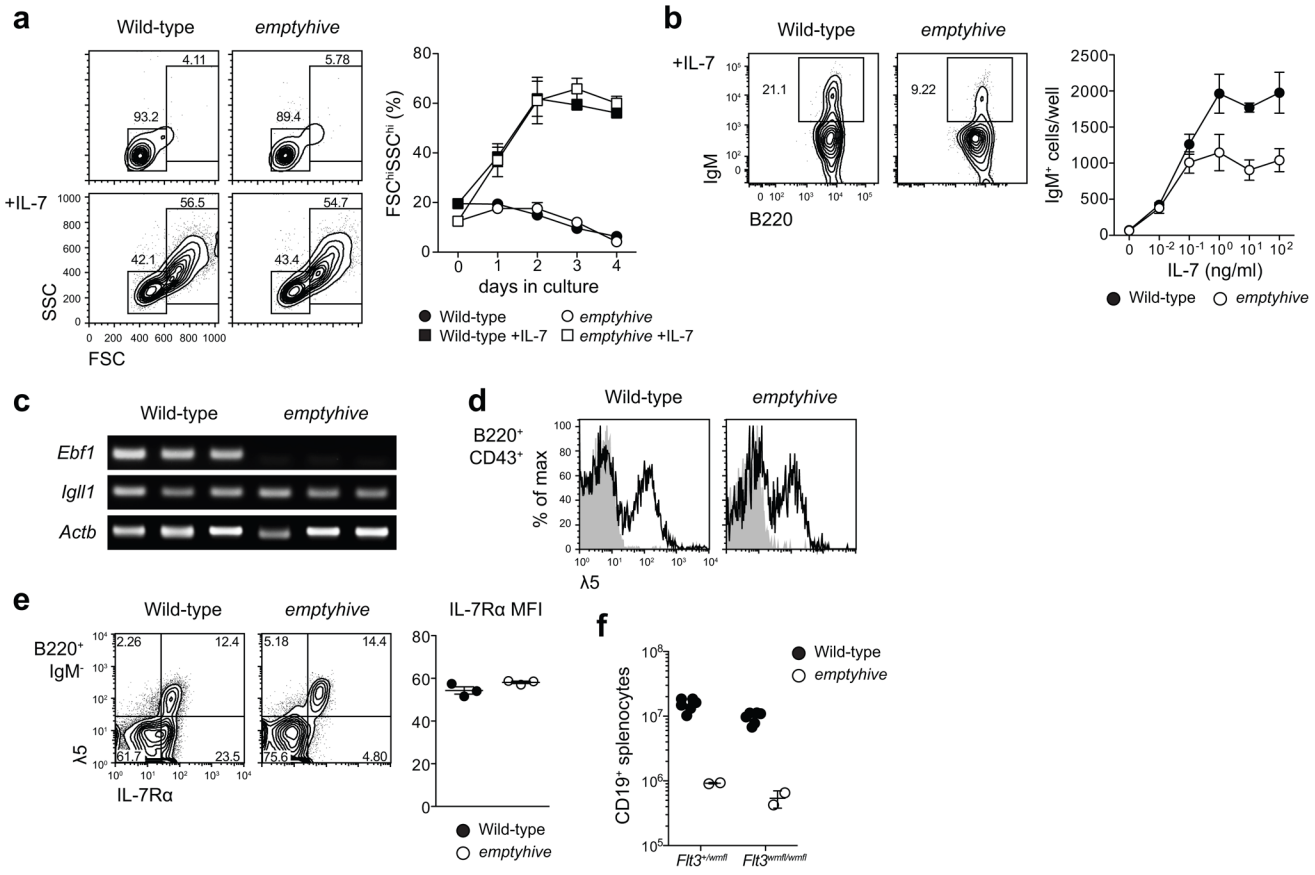


Figure 4.

Sensitivity to IL-7 and a failure to sustain expression of *Ebf1*. (**a**) $B220^+$ surface IgM^-bone marrow cells were sorted by flow cytometry and cultured *ex vivo* in the presence or absence of 100 ng/ml IL-7, and percentages of 7-AAD^- lymphoblasts ($FSC^{hi}SSC^{hi}$) were measured at daily intervals. Symbols and error bars represent the mean and standard error of three mice per genotype. (**b**) $B220^+$ surface IgM^- bone marrow cells sorted from wild-type (CD45.1) or *emptyhive* (CD45.2) mice were cocultured in the presence of various concentrations of IL-7. Following four days of culture, frequencies and numbers of 7-AAD^-surface IgM^+ cells were measured. Symbols and error bars represent the mean and standard error of three mice per genotype. (**c**) RT-PCR PCR of cDNA from pre-pro-B cells (7-$AAD^-B220^+IgM/IgD^-CD19^-NK1.1^-Ly6C^-$). Each lane represents an individual mouse. (**d**) λ5 (CD179b) expression on the surface of $B220^+CD43^+$ bone marrow lymphocytes. Shaded histograms represent rat IgG2a isotype control, while solid histograms show λ5 staining. (**e**) IL-7Rα (CD127) expression on the surface of $B220^+IgM^-$ bone marrow lymphocytes (dot plots, left), or $B220^+IgM^-λ5^+$ (mean fluorescence intensity, right). (**f**) Splenic B cell numbers in *emptyhive* mice with combined mutation of *Flt3*. All data are representative of two independent experiments, each with three mice per genotype.

NIH-PA Author Manuscript

NIH-PA Author Manuscript

NIH-PA Author Manuscript

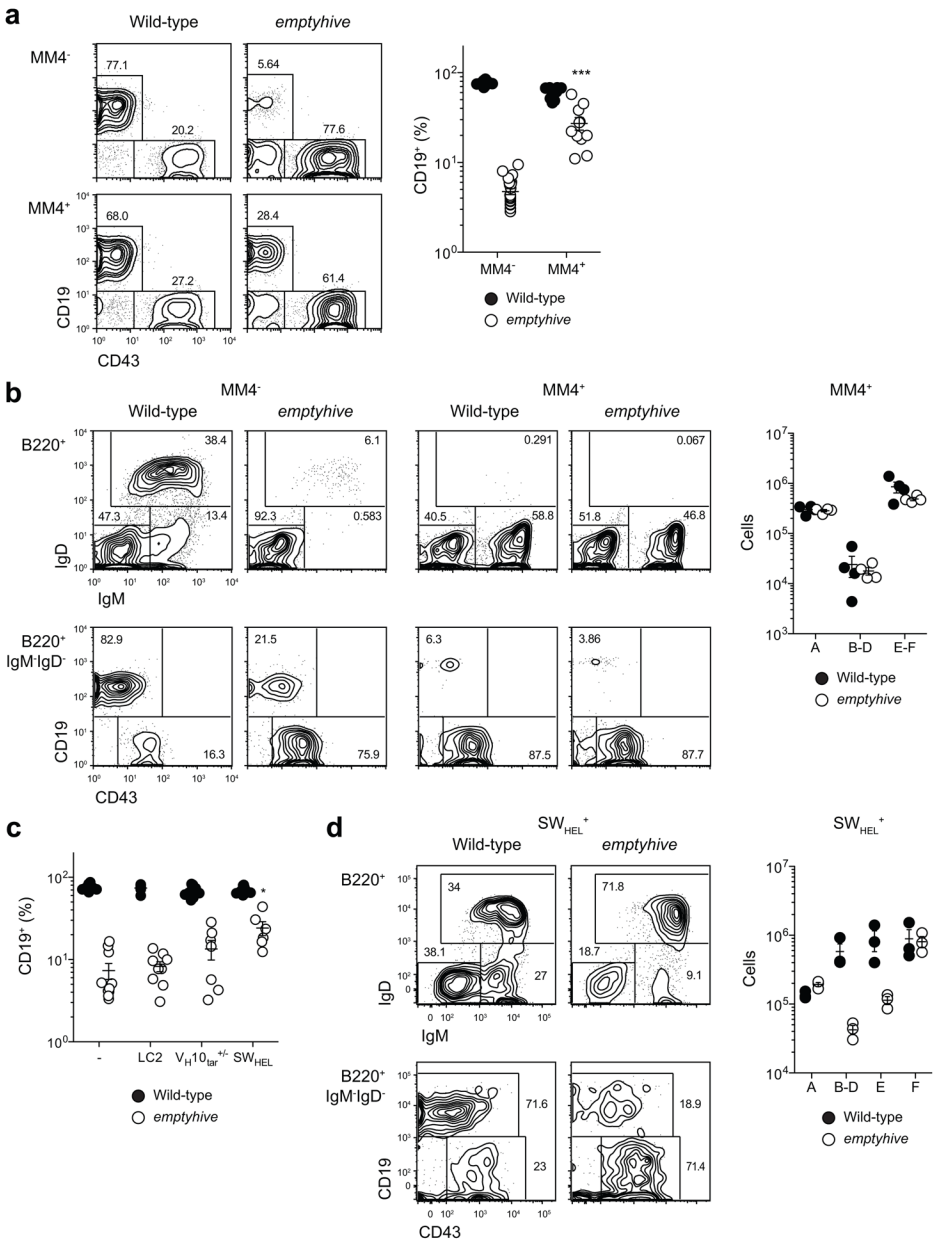


Figure 5.

Partial correction of the *emptyhive* phenotype by a BCR transgene. The *emptyhive* mutation was combined with the MM4 transgene (**a, b**) or the LC2 light chain transgene, V_H10_{tar} knockin allele, or both (SW_{HEL}) (**c, d**). Frequencies of $CD19^+$ cells in blood (**a**, **c**), or B cell subsets in bone marrow (**b**, **d**) as determined by flow cytometry. An unpaired *t*-test was performed in (**a**) with comparison to the *emptyhive* non-transgenic group. For (**c**), a one-way ANOVA followed by Bonferroni post test was used, with reference to the *emptyhive* non-transgenic group. $*P < 0.05$, $***P < 0.001$. Each symbol represents an individual mouse, and data are representative of two independent experiments.

NIH-PA Author Manuscript

NIH-PA Author Manuscript

NIH-PA Author Manuscript

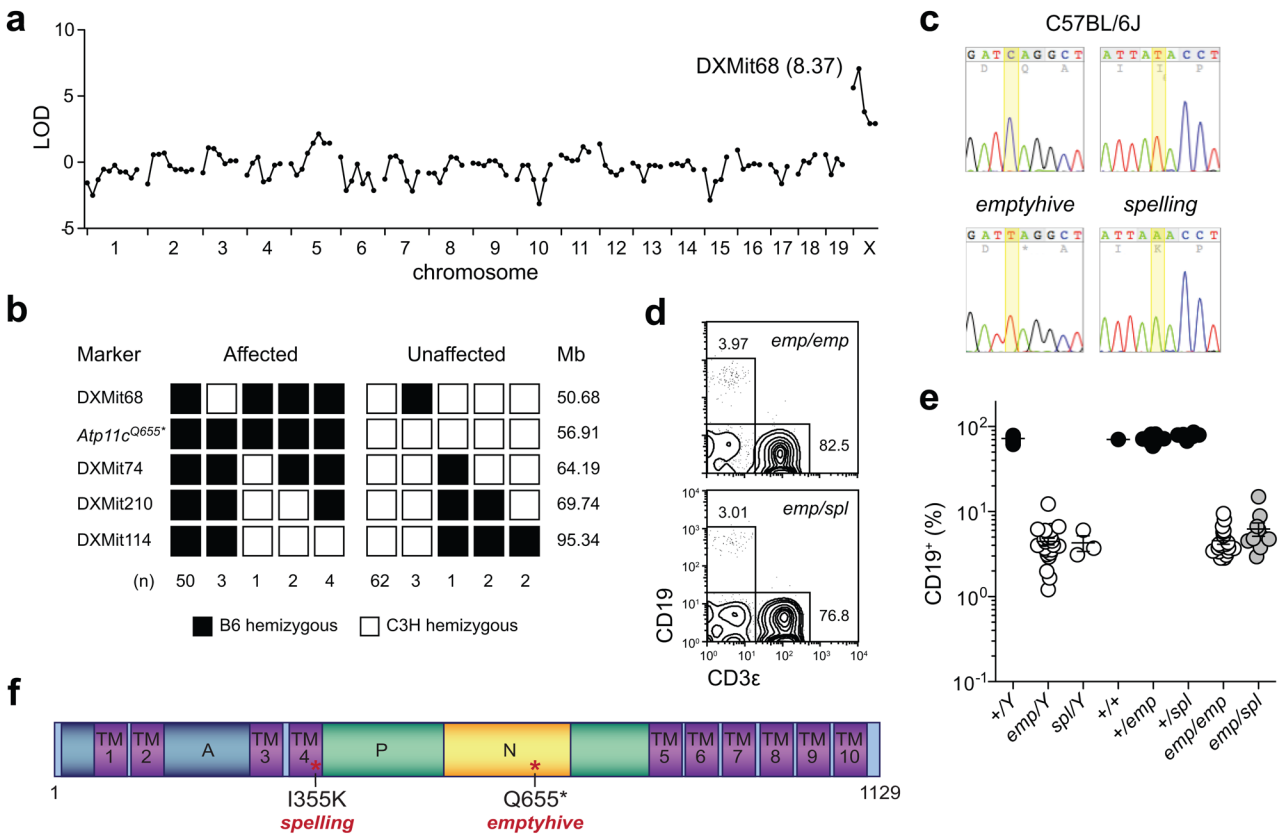


Figure 6.

The *emptyhive* phenotype is caused by a recessive mutation of *Atp11c*. Chromosomal (**a**) and fine (**b**) mapping of the *emptyhive* phenotype. (**c**) Sequence traces of the mutated nucleotides (C2113T, Q655*; T1214A, I355K) in *Atp11c* as detected in *emptyhive* and *spelling* hemizygous males. (**d**, **e**) Allelism test of *spelling* and *emptyhive* alleles. Progeny from an $Atp11c^{spl/Y} \times Atp11c^{emp/+}$ mating were tested for phenotypic complementation by measuring the frequency of B cells in blood. Each symbol represents an individual mouse. (**f**) Predicted ATP11C protein domain structure. TM, transmembrane domain; P, phosphorylation domain; A, actuator domain; N, nucleotide binding domain.

NIH-PA Author Manuscript
NIH-PA Author Manuscript
NIH-PA Author Manuscript

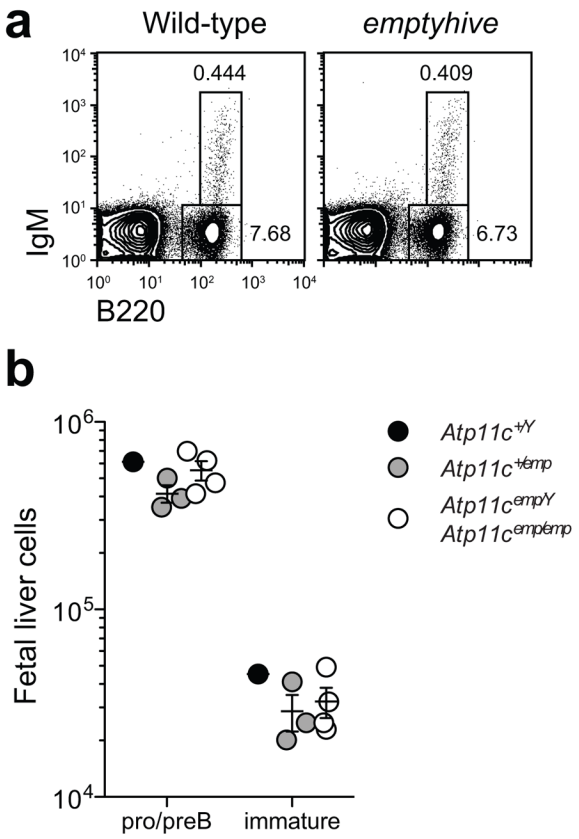


Figure 7.

Intact B lymphopoiesis in fetal liver. Percentages (**a**) and absolute numbers (**b**) of fraction A-D ($B220^+IgM^-$) and immature ($B220^+IgM^+$, fraction E) B cells in the fetal liver of E18.5 embryonic siblings from $Atp11c^{emp/Y} \times Atp11c^{+/emp}$ matings. Each symbol represents an individual embryo, and data are representative of two experiments with 8–14 embryos per experiment.

X-linked cholestasis in mouse due to mutations of the P4-ATPase ATP11C

Owen M. Siggs[a], Bernd Schnabl[b], Bill Webb[c], and Bruce Beutler[a,1]

[a]Department of Genetics and [c]Center for Metabolomics and Mass Spectrometry, The Scripps Research Institute, La Jolla, CA 92037; and [b]Department of Medicine, University of California at San Diego, School of Medicine, La Jolla, CA 92093

Contributed by Bruce Beutler, March 28, 2011 (sent for review February 15, 2011)

Transporters at the hepatic canalicular membrane are essential for the formation of bile and the prevention of cholestatic liver disease. One such example is ATP8B1, a P4-type ATPase disrupted in three inherited forms of intrahepatic cholestasis. Mutation of the X-linked mouse gene *Atp11c*, which encodes a paralogous P4-type ATPase, precludes B-cell development in the adult bone marrow, but also causes hyperbilirubinemia. Here we explore this hyperbilirubinemia in two independent *Atp11c* mutant mouse lines, and find that it originates from an effect on nonhematopoietic cells. Liver function tests and histology revealed only minor pathology, although cholic acid was elevated in the serum of mutant mice, and became toxic to mutant mice when given as a dietary supplement. The majority of homozygous mutant females also died of dystocia in a maternal genotype-specific manner. ATP11C therefore represents a multifunctional transporter, essential for adult B-cell development, the prevention of intrahepatic cholestasis, and parturition, and is a new candidate for genetically undiagnosed cases of cholestasis and dystocia in humans.

gallbladder | uterus | enterohepatic circulation | jaundice | bile acid

Bile is essential for the emulsification of dietary lipids and fat-soluble vitamins, for the catabolism of cholesterol, and for the expulsion of toxic metabolites such as bilirubin. The detergent properties of bile are conferred by bile acids, which are synthesized in the liver from cholesterol (1). Following their synthesis in liver, bile acids (along with other constituents of bile) are transported across the canalicular membrane of hepatocytes, drain into the gallbladder via bile ducts, and are expelled into the duodenum in response to cholecystokinin, secreted by epithelial cells of the duodenum.

Cholestasis is an acquired or inherited syndrome associated with the retention of bile constituents in the circulation. Among the inherited forms, progressive familial intrahepatic cholestasis (PFIC) is a degenerative liver disease caused by mutations affecting canalicular hepatocyte membrane transporters (2). PFIC1 is caused by mutation of *ATP8B1* (3), encoding a P4-type ATPase involved in the translocation of phosphatidylserine (PS) from the exoplasmic to cytoplasmic membrane leaflets (4). PFIC2 is caused by mutations of *ABCB11*, encoding the bile salt export pump (BSEP) (5). BSEP is the primary transporter of hydrophobic bile acids, and as a consequence, patients with PFIC2 have extremely low concentrations of bile salts in bile (6).

Finally, mutation of *ABCB4* leads to PFIC3 (7), which can be clinically distinguished from PFIC1 and PFIC2 by elevated quantities of serum γ-glutamyl transferase (GGT). *ABCB4* encodes the MDR3 protein (MDR2 in mouse), which is essential for the translocation of phosphatidylcholine from the inner to outer leaflet of the canalicular membrane (8), as highlighted by the near absence of phosphatidylcholine from the bile of PFIC3 patients and *Abcb4* mutant mice (9).

Dubin–Johnson syndrome, caused by mutations of *ABCC2*, is also caused by inactivation of a canalicular transporter (MRP2) (2). Hyperbilirubinemia is common to patients with PFIC and Dubin–Johnson syndrome, but for different reasons. In the case of PFIC, a failure of transport leads to liver damage, which in turn prevents the expulsion of bile acids and bilirubin, leading to hyperbilirubinemia. MRP2, on the contrary, is a key transporter of conjugated bilirubin, and patients with Dubin–Johnson syndrome therefore develop hyperbilirubinemia without excessive retention of bile acids.

The similar clinical outcomes of *ATP8B1* and *ABCB4* mutations, and *ABCB11* and *ABCC2* mutations, all highlight the importance of phospholipid asymmetry and its role in canalicular transport. Phospholipid asymmetry is known to be influenced by the P4-type ATPases, a group of hypothetical aminophospholipid flippases (to which ATP8B1 belongs), which are thought to enrich phosphatidylserine and/or phosphatidylethanolamine at the cytoplasmic membrane leaflet (10). However, beyond ATP8B1, little is known of the functions of the 13 other mammalian P4-type ATPases (11).

We and others have recently discovered that mutation of the P4-type ATPase ATP11C in mouse leads to a syndrome of B-cell lymphopenia associated with hyperbilirubinemia (12, 13), although the origins of hyperbilirubinemia were uncertain. Here we detail a key nonhematopoietic role for ATP11C, specifically in the prevention of intrahepatic cholestasis.

Results

Intrahepatic Hyperbilirubinemia in *Atp11c* Mutant Mice. While investigating B-cell lymphopenia in *Atp11c* mutant mice (12), we observed strong yellow pigmentation in the plasma of mutant mice (Fig. 1*A*). Yellow plasma pigmentation segregated exclusively with B-cell lymphopenia in the $Atp11c^{emptyhive}$ pedigree (Fig. 1*B*), and was also apparent in mice with an independent chemically induced allele, $Atp11c^{spelling}$ (Fig. 1*B*). Compound heterozygosity for both alleles also led to plasma pigmentation (Fig. 1*C*), indicating that it was not caused by a genetically linked incidental mutation, but by mutation of the *Atp11c* locus itself. Measurement of plasma bilirubin revealed a 10-fold increase in both total and direct bilirubin (Fig. 1*D*). Hyperbilirubinemia was most dramatic in young mice, and declined progressively with age (Fig. 1*E*).

Hyperbilirubinemia may be a consequence of several physiological defects, including increased hemolysis (prehepatic), autoimmune hepatitis or hepatocyte death (intrahepatic), or biliary obstruction (posthepatic). Combining the *Atp11c* mutation with a null allele of *Rag1* allowed us to exclude autoreactive lymphocytes as a cause (Fig. 2*A*), as did bone marrow transplantation experiments, which further established that plasma pigmentation was caused by radioresistant cell lineages (Fig. 2*B*), rather than increased hemolysis. These findings were consistent with the increase of direct (conjugated) bilirubin (Fig. 1*D*), which is not expected to occur in prehepatic hyperbilirubinemia.

Author contributions: O.M.S. and B.B. designed research; O.M.S., B.S., and B.W. performed research; O.M.S., B.S., and B.B. analyzed data; and O.M.S. and B.B. wrote the paper.

The authors declare no conflict of interest.

[1]To whom correspondence should be addressed. E-mail: bruce@scripps.edu.

This article contains supporting information online at www.pnas.org/lookup/suppl/doi:10.1073/pnas.1104631108/-/DCSupplemental.

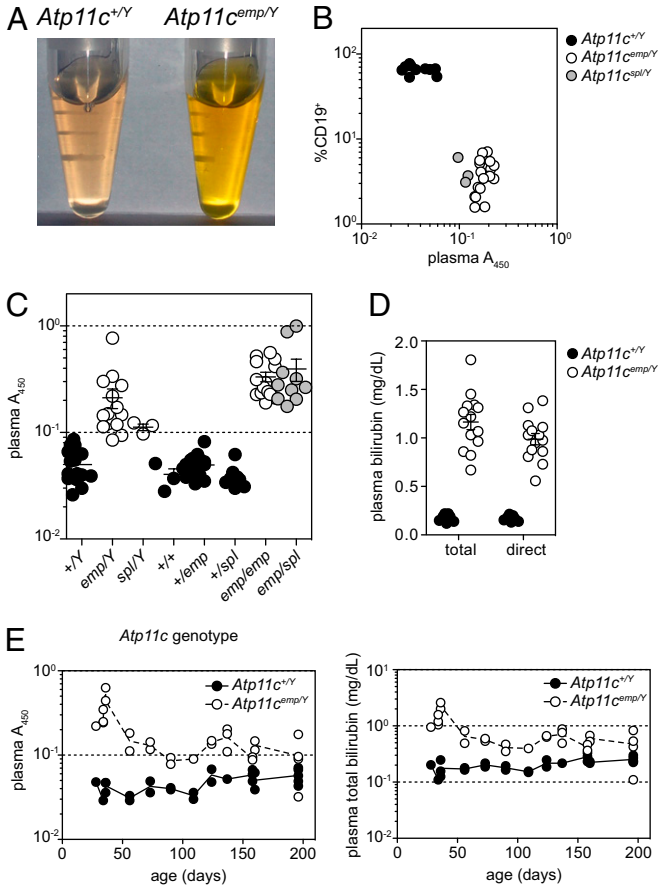


Fig. 1. Hyperbilirubinemia caused by mutations of *Atp11c*. Plasma pigmentation (*A*) and its relationship with B-cell lymphopenia (*B*) in *Atp11c* mutant mice. (*C*) Allelism testing of *emptyhive* and *spelling* alleles of *Atp11c*. (*D*) Quantitation of total and direct bilirubin in plasma, and the severity of plasma hyperbilirubinemia and pigmentation across various ages (*E*). Error bars in *C* and *D* represent SEM. Data are representative of at least three independent experiments.

Histological and Biochemical Anomalies. Histological analysis of H&E-stained liver sections from 3-mo-old mice indicated occasional portal triad-associated inflammation in mutant livers (Fig. S1*A*). Both Sirius red and trichrome blue staining were slightly more pronounced in mutant portal regions compared with littermate controls, which indicated an increased deposition of extracellular matrix (ECM), and suggested chronic, albeit mild, damage (Fig. S1*B*). Oil red O staining did not reveal an increase in lipid deposition, although apoptotic cells, as revealed by TUNEL staining, were more prevalent in 6-mo-old mutant livers (but not in 3-mo-old mutants; Fig. S1*B*). Variation in nuclear volume suggested that TUNEL-positive cells were of both parenchymal and nonparenchymal origin. Plasma pigmentation was nonetheless independent of the death domain-containing receptor Fas and the proapoptotic Bcl2 family member Bim (14, 15), as combined mutation of *Fas* or *Bcl2l11* and *Atp11c* did not affect it (Fig. S2).

Quantities of aspartate aminotransferase (AST), alanine aminotransferase (ALT), GGT, and alkaline phosphatase in plasma were also equivalent between 3-mo-old *Atp11c* mutants and controls, although total cholesterol was approximately 30% higher in mutant plasma, predominantly because of an increase in the LDL form (Table S1).

The collective implications of these data were that hyperbilirubinemia in *Atp11c* mutant mice appeared to be of hepatocellular origin. This appears consistent with the predominant expression of ATP11C-encoding mRNA in the liver (Fig. S3*A*), primarily in hepatocytes and liver endothelial cells (Fig. S3*B*).

High Incidence of Dystocia in Homozygous *Atp11c* Mutant Females. An additional pathological effect of the *Atp11c* mutation was a high frequency of dystocia in homozygous mutant females (Fig. 3*A*). More than 50% of $Atp11c^{emp/emp}$ females suffered dystocia in their first pregnancy, compared with fewer than 5% in $Atp11c^{+/emp}$ females. This phenomenon depended upon the genotype of the mother, rather than that of the pups, as $Atp11c^{+/Y} \times Atp11c^{emp/emp}$ matings had as many (if not more) cases of dystocia than $Atp11c^{emp/Y} \times Atp11c^{emp/emp}$. Surviving $Atp11c^{emp/emp}$ females almost always gave additional litters without dystocia, with an average litter size of 4.05 ($n = 19$, SD = 4.55 from 13 $Atp11c^{emp/emp}$ females) compared with 4.79 for $Atp11c^{+/emp}$ females ($n = 78$, SD = 4.79 from 35 females). Neither plasma pigmentation nor hyperbilirubinemia was more severe in $Atp11c^{emp/emp}$ females at 18.5 d post coitum, compared with their virgin counterparts (Fig. 3*B*).

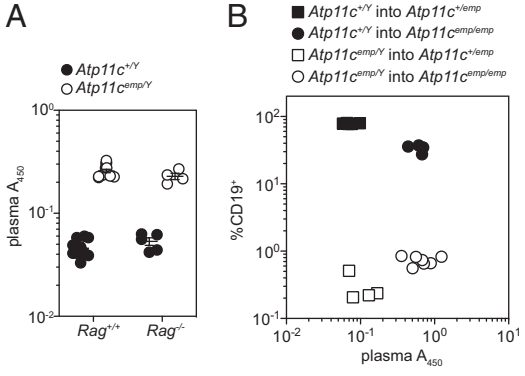


Fig. 2. Plasma hyperpigmentation is independent of B and T lymphocytes. Plasma pigmentation of *Rag1*/*Atp11c* double mutant mice (*A*) and reciprocal bone marrow chimeric mice (*B*). Error bars in *A* represent SEM. Data are representative of three (*A*) or two (*B*) independent experiments.

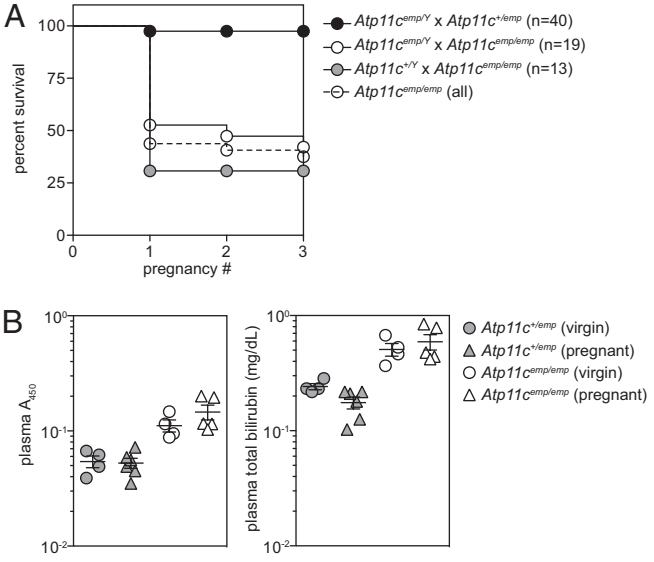


Fig. 3. High frequency of dystocia in $Atp11c^{emp/emp}$ females. (*A*) Survival curve of homozygous and heterozygous *Atp11c* mutant female littermates following pregnancies to hemizygous mutant or WT males. (*B*) Plasma absorbance (A_{450}) and total bilirubin measurements from the plasma of age-matched virgin or 18.5 d post coitum pregnant females. Error bars in *B* represent SEM.

Table 1. Ions on LC/MS with the greatest difference between WT and *Atp11c* mutant serum

No.	m/z	Retention time	Group	Atp11c+/emp (n = 4) Mean	Atp11c+/emp (n = 4) SD	Atp11cemp/emp (n = 3) Mean	Atp11cemp/emp (n = 3) SD	Mean difference	Fold change	P value
1	373.289	1,039.625	152	2.30×10^6	3.70×10^6	2.36×10^7	7.29×10^6	2.13×10^7	10	3.6×10^{-3}
2	817.603	1,004.24	290	2.73×10^5	4.20×10^5	9.69×10^6	5.67×10^6	9.42×10^6	36	1.9×10^{-2}
3	546.309	1,136.01	20	3.81×10^5	1.10×10^5	8.59×10^6	1.07×10^6	8.21×10^6	23	1.9×10^{-5}
4	761.323	1,098.94	203	3.25×10^4	1.71×10^4	7.71×10^6	1.82×10^6	7.67×10^6	237	3.3×10^{-4}
5	1031.612	882.73	192	4.32×10^5	6.62×10^5	6.68×10^6	4.14×10^6	6.25×10^6	15	2.8×10^{-2}
6	584.269	1,680.245	331	4.66×10^5	6.49×10^5	4.68×10^6	1.11×10^6	4.22×10^6	10	1.4×10^{-3}
7	257.156	56.77	18	4.19×10^5	2.38×10^5	4.24×10^6	1.23×10^6	3.82×10^6	10	1.5×10^{-3}
8	761.326	1,077.81	343	1.13×10^4	7.38×10^3	2.55×10^6	9.61×10^5	2.54×10^6	225	2.8×10^{-3}
9	373.285	927.82	100	1.20×10^4	1.32×10^4	2.05×10^6	6.72×10^5	2.04×10^6	171	1.5×10^{-3}
10	599.307	1,313.93	229	1.76×10^3	3.08×10^3	2.03×10^6	8.50×10^5	2.03×10^6	1,155	4.3×10^{-3}

Ions with a fold change greater than or equal to 10 and a mean peak intensity difference greater than 1 million were ranked by mean peak intensity difference. Multiple ions from a common retention group (and therefore likely to originate from the same molecule) are represented only once.

***Atp11c* Mutant Mice Are Cholestastic.** As a result of the absence of severe liver pathology, we screened for further metabolic abnormalities (adapted from ref. 16), subjecting mutant and WT serum to liquid chromatography/mass spectrometry (LC/MS). Ion peaks were sorted into groups based on ion retention time, and groups containing ions with the greatest difference in mean peak intensity were scrutinized further (Table 1). Ion molecular weights were cross-referenced with METLIN database and Human Metabolome Database, and one candidate molecule (cholic acid) was selected for validation by tandem MS (MS/MS; Fig. S4). LC/MS confirmed that cholic acid was present in higher quantities in *Atp11c* mutant serum (Fig. 4 *A* and *B*), with an independent assay confirming that total bile acid concentrations were also increased (Fig. 4*C*).

Exogenous Bile Acid Toxicity in *Atp11c* Mutant Mice. These findings, along with earlier data, were indicative of intrahepatic cholestasis, and led us to suspect that feeding mutant mice with a cholic acid-supplemented diet might exacerbate the phenotype, as is observed in mice with mutation of *Atp8b1* (17) or *Abcb11* (18). Indeed, *Atp11c* mutants lost weight more rapidly than their WT littermates (Fig. 5*A*), culminating in uniform lethality in mutant males by day 15 (Fig. 5*B*). Weight loss was also associated with dramatic increases in plasma bilirubin (Fig. 5*C*).

Two striking observations made in cholic acid-fed mutant mice at necropsy were a pronounced enlargement of the gallbladder (Fig. 5*D*) and jaundiced skin (Fig. 5*E*), neither of which was observed in *Atp11c* mutants on a normal diet. Sirius red staining was also more apparent in mutant livers (Fig. 5*G*). Gallbladder enlargement did not appear to be caused by biliary obstruction, as no precipitates were apparent within the gallbladder, nor was there any histological evidence of ductular proliferation.

This potential disruption of enterohepatic bile circulation seen in *Atp11c* mutant mice could be explained by ATP11C acting in bile acid transport, either as a pump, channel, or sensor. If this were the case, one would expect that dietary supplementation of cholic acid would fail to suppress expression of cholesterol 7α-hydroxylase (encoded by *Cyp7a1*), a rate-limiting enzyme in bile acid synthesis from cholesterol, which occurs in a farnesoid X receptor-dependent manner (19). This was not the case, however, as *Cyp7a1* expression was equally low in mutants as in WT littermates after cholic acid feeding (Fig. 5*F*). *Atp11c* mRNA was nonetheless increased in *Atp11c*$^{emp/Y}$ mutant mice and in mice fed a cholic acid-supplemented diet (Fig. 5*F*), suggesting that *Atp11c* is transcriptionally induced in response to cholestasis.

Discussion

The present findings reveal an additional, extrahematopoietic function for the P4-type ATPase ATP11C, namely in the prevention of cholestasis. This mild cholestatic phenotype of *Atp11c* mutant mice resembles other mouse models of PFIC, but with notable distinctions. Chief among them is hyperbilirubinemia, which was greatest in younger mutant mice, and declined progressively with age. The reason for this is yet to be determined, but may reflect an increased dependence on ATP11C-facilitated bilirubin excretion in younger mice, perhaps because of behavioral differences (20) or competition between substrates of ATP11C. Hyperbilirubinemia is observed in *Atp11c* and *Abcb4* mutants (9), but not in *Abcb11* or *Atp8b1* mutants (17, 21), although, unlike in *Abcb4* mutants, plasma ALT and AST were not

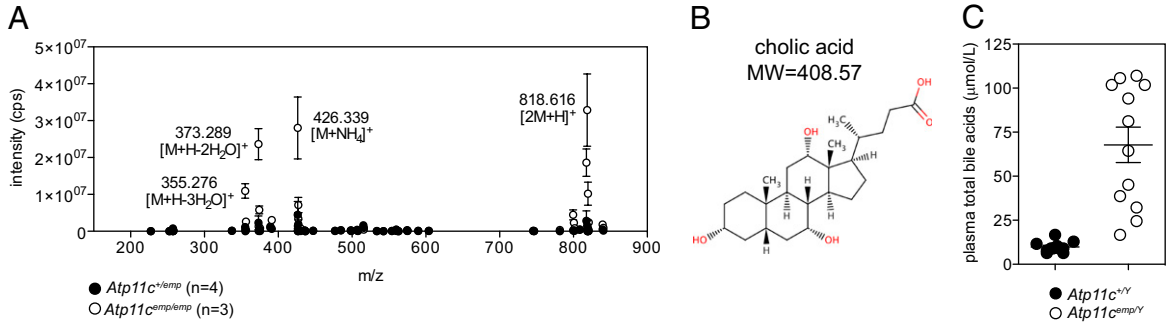


Fig. 4. *Atp11c* mutant mice are cholestatic. (*A*) LC/MS ion intensity profile for the 1039.625s retention group. The ion at 373.289 (*m/z*) showed the greatest mean difference between *Atp11c* mutant (n = 3) and littermate control (n = 4) serum. Hypothetical ion identities are shown in parentheses below each *m/z* value, which are all consistent with the chemical structure and molecular weight of cholic acid (*B*). (*C*) Total bile acids as measured from the plasma of *Atp11c* mutant and littermate control mice. Error bars in *A* and *C* represent SEM.

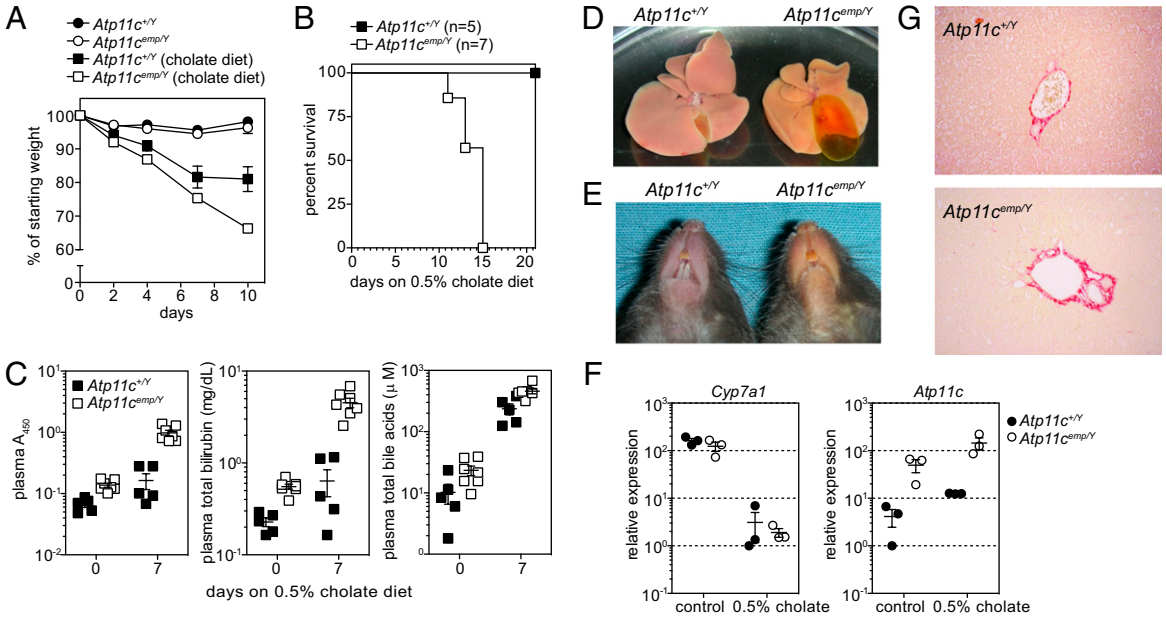


Fig. 5. Severe pathology in Atp11c mutant mice induced by a cholic acid-supplemented diet. *Atp11c* mutant and control males were fed with a cholic acid-supplemented ($n = 7$ and $n = 5$, respectively) or control diet ($n = 7$ and $n = 5$, respectively), and monitored for weight loss (*A*), mortality (*B*), and changes in plasma constituents (*C*). Gallbladder distention (*D*) and jaundice (*E*) as observed in littermates on a cholic acid diet for 13 d. (*F*) Relative expression of *Cyp7a1* and *Atp11c* mRNA in the livers of mice after 7 d of a cholic acid-supplemented or control diet (normalized to *Actb*). (*G*) Sirius red staining of liver sections after 13 d of a cholic acid-supplemented diet. Error bars in *A*, *C*, and *F* represent SEM.

elevated in 3-mo-old *Atp11c* mutants. TUNEL staining, however, was more prevalent in 6-mo-old *Atp11c* mutants, suggesting that liver damage is a mild but progressive consequence of the mutation. Ductular proliferation was also not apparent in *Atp11c* mutant sections, indicating that hepatocyte death and biliary obstruction are more prevalent in *Abcb4* mutant mice (9).

More pathological distinctions emerged after dietary supplement of cholic acid, notably an enlargement of the gallbladder in *Atp11c*, but not *Atp8b1* or *Abcb11*, mutant strains (17, 22). This does not seem to be a result of a physical obstruction such as gallstones or acalculous cholecystitis ("sludge"), as bile duct proliferation is not observed (as it is following bile duct ligation) (23). Other explanations could include a failure of cholestokinin signaling (with failure of gallbladder contraction or relaxation of the sphincter of Oddi), or an inability to control FGF15-mediated gallbladder filling (24).

Similar to *Abcb11* mutants, cholestatic disease is very mild in *Atp11c* mutant mice, yet mice that consume cholic acid as a dietary supplement die within a matter of days (22). BSEP is known to be a major canalicular transporter of hydrophobic bile acids, including cholic acid (21), and this sensitivity to dietary cholic acid can be attributed to the strong cholestatic effects of cholic acid, but not the primary murine bile acids (α- and β-muricholic acid). This raises the possibility that ATP11C is involved in the transport of cholestatic bile acids, perhaps in concert with BSEP, that are not normally prevalent in mice. Other transporters are likely to be affected also, such as MRP2 (encoded by *Abcc2*), which transports conjugated bilirubin (but not cholic acid) (25).

We have excluded the possibility that ATP11C acts as a nonredundant sensor or transporter of cholic acid between the portal circulation and the hepatocyte, as farnesoid X receptor-mediated repression of *Cyp7a1* in the liver remains intact after cholic acid feeding (19). We cannot, however, exclude that ATP11C acts as a transporter between the hepatocyte and the bile canaliculi, and it will be critical to determine the subcellular localization of ATP11C, and how mutation of it affects the flow of bile constituents between the hepatocyte and bile ducts.

Why is there such a high frequency of dystocia in *Atp11c* mutant females? Liver pathology did not appear to be more severe during late pregnancy, although the profile of bile acids in *Atp11c* mutant plasma might somehow be toxic to late-term embryos, or preclude their delivery. Another possibility is that smooth muscle function is compromised both in the uterus (where *Atp11c* transcript is detected; Fig. S3*A*) and in the gallbladder, during parturition and cholic acid feeding, respectively. Although dystocia has not been reported in other mouse models of PFIC, and is not characteristic of intrahepatic cholestasis of pregnancy in the clinic (26), *Atp11c* mutants may represent a unique model to understand the pathology of dystocia and other defects of parturition.

An important difference between our $Atp11c^{emptyhive}$ mutant strain (12) and an independent strain [$Atp11c^{ambrosius}$ (13)] is the observation of hepatocellular carcinoma (HCC) in 6 mo-old *ambrosius* mutant mice. We have not observed this in our strain, even in mice beyond 1 y of age. The inbred genetic background is consistent in each case (C57BL/6J), although modifying effects of incidental mutations induced in either stock have not been excluded. As HCC is apparent in older *Abcb4* mutant mice (27), perhaps a more likely explanation is that HCC in *ambrosius* mutant mice has an environmental cue (of microbial or dietary origin) present in one facility but not the other.

How might ATP11C function in both hepatocytes and adult B-cell progenitors? Canalicular membrane asymmetry is known to be critical for the formation of bile (9) and for hepatocytes to resist the detergent effects of bile (28), and ATP11C is presumably involved in one or both of these processes. Another conceivable possibility is that ATP11C mediates trafficking of other canalicular transporters. As much less is known of the consequences of altered membrane asymmetry in B-cell progenitors, understanding the hepatic function of ATP11C could provide important insights into lymphocyte development. Studies of canalicular membrane structure and function, by EM and functional analysis of other known canalicular transporters, will

be important in this respect. Bile acid metabolites are also known to affect B-cell function. For instance, 25-hydroxycholesterol, an oxysterol metabolite of cholesterol and precursor for bile acid synthesis, can suppress secretion of IgA (29). The observation that *Atp11c*$^{emp/Y}$ mutant mice also have a significant deficiency of IgA (12) might reflect a surplus of 25-hydroxycholesterol, although whether this also accounts for the development defects remains to be determined.

What about the substrate of ATP11C? These mutant strains establish a previously unappreciated biochemical link between hepatocytes and B-cell progenitors, and identification of the substrate(s) of ATP11C will be of central importance to resolving its function. Yabas et al. have shown that mutant B-cell precursors are less efficient at internalizing exogenous PS at the cell membrane (13), but whether PS is the critical substrate remains to be seen. PS asymmetry is known to important not just at the cell membrane, but also at other organellar membranes (30), any number of which could affect pathways required for B-cell development. ATP8B1 also appears to be vital for inward translocation of PS at the cell surface, although other substrates have been proposed (31). Whatever their substrate, these mutants promise to provide new insight into disorders of lymphopoiesis, parturition, and cholestatic disease.

Materials and Methods

Mice. All animal procedures were in accordance with institutional guidelines. *Atp11c*^{emptyhive}, *Atp11c*^{spelling}, and *Rag1*^{maladaptive} (Mouse Genome Informatics database no. 3851764) alleles were generated on a pure C57BL/6J background by *N*-ethyl-*N*-nitrosourea mutagenesis as previously described (12), and are described at http://mutagenetix.scripps.edu. *Fas*^{lpr} mice were obtained from Jackson Laboratories, and *Bcl2l11*$^{tm1.1Ast}$ mice have been described previously (32). The *emptyhive* strain was maintained by hemizygote–to-heterozygote breeding, with male littermates used for experiments unless otherwise indicated. Mice were maintained on a PicoLab Mouse Diet 20 (LabDiet 5058), and sentinels present in the same room were routinely negative for serum antibodies against *Mycoplasma pulmonis*, mouse rotavirus, mouse hepatitis virus, murine norovirus, mouse parvovirus, minute virus of mice, Sendai virus, and Theiler murine encephalomyelitis virus.

Bone Marrow Chimeras. Recipient mice were γ-irradiated with a dose of 10 Gy (^{137}Cs source). The following day, mice received 5×10^6 bone marrow cells pooled from two donors via tail vein injection, and were maintained on trimethoprim/sulfamethoxazole antibiotic water until they were killed for analysis 8 wk later.

Cholate-Supplemented Diet. Mice were fed a basal 14% protein diet (TD.00357; Harlan) with or without a supplement of 0.5% sodium cholate. Mice were weighed at biweekly intervals, bled weekly for serum analysis, and monitored daily for survival.

Quantitative PCR. Total RNA was prepared from liver (RNeasy kit; Qiagen) and reverse-transcribed into cDNA (Retroscript; Ambion). Quantitative PCR reactions (SYBR Master Mix; BioPioneer) were analyzed on a 7300 Real-Time PCR System (Applied Biosystems). Relative quantities of *Cyp7a1* cDNA were calculated by reference to *Actb* using the comparative C_T method. Isolation of cDNA from MACS-sorted liver cell fractions has been described previously (23). Primer sequences were as follows: *Actb*, GGCTGTATTCCCCTCCATCG (forward); *Actb*, CCAGTTGGTAACAATGCCATGT (reverse); *Atp11c*, CTCGTTTCTCTTCTCCAGCA (forward); *Atp11c*, AGTGTGTTTTGTGGACGGC (reverse); *Cyp7a1*, GGGATTGCTGTGGTAGTGAGC (forward); and *Cyp7a1*, GGTATGGAATCAACCCGTTGTC (reverse).

Histology. Livers were fixed in 10% neutral buffered formalin and embedded in paraffin wax, and 5-μm sections were stained with H&E, Sirius red, or trichrome blue. Oil red O staining was performed on frozen sections. TUNEL staining was performed on paraffin sections according to the manufacturer's instructions (Roche).

Plasma Analysis. Blood from the retroorbital plexus of isoflurane-anesthetized mutant mice was collected in cluster tubes (Costar) containing 20 μL of 6% EDTA solution (wt/vol in water) or allowed to clot in serum separator tubes and centrifuged for 5 min at $10{,}000 \times g$. Mice were fasted overnight before bleeding where indicated. Serum absorbance was measured at 450 nm (subtracting absorbance at 540 nm) on a MAXline Emax Microplate Reader (Molecular Devices). Total and direct bilirubin (StanBio) and total bile acids (Diazyme) were measured according the manufacturer's instructions. All other plasma chemistry parameters, including ALT, alkaline phosphatase, and GGT were measured by standard clinical chemistry (University of California, San Diego, Murine Hematology Core).

Serum MS. Mutant and WT littermates were fasted overnight, and the following morning blood was collected from the retroorbital plexus into serum separator tubes and allowed to clot. Serum was then subjected to positive ion-mode LC/MS on an Agilent 6520 Q-TOF mass spectrometer, with the output annotated by XCMS software (33). Ion peak intensities for mutant and WT groups were ranked by mean peak difference, and those with a peak difference greater than 1 million were ranked according to fold difference. Ions with the largest peak differences were then compared with the METLIN database (http://metlin.scripps.edu/) and Human Metabolome Database (http://www.hmdb.ca/) for potential candidate metabolites. For candidate validation, standards (including cholic acid, C1129; Sigma) were run in parallel with mutant serum on an Agilent 6520 Q-TOF in tandem mode (MS/MS).

ACKNOWLEDGMENTS. We thank A. Knisely A. Hofmann, and M. Katsumi for valuable comments; E. Moresco for help preparing the manuscript; M. Gutierrez for animal care; D. Ditto and the University of California at San Diego, Murine Hematology Core for clinical chemistry; P. Krebs and M. Chadwell for help with histology; and S. Won for first noticing plasma pigmentation. This work was supported by the National Institute of Allergy and Infectious Diseases Broad Agency Announcement Contract HHSN272200700038C (to B.B.), with fellowship support from the General Sir John Monash Foundation (O.M.S.).

1. Russell DW (2003) The enzymes, regulation, and genetics of bile acid synthesis. *Annu Rev Biochem* 72:137–174.
2. Trauner M, Meier PJ, Boyer JL (1998) Molecular pathogenesis of cholestasis. *N Engl J Med* 339:1217–1227.
3. Bull LN, et al. (1998) A gene encoding a P-type ATPase mutated in two forms of hereditary cholestasis. *Nat Genet* 18:219–224.
4. Ujhazy P, et al. (2001) Familial intrahepatic cholestasis 1: Studies of localization and function. *Hepatology* 34:768–775.
5. Strautnieks SS, et al. (1998) A gene encoding a liver-specific ABC transporter is mutated in progressive familial intrahepatic cholestasis. *Nat Genet* 20:233–238.
6. Jansen PL, et al. (1999) Hepatocanalicular bile salt export pump deficiency in patients with progressive familial intrahepatic cholestasis. *Gastroenterology* 117:1370–1379.
7. de Vree JM, et al. (1998) Mutations in the MDR3 gene cause progressive familial intrahepatic cholestasis. *Proc Natl Acad Sci USA* 95:282–287.
8. Ruetz S, Gros P (1994) Phosphatidylcholine translocase: A physiological role for the mdr2 gene. *Cell* 77:1071–1081.
9. Smit JJ, et al. (1993) Homozygous disruption of the murine mdr2 P-glycoprotein gene leads to a complete absence of phospholipid from bile and to liver disease. *Cell* 75: 451–462.
10. Holthuis JCM, Levine TP (2005) Lipid traffic: Floppy drives and a superhighway. *Nat Rev Mol Cell Biol* 6:209–220.
11. Folmer DE, Elferink RPJO, Paulusma CC (2009) P4 ATPases - lipid flippases and their role in disease. *Biochim Biophys Acta* 1791:628–635.
12. Siggs OM, et al. (2011) The P4-type ATPase ATP11C is essential for B lymphopoiesis in adult bone marrow. *Nat Immunol*, 10.1038/ni.2012.
13. Yabas M, et al. (2011) ATP11C is critical for the internalization of phosphatidylserine and differentiation of B lymphocytes. *Nat Immunol*, 10.1038/ni.2011.
14. Kaufmann T, et al. (2009) Fatal hepatitis mediated by tumor necrosis factor TNFalpha requires caspase-8 and involves the BH3-only proteins Bid and Bim. *Immunity* 30: 56–66.
15. Malhi H, Gores GJ (2008) Cellular and molecular mechanisms of liver injury. *Gastroenterology* 134:1641–1654.
16. Wikoff WR, Pendyala G, Siuzdak G, Fox HS (2008) Metabolomic analysis of the cerebrospinal fluid reveals changes in phospholipase expression in the CNS of SIV-infected macaques. *J Clin Invest* 118:2661–2669.
17. Pawlikowska L, et al. (2004) A mouse genetic model for familial cholestasis caused by ATP8B1 mutations reveals perturbed bile salt homeostasis but no impairment in bile secretion. *Hum Mol Genet* 13:881–892.
18. Wang H, et al. (2003) Nicotinic acetylcholine receptor alpha7 subunit is an essential regulator of inflammation. *Nature* 421:384–388.
19. Sinal CJ, et al. (2000) Targeted disruption of the nuclear receptor FXR/BAR impairs bile acid and lipid homeostasis. *Cell* 102:731–744.
20. Groen A, Kunne C, Oude Elferink RP (2006) Increased serum concentrations of secondary bile salts during cholate feeding are due to coprophagy. A study with wild-type and Atp8b1-deficient mice. *Mol Pharm* 3:756–761.

21. Wang R, et al. (2001) Targeted inactivation of sister of P-glycoprotein gene (spgp) in mice results in nonprogressive but persistent intrahepatic cholestasis. *Proc Natl Acad Sci USA* 98:2011–2016.
22. Wang R, et al. (2003) Severe cholestasis induced by cholic acid feeding in knockout mice of sister of P-glycoprotein. *Hepatology* 38:1489–1499.
23. Taura K, et al. (2008) Hepatic stellate cells secrete angiopoietin 1 that induces angiogenesis in liver fibrosis. *Gastroenterology* 135:1729–1738.
24. Choi M, et al. (2006) Identification of a hormonal basis for gallbladder filling. *Nat Med* 12:1253–1255.
25. Borst P, Elferink RO (2002) Mammalian ABC transporters in health and disease. *Annu Rev Biochem* 71:537–592.
26. Geenes V, Williamson C (2009) Intrahepatic cholestasis of pregnancy. *World J Gastroenterol* 15:2049–2066.
27. Mauad TH, et al. (1994) Mice with homozygous disruption of the mdr2 P-glycoprotein gene. A novel animal model for studies of nonsuppurative inflammatory cholangitis and hepatocarcinogenesis. *Am J Pathol* 145:1237–1245.
28. Paulusma CC, et al. (2006) Atp8b1 deficiency in mice reduces resistance of the canalicular membrane to hydrophobic bile salts and impairs bile salt transport. *Hepatology* 44:195–204.
29. Bauman DR, et al. (2009) 25-Hydroxycholesterol secreted by macrophages in response to Toll-like receptor activation suppresses immunoglobulin A production. *Proc Natl Acad Sci USA* 106:16764–16769.
30. Leventis PA, Grinstein S (2010) The distribution and function of phosphatidylserine in cellular membranes. *Annu Rev Biophys* 39:407–427.
31. Ray NB, et al. (2010) Dynamic regulation of cardiolipin by the lipid pump Atp8b1 determines the severity of lung injury in experimental pneumonia. *Nat Med* 16: 1120–1127.
32. Bouillet P, et al. (1999) Proapoptotic Bcl-2 relative Bim required for certain apoptotic responses, leukocyte homeostasis, and to preclude autoimmunity. *Science* 286: 1735–1738.
33. Smith CA, Want EJ, O'Maille G, Abagyan R, Siuzdak G (2006) XCMS: Processing mass spectrometry data for metabolite profiling using nonlinear peak alignment, matching, and identification. *Anal Chem* 78:779–787.

Supporting Information

Siggs et al. 10.1073/pnas.1104631108

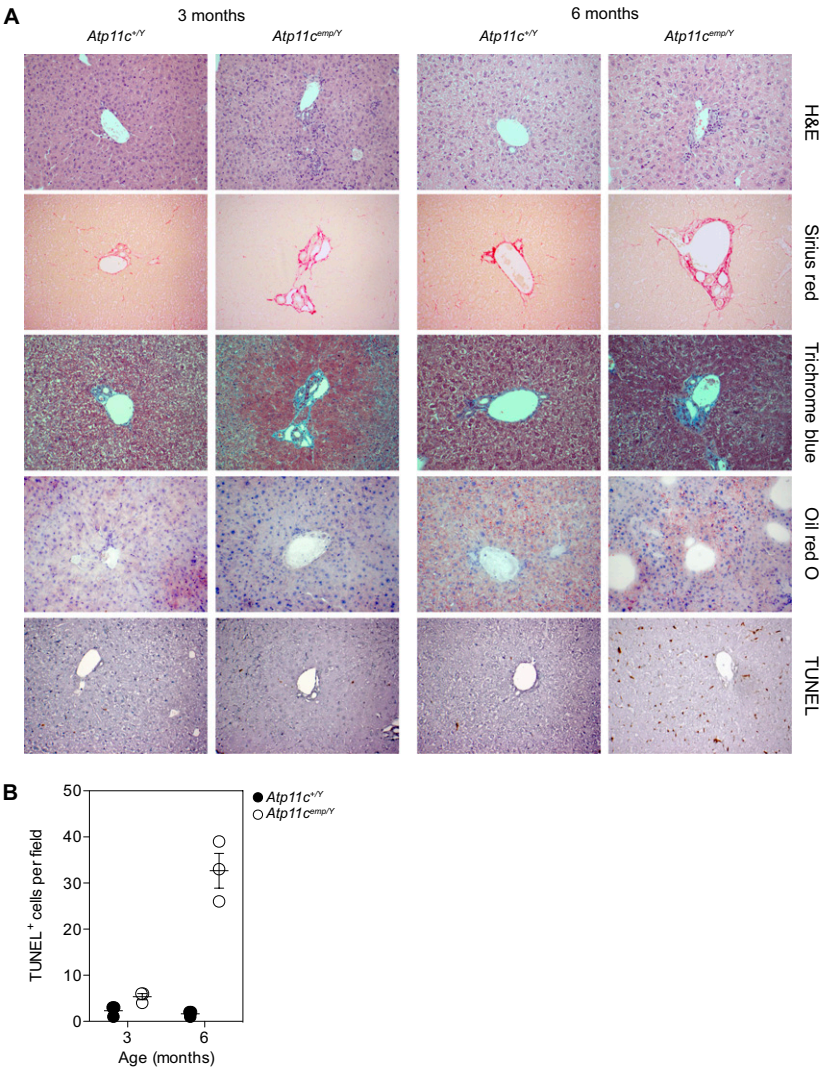


Fig. S1. Mild liver pathology in *Atp11c* mutant mice. (*A*) H&E, Sirius red, trichrome blue, Oil red O, and TUNEL-stained liver sections of 3-mo-old and 6-mo-old *Atp11c* mutants and sex-matched littermate controls. (*B*) Quantification of TUNEL-positive cells. Each point represents the number of TUNEL-positive cells in single high-power field. Data are representative of one to three individuals per genotype.

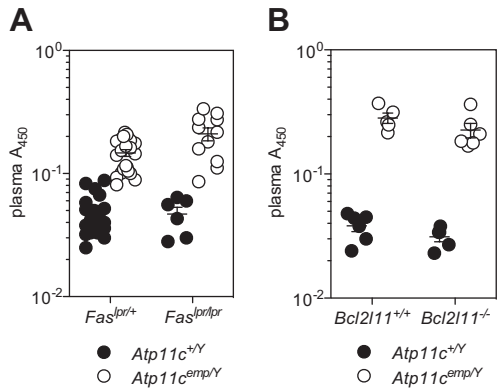


Fig. S2. *Atp11c* mutant plasma pigmentation is not corrected by mutation of Fas or Bim. Plasma pigmentation as measured in (*A*) *Fas*;*Atp11c* and (*B*) *Bcl2l11*; *Atp11c* double mutant mice and littermate controls. Each point represents an individual mouse. Error bars represent SEM.

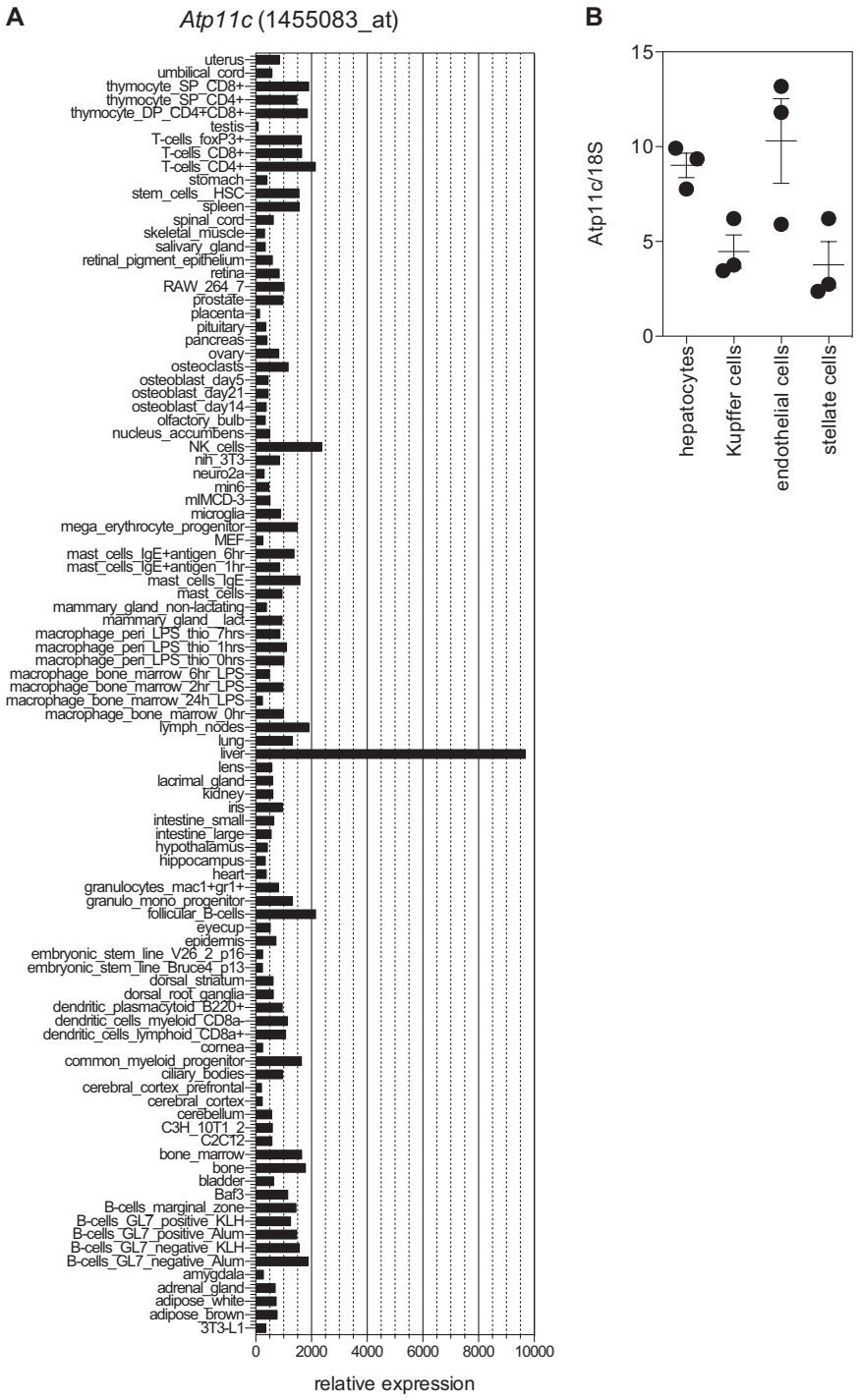


Fig. S3. Tissue- and cell type-specific expression of *Atp11c* message. (*A*) Relative tissue-specific expression of *Atp11c* (probe 1455083_at; Affymetrix) according to the BioGPS database (1). (*B*) *Atp11c* expression as measured in MACS-sorted liver cell subsets (relative to 18S ribosomal RNA).

1. Lattin JE, et al. (2008) Expression analysis of G protein-coupled receptors in mouse macrophages. *Immunome Res* 4:5.

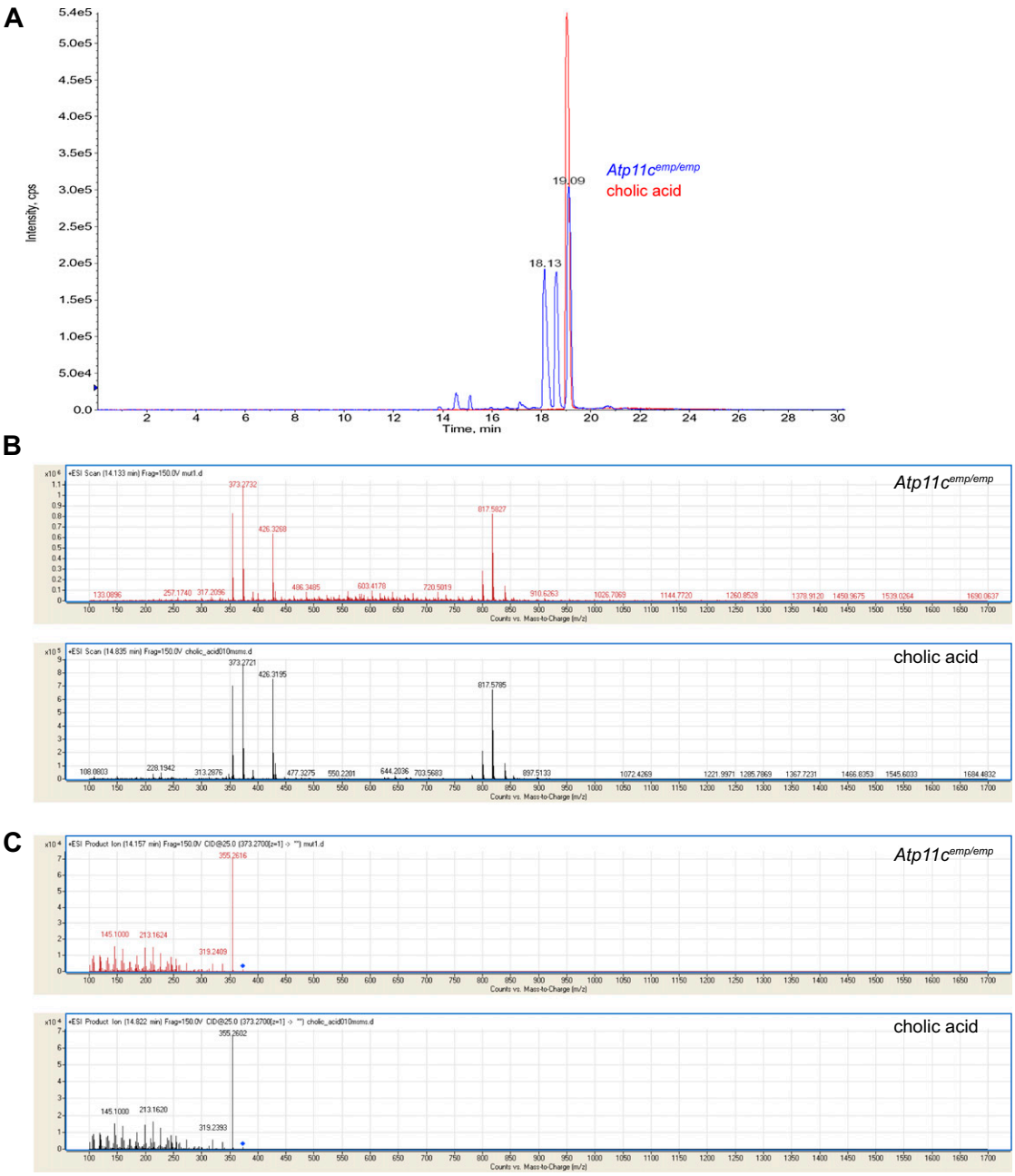


Fig. S4. MS/MS profile of cholic acid and *Atp11c* mutant serum. (*A*) Retention time of a cholic acid standard (red) run in parallel with *Atp11c* mutant serum (blue). *m/z* values (*B*) and fragmentation patterns (*C*) of ions within the common retention group.

Table S1. Blood chemistry parameters

	Atp11$^{c+/Y}$ (n = 3)		Atp11c$^{emp/Y}$ (n = 3)		
Parameter	Mean	SD	Mean	SD	P value
Bicarbonate, mmol/L	12.67	3.06	15.33	3.79	0.3984
Chloride, mmol/L	106.33	0.58	106.67	2.31	0.8287
Sodium, mmol/L	150.67	0.58	149.00	1.00	0.0824
Potassium, mmol/L	4.77	0.61	4.70	0.53	0.8934
Calcium, mg/dL	10.60	0.35	10.20	0.20	0.1759
Albumin, g/dL	3.37	0.06	3.30	0.26	0.7081
Total protein, g/dL	4.97	0.21	4.83	0.21	0.4766
Phosphorous, mg/dL	13.00	3.15	11.17	1.76	0.4410
Creatinine, mg/dL	0.13	0.01	0.18	0.03	0.1987
BUN, mg/dL	24.67	5.03	25.33	4.16	0.8686
AST, U/L	52.00	14.00	64.00	14.42	0.3596
Alkaline phosphatase, U/L	74.00	12.17	78.67	23.44	0.7795
ALT, U/L	22.67	4.16	29.33	6.43	0.2177
GGT, U/L	<3	0	<3	0	N/A
Glucose, mg/dL	235.33	69.87	213.33	58.32	0.6976
Cholesterol, mg/dL	148.75	21.97	201.00	18.25	0.0355
Triglycerides, mg/dL	121.25	56.17	84.00	9.00	0.3694
LDL cholesterol, mg/dL	13.67	6.43	44.00	8.19	0.0084
HDL cholesterol, mg/dL	116.25	13.52	144.00	10.39	0.0516
Lipase, U/L	30.00	6.50	27.00	5.20	0.5676

*$P < 0.05$.

blood
Leading the world in reporting basic and applied hematology research
JOURNAL OF THE AMERICAN SOCIETY OF HEMATOLOGY
Original Article | Current Issue | About Blood | Submissions | Subscriptions | Contact Us

Blood. Jun 14, 2012; 119(24): 5769–5771. PMCID: PMC3382936
Prepublished online May 1, 2012. doi: 10.1182/blood-2012-03-417949

iRhom2 is required for the secretion of mouse TNFα

Owen M. Siggs,[1,*] Nengming Xiao,[1,*] Ying Wang,[2] Hexin Shi,[2] Wataru Tomisato,[1,2] Xiaohong Li,[1,2] Yu Xia,[1] and Bruce Beutler[1,2]

[1]Department of Genetics, The Scripps Research Institute, LA Jolla, CA; and
[2]Center for Genetics of Host Defense, University of Texas Southwestern Medical Center, Dallas, TX
Corresponding author.
*O.M.S. and N.X. contributed equally to this work.

Received March 19, 2012; Accepted April 25, 2012.

Copyright © 2012 by The American Society of Hematology

Abstract

TNFα is a powerful inflammatory stimulus, central both to the control of infection, and as an agent of inflammatory disease. The most potent inducers of TNFα secretion signal through the Toll-like receptors, and we describe here a chemically-induced mutation that impairs this response in macrophages. A missense mutation was revealed in the gene encoding the inactive rhomboid protease iRhom2, which was not complemented by a null allele of the same gene. Neither the missense nor the null allele affected TLR-induced secretion of IL-6. Moreover, unlike a mutation in TNFα, the iRhom2 missense mutation did not cause enhanced susceptibility to colitis induced by dextran sodium sulfate. These results establish a specific role for iRhom2 in the secretion of TNFα, and present a new target for the modulation of inflammation.

Introduction

TLR activation triggers a signaling pathway that culminates in the activation of NF-κB and the synthesis of proinflammatory cytokines such as TNFα. TNFα, which is synthesized as a membrane-bound precursor, is liberated from the cell surface by the TNFα converting enzyme (TACE, also known as ADAM17).[1,2] Mammalian TACE is also required for the cleavage of other membrane-bound ligands, including the EGFR ligand TGFα,[3] whose counterpart in *Drosophila* is cleaved by the unrelated protease *rhomboid-1*.[4,5] The rhomboid protease family is also present in mammals, and includes members with no predicted catalytic function, known as iRhoms.[6] Until very recently, the physiologic function of these proteins was unknown.

To reveal new regulators of TLR-induced TNFα, we have stimulated peritoneal macrophages from the progeny of chemically-mutagenized mice.[7] This screen has revealed mutant alleles throughout the pathway, from TLRs and the proteins that control their expression,[8] to TNFα itself.[9] Here we describe a new mutation affecting TLR-induced TNFα secretion that did not affect secretion of IL-6. The causative mutation lay in the gene encoding iRhom2, a catalytically inactive member of the rhomboid protease family.

Methods

Mice and positional cloning

Rhbdf2^{sinecure} was generated on a C57BL/6J background by *N*-ethyl-*N*-nitrosourea mutagenesis as previously described.[10] The index *sinecure* mutant (C57BL/6J, male) was outcrossed to C57BL/10J

females (The Jackson Laboratory) for mapping, and F1 daughters were backcrossed to their father. Mice were grouped into mutant and wild-type cohorts (20 and 15 mice, respectively) based on TNFα secretion in response to MALP-2. Individual mice were typed at 70 polymorphic markers across the genome, and genotype frequencies were used to calculate LOD scores at each position. *Rhbdf2* amplicons from wild-type and *sinecure* genomic DNA were sequenced using an ABI 3730xl capillary sequencer. C57BL/6J mice used for mutagenesis were obtained from The Jackson Laboratory. All other mice were obtained from the TSRI breeding colony. *Ticam1*^{Lps2} and *Irak2*^{otiose} mutants have been described previously.[11,12] *Rhbdf2*$^{tm1a(KOMP)Wtsi}$ ES cells (MGI:4362881, C57BL/6N background[13]) were obtained from the KOMP repository at UC Davis. After expansion, cells were injected into FVB blastocysts and transplanted into pseudopregnant females. Chimeric male offspring were mated to C57BL/6J-*Tyr*$^{c-2J}$ albino females to confirm germ line transmission. Black offspring were genotyped by PCR. Mice heterozygous for the *Rhbdf2*$^{tm1a(KOMP)Wtsi}$ allele were then mated with each other, with homozygous *sinecure* mutants, or with C57BL/6J. All animal procedures were in accordance with guidelines of the Institutional Animal Care and Use Committee of The Scripps Research Institute and University of Texas Southwestern Medical Center.

Macrophage stimulation and cytokine ELISA

To screen the progeny of ENU-mutagenized mice, thioglycollate-elicited peritoneal cells were stimulated and TNFα measured by L-929 bioassay as previously described.[14] Subsequently, TNFα and IL-6 were measured by ELISA after MALP-2 (200 pg/mL) or LPS (1 ng/mL) stimulation as described previously.[15]

DSS-induced colitis

Sex- and age-matched littermates received 3% (wt/vol) dextran sulfate sodium (DSS; MP Biomedicals) in drinking water for 7 days, with weight recorded daily and normalized to day 0.

Results and discussion

During the course of a forward genetic screen for regulators of TLR-induced TNFα we identified an individual with a mildly impaired response (Figure 1A). This phenotype, named *sinecure*, was inherited as a recessive trait most apparent after stimulation with the TLR2/6 agonist MALP-2. *Sinecure* mice were otherwise healthy and fertile, with no other externally obvious phenotypes.

To isolate the causative mutation of the *sinecure* phenotype, we outcrossed the index *sinecure* male to C57BL/10J females, and backcrossed him to his F1 daughters. Macrophages from progeny were stimulated with MALP-2, and grouped into wild-type or mutant cohorts based on their TNFα response. After genotyping individual mice at 70 polymorphic loci across the genome, the *sinecure* phenotype showed strong linkage to distal chromosome 11 (Figure 1B). This interval was refined to a 17.5 Mb region using additional markers (Figure 1C), encompassing an estimated 282 protein-coding genes. Among these, *Rhbdf2* was proposed as a candidate because of its strikingly high expression in macrophages,[16] and was sequenced directly. A single nonsynonymous mutation was identified: an A to T transversion at position 1680 of the *Rhbdf2* transcript, in exon 10 of 19 total exons (Figure 1D), corresponding to an isoleucine to phenylalanine substitution at amino acid 387 of the iRhom2 protein (Figure 1E-F).

To establish that the missense mutation in *Rhbdf2* was responsible for the *sinecure* phenotype, we derived mice with an independent mutation of *Rhbdf2*. This allele was created by the targeted insertion of a gene trap cassette between exons 3 and 4.[13] Since exon 3 is the first coding exon of all coding transcripts of *Rhbdf2*, this insertion is predicted to result in a null allele, and is hereafter referred to as *Rhbdf2*^{KO}. Like *Rhbdf2*^{sinecure} homozygotes, mice homozygous for the *Rhbdf2*^{KO} allele were fully viable and fertile, with no externally visible phenotypes, and their peritoneal macrophages secreted less TNFα in response to both MALP-2 and LPS stimulation (Figure 2A). This response was lower than that of *Rhbdf2*$^{sin/sin}$ cells (indicating that the iRhom2^{I387F} substitution was a probable hypomorph), but not as low as

Ticam1$^{Lps2/Lps2}$;*Irak4*$^{oti/oti}$ cells, suggesting that either the *Rhbdf2*^{KO} allele was not a complete null, or that an iRhom2-independent pathway of TNFα secretion exists. iRhom2 might therefore act purely as a catalyst of TNFα secretion, or alternatively is functionally redundant with other protein(s). Mice with a compound heterozygous mutation of *Rhbdf2* (*Rhbdf2*$^{sin/KO}$) showed a similar reduction of TNFα secretion (Figure 2A), indicating that the *Rhbdf2* mutation in both strains was the cause of the impaired TNFα response. Unlike compound homozygosity for *Ticam1*$^{Lps2/Lps2}$ and *Irak4*$^{oti/oti}$ mutations, which blocks all known signals emanating from all TLRs, neither *Rhbdf2* mutation had any effect on IL-6 secretion (Figure 2B). The point of influence for iRhom2 therefore appears to be downstream of NF-κB activation and cytokine gene transcription.

Since TACE is a key mediator of TNFα secretion, but not the secretion of other cytokines, regulation of TACE activity would seem a likely function for iRhom2, particularly given that iRhom2 is localized to the ER,[17] and both rhomboid proteins and TACE are known to play important roles during EGFR ligand processing.[3–5] Two groups have independently reached similar conclusions, and have further revealed a specific interaction between iRhom2 and the protein precursor of TACE.[18,19]

It remains to be seen if iRhom2 is required for the function of proteases other than TACE,[20] or indeed for the processing of other proteins by TACE, such as FLT3L and EGFR ligands. Using a DSS-induced colitis model system, we tested whether iRhom2 was necessary in vivo for the processing of EGFR ligands, which initiate signaling known to be important for the regeneration of the gut epithelium.[21] Unlike TACE and EGFR mutants,[21,22] the *Rhbdf2* mutation did not affect sensitivity to DSS-induced weight loss (supplemental Figure 1, available on the *Blood* Web site; see the Supplemental Materials link at the top of the online article), implying that iRhom2 was physiologically redundant for the processing of EGFR ligands. In support of this conclusion, *Rhbdf2*^{sinecure} homozygotes did not exhibit the epidermal phenotypes that are characteristic of EGFR and TACE mutant mice. This potential redundancy is consistent with the myeloid-enriched mRNA expression of iRhom2 (supplemental Figure 2), and may make iRhom2 an attractive target for the treatment of inflammatory disease. Yet unlike most other rhomboid proteins (and indeed even TACE), iRhom2 is not an active protease, and may therefore be a challenging target for small molecule inhibition.

Supplementary Material

Supplemental Figures:

Acknowledgments

The authors thank M. Gutierrez for animal care, C. Ross and T. Robinson for sequencing, and D. La Vine for illustrations.

This work was supported by the National Institute of Allergy and Infectious Diseases of the National Institutes of Health (HHSN272200700038C to B.B.), and The General Sir John Monash Foundation (O.M.S.).

Footnotes

The online version of this article contains a data supplement.

The publication costs of this article were defrayed in part by page charge payment. Therefore, and solely to indicate this fact, this article is hereby marked “advertisement” in accordance with 18 USC section 1734.

Authorship

Contribution: O.M.S. identified the *sinecure* mutation and coordinated and wrote the paper; N.X. identified and mapped the *sinecure* phenotype; Y.W. and H.S. examined the TLR-induced cytokine response; W.T. performed DSS experiments; X.L. performed microinjections of the *Rhbdf2* knockout cell line; Y.X.

provided bioinformatics support; and B.B. oversaw the study and corrected the paper.

Conflict-of-interest disclosure: The authors declare no competing financial interests.

Correspondence: Owen M. Siggs, Department of Genetics, The Scripps Research Institute, 10550 North Torrey Pines Rd, La Jolla, CA 92037; e-mail: siggs@scripps.edu; and Bruce Beutler, Center for Genetics of Host Defense, University of Texas Southwestern Medical Center, 5323 Harry Hines Blvd, Dallas, TX 75390; e-mail: bruce.beutler@utsouthwestern.edu.

References

1. Black RA, Rauch CT, Kozlosky CJ, et al. A metalloproteinase disintegrin that releases tumour-necrosis factor-alpha from cells. Nature. 1997;385(6618):729–733. [PubMed: 9034190]

2. Moss ML, Jin SL, Milla ME, et al. Cloning of a disintegrin metalloproteinase that processes precursor tumour-necrosis factor-alpha. Nature. 1997;385(6618):733–736. [PubMed: 9034191]

3. Peschon JJ, Slack JL, Reddy P, et al. An essential role for ectodomain shedding in mammalian development. Science. 1998;282(5392):1281–1284. [PubMed: 9812885]

4. Lee JR, Urban S, Garvey CF, Freeman M. Regulated intracellular ligand transport and proteolysis control EGF signal activation in Drosophila. Cell. 2001;107(2):161–171. [PubMed: 11672524]

5. Urban S, Lee JR, Freeman M. Drosophila rhomboid-1 defines a family of putative intramembrane serine proteases. Cell. 2001;107(2):173–182. [PubMed: 11672525]

6. Freeman M. Rhomboid proteases and their biological functions. Annu Rev Genet. 2008;42:191–210. [PubMed: 18605900]

7. Beutler B, Jiang Z, Georgel P, et al. Genetic analysis of host resistance: Toll-like receptor signaling and immunity at large. Annu Rev Immunol. 2006;24:353–389. [PubMed: 16551253]

8. Tabeta K, Hoebe K, Janssen EM, et al. The Unc93b1 mutation 3d disrupts exogenous antigen presentation and signaling via Toll-like receptors 3, 7 and 9. Nat Immunol. 2006;7(2):156–164. [PubMed: 16415873]

9. Rutschmann S, Hoebe K, Zalevsky J, et al. PanR1, a dominant negative missense allele of the gene encoding TNF-alpha (Tnf), does not impair lymphoid development. J Immunol. 2006;176(12):7525–7532. [PubMed: 16751399]

10. Georgel P, Du X, Hoebe K, Beutler B. ENU mutagenesis in mice. Methods Mol Biol. 2008;415:1–16. [PubMed: 18370145]

11. Hoebe K, Du X, Georgel P, et al. Identification of Lps2 as a key transducer of MyD88-independent TIR signalling. Nature. 2003;424(6950):743–748. [PubMed: 12872135]

12. Croker BA, Lawson BR, Rutschmann S, et al. Inflammation and autoimmunity caused by a SHP1 mutation depend on IL-1, MyD88, and a microbial trigger. Proc Natl Acad Sci U S A. 2008;105(39):15028–15033. [PMCID: PMC2567487] [PubMed: 18806225]

13. Skarnes WC, Rosen B, West AP, et al. A conditional knockout resource for the genome-wide study of mouse gene function. Nature. 2011;474(7351):337–342. [PMCID: PMC3572410] [PubMed: 21677750]

14. Hoebe K, Du X, Goode J, Mann N, Beutler BA. Lps2: a new locus required for responses to lipopolysaccharide, revealed by germline mutagenesis and phenotypic screening. J Endotoxin Res. 2002;9(4):250–255. [PubMed: 12935356]

15. Siggs OM, Berger M, Krebs P, et al. A mutation of Ikbkg causes immune deficiency without impairing degradation of IkappaB alpha. Proc Natl Acad Sci U S A. 2010;107(7):3046–3051.

[PMCID: PMC2840324] [PubMed: 20133626]

16. Su AI, Wiltshire T, Batalov S, et al. A gene atlas of the mouse and human protein-encoding transcriptomes. Proc Natl Acad Sci U S A. 2004;101(16):6062–6067. [PMCID: PMC395923] [PubMed: 15075390]

17. Zettl M, Adrain C, Strisovsky K, Lastun V, Freeman M. Rhomboid family pseudoproteases use the ER quality control machinery to regulate intercellular signaling. Cell. 2011;145(1):79–91. [PMCID: PMC3149277] [PubMed: 21439629]

18. Adrain C, Zettl M, Christova Y, Taylor N, Freeman M. Tumor necrosis factor signaling requires iRhom2 to promote trafficking and activation of TACE. Science. 2012;335(6065):225–228. [PMCID: PMC3272371] [PubMed: 22246777]

19. McIlwain DR, Lang PA, Maretzky T, et al. iRhom2 regulation of TACE controls TNF-mediated protection against listeria and responses to LPS. Science. 2012;335(6065):229–232. [PMCID: PMC4250273] [PubMed: 22246778]

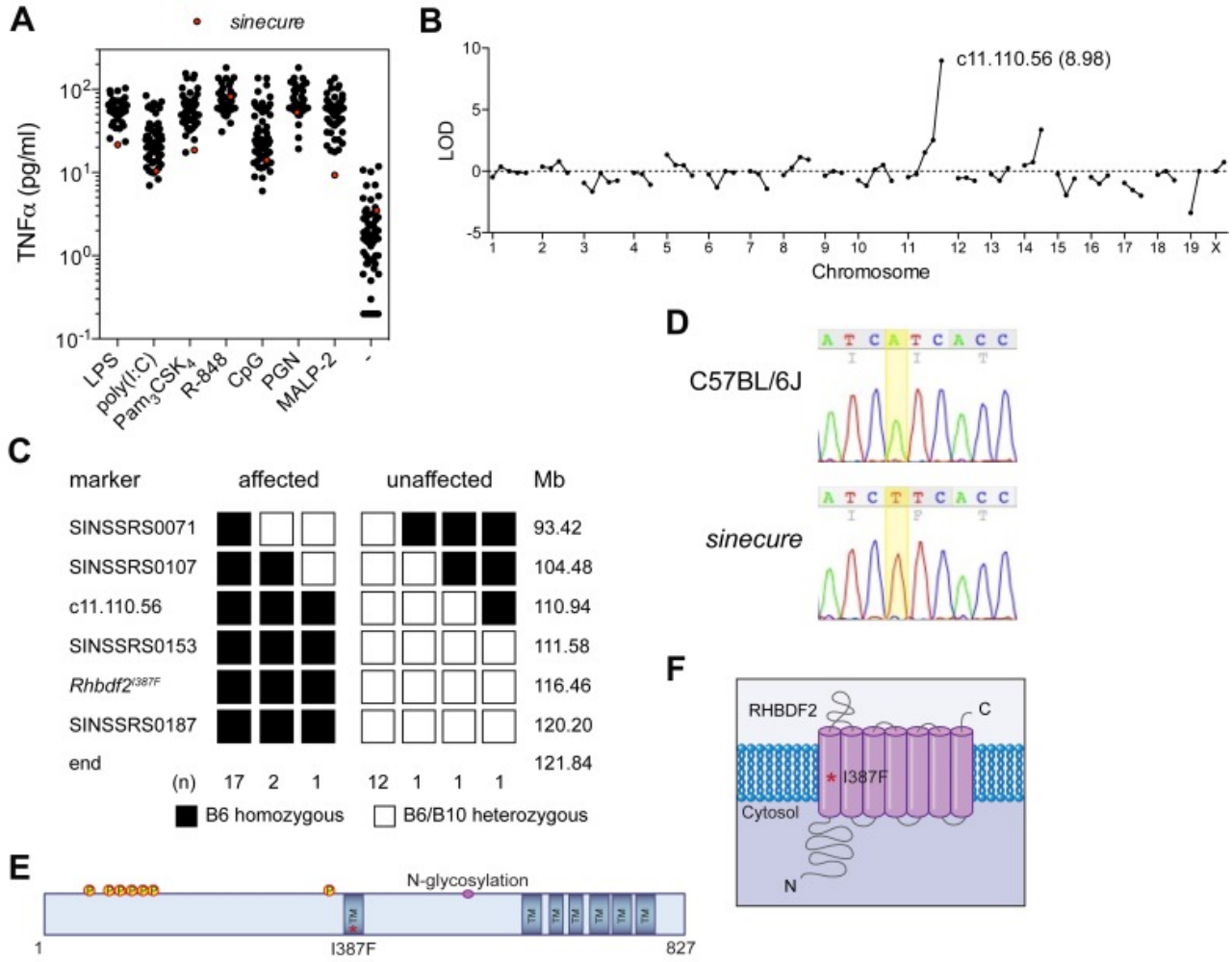
20. Blobel CP. ADAMs: key components in EGFR signalling and development. Nat Rev Mol Cell Biol. 2005;6(1):32–43. [PubMed: 15688065]

21. Brandl K, Sun L, Neppl C, et al. MyD88 signaling in nonhematopoietic cells protects mice against induced colitis by regulating specific EGF receptor ligands. Proc Natl Acad Sci U S A. 2010;107(46):19967–19972. [PMCID: PMC2993336] [PubMed: 21041656]

22. Chalaris A, Adam N, Sina C, et al. Critical role of the disintegrin metalloprotease ADAM17 for intestinal inflammation and regeneration in mice. J Exp Med. 2010;207(8):1617–1624. [PMCID: PMC2916135] [PubMed: 20603312]

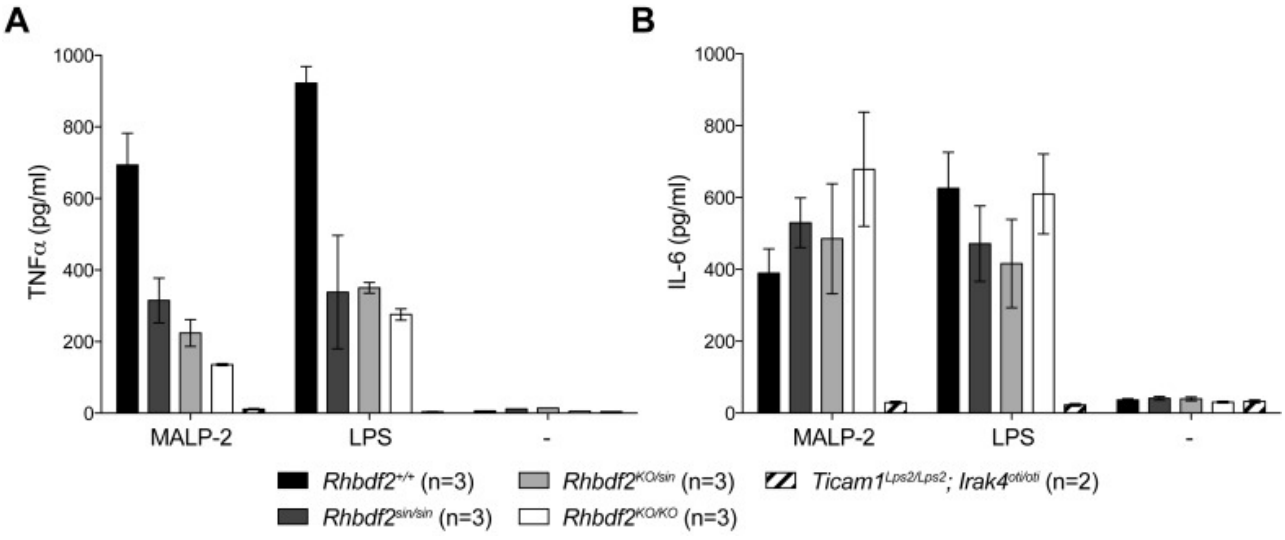
Figures and Tables

Figure 1



A recessive mutation in *Rhbdf2* is associated with reduced TLR-induced TNFα secretion. (A) Phenotype of the index *sinecure* mouse. Peritoneal macrophages from 62 G3 descendants of ENU-mutagenized sires were stimulated with a panel of TLR ligands, and TNFα production measured by L-929 bioassay. Genome-wide (B) and fine (C) mapping of the *sinecure* mutation to distal chromosome 11. (D) A homozygous transversion mutation in *Rhbdf2*, corresponding to an isoleucine to phenylalanine missense mutation (E) in the N-terminal transmembrane domain (TM) of iRhom2 protein. Predicted phosphorylation (P) and glycosylation sites are also indicated. (F) Topology of the iRhom2 protein, indicating the position of the *sinecure* missense mutation.

Figure 2



Mutant alleles of *Rhbdf2* are noncomplementary and cause a specific block in TNFα secretion. Thioglycollate-elicited peritoneal cells were isolated from mice of the indicated genotypes, and cultured in the presence of 200 pg/mL MALP-2, 1 ng/mL LPS, or media alone (-) for 4 hours. TNFα (A) and IL-6 (B) was then measured in the culture

supernatant.

Articles from Blood are provided here courtesy of **American Society of Hematology**

Published December 26, 2011

ZBTB1 is a determinant of lymphoid development

Owen M. Siggs, Xiaohong Li, Yu Xia, and Bruce Beutler

Department of Genetics, The Scripps Research Institute, La Jolla, CA 92037

In this study, we describe a chemically induced mouse mutation that caused a complete and cell-intrinsic T cell deficiency. Development of other lymphoid lineages was also partially impaired and was severely compromised under competitive conditions. Positional cloning, retroviral transduction, and a somatic reversion event revealed that the causative mutation lay within *Zbtb1* (*zinc finger and BTB domain containing 1*), a gene conserved throughout vertebrate evolution. Our data establish ZBTB1 as a critical determinant of T cell development and lymphopoiesis in general, most likely by acting as a transcriptional regulator.

CORRESPONDENCE
Owen M. Siggs:
siggs@scripps.edu
OR
Bruce Beutler:
bruce.beutler@utsouthwestern.edu

Abbreviations used: BTB-ZF, Broad complex, Tramtrack, and Bric à brac–zinc finger; CLP, common lymphoid progenitor; EdU, 5-ethynyl-2′deoxyuridine; ENU, *N*-ethyl-*N*-nitrosourea; ETP, early thymic precursor; HSC, hematopoietic stem cell.

Lymphocytes arise from multipotent progenitors in the bone marrow (Kondo et al., 1997), deviating from the myeloid lineage and completing their differentiation under the influence of a suite of transcriptional regulators (Busslinger, 2004; Rothenberg and Taghon, 2005), including Ikaros (Georgopoulos et al., 1994), Pax5 (Nutt et al., 1999), and Notch1 (Radtke et al., 1999). The transcriptional regulators that guide this process are of special interest because many are also involved in lymphoid tumorigenesis (Ye et al., 1993; Weng et al., 2004; Mullighan et al., 2007, 2008), whereas others can be manipulated for directed reprogramming of cell fate (Cobaleda et al., 2007).

Among all known transcriptional regulators of lymphopoiesis, the BTB-ZF (Broad complex, Tramtrack, and Bric à brac–zinc finger) family of proteins is well represented. These proteins influence lymphoid development from the common lymphoid progenitor (CLP) stage (Kosan et al., 2010), to the T versus B fate decision (Maeda et al., 2007), to $CD4^+$ versus $CD8^+$ T cell selection (He et al., 2005), and even as late as the differentiation of Tfh (Johnston et al., 2009; Nurieva et al., 2009; Yu et al., 2009) and NKT (Kovalovsky et al., 2008; Savage et al., 2008) effector lineages.

In this study, we have used chemical mutagenesis in mice to reveal the physiological function of the BTB-ZF protein ZBTB1 (zinc finger and BTB domain containing 1). ZBTB1 was essential for T cell development and also for the development of B and NK cells under competitive conditions.

RESULTS AND DISCUSSION

Severe T cell lymphopenia

While surveying the descendants of chemically mutagenized mice for lymphocyte deficiencies (Siggs et al., 2011), we identified a single male mouse devoid of T cells. This phenotype, nicknamed *scanT* because of the low (or scant) frequency of T cells, was transmitted as a recessive trait (Fig. 1, A and B). *scanT* mutant mice were born at the expected Mendelian ratio, were typically fertile, and were outwardly normal in behavior.

scanT thymi were severely hypoplastic (Fig. 1 C), containing around 2% of the number of wild-type cells, and lacked corticomedullary definition (Fig. 1 D). Thymocyte development was impaired from the early thymic precursor (ETP) stage and beyond (Fig. 1, E and F). Of the lymphocytes that were present in the thymus, almost all were B cells, representing a 20-fold increase over wild-type numbers (Fig. 1 F).

X. Li's and B. Beutler's present address is Center for Genetics of Host Defense, University of Texas Southwestern Medical Center, Dallas, TX 75390.

© 2012 Siggs et al. This article is distributed under the terms of an Attribution–Noncommercial–Share Alike–No Mirror Sites license for the first six months after the publication date (see http://www.rupress.org/terms). After six months it is available under a Creative Commons License (Attribution–Noncommercial–Share Alike 3.0 Unported license, as described at http://creativecommons.org/licenses/by-nc-sa/3.0/).

The Rockefeller University Press $30.00
J. Exp. Med. Vol. 209 No. 1 19-27
www.jem.org/cgi/doi/10.1084/jem.20112084

Supplemental Material can be found at:
http://jem.rupress.org/content/suppl/2011/12/22/jem.20112084.DC1.html

The Journal of Experimental Medicine

Downloaded from jem.rupress.org on January 19, 2012

Published December 26, 2011

Mutation of a previously uncharacterized zinc finger protein

We mapped the *scanT* genetic lesion first by genome-wide linkage to chromosome 12 (Fig. 2 A) and then by fine mapping to a 5-Mbp interval between markers D12Mit33 and D12Mit4 (Fig. 2 B). Because none of the 35 annotated protein-encoding genes in the interval (Table S1) had previously been implicated in T cell development, we sequenced the coding exons and flanking splice junctions of three (*Zbtb1*, *Zbtb25*, and *Ppp2r5e*) based on their predominant expression in lymphocytes (http://biogps.gnf.org/). 93.4% of all target nucleotides (6,081/6,511) were covered on both strands of wild-type and *scanT* samples with a Phred quality score of >30, and a single missense transition was identified in *Zbtb1* (C74R; Fig. 2 C). PolyPhen-2 (Adzhubei et al., 2010) assigned a score of 0.954 to this mutation, predicting a deleterious effect with 93% confidence. 43.2% of the total coding critical region (59,447/137,702 nt) was also covered at least three times by SOLiD 3 sequencing, with no additional mutations found.

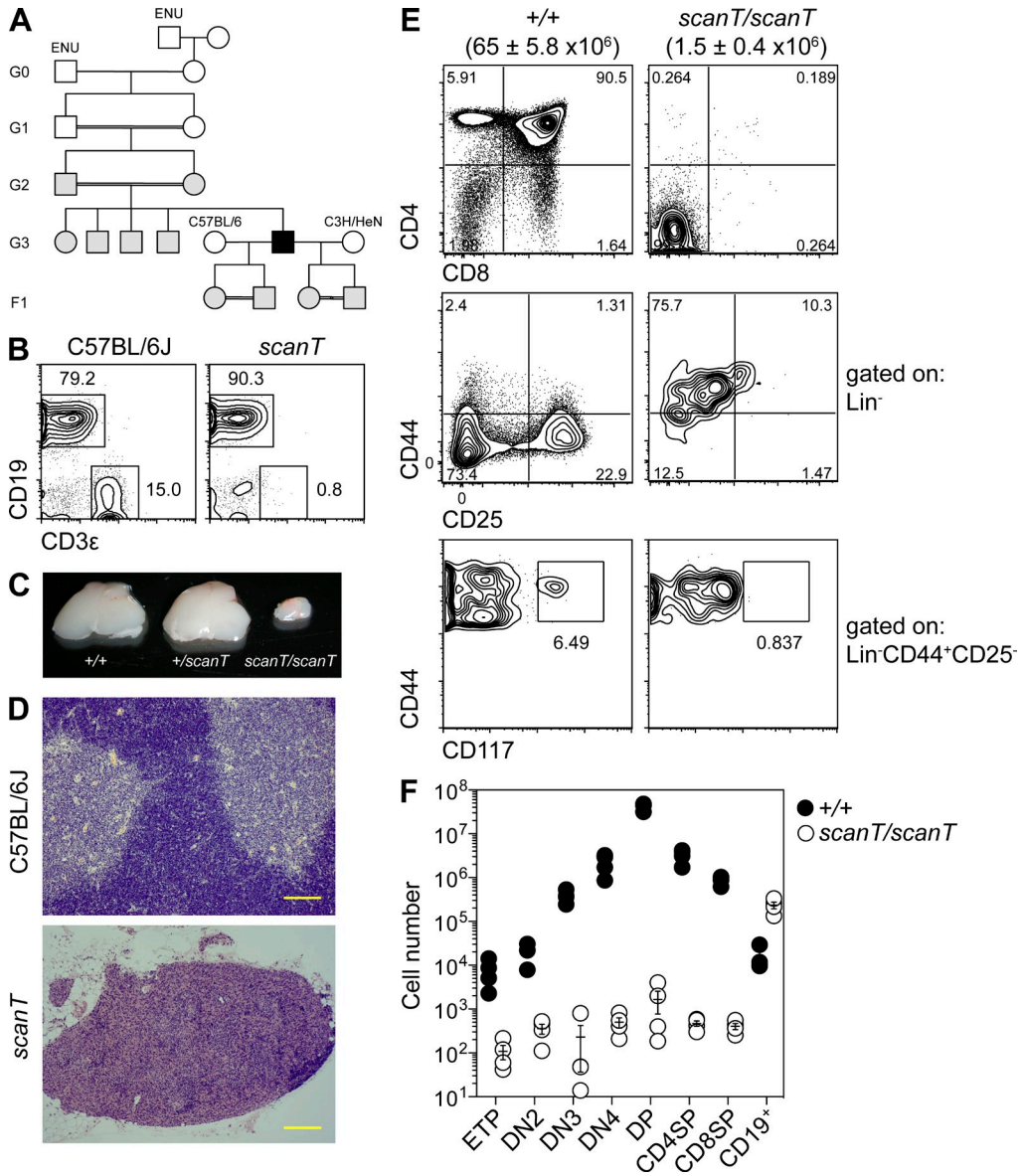


Figure 1. T cell aplasia in *scanT* mice. (A) Initial generations of the *scanT* pedigree. Black symbols, T-deficient phenotype; gray symbols, wild-type phenotype; open symbols, not tested. (B) Percentages of B ($CD19^+$) and T ($CD3\varepsilon^+$) cells in the peripheral blood of 8-wk-old mice as measured by flow cytometry. (C–F) Relative size (C), histological appearance (H&E; D), and cellular composition (E and F) of the thymus of wild-type and mutant siblings at 8 wk of age. Lineage markers in E and F were CD11b, $CD3\varepsilon$, B220, Ter119, Ly6G, NK1.1, and $CD8\alpha$. Subsets in F were gated as follows: ETP ($Lin^-CD44^+CD25^-CD117^+$), DN2 ($Lin^-CD44^+CD25^+$), DN3 ($Lin^-CD44^-CD25^+$), DN4 ($Lin^-CD44^-CD25^-$), DP ($CD4^+CD8\alpha^+$), CD4SP ($CD4^+CD8\alpha^-$), and CD8SP ($CD4^-CD8\alpha^+$). Data are representative of one (A and D), two to three (E and F), or more than three (B and C) independent experiments. Error bars represent standard error, and symbols in F represent individual mice. Numbers in parentheses in E represent mean thymic cellularity and standard error. Bars, 100 µm.

Downloaded from jem.rupress.org on January 19, 2012

Published December 26, 2011

Zbtb1 encodes a 713-aa member of the POK (POZ [Poxviruses and zinc finger] and Krüppel) or BTB-ZF family of transcriptional regulators and had no previously described function. Mouse ZBTB1 is 94% identical to its counterpart in man. Two characteristic domains are shared by BTB-ZF family members: an N-terminal BTB/POZ domain and a series of C-terminal C_2H_2 Krüppel-type zinc finger motifs. ZBTB1 itself contains an N-terminal BTB domain, eight zinc finger motifs, and two nuclear localization sequences (Matic et al., 2010). The residue mutated in the *scanT* pedigree (C74) is predicted to lie within the A3 helix of the BTB domain (Fig. 2 D and Fig. S1; Stogios et al., 2005) and is highly conserved across the vertebrate lineage (Fig. 2 E). Two unique transcripts are predicted to arise from the *Zbtb1/ZBTB1* locus, both of which harbor the *scanT* mutation, yet only one of which (Ensembl release 65 accession no. ENST00000394712) is predominantly expressed in T cells and other leukocytes in mouse and man (Fig. S2). The other (Ensembl release 65 accession no. ENST00000358738) is known to be transcribed in HeLa cells by the nonconventional single-polypeptide nuclear RNA polymerase IV (Kravchenko et al., 2005).

To confirm that the mutation in *Zbtb1* was responsible for the *scanT* phenotype, wild-type *Zbtb1* was retrovirally

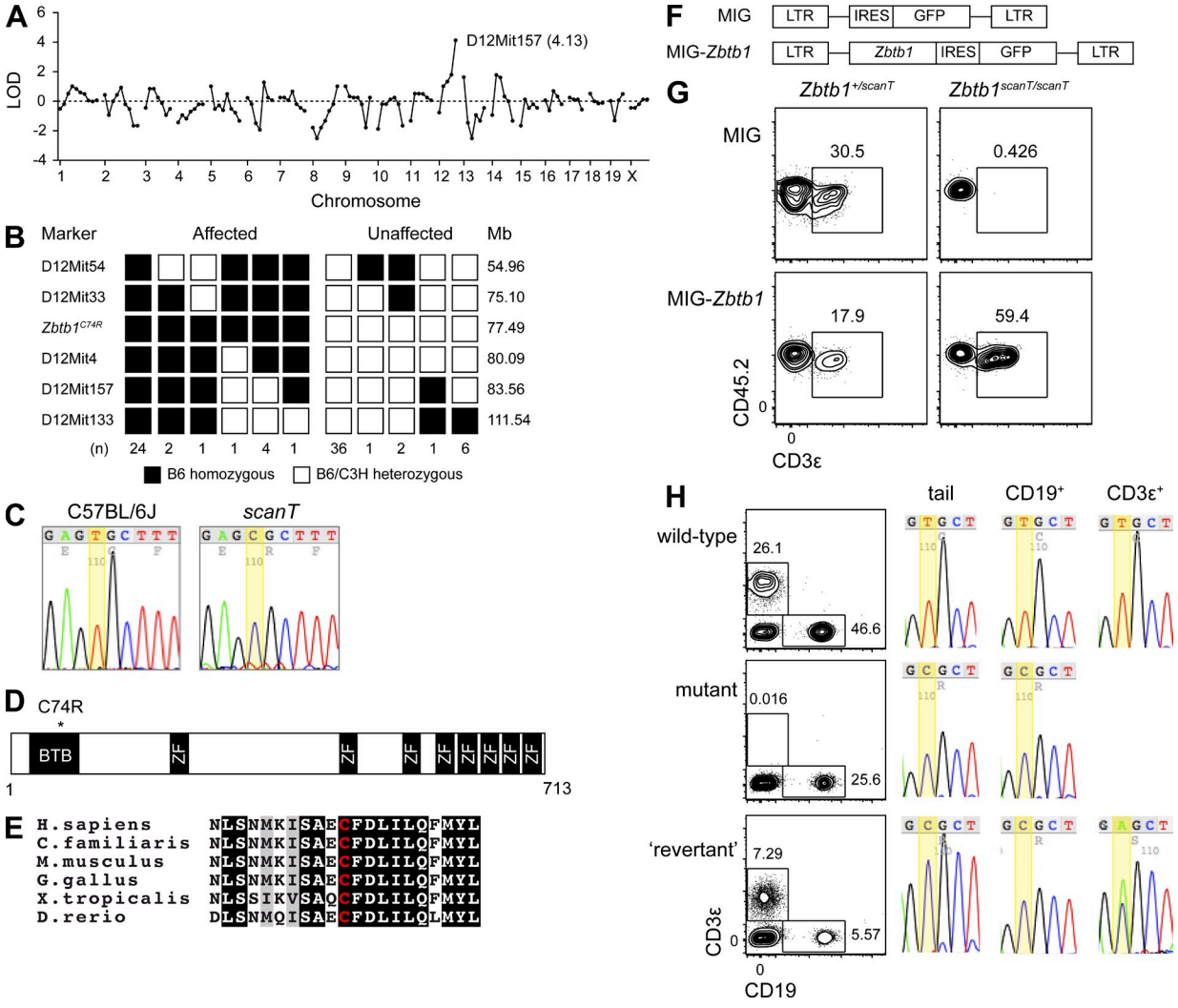


Figure 2. Identification of a missense mutation in ZBTB1. (A and B) Chromosomal mapping (A) and fine mapping (B) of the *scanT* phenotype. LOD, logarithm of odds score. (C) DNA sequence chromatograms of the mutated nucleotide in *Zbtb1* (thymine to cytosine), resulting in the substitution of arginine for cysteine at codon 74. (D) Predicted ZBTB1 protein domain structure. (E) Conservation of ZBTB1 sequence across multiple vertebrates, with the amino acid corresponding to $ZBTB1^{C74}$ highlighted in red. ZBTB1 counterparts were not found in nonvertebrate proteomes. (F) Schematic of the MIG-*Zbtb1* and control retroviral constructs. MIG, MSCV-IRES-GFP; LTR, long terminal repeat. (G) Bone marrow cells from *scanT* mice or heterozygous controls ($CD45.2^+$) were transduced with a retroviral construct expressing *Zbtb1* and transferred into irradiated $CD45.1^+$ recipients ($\sim 2 \times 10^6$ cells/mouse). Transduced $CD3\varepsilon^+$ cells were identified in blood 4 mo after transfer by coexpression of GFP. (H) Phenotypic reversion associated with somatic mutation of *Zbtb1*. DNA was prepared from tail clippings and flow-sorted $CD19^+$ and $CD3\varepsilon^+$ lymph node cells and sequenced at the locus mutated in the *scanT* pedigree. Contour plots were obtained from blood. Data in G are representative of three independent experiments. (C and H) Yellow highlighting indicates the position of the nucleotide mutated in the *scanT* pedigree..

Downloaded from jem.rupress.org on January 19, 2012

Published December 26, 2011

transduced into *scanT* hematopoietic progenitors (Fig. 2 F). GFP$^+$ T cells were recovered from recipients of *Zbtb1*-transduced *scanT* progenitors (Fig. 2 G), presumably as a consequence of restored thymic development. These data indicated that the mutation in *Zbtb1* could account for T cell deficiency in scanT mice.

In a minority of cases (3/16 in a 3-mo-old cohort of *Zbtb1*^{scanT} homozygotes), T cells were detected at diminished frequencies in the blood of germline mutant mice. We hypothesized that these cells arose from a somatic mutation that suppressed the *scanT* phenotype, considering the strong selective advantage that such a mutation would confer and given that a similar phenomenon is known to occur in human T cell–deficient SCID (Hirschhorn et al., 1996). To test for somatic suppressor mutations, DNA was isolated from sorted T and B cells. Sequencing of the mutated *Zbtb1* locus revealed a heterozygous mutation within the T cell compartment of one phenotypic revertant (but not the other

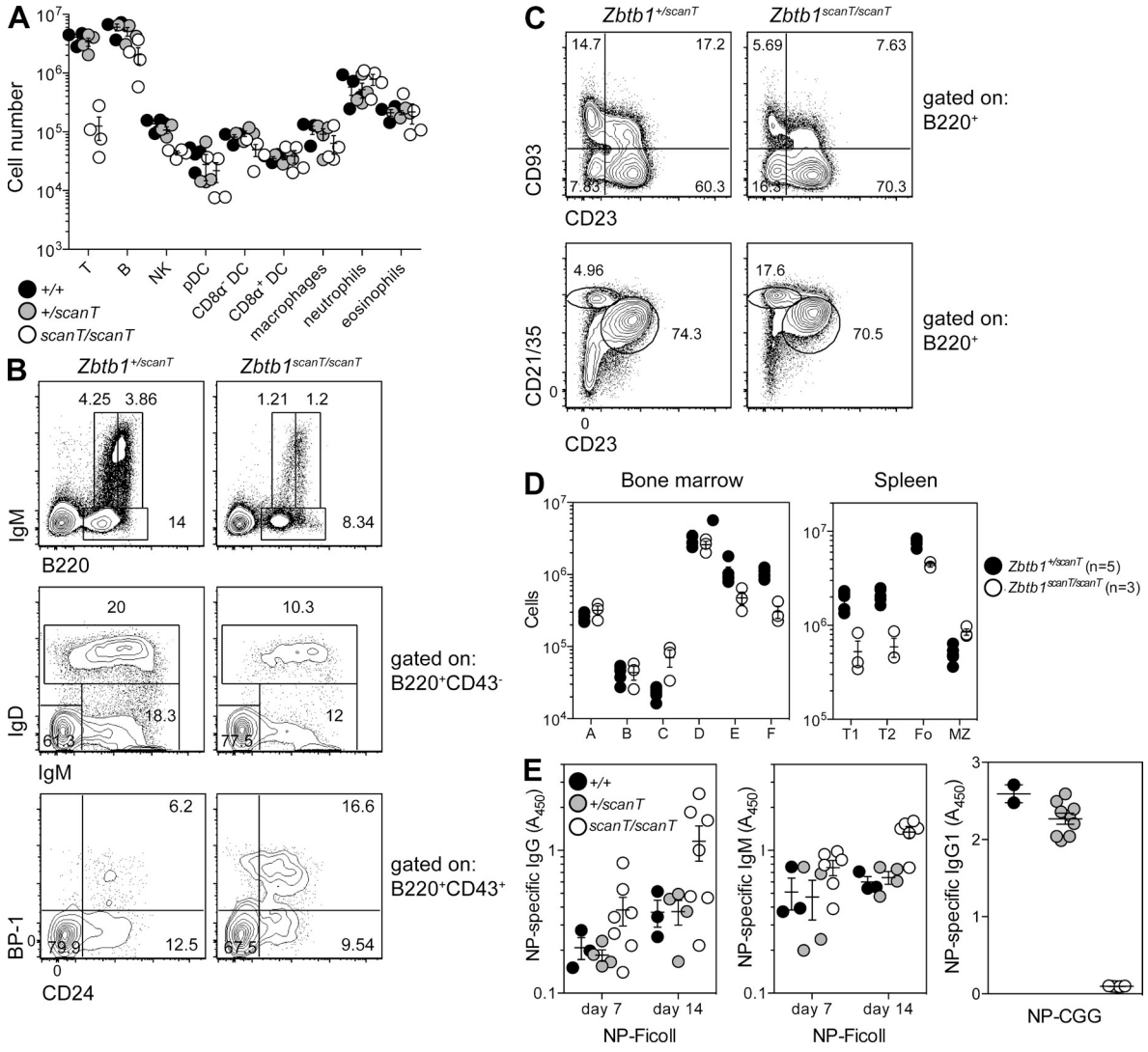


Figure 3. ***scanT*** **mice have generalized deficiencies of lymphoid but not myeloid cells.** (A) Total numbers of major lymphoid and myeloid cell subsets in the spleen of 8-wk-old sex-matched littermates, gated as follows: T (CD3ε$^+$), B (CD19$^+$), NK (NK1.1$^+$CD3ε$^-$), plasmacytoid DCs (pDC; Lin$^-$PDCA1$^+$SiglecH$^+$), CD8α$^-$ DCs (Lin$^-$CD11c$^+$CD11b$^+$CD8α$^-$), CD8α$^+$ DCs (Lin$^-$CD11c$^+$CD11b$^-$CD8α$^+$), macrophages (Lin$^-$CD11b$^+$F4/80$^+$SSC^{lo}), neutrophils (Lin$^-$CD11b$^+$F4/80$^-$Ly6G^{hi}), and eosinophils (Lin$^-$CD11b$^+$F4/80$^+$SSC^{hi}). Lineage markers included CD19, TCR-β, NK1.1, and the viability dye 7-AAD. (B–D) Frequencies (B and C) and numbers (D) of major B cell subsets in bone marrow and spleen. Subsets in bone marrow were gated as follows: A (CD11b$^-$CD3e$^-$Ter119$^-$Ly6G$^-$NK1.1$^-$IgM$^-$B220$^+$CD19$^-$CD24$^-$BP-1$^-$), B (B220$^+$IgM$^-$CD43$^+$CD24$^+$BP-1$^-$), C (B220$^+$IgM$^-$CD43$^+$CD24$^+$BP-1$^+$), D (B220$^+$CD43$^-$IgM$^-$IgD$^-$), E (B220$^+$CD43$^-$IgM$^+$IgD$^-$), and F (B220$^+$CD43$^-$IgM$^+$IgD$^+$). Subsets in spleen were gated as follows: T1 (B220$^+$CD93$^+$CD23$^-$), T2 (B220$^+$CD93$^+$CD23$^+$), Fo (follicular; B220$^+$CD93$^-$CD23$^+$CD21/35^{int}), and MZ (marginal zone; B220$^+$CD93$^-$CD23$^-$CD21/35^{hi}). (E) NP (4-hydroxy-3-nitrophenylacetyl)-specific antibodies in the serum of mice immunized with NP-Ficoll or NP-CGG at 7 or 14 d (NP-Ficoll) or 14 d (NP-CGG) after immunization, presented as absorbance at 450 nm (A_{450}). (A–E) Data are representative of one (E) or two (A–D) independent experiments with four or more mice per group. Error bars represent standard error, and symbols represent individual mice.

Downloaded from jem.rupress.org on January 19, 2012

Published December 26, 2011

two; Fig. 2 H), indicating that most, if not all, T cells in this mouse were clonally derived. This mutation either occurred after the CLP stage or did not confer a selective advantage in the B cell lineage because it was not observed in DNA from CD19$^+$ cells (Fig. 2 H). The mutation in question occurred at the same nucleotide as the *scanT* mutation (the first base of codon 74), yet rather than a reversion to the wild-type codon (TGC, encoding cysteine) changed the codon to serine (AGC). Given the physical similarities of serine and cysteine, we propose that *Zbtb1*^{C74S} is permissive to T cell development and T cell clonal expansion, whereas *Zbtb1*^{C74R} is not.

Defects in lymphoid but not myeloid development

The effects of *Zbtb1* mutation were not restricted to the T cell lineage. Numbers of all lymphocyte lineages (T, B, and NK) were reduced in the spleens of mutant mice, whereas numbers of myeloid cells were not (Fig. 3 A). An examination of B cell development in mutant bone marrow revealed an accumulation of B cell progenitors at the Hardy Fraction C stage, followed by a reduction of progenitors at each subsequent stage (Fig. 3, B and D). In the mutant spleen, numbers of transitional and follicular B cells were significantly reduced by an average of 72% and 44%, respectively (Fig. 3, C and D). The relatively minor reduction in follicular as compared with transitional B cell numbers may indicate mild compensatory expansion in the follicular compartment. Mutant B cells nevertheless responded to T-independent (but not T dependent) immunization (Fig. 3 E), implying a developmental rather than a functional B cell defect.

A cell-intrinsic defect

To distinguish between potential hematopoietic and non-hematopoietic origins of the *Zbtb1* mutant phenotype, we created radiation chimeras. *Rag1* mutants reconstituted with *Zbtb1* mutant bone marrow developed B cells but not T cells (Fig. 4 A). This defect was intrinsic to *Zbtb1* mutant T cell progenitors, rather than other radiosensitive hematopoietic cells, because T cells in mixed bone marrow chimeras were exclusively derived from wild-type donors (Fig. 4 B). In fact, all blood lymphocytes (but not CD11b$^+$ myeloid cells) were wild-type donor derived, implying a general competitive failure of *Zbtb1* mutant lymphoid progenitors (Fig. 4 B). Finer phenotyping of the spleen, bone marrow, and thymus of mixed bone marrow chimeric mice confirmed this to be the case. B, T, and NK cells in the spleen were exclusively wild-type derived (CD45.1$^+$), whereas little or no competitive disadvantage was seen in the myeloid compartments (Fig. 4 C). Cells of wild-type origin dominated the B cell compartment from the Fraction A stage onward and similarly outcompeted *Zbtb1* mutant NK progenitors in bone marrow and T cell progenitors in the thymus (Fig. 4 C).

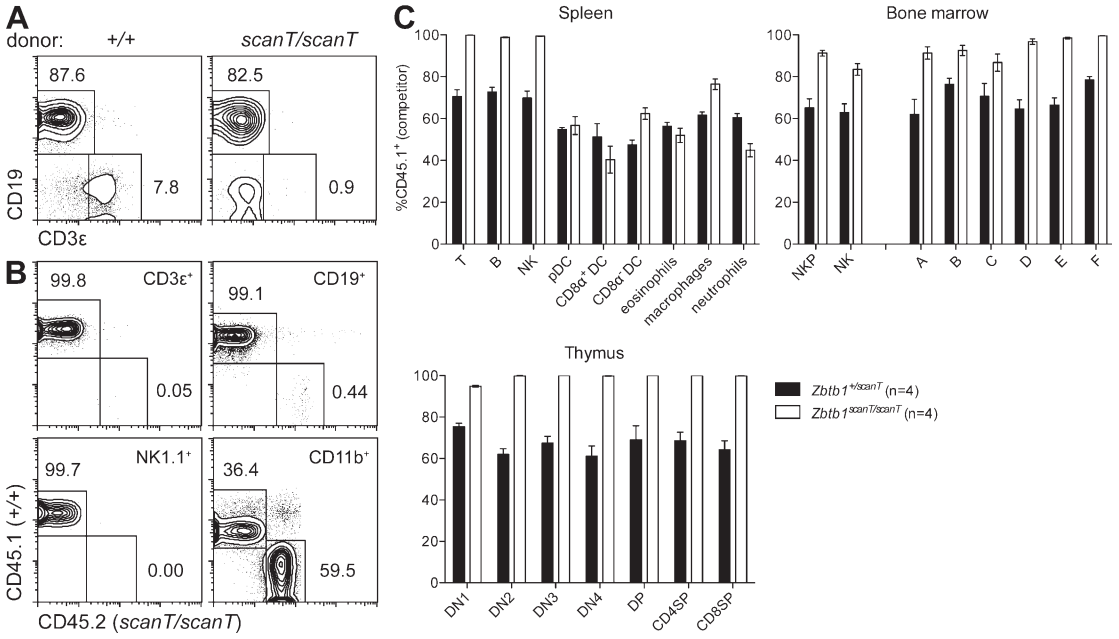


Figure 4. A cell-intrinsic T cell deficiency and competitive failure of lymphoid reconstitution. (A and B) Lethally irradiated *Rag1* mutant mice (CD45.2$^+$) were reconstituted with unmixed *scanT* or wild-type bone marrow (CD45.2$^+$; A) or a mixture of *scanT* or wild-type marrow (CD45.2$^+$) with wild-type bone marrow (CD45.1$^+$; B). Chimerism was measured 8 wk after transplant. Panels in B have been gated on the indicated cell subset. (C) Lethally irradiated wild-type recipients (CD45.1$^+$) were transplanted with an equal mixture of wild-type (CD45.1$^+$) and heterozygous or homozygous mutant (CD45.2$^+$) bone marrow. Wild-type donor chimerism (CD45.1$^+$) was measured 8 wk later in the spleen, bone marrow, and thymus. Subsets were gated as in Fig. 3, with the addition of NK progenitors (NKP; 7-AAD$^-$CD19$^-$TCR-β$^-$CD122$^+$NK1.1$^-$). (A–C) Data are representative of one (A) or three (B and C) independent experiments with at least three mice per group. Error bars represent standard error.

Downloaded from jem.rupress.org on January 19, 2012

Published December 26, 2011

Uncompromised hematopoietic progenitor function

However, the *scanT* mutation did not appear to affect hematopoietic development before lymphoid specification. Percentages and numbers of early hematopoietic progenitors, including CLPs, were comparable in heterozygous and homozygous mutant bone marrow (Fig. 5, A and B) and were reconstituted at equivalent percentages in mixed bone marrow chimeras (Fig. 5 C). Hematopoietic stem cell (HSC) turnover, as measured by incorporation of the thymidine analogue 5-ethynyl-2′deoxyuridine (EdU), occurred at similar rates in wild-type and mutant mice (Fig. 5 D). Wild-type and *Zbtb1* mutant bone marrow also generated equivalent numbers of hematopoietic colonies in the spleens of lethally irradiated recipients, both at days 8 (indicative of megakaryocyte/erythroid progenitor function) and 12 (reflective of multipotent progenitor function; Fig. 5 E; Na Nakorn et al., 2002). Myeloid engraftment did not occur in unconditioned *Zbtb1* mutant recipients of wild-type bone marrow, which is consistent with the interpretation of intact HSC function (Fig. 5 F).

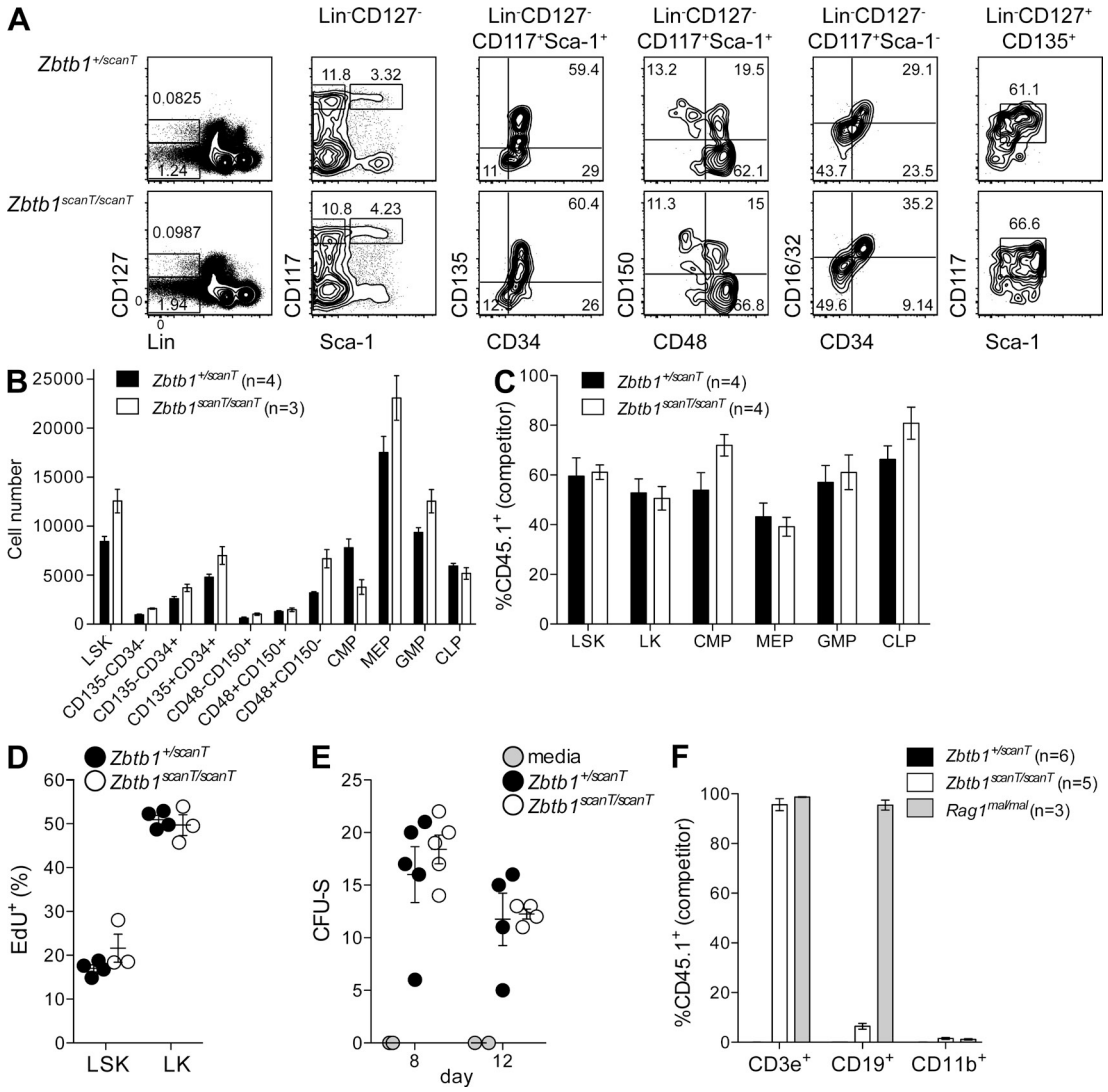


Figure 5. Normal development and function of hematopoietic progenitors. (A and B) Frequencies (A) and numbers (B) or hematopoietic progenitors in heterozygous and homozygous *Zbtb1* mutant bone marrow. LT-HSC (long-term HSC; $CD135^-CD34^-$ or $CD150^+CD48^-$), ST-HSC (short-term HSC; $CD135^-CD34^+$ or $CD150^+CD48^+$), MPP (multipotent progenitors; $CD135^+CD34^+$ or $CD150^-CD48^+$), CMP (common myeloid progenitors; $CD16/32^-CD34^+$), GMP (granulocyte/monocyte progenitors; $CD16/32^+CD34^+$), MEP (megakaryocyte/erythroid progenitors; $CD16/32^-CD34^-$), and CLP ($CD117^{int}Sca\text{-}1^{int}$) were gated as indicated. (C) Chimerism of a subset of hematopoietic progenitors outlined in A, 8 wk after reconstitution of lethally irradiated $CD45.1^+$ recipients with an equal mixture of $CD45.1^+$ and *Zbtb1*$^{+/scanT}$ ($CD45.2^+$) or $CD45.1^+$ and *Zbtb1*$^{scanT/scanT}$ ($CD45.2^+$) bone marrow cells. (D) Incorporation of the thymidine analogue EdU 4 h after injection. (E) Spleen colony forming units (CFU-S) counted 8 or 12 d after transfer of 10^5 bone marrow cells (or media alone) into lethally irradiated recipients. (F) Engraftment of 2×10^6 $CD45.1^+$ bone marrow cells in unconditioned recipients 8 wk after injection. Lineage markers in A–D were CD11b, CD3ε, B220, Ter119, Ly6G, NK1.1, and CD8α. (A–F) Data are representative of one (D and F), two (A–C), and three (E) independent experiments with at least three mice per group. Error bars represent standard error, and symbols in D and E represent individual mice.

Downloaded from jem.rupress.org on January 19, 2012

Published December 26, 2011

In certain aspects, *Zbtb1* mutants reflect the phenotype of mice lacking Notch1. Both *Zbtb1* and *Notch1* mutants are profoundly T cell deficient and show an accumulation of B cells in the thymic rudiment (Radtke et al., 1999). Yet although *Zbtb1* mutants have a competitive disadvantage in the B and NK lineages, *Notch1* mutants do not (Radtke et al., 1999). Germline mutation of *Zbtb1* appears permissive to embryonic development, whereas mutation of *Notch1* is not (Swiatek et al., 1994), indicating a more specialized role for ZBTB1 in determining lymphoid fate. This is consistent with the conservation of *Zbtb1* only among vertebrate genomes and might implicate the human *ZBTB1* locus in genetically obscure cases of T cell–deficient SCID (Fischer, 2007).

Although there are no previous studies of a physiological role for ZBTB1, one describes some of its biochemical characteristics (Matic et al., 2010). ZBTB1, like many of its BTB-ZF counterparts, acts as a potent transcriptional repressor, as determined by the repressive activity of a Gal4-ZBTB1 fusion protein. This repressive activity, as well as the colocalization of ZBTB1 with the SMRT transcriptional repressor, is also regulated by SUMOylation (Matic et al., 2010).

Our data raise several questions about the function of ZBTB1 in T cell and lymphoid specification. In particular, why is ZBTB1 critical for T cell development but only essential for B and NK development under competition? Can the reduction in ETP numbers be explained by their failure to migrate to the thymus, by a failure to proliferate within it, or a combination of both? Programmed death of T cell progenitors is unlikely to account for this because T cells also fail to develop in the absence of the proapoptotic protein BIM (which can rescue erythropoiesis in mice deficient for the BTB-ZF relative LRF; Fig. S3; Maeda et al., 2009).

In summary, our work defines ZBTB1 as a regulator of lymphoid development, joining the ranks of several other lymphoid-promoting BTB-ZF proteins. As is the case with other BTB-ZF family members, ZBTB1 presumably acts as a transcriptional suppressor, and the determination of precisely which genes it regulates will be of central importance to our understanding of lymphopoiesis.

MATERIALS AND METHODS

Mice and positional cloning. *Zbtb1*^{scanT} was generated on a pure C57BL/6J (The Jackson Laboratory) background by *N*-ethyl-*N*-nitrosourea (ENU) mutagenesis as previously described (Georgel et al., 2008). The index *scanT* mutant (C57BL/6J) was outcrossed to C3H/HeN females (Taconic), and F1 progeny were intercrossed. Blood was collected from the retroorbital plexus of 26 F2 progeny, and mice were grouped into mutant and wild-type cohorts (7 and 19 mice, respectively) based on relative percentages of CD19$^+$ and CD3ε$^+$ cells as measured by flow cytometry. Individual mice were typed at 128 microsatellite markers spaced across the genome (complete list available in the Supplemental material), with expected and observed genotype frequencies used to calculate LOD (logarithm of odds) scores at each marker. For fine mapping, an extra 71 F3 backcross progeny were genotyped at additional loci within the critical region. Candidate gene amplicons from wild-type and *scanT* genomic DNA were sequenced using a capillary sequencer (3730xl; Applied Biosystems). Genomic DNA from a single *scanT* homozygote was used to create a fragment library for single slide whole-genome sequencing on the SOLiD 3 platform (Applied Biosystems). *Rag1*^{maladaptive} mice (C57BL/6J, MGI:3851764) were generated in-house by ENU mutagenesis, and B6.SJL-*Ptprc*^{a} *Pep3*^{b}/BoyJ (CD45.1, backcrossed >22 generations to C57BL/6), *Bcl2l11*$^{tm1.1Ast}$ (backcrossed 13 generations to C57BL/6; Bouillet et al., 1999), and C57BL/6J males used for mutagenesis were obtained from the Jackson Laboratory. All other C57BL/6J mice were obtained from The Scripps Research Institute breeding colony. All animal procedures were performed in accordance with guidelines of the Institutional Animal Care and Use Committee of The Scripps Research Institute, and all experiments were conducted with homozygous mutants and sex-matched littermate controls.

Flow cytometry. Blood from the retroorbital plexus of isoflurane-anesthetized mice was collected in cluster tubes (Costar) containing 20 µl of 6% (wt/vol) EDTA in water. 50 µl of blood was subjected to two rounds of red blood cell lysis with ammonium chloride before staining. Lymphocyte suspensions from bone marrow (femurs and tibias from one hind leg), spleen, and thymus were counted (Z2 Coulter Counter; Beckman Coulter) and were stained with a combination of the following mouse-specific antibodies: FITC-conjugated IgM (goat polyclonal; 1020-02; SouthernBiotech); FITC-conjugated CD24 (30-F1), CD48 (HM48-1), F4/80 (BM8), CD127 (A7R34); PE-conjugated CD122 (5H4), CD135 (A2F10), CD150 (9D1), IgD (11-26), PDCA1 (927), TCR-β (H57-597; PerCP-Cy5.5); CD117 (2B8; eFluor710), APC-conjugated CD8α (53-6.7), CD11b (M1/70), CD93 (AA4.1), IgM (II/41), Ly6G (RB6-8C5), NK1.1 (PK136), TER119 (TER-119; eBioscience); FITC-conjugated CD4 (GK1.5), CD23 (B3B4), CD25 (7D4), CD34 (RAM34), PE-conjugated BP-1 (BP-1), CD11b (M1/70), CD19 (1D3), CD21/35 (7G6), CD44 (IM7), PerCP-Cy5.5–conjugated B220 (RA3-6B2), CD8α (53–6.7), CD19 (1D3), NK1.1 (PK136), APC-conjugated CD11c (HL3) and CD43 (S7), CD44 (IM7; Horizon V500; BD); APC-conjugated SiglecH (551), CD3ε (145-2C11), APC-Cy7–conjugated Sca-1 (D7) and CD45.2 (104), PE-Cy7–conjugated CD16/32 (93) and CD19 (6D5), CD45.1 (A20; Pacific blue), and CD16/32 (93; purified; BioLegend). Samples were acquired on a FACSCalibur or LSRFortessa (BD), and data were analyzed with FlowJo software (Tree Star). 7-AAD was purchased from eBioscience, and EdU labeling and staining were performed according to the manufacturer's instructions (Invitrogen) 4 h after a single intraperitoneal injection of 100 mg/kg EdU. For sorting experiments, lymph node or suspensions were labeled with antibodies, and target populations were sorted by a FACSAria II (BD) into serum for genomic DNA extraction.

Immunizations. Immunizations were performed as described previously (Siggs et al., 2011).

Hematopoietic chimeras. Recipient mice were γ-irradiated with a split dose of 11 Gy (2 × 5.5 Gy, ^{137}Cs source). The next day, mice were injected with 2 × 10^6 bone marrow cells via the retroorbital plexus and were maintained on trimethoprim/sulfamethoxazole antibiotic water until sacrificed for analysis 8 wk later. For colony forming unit assays, mice received 10^5 bone marrow cells and were sacrificed 8 or 12 d later. Spleens were fixed overnight in Bouin's solution (Sigma-Aldrich), and colonies were counted the next day. For unconditioned chimeras, unconditioned recipients received a single retroorbital injection of 2 × 10^6 bone marrow cells.

Retroviral transduction. The open reading frame of *Zbtb1* was cloned into the BglII–EcoRI site of pMIG (MSCV2.2-IRES-GFP; Addgene #9044, deposited by W. Hahn [Dana-Farber Cancer Institute, Boston, MA]) to generate the pMIG-*Zbtb1* vector. Vectors were transfected into the Plat-E packaging cell line using Fugene 6 (Roche), and retrovirus-containing supernatant was collected 24 and 48 h later. Bone marrow donor mice were primed 5 d before harvest with 150 mg/kg 5-fluorouracil (Sigma-Aldrich), and bone marrow cells were prestimulated overnight with 10 ng/ml of mouse recombinant IL-3, 10 ng/ml IL-6, 50 ng/ml SCF, 50 ng/ml TPO, and 5 ng/ml FLT3L (all from PeproTech). The next day, 3 ml/well of retroviral supernatant was centrifuged (2,000 rpm for 2 h at 32°C) onto RetroNectin-coated 6-well plates (20 µg/ml; Takara Bio Inc.), and cells were

Downloaded from jem.rupress.org on January 19, 2012

Published December 26, 2011

cultured on coated plates in the presence of 4 μg/ml Polybrene (Sigma-Aldrich) for 48 h. Recipient CD45.1$^+$ mice were γ-irradiated with a split dose of 11 Gy (^{137}Cs source) and the next day injected with ∼2 × 10^6 transduced bone marrow cells via the retroorbital plexus.

Histology. Thymi were fixed in 10% neutral buffered formalin and embedded in paraffin wax, and 5-μm sections were stained with hematoxylin and eosin (H&E).

PolyPhen-2. The deleterious effect of the *scanT* mutation was predicted using the HumVar-trained PolyPhen-2 server (version 2.1.0; Adzhubei et al., 2010).

Online supplemental material. Fig. S1 compares the sequence of ZBTB1 with other BTB-ZF proteins. Fig. S2 shows the tissue-specific expression of *Zbtb1* transcripts. Fig. S3 shows flow cytometric analysis of lymphocyte populations in *Zbtb1*;*Bcl2l11* double mutant mice. Table S1 is a list of protein-encoding genes in the *scanT* critical region. The whole genome mapping panel for C57BL/6J versus C3H/HeN is also included in the supplemental material. Online supplemental material is available at http://www.jem.org/cgi/content/full/jem.20112084/DC1.

We thank M. Gutierrez for animal care; C. Domingo, L. Hanley, and E. Pirie for ENU pedigree generation; S. Kalina and T. Robinson for genotyping; C. Ross and P. Lin for sequencing; C. Arnold for assistance with immunizations; and D. Yu (Monash University, Clayton, Victoria, Australia) for advice on retroviral transduction.

This work was supported by the Bill & Melinda Gates Foundation, the National Institute of Allergy and Infectious Diseases of the National Institutes of Health (grant HHSN272200700038C to B. Beutler), and The General Sir John Monash Foundation (O.M. Siggs).

The authors have no conflicting financial interests.

Author contributions: O.M. Siggs designed research, performed all experiments, analyzed data, and wrote the manuscript. X. Li propagated the *scanT* strain by intracytoplasmic sperm injection, Y. Xia provided bioinformatics support, and B. Beutler managed the mutagenesis operation and corrected the manuscript.

Submitted: 29 September 2011
Accepted: 5 December 2011

REFERENCES

Adzhubei, I.A., S. Schmidt, L. Peshkin, V.E. Ramensky, A. Gerasimova, P. Bork, A.S. Kondrashov, and S.R. Sunyaev. 2010. A method and server for predicting damaging missense mutations. *Nat. Methods*. 7:248–249. http://dx.doi.org/10.1038/nmeth0410-248

Bouillet, P., D. Metcalf, D.C.S. Huang, D.M. Tarlinton, T.W. Kay, F. Köntgen, J.M. Adams, and A. Strasser. 1999. Proapoptotic Bcl-2 relative Bim required for certain apoptotic responses, leukocyte homeostasis, and to preclude autoimmunity. *Science*. 286:1735–1738. http://dx.doi.org/10.1126/science.286.5445.1735

Busslinger, M. 2004. Transcriptional control of early B cell development. *Annu. Rev. Immunol*. 22:55–79. http://dx.doi.org/10.1146/annurev.immunol.22.012703.104807

Cobaleda, C., W. Jochum, and M. Busslinger. 2007. Conversion of mature B cells into T cells by dedifferentiation to uncommitted progenitors. *Nature*. 449:473–477. http://dx.doi.org/10.1038/nature06159

Fischer, A. 2007. Human primary immunodeficiency diseases. *Immunity*. 27:835–845. http://dx.doi.org/10.1016/j.immuni.2007.11.012

Georgel, P., X. Du, K. Hoebe, and B. Beutler. 2008. ENU mutagenesis in mice. *Methods Mol. Biol*. 415:1–16. http://dx.doi.org/10.1007/978-1-59745-570-1_1

Georgopoulos, K., M. Bigby, J.H. Wang, A. Molnar, P. Wu, S. Winandy, and A. Sharpe. 1994. The Ikaros gene is required for the development of all lymphoid lineages. *Cell*. 79:143–156. http://dx.doi.org/10.1016/0092-8674(94)90407-3

He, X., X. He, V.P. Dave, Y. Zhang, X. Hua, E. Nicolas, W. Xu, B.A. Roe, and D.J. Kappes. 2005. The zinc finger transcription factor Th-POK regulates CD4 versus CD8 T-cell lineage commitment. *Nature*. 433:826–833. http://dx.doi.org/10.1038/nature03338

Hirschhorn, R., D.R. Yang, J.M. Puck, M.L. Huie, C.K. Jiang, and L.E. Kurlandsky. 1996. Spontaneous in vivo reversion to normal of an inherited mutation in a patient with adenosine deaminase deficiency. *Nat. Genet*. 13:290–295. http://dx.doi.org/10.1038/ng0796-290

Johnston, R.J., A.C. Poholek, D. DiToro, I. Yusuf, D. Eto, B. Barnett, A.L. Dent, J. Craft, and S. Crotty. 2009. Bcl6 and Blimp-1 are reciprocal and antagonistic regulators of T follicular helper cell differentiation. *Science*. 325:1006–1010. http://dx.doi.org/10.1126/science.1175870

Kondo, M., I.L. Weissman, and K. Akashi. 1997. Identification of clonogenic common lymphoid progenitors in mouse bone marrow. *Cell*. 91:661–672. http://dx.doi.org/10.1016/S0092-8674(00)80453-5

Kosan, C., I. Saba, M. Godmann, S. Herold, B. Herkert, M. Eilers, and T. Möröy. 2010. Transcription factor miz-1 is required to regulate interleukin-7 receptor signaling at early commitment stages of B cell differentiation. *Immunity*. 33:917–928. http://dx.doi.org/10.1016/j.immuni.2010.11.028

Kovalovsky, D., O.U. Uche, S. Eladad, R.M. Hobbs, W. Yi, E. Alonzo, K. Chua, M. Eidson, H.-J. Kim, J.S. Im, et al. 2008. The BTB-zinc finger transcriptional regulator PLZF controls the development of invariant natural killer T cell effector functions. *Nat. Immunol*. 9:1055–1064. http://dx.doi.org/10.1038/ni.1641

Kravchenko, J.E., I.B. Rogozin, E.V. Koonin, and P.M. Chumakov. 2005. Transcription of mammalian messenger RNAs by a nuclear RNA polymerase of mitochondrial origin. *Nature*. 436:735–739. http://dx.doi.org/10.1038/nature03848

Maeda, T., T. Merghoub, R.M. Hobbs, L. Dong, M. Maeda, J. Zakrzewski, M.R.M. van den Brink, A. Zelent, H. Shigematsu, K. Akashi, et al. 2007. Regulation of B versus T lymphoid lineage fate decision by the proto-oncogene LRF. *Science*. 316:860–866. http://dx.doi.org/10.1126/science.1140881

Maeda, T., K. Ito, T. Merghoub, L. Poliseno, R.M. Hobbs, G. Wang, L. Dong, M. Maeda, L.C. Dore, A. Zelent, et al. 2009. LRF is an essential downstream target of GATA1 in erythroid development and regulates BIM-dependent apoptosis. *Dev. Cell*. 17:527–540. http://dx.doi.org/10.1016/j.devcel.2009.09.005

Matic, I., J. Schimmel, I.A. Hendriks, M.A. van Santen, F. van de Rijke, H. van Dam, F. Gnad, M. Mann, and A.C.O. Vertegaal. 2010. Site-specific identification of SUMO-2 targets in cells reveals an inverted SUMOylation motif and a hydrophobic cluster SUMOylation motif. *Mol. Cell*. 39:641–652. http://dx.doi.org/10.1016/j.molcel.2010.07.026

Mullighan, C.G., S. Goorha, I. Radtke, C.B. Miller, E. Coustan-Smith, J.D. Dalton, K. Girtman, S. Mathew, J. Ma, S.B. Pounds, et al. 2007. Genome-wide analysis of genetic alterations in acute lymphoblastic leukaemia. *Nature*. 446:758–764. http://dx.doi.org/10.1038/nature05690

Mullighan, C.G., C.B. Miller, I. Radtke, L.A. Phillips, J. Dalton, J. Ma, D. White, T.P. Hughes, M.M. Le Beau, C.-H. Pui, et al. 2008. BCR-ABL1 lymphoblastic leukaemia is characterized by the deletion of Ikaros. *Nature*. 453:110–114. http://dx.doi.org/10.1038/nature06866

Na Nakorn, T., D. Traver, I.L. Weissman, and K. Akashi. 2002. Myeloerythroid-restricted progenitors are sufficient to confer radioprotection and provide the majority of day 8 CFU-S. *J. Clin. Invest*. 109:1579–1585.

Nurieva, R.I., Y. Chung, G.J. Martinez, X.O. Yang, S. Tanaka, T.D. Matskevitch, Y.-H. Wang, and C. Dong. 2009. Bcl6 mediates the development of T follicular helper cells. *Science*. 325:1001–1005. http://dx.doi.org/10.1126/science.1176676

Nutt, S.L., B. Heavey, A.G. Rolink, and M. Busslinger. 1999. Commitment to the B-lymphoid lineage depends on the transcription factor Pax5. *Nature*. 401:556–562. http://dx.doi.org/10.1038/44076

Radtke, F., A. Wilson, G. Stark, M. Bauer, J. van Meerwijk, H.R. MacDonald, and M. Aguet. 1999. Deficient T cell fate specification in mice with an induced inactivation of Notch1. *Immunity*. 10:547–558. http://dx.doi.org/10.1016/S1074-7613(00)80054-0

Rothenberg, E.V., and T. Taghon. 2005. Molecular genetics of T cell development. *Annu. Rev. Immunol*. 23:601–649. http://dx.doi.org/10.1146/annurev.immunol.23.021704.115737

Downloaded from jem.rupress.org on January 19, 2012

Published December 26, 2011

Savage, A.K., M.G. Constantinides, J. Han, D. Picard, E. Martin, B. Li, O. Lantz, and A. Bendelac. 2008. The transcription factor PLZF directs the effector program of the NKT cell lineage. *Immunity*. 29:391–403. http://dx.doi.org/10.1016/j.immuni.2008.07.011

Siggs, O.M., C.N. Arnold, C. Huber, E. Pirie, Y. Xia, P. Lin, D. Nemazee, and B. Beutler. 2011. The P4-type ATPase ATP11C is essential for B lymphopoiesis in adult bone marrow. *Nat. Immunol.* 12:434–440. http://dx.doi.org/10.1038/ni.2012

Stogios, P.J., G.S. Downs, J.J.S. Jauhal, S.K. Nandra, and G.G. Privé. 2005. Sequence and structural analysis of BTB domain proteins. *Genome Biol.* 6:R82. http://dx.doi.org/10.1186/gb-2005-6-10-r82

Swiatek, P.J., C.E. Lindsell, F.F. del Amo, G. Weinmaster, and T. Gridley. 1994. Notch1 is essential for postimplantation development in mice. *Genes Dev.* 8:707–719. http://dx.doi.org/10.1101/gad.8.6.707

Weng, A.P., A.A. Ferrando, W. Lee, J.P. Morris IV, L.B. Silverman, C. Sanchez-Irizarry, S.C. Blacklow, A.T. Look, and J.C. Aster. 2004. Activating mutations of NOTCH1 in human T cell acute lymphoblastic leukemia. *Science*. 306:269–271. http://dx.doi.org/10.1126/science.1102160

Ye, B.H., F. Lista, F. Lo Coco, D.M. Knowles, K. Offit, R.S. Chaganti, and R. Dalla-Favera. 1993. Alterations of a zinc finger-encoding gene, BCL-6, in diffuse large-cell lymphoma. *Science*. 262:747–750. http://dx.doi.org/10.1126/science.8235596

Yu, D., S. Rao, L.M. Tsai, S.K. Lee, Y. He, E.L. Sutcliffe, M. Srivastava, M. Linterman, L. Zheng, N. Simpson, et al. 2009. The transcriptional repressor Bcl-6 directs T follicular helper cell lineage commitment. *Immunity*. 31:457–468. http://dx.doi.org/10.1016/j.immuni.2009.07.002

Downloaded from jem.rupress.org on January 19, 2012

Published December 26, 2011

JEM

SUPPLEMENTAL MATERIAL

Siggs et al., http://www.jem.org/cgi/content/full/jem.20112084/DC1

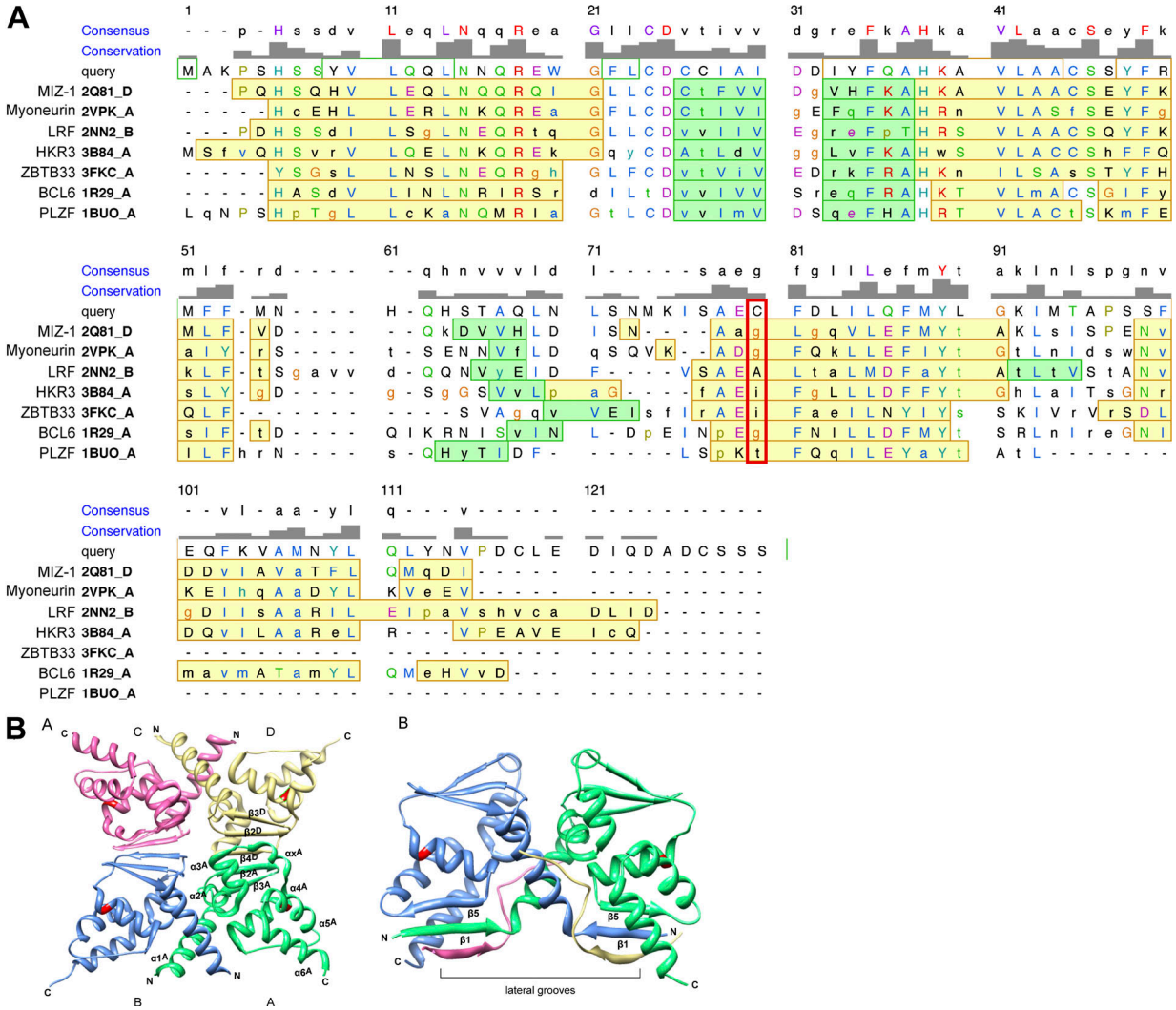


Figure S1. BTB domain alignment with structural features. (A) Sequence comparison of the ZBTB1 BTB domain alongside selected BTB-ZF proteins with publicly available Protein Data Bank crystal structures, generated by the BLAST feature of University of California, San Francisco Chimera. Yellow shading represents α-helices, and β-sheets are depicted in green. Conserved residues are capitalized. The amino acid affected by the *scanT* mutation is boxed in red. (B) Crystal structure representations of a MIZ-1 tetramer (left) and BCL6 dimer (blue and green) bound to a 17-aa region of the SMRT corepressor (pink and yellow; right). The amino acid corresponding to cysteine 74 of ZBTB1 (mutated in *scanT*) is indicated in red.

The Journal of Experimental Medicine

Downloaded from jem.rupress.org on January 19, 2012

Published December 26, 2011

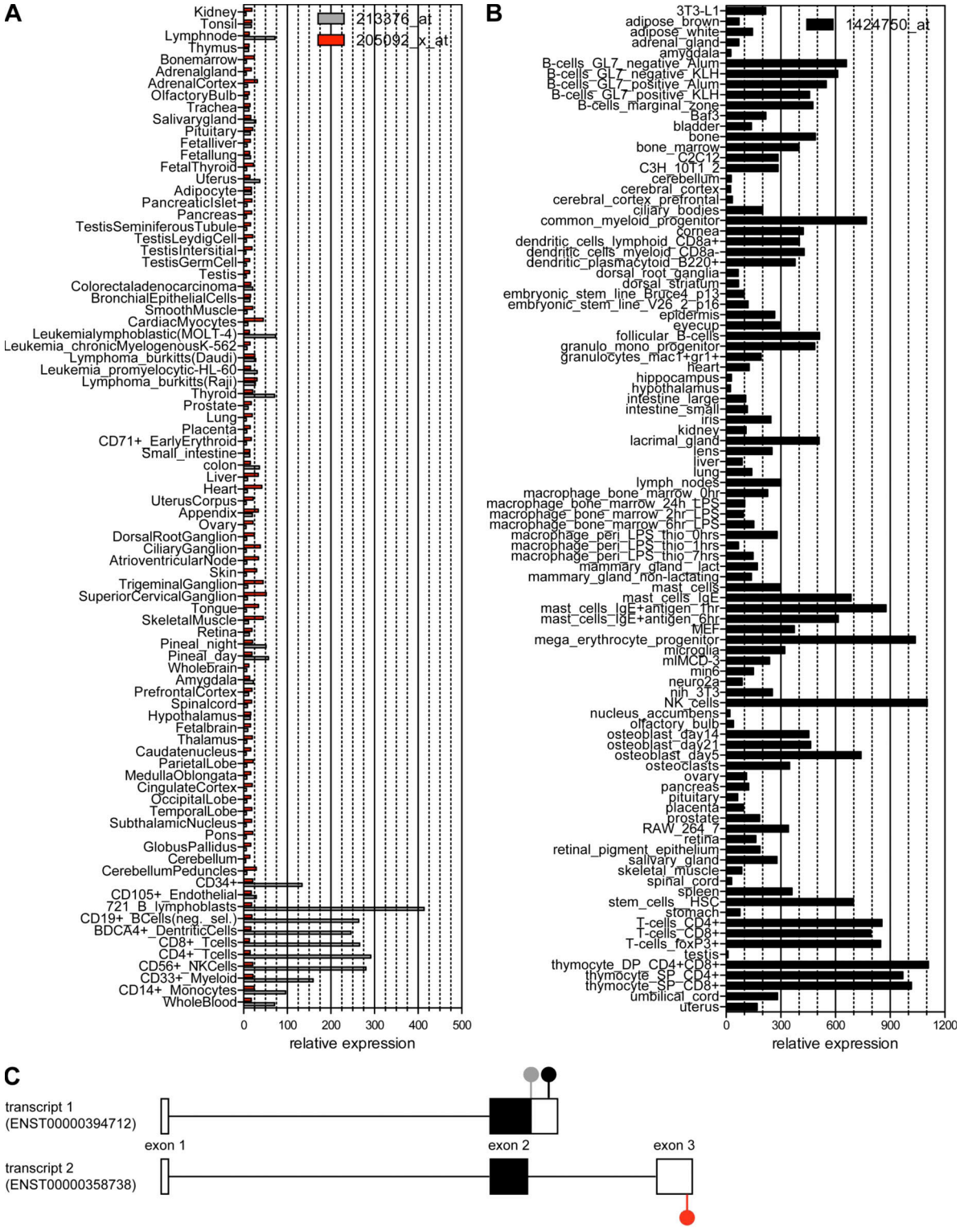


Figure S2. Enrichment of *Zbtb1* expression in leukocyte lineages of mouse and man. (A) Expression of *ZBTB1* transcripts in human cells and tissues (Human U133A/GNF1H Gene Atlas, GEO DataSets accession no. GSE1133; Su et al., 2004). (B) Expression of mouse *Zbtb1* (Mouse MOE430 Gene Atlas, GEO DataSets accession no. GSE10246; Lattin et al., 2008). (C) Relative locations of mouse and human Affymetrix probe sets (color-coded with A and B) in ZBTB1-encoding transcripts. Ensembl accession numbers correspond to human transcripts.

Downloaded from jem.rupress.org on January 19, 2012

Published December 26, 2011

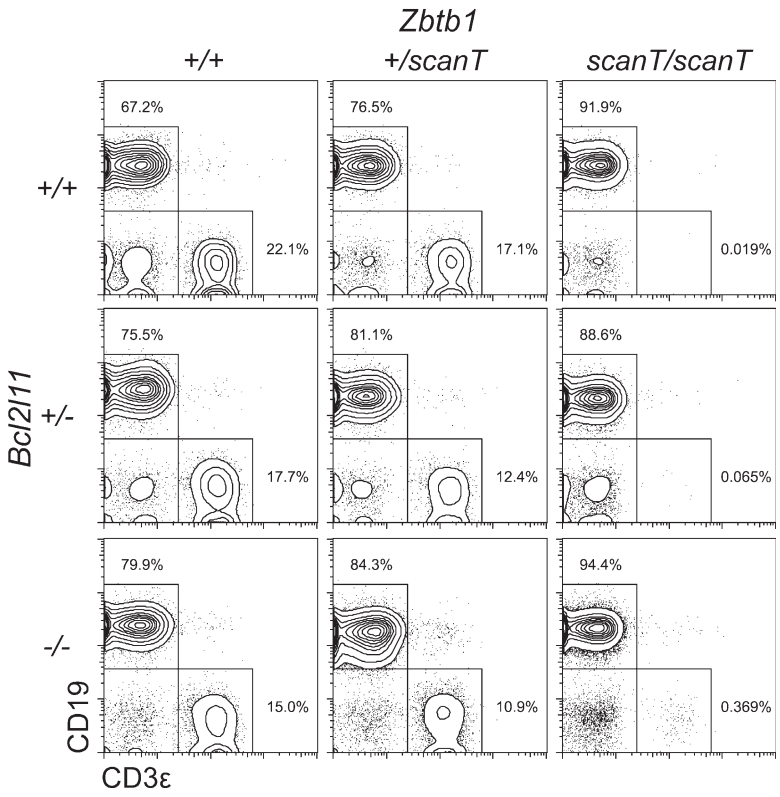


Figure S3. T cell deficiency is independent of BIM. *Zbtb1*$^{+/scanT}$ *Bcl2l11*$^{+/-}$ double heterozygotes were intercrossed, and frequencies of CD19^{+} and CD3ε^{+} blood lymphocytes were examined in the progeny. Data are from a single experiment, with plots representative of one to seven mice per genotype.

Downloaded from jem.rupress.org on January 19, 2012

Published December 26, 2011

Table S1. List of genes within the *scanT* critical region

Ensembl gene ID	Gene start	Gene end	Strand	Associated gene name
	bp	*bp*		
ENSMUSG00000044912	75,098,744	75,368,903	1	*Syt16*
ENSMUSG00000071265	75,389,722	75,396,932	1	*1700086L19Rik*
ENSMUSG00000029878	75,398,461	75,401,455	1	*Dbpht2*
ENSMUSG00000079062	75,403,467	75,404,326	−1	*AC158365.1*
ENSMUSG00000079061	75,416,097	75,417,381	−1	*AC158365.2*
ENSMUSG00000034402	75,998,207	76,278,319	−1	*Kcnh5*
ENSMUSG00000046768	76,409,309	76,502,443	1	*Rhoj*
ENSMUSG00000048982	76,512,707	76,517,768	−1	*Gphb5*
ENSMUSG00000021051	76,551,870	76,697,187	−1	***Ppp2r5e***
ENSMUSG00000045690	76,731,583	76,770,494	−1	*Wdr89*
ENSMUSG00000021054	76,815,256	76,836,662	−1	*Sgpp1*
ENSMUSG00000063450	76,919,121	77,211,913	1	*Syne2*
ENSMUSG00000021055	77,221,406	77,278,246	−1	*Esr2*
ENSMUSG00000021056	77,299,679	77,347,721	−1	*Tex21*
ENSMUSG00000021048	77,356,395	77,420,789	1	*Mthfd1*
ENSMUSG00000021057	77,425,878	77,431,041	1	*Akap5*
ENSMUSG00000056459	77,449,932	77,469,986	−1	***Zbtb25***
ENSMUSG00000033454	77,471,253	77,496,263	1	***Zbtb1***
ENSMUSG00000059970	77,505,163	77,507,921	1	*Hspa2*
ENSMUSG00000052221	77,518,608	77,540,460	1	*AC124453.1*
ENSMUSG00000073000	77,545,547	77,552,323	1	*AC124453.3*
ENSMUSG00000052609	77,634,569	77,680,027	1	*Plekhg3*
ENSMUSG00000021061	77,681,475	77,811,534	−1	*Spnb1*
ENSMUSG00000033373	77,866,525	78,022,399	1	*Fntb*
ENSMUSG00000042808	77,893,324	77,896,493	−1	*Gpx2*
ENSMUSG00000021062	77,898,947	77,923,895	−1	*Rab15*
ENSMUSG00000059436	78,038,261	78,063,188	−1	*Max*
ENSMUSG00000021065	78,340,052	78,577,325	1	*Fut8*
ENSMUSG00000047454	79,327,721	79,785,725	1	*Gphn*
ENSMUSG00000056987	79,792,522	79,835,500	1	*Fam71d*
ENSMUSG00000021112	79,849,979	79,941,573	1	*Mpp5*
ENSMUSG00000021114	79,943,976	79,962,513	−1	*Atp6v1d*
ENSMUSG00000021116	79,962,806	79,987,997	1	*Eif2s1*
ENSMUSG00000021118	79,989,678	80,007,951	−1	*Plek2*
ENSMUSG00000046157	80,062,784	80,108,324	−1	*Tmem229b*

Downloaded from jem.rupress.org on January 19, 2012

REFERENCES

Lattin, J.E., K. Schroder, A.I. Su, J.R. Walker, J. Zhang, T. Wiltshire, K. Saijo, C.K. Glass, D.A. Hume, S. Kellie, and M.J. Sweet. 2008. Expression analysis of G Protein-Coupled Receptors in mouse macrophages. *Immunome Res.* 4:5. http://dx.doi.org/10.1186/1745-7580-4-5

Su, A.I., T. Wiltshire, S. Batalov, H. Lapp, K.A. Ching, D. Block, J. Zhang, R. Soden, M. Hayakawa, G. Kreiman, et al. 2004. A gene atlas of the mouse and human protein-encoding transcriptomes. *Proc. Natl. Acad. Sci. USA.* 101:6062–6067. http://dx.doi.org/10.1073/pnas.0400782101

The whole genome mapping panel for C57BL/6J versus C3H/HeN appears on the following three pages.

Published December 26, 2011

Panel	Chr	ChrLength(Mb)	Marker	ChrLoc(Mb)	Predicted Length	B6 Length	C3H Length	Forward Primer	Reverse Primer	Vendor	Color	Row	Column
A1	1	197	d1mit242	4.19	84	83.82	147	TGTCAATCAGTAAGGCACAAGG	CATGTGATTTGTTTATTCAATCACC	Sigma	6fam	E	1
A1	1		D1Mit169.1	24.07	220	218	221	CIDR	CIDR	ABI-Cidr	ned	D	1
A1	1		d1mit243	35.13	145	146	132.72	CCAGGGCAATTGGATACAAT	GTTGTGCCAAAATGGAGGAC	ABI	ned	A	2
A1	1		d1mit161	59.28	112	112.97	115.08	ACCAGCCCTCCTTTTTTGTT	CTTGCCTCTTCAGGCACCT	Sigma	6fam	C	1
A1	1		D1Mit380.1	72.98	117	115.71	148.52	CIDR	CIDR	ABI-Cidr	vic	B	2
A1	1		d1mit10	92.58	139	135.1	141.45	AAACCATGCAGGTACTGATATGG	GAAGAAATTAACTGAGAGCAAGGC	Sigma	6fam	A	1
E1	1		d1mit136	103.89	103	105	111	TAGCCCTACACACTGTAGAAATGC	TGAACACAAAGTAGTAAATGCGTG	ABI	ned	H	9
A1	1		D1Mit495.1	129.52	144	145.56	139.48	CIDR	CIDR	ABI-Cidr	ned	H	1
A1	1		D1Mit159.1	161.59	206	206.6	187.54	CIDR	CIDR	ABI-Cidr	vic	B	1
C1	1		d1mit115	179.61	147	151.24	146.99	AAGGGAATGGAATTAGGGTCA	TAACGGACACCCATTTTAAACA	ABI	ned	E	5
A1	1		D1Mit292.1	193.23	212	210.33	208.26	CIDR	CIDR	ABI-Cidr	6fam	G	1
C1	2	182	d2mit1	3.8	123	130.73	126.49	CTTTTTCGTATGTGGTGGGG	AACATTGGGCCTCTATGCAC	ABI	ned	F	5
A1	2		d2mit365	27.66	100	108.2	112.37	GAGATCCCACTGATGATACAAGC	AGATGTGCCCAAGGGTCC	ABI	vic	F	2
B1	2		d2mit237	40.85	123	126.6	112.04	TTCCAAGTCACCTATTATCAAAAGG	TTGATACGGACACCAGCAAA	ABI	ned	H	4
A1	2		d2mit242	57.2	136	138	142	TTCCACACTCATGCCTATATGC	AAATGAACCTCTCAGGATCATATACC	ABI	6fam	E	2
A1	2		d2mit75	80.42	113	114.46	108.75	TCAGCATGTGGATGAATACACA	AACTTTTTAAAAACTACGAGCGTG	ABI	6fam	G	2
B1	2		d2mit100	106.38	112	114	129	GTGTTCCTAAGGTTGTATTTTGGC	GAAATTTGACAATTGCTAGGTGC	ABI	6fam	C	3
C1	2		d2mit277	123.26	277	279	126.24?	ATTCTGCATTCAAGCAAATTCA	CTTGAAAGTAGTTGGTTGGTTGG	ABI	vic	G	5
C1	2		D2Mit285.1	152.68	151	151.57	162.13	CIDR	CIDR	ABI-Cidr	ned	A	5
B1	2		D2Mit148.1	178.54	116	115.15	118.7	CIDR	CIDR	ABI-Cidr	6fam	G	4
D1	3	160	d3mit221	7.89	146	146.39	158.59	ATATAAGGACATAAACAGGCATTTCT	AAAATGTAGATCCCTTCATACATGC	Sigma	6fam	C	7
B1	3		D3Mit203.1	26.84	263	261	247	CIDR	CIDR	ABI-Cidr	6fam	D	3
G1	3		d3mit182	50.39	151	162	166?	TTATCTTGTTGGGGAGGTGG	AGAGAACTGATTCCTTTAAGTTGTCC	ABI	vic	F	14
C1	3		d3mit154	68.61	145	145.99	141.24	TGGAGGTTTGGAAGTGGC	AGAGTGTTTCTAGATGCCTGCC	Sigma	6fam	B	5
A1	3		D3Mit98.1	85.99	95	92.59	106.26	CIDR	CIDR	ABI-Cidr	ned	C	2
B1	3		d3mit57	115.53	157	163	161	TCCAGTTACTTGGTGAACTCCA	ATATGTGTACATGTTCATGGTGTG	ABI	vic	A	3
A1	3		d3mit116	154.2	259	268.09	282	TCACTGCCCATCTTTGTAACC	CCCAGAGACCCGGAATAGAA	ABI	vic	H	2
F1	4	156	d4mit235	8.26	116	118	101	AGGCCAAAGGTTGGATTTCT	GAGACTTGAAATTGAAGCATTTAGG	ABI	ned	G	11
D1	4		d4mit268	20.54	148	150.88	152.96	TAATCTGATCCAAACACTAAATCAGA	GCAGCCTTATGGAAACTTTCA	ABI	6fam	E	8
B1	4		d4mit236	39.06	202	201	183.97	TCTTAGCATGCTTACCGCCT	GGCCCGTAGGATGACTGTC	Sigma	6fam	F	3
B1	4		d4mit178	66.84	147	156.22	174.4	GCCCTGAAGGTAAATCAGTAACT	GCTCAGGAGGTACATTGCCT	ABI	ned	E	3
H1	4		d4mit301	88.75	104	103.55	111.81	CATTCTAAAATATGCTCCAAGTGTG	CGAGAATGTGGTTATTAAACTATTCC	Sigma	6fam	B	15
C1	4		d4mit176	101.16	138	140.7	147.32	AGATAATCCTCCAGACAGACATCC	GTAAGGATATACCTATGAAGGGTTCG	ABI	vic	C	6
E1	4		D4Mit203.1	129.25	98	96.28	105.86	CIDR	CIDR	ABI-Cidr	6fam	A	10
E1	4		d4mit253	152.38	147	144.58	140.23	ATGATTCCCTCTTCTGGCCT	AATGACTACAACAGGACATTCATTT	Sigma	6fam	B	10
B1	5	153	d5mit193	4.23	136	138.15	148.99	TGTCTTTAAAGTGGCCCAGG	TGTTTTCTATGTGTTTTATATGCTTCA	ABI	vic	B	4
B1	5		d5mit348	24.43	123	125.67	131.53?	CTGACCAGAACACAGCATAGTACA	TTTAAAATAGGAAAAGCATTCTTTCC	ABI	ned	C	4
B1	5		d5mit352	35.96	110	117	125	CCCAGAGCCCACATCAAG	TAGGTGGGTGTGTCTCTCCC	ABI	ned	D	4
D1	5		d5mit81	50.72	210	206.89	193.04	GGGAGTTCCAGGTTCATTGA	ATGTGCATTATGGCATGTAAATG	ABI	6fam	A	8
E1	5		D5Mit309.1	79.93	141	137.98	146.57	CIDR	CIDR	ABI-Cidr	6fam	E	10
C1	5		d5mit239	107.84	146	155.41	134.87	ATTGCAGACATAAAGGATATTTTGG	GCCAGCCTGGCTTACATAAG	ABI	vic	A	6
D1	5		d5mit425	120.33	124	126	129	TCGCCTTTCTTTCCCTCC	AAAATTACATTTGCATCTGGGG	ABI	6fam	F	8
B1	5		d5mit98	138.66	156	164	171	TCCTTCATTTTATCTTCTGCCC	TGAATTCACTCTCGCACCTG	ABI	ned	A	4
C1	6	150	d6mit166	5.32	100	100.24	110.49	CATTTTATTTTATTGATGGATGTGTG	GTTGTCTTATGGCTGCCATG	Sigma	6fam	D	6
E1	6		d6mit307	29.07	99	98.66	91.88	TTTTAATCTTTTGCCTCTTTCTCG	TGGGCTCAGGCACTTCTTAT	Sigma	6fam	F	10
D1	6		D6Mit274.1	48.68	111	108.85	89.57	CIDR	CIDR	ABI-Cidr	6fam	G	8
H1	6		d6mit209	75.49	134	142.79	147.21	CTCCCCCTCTGTGTGATTGT	TTATTACACCAGACCCATGTGG	ABI	ned	F	16
H1	6		D6Mit284.1	92.56	206	206.45	195.12	CIDR	CIDR	ABI-Cidr	ned	G	16
H1	6		d6mit328	112.73	125	122.55	129	ACCTGGGTAAACAGGGAAGC	ACATCTTTGTCTGGATTTTGGG	ABI	6fam	H	16
C1	6		d6mit59	138.93	169	165.55	175.02	GCCATCCTTTGTAATAACAAACA	CGTCTGGGAAAACCTCAAAA	Sigma	6fam	B	6
F1	7	153	d7mit152	4.65	129	122.3	118.48	GCCTAGCACACGCCAAAG	CCTTGTGCATGGTTGCTATG	Sigma	6fam	H	11
D1	7		d7mit76	19.58	224	224	255	CATGAGCACGTGGAGAAAGA	CGTGGAAACCTGATAAACTGA	Sigma	6fam	B	8
F1	7		d7mit27	51.22	246	252	260	TGAACTGGGGAGGAAAGTTG	AACATGAAAAGACATTCCCCC	ABI	6fam	E	11
F1	7		d7mit317	79.64	102	96.88	90	ATGTCTCCTTGACATTGGGC	TCTTGTAATCTCACATCTAAGTGTGTG	Sigma	6fam	E	12

Downloaded from jem.rupress.org on January 19, 2012

Published December 26, 2011

F1	7		D7Mit350.1	90.73	223	220	226	CIDR	CIDR	ABI-Cidr	ned	A	12
C1	7		D7Mit98.1	122.06	186	186.13	180.17	CIDR	CIDR	ABI-Cidr	6fam	E	6
E1	7		d7mit71	138.17	117	118.3	114.21	CCACCTGGAATACATGTAACCC	TAAGATCCAAGAGATGGGTTAAGC	Sigma	6fam	G	10
H1	8	132	d8mit124	14.72	129	124.33	130.14	CAACTGTGTATCATAAACTGGGAA	GAAGAATCACTCAGCAGTGTATGG	Sigma	6fam	A	16
E1	8		d8mit3	25.72	172	174.27	180.41	TCCCATTCTCGCATAAGTCC	GATGGGAAGACAGGGTAGCA	Sigma	6fam	C	10
H1	8		d8mit339	41.39	123	125	107	ACCTATGGTACACACACATCGC	CAAACATTTTTAGGCATTTAGATCC	ABI	ned	D	16
H1	8		d8mit25	67.12	117	124	134	TCAGACTAATGTCCAGTAGCAAGC	ATTGCATGTCCATGTCTGGA	ABI	ned	B	16
B1	8		D8Mit45.1	89.83	95	96.2	102.58	CIDR	CIDR	ABI-Cidr	vic	E	4
F1	8		d8mit183	103.57	149	158	165	TCTCAAATAACTATCAACTCTTAGGGG	TCTTTGAACTGGCTATAATCACTCA	ABI	ned	F	12
G1	8		D8Mit88.1	117.36	131	129.57	142.95	CIDR	CIDR	ABI-Cidr	6fam	D	14
H1	9	124	d9_14.1	14.13	288	288	284.6	GGCCATGAAAGTGAATGATGATAGGTG	GCTGTGAACATAAAGGCAAGCGTTC	Sigma	6fam	E	16
C1	9		D9Mit2.1	37.2	191	190.27	194.37	CIDR	CIDR	ABI-Cidr	ned	F	6
F1	9		d9mit4	51.93	122	126	136	TGCTGAGCAAGCTATGAGGA	GACAGCCCATCACAGCTACA	ABI	vic	G	12
F1	9		D9Mit336.1	65.43	175	175.43	158.76	CIDR	CIDR	ABI-Cidr	ned	C	12
F1	9		d9mit196	85.79	143	152	162	GCCTTCTGTTCAGAACTTTCTG	TCTGTATTTAAGCATGCATGTGC	ABI	6fam	B	12
F1	9		D9Mit355.1	98.72	117	116.38	126.94	CIDR	CIDR	ABI-Cidr	ned	D	12
E1	9		d9mit151	121.39	114	123	119	TGGTCAAGGTGTGGTATCGA	AAAACTCAGCATCCAATGGG	ABI	vic	D	10
C1	10	130	d10mit298	8.51	150	151.84	162.51	TCCTGTTCACTGACTGTCTTCC	AAACAACCAGGCTCCCAAG	Sigma	6fam	C	5
F1	10		D10Mit213.1	20.13	260	258.01	244.95	CIDR	CIDR	ABI-Cidr	ned	C	11
G1	10		d10mit194	46.56	81	79.76	90.89	GATTGTTTGTAAAGACATGATCACG	AGATGTGGAATAGGAAGTATGATCG	Sigma	6fam	H	13
F1	10		D10Mit31.1	67.72	138	135	139	CIDR	CIDR	ABI-Cidr	ned	F	11
F1	10		d10mit230	89.66	115	119.25	116	AGATAGCCTAGGGGGTGCAT	ATCAGTTTCCAATCGCTGCT	ABI	6fam	B	11
D1	10		D10Mit233.1	113.82	136	132.95	111.91	CIDR	CIDR	ABI-Cidr	ned	H	8
D1	10		d10mit271	123.78	117	119	106	ACAACCAAAGGTCTTTGTAGAAGA	AATATATAGGCACACCTTAATAGCCA	ABI	vic	D	7
C1	11	122	D11Mit2.1	12.22	104	102.03	117.1?	CIDR	CIDR	ABI-Cidr	6fam	H	5
B1	11		d11mit205	33.09	104	108	111	GGCAGAGTCTAGTCTGATATCTTGG	CAGTGCACAGCCAGGTTG	ABI	vic	G	3
E1	11		d11mit235	44.19	180	185	200	GAGAGGGCAGTAGCAGCAAC	ATTTATGAGAAGGTCTGAAGGGC	ABI	ned	A	9
B1	11		D11Mit4.1	68.42	176	176.35	170.26	CIDR	CIDR	ABI-Cidr	vic	H	3
C1	11		d11mit284	88.99	86	87.99	101.97	GCTCGACCTAGGGGAAGAAG	AGAATGCTGTGCAACTGGTG	ABI	ned	G	6
D1	11		D11Mit333.1	108.58	99	99.56	79.87	CIDR	CIDR	ABI-Cidr	ned	E	7
C1	12	121	d12mit269	16.76	118	120	126	TCCCACAATCTATTCTTGGACC	ATACGTTTCCCAGAGGACATG	ABI	vic	H	6
D1	12		D12Mit60.1	35.47	121	118.48	112.75	CIDR	CIDR	ABI-Cidr	ned	F	7
G1	12		d12mit54	54.96	150	151.49	144.39	TGGTGAAATTCACTCCTTTGG	CCCTGTGCTGGTAGGTGTG	Sigma	6fam	H	14
H1	12		d12mit158	83.72	150	159	141	CATTGGGCAATGGAATTTG	ATGAGAGAAAACCAGAAACAAAGG	ABI	6fam	C	15
C1	12		d12mit133	111.54	113	121	115	TGAGCAAAAGTTATTGGGTGG	GGAGATATTGCTTATGTCTCCCC	ABI	vic	D	5
H1	13	120	d13mit57	17.09	140	135.74	144.16	GATATACTTGTTTGCACACTTGGG	AGAGAGTATGTGCCACCATGG	Sigma	6fam	E	15
D1	13		d13mit245	45.16	137	139	147.52	TGATGAGTCCCAGACCAACA	ATTCCAGTGGTTAGGCATGG	ABI	ned	G	7
B1	13		d13mit281	68.86	99	101	97	TGTCTAAGTGCACGTGGAGC	ATGTGAATTGATTTTGTGGGC	ABI	vic	F	4
H1	13		d13mit314	86.07	113	115.14	119.22	AGACTGAGCAGGTTGTATTTAGGC	CTTATTTTTAAATTGGTTTTACACACA	Sigma	6fam	D	15
D1	13		D13Mit144.1	96.87	138	136.28	140.77	CIDR	CIDR	ABI-Cidr	vic	A	7
G1	13		D13Mit260.1	113.16	206	205.81	195.02	CIDR	CIDR	ABI-Cidr	6fam	A	13
E1	14	125	d14mit49	14.72	250	245	205.03	TTCACTGAATAAAAAGACTCCTCG	TCCTTTACTTGGTGTACGTCTGC	Sigma	6fam	E	9
D1	14		d14mit174	32.46	146	148.91	153.04	ACTGCAGAGTCCACACAAGTG	TCTGAGCCACTATGCCTGG	ABI	ned	B	7
E1	14		D14Mit5.1	60.34	194	193.28	180.83	CIDR	CIDR	ABI-Cidr	6fam	F	9
H1	14		d14mit92	91.51	89	95	116.37?	CTGCTGCAGAATTAATTGATTTT	GGATATATGGATTTATACAGACACACA	ABI	ned	F	15
G1	14		d14mit197	105.72	101	97.49	93.5	TCCCATAGCAAATCTCTAGGTAGG	CATTCTGCAATAGATTTCTTGGG	Sigma	6fam	E	13
D1	14		d14mit135	121.21	172	168.51	172.44	TTTATTTTATGTGTGATTGTGCACA	TGTGTGCGTGTCACACTGAT	Sigma	6fam	H	7
E1	15	103	d15mit176	12.33	150	159	157	GCTTTCTCCTGGATAACAGGC	CTCTCCTTTTGACTACCCTAGCC	ABI	ned	C	9
H1	15		d15mit201	29.44	99	98.94	92.35	TTTTGGAGTCTTTCAGTTTTCTCC	TTGAGTGGTATAATTTTGATTTACACA	Sigma	6fam	G	15
E1	15		D15Mit143.1	51.99	135	123?	131.85	CIDR	CIDR	ABI-Cidr	vic	B	9
B1	15		D15Mit67.1	70.03	182	180.89	179.05	CIDR	CIDR	ABI-Cidr	vic	B	3
G1	15		D15Mit242.1	90.22	100	97.71	99.74	CIDR	CIDR	ABI-Cidr	6fam	B	13
G1	16	98	d16mit181	6.32	109	110.56	120.83	CTGTGTGAACGTGTTAGTATGTATGC	CATGGTTGACAATTGGCTTG	Sigma	6fam	E	14
G1	16		d16mit101	23.74	150	147.59	143.22	TTATGAAATGTTTTATCTTTTGGGG	CTCCAGATGTAGAAATTAAAATCTTGG	Sigma	6fam	F	13

Downloaded from jem.rupress.org on January 19, 2012

Published December 26, 2011

G1	16		d16mit125	42.38	150	154	146	CAGAGATTACAAGCATACATCTTAGC	CAAACAACAAAACACATTCAACTC	ABI	ned	G	13
G1	16		D16Mit139.1	65.67	155	154.25	181.41	CIDR	CIDR	ABI-Cidr	6fam	C	13
D1	16		D16Mit153.1	87.58	153	151.56	155.66	CIDR	CIDR	ABI-Cidr	vic	D	8
E1	17	95	d17mit57	10.06	300	301.99	319.5	GCTGATAAACGTGGTGGCTT	GTTTAGTGGCTTCAAGTCACCC	Sigma	6fam	G	9
A1	17		phmx17.1	31.84	330	334.23	326.42	GATACAATGGGTCAGGTGGG	GTAGTCCTGGCTGGCTTCAG	ABI	vic	D	2
G1	17		d17mit181	57.39	124	130	124	TTTCCGAGGATTGGAAAAAA	GAGACCACACGCACTCACAC	ABI	6fam	D	13
G1	17		d17mit76	86.03	124	126	93	CTCCTCACCCAGATTCTTGTAA	TTTCGCAAGTTATTTTAACCCG	ABI	ned	A	14
G1	18	91	d18mit146	12.56	143	151	142	ATGTCCCTCTGCTCTTTAGTTACC	GGACCACAGAGTCATTCCGT	Sigma	6fam	B	14
G1	18		d18mit225	30.78	116	114.86	117.08	AGGACAAATAAATAAAAAGAGTGTGTG	CTTCCATATTGCTGTAACTTAAATGG	ABI	6fam	C	14
H1	18		d18mit238	57.18	122	124	128	TGTATCCTTTGTACTTAGAGACACAGC	ACATGCCTGACAAATTTATTTGG	ABI	vic	A	15
A1	18		D18Mit186.1	72.18	93	92.64	72.81	CIDR	CIDR	ABI-Cidr	6fam	F	1
H1	19	61	d19mit59	5.32	199	194.24	136.46	CTCTAACTATCCTCTGACCTTCACA	TTTTAAGCAGAACATTGAGGACC	Sigma	6fam	H	15
H1	19		d19mit96	21.92	119	126.84	118.45	CTTAACTGCAGTTTTAAAAGACATTTG	CATTTGAGAGAATGTTTGAACATACA	ABI	vic	C	16
F1	19		D19Mit17.1	45.63	107	103.48	97.71	CIDR	CIDR	ABI-Cidr	6fam	D	11
E1	19		d19mit33	56.27	262	259	322	CCTTTTCAAGAGCATCCTTAAA	GGTGGGACTTGAGAGATGCA	ABI	6fam	D	9
G1	x	167	dxmit81	33.74	200	211.66	213.78	GAGGAGCATCAACCTTCTCG	GAGGTGGGGAGAAACAGAGG	ABI	vic	G	14
F1	x		DXMit68.1	50.68	147	147.78	138.32	CIDR	CIDR	ABI-Cidr	ned	A	11
F1	x		dxmit114	95.34	146	155.28	161.71	ATGGCATCCACAGTACCACA	GTAAAATCAATTTGTGAATAAGGAAGC	ABI	vic	H	12
D1	x		DXMit172.1	119.2	219	218.72	200.09	CIDR	CIDR	ABI-Cidr	vic	C	8
E1	x		DXMit121.1	157.87	127	123.2	121.32	CIDR	CIDR	ABI-Cidr	ned	H	10

Notes:

1. Based on NCBI Build v37.1
2. Dyes- VIC (Applied Biosystems) excitation λ=488 nm, emission λ= 552 nm (green)
   NED excitation λ=_ nm, emission λ=_ nm (yellow)
   6FAM excitation λ=_ nm, emission λ=_ nm (blue)
3. CIDR markers are proprietary, and primer sequences are not publicly available.

Downloaded from jem.rupress.org on January 19, 2012

Disruption of copper homeostasis due to a mutation of *Atp7a* delays the onset of prion disease

Owen M. Siggs[a,1], Justin T. Cruite[b,1], Xin Du[a], Sophie Rutschmann[a,2], Eliezer Masliah[c], Bruce Beutler[a,3,4], and Michael B. A. Oldstone[b,4]

Departments of [a]Genetics and [b]Immunology and Microbial Sciences, The Scripps Research Institute, La Jolla, CA 92037; and [c]Department of Pathology, University of California at San Diego, La Jolla, CA 92037

Contributed by Bruce Beutler, July 6, 2012 (sent for review June 8, 2012)

Copper influences the pathogenesis of prion disease, but whether it is beneficial or detrimental remains controversial. Copper homeostasis is also essential for normal physiology, as highlighted by the spectrum of diseases caused by disruption of the copper transporting enzymes ATP7A and ATP7B. Here, by using a forward genetics approach in mice, we describe the isolation of three alleles of *Atp7a*, each with different phenotypic consequences. The mildest of the three, *Atp7a*^{brown}, was insufficient to cause lethality in hemizygotes or mottling of the coat in heterozygotes, but did lead to coat hypopigmentation and reduced copper content in the brains of hemizygous males. When challenged with Rocky Mountain Laboratory scrapie, the onset of prion disease was delayed in *Atp7a*^{brown} mice, and significantly less proteinase-resistant prion protein was found in the brains of moribund *Atp7a*^{brown} mice compared with WT littermates. Our results establish that ATP7A-mediated copper homeostasis is important for the formation of pathogenic proteinase-resistant prion protein.

neurodegeneration | *N*-ethyl-*N*-nitrosourea (ENU) mutagenesis | Menkes disease | ATPase | pigmentation

Prion diseases are fatal infectious neurodegenerative diseases caused by the misfolding and aggregation of the cellular prion protein, PrP, into the β-sheet–rich, proteinase-resistant, disease-associated form, PrP^{res}. Diseases caused by prions include Creutzfeldt–Jakob disease in humans, bovine spongiform encephalopathy in cattle, scrapie in sheep, and chronic wasting disease in cervids, yet the normal function of cellular prion protein remains a mystery. PrP is known to bind copper, and copper can induce expression of the PrP-encoding gene *Prnp* (1–4). Histidine residues within the highly conserved octarepeat of PrP bind copper (5–8), and additional copies of the octarepeat within PrP are associated with early-onset prion disease. Octarepeat expansion can increase the copper-binding affinity of PrP by as much as 10-fold, suggesting that copper plays a significant role in prion pathogenesis (8). Copper also binds to histidines within region 95–115 of PrP.

The role of copper in prion disease pathogenesis is complex, and interpretations to date have been contradictory. Binding of copper to PrP destabilizes the native α-helical PrP and leads to an increase in β-sheet structure and conversion to the proteinase-resistant form (9–13), yet it has been reported that copper inhibits PrP^{res} amplification (14). Copper is known to promote prion infectivity (15), yet it is also important in limiting neuropathology caused by reactive oxygen species (16). Although copper chelation delays disease onset in mice (17), similar delays are observed in mice and hamsters maintained on a high-copper diet (18, 19). Mice fed a copper-depleted diet are also reported to be more sensitive to prion pathogenesis following i.p. inoculation (18).

The physiological consequences of copper deficiency were first recognized among a group of sheep in western Australia, which were noticed for their "stringy" coats, anemia, and the fact that they consistently gave birth to ataxic lambs (20). The affected ewes were subsequently found to be copper-deficient, and drenching them with copper sulfate solution would reverse anemia, improve their coat condition, and prevent ataxia in their lambs (21). A similar link was established many years later in man, when patients with Menkes disease, an X-linked neurodegenerative condition, were discovered to be copper-deficient (22).

Menkes disease is caused by mutation of *ATP7A*, which encodes the P1B-type ATPase ATP7A (23). Along with the closely related ATPase ATP7B, ATP7A is a critical transporter of copper. Mutation of *ATP7A* is known to cause at least three distinct disorders (24), including Menkes disease (25–27), occipital horn syndrome (considered to be a milder form of Menkes disease) (28), and isolated distal motor neuropathy (29). Conversely, mutation of *ATP7B* causes Wilson disease (30, 31), which is characterized by neuronal and hepatic pathologic processes associated with copper accumulation.

Copper homeostasis is essential for two reasons. First, copper is an essential cofactor for enzymes such as superoxide dismutase, dopamine hydroxylase, tyrosinase, and lysyl oxidase, accounting for the characteristic defects in neurological function, pigmentation, and connective tissue formation seen in Menkes disease (32). Conversely, copper can promote the production of reactive oxygen species, and is therefore highly toxic in excess.

Here we describe the isolation of an *Atp7a* mutant mouse strain with an inherited copper deficiency. In hemizygous males, a 60% reduction in cerebral copper content was associated with delayed PrP^{res} conversion and prion pathogenesis.

Results

Positional Cloning of *brown* Phenotype. During the course of a C57BL/6J mouse mutagenesis program, we identified a male G3 mouse with a brown coat. This phenotype, designated simply as *brown*, was not seen in either parent, suggesting that it was inherited as an autosomal or X-linked recessive trait (ref. 33; http://mutagenetix.utsouthwestern.edu/phenotypic/phenotypic_rec.cfm?pk=469). To determine the chromosomal location of the causative mutation, the index *brown* male was outcrossed to C3H/HeN females, and then backcrossed to his F1 daughters. Among a total of 17 offspring, six were phenotypically normal (one female, five male) and 11 shared the coat color phenotype of their sire (seven female, four male). Each mouse was genotyped at 128 polymorphic markers across the genome, and individual genotypes were tabulated to calculate logarithm (base 10) of odds scores at each marker. This revealed a single peak score of 3.86 at DXMit172, flanked by the distal marker DXMit114 and proximal

Author contributions: O.M.S., J.T.C., B.B., and M.B.A.O. designed research; O.M.S., J.T.C., and E.M. performed research; X.D. and S.R. contributed new reagents/analytic tools; O.M.S., J.T.C., B.B., and M.B.A.O. analyzed data; and O.M.S., J.T.C., B.B., and M.B.A.O. wrote the paper.

The authors declare no conflict of interest.

[1]O.M.S. and J.T.C. contributed equally to this work.

[2]Present address: Faculty of Medicine, Imperial College London, London W12 0NN, United Kingdom.

[3]Present address: Center for Genetics of Host Defense, University of Texas Southwestern Medical Center, Dallas, TX 75390.

[4]To whom correspondence may be addressed. E-mail: bruce.beutler@utsouthwestern.edu or mbaobo@scripps.edu.

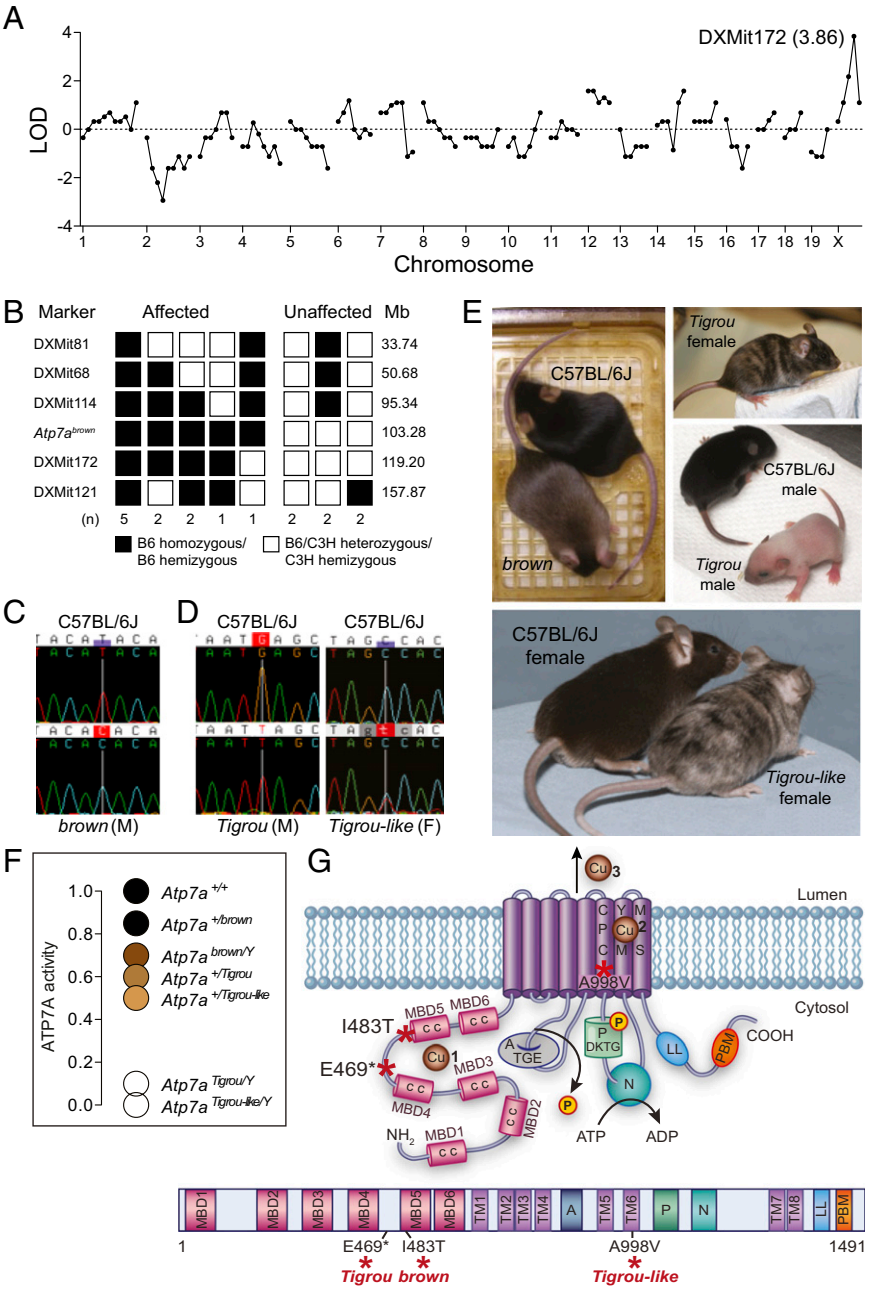


Fig. 1. A hemizygous viable allele of *Atp7a*. (*A*) Linkage mapping of the *brown* mutation to chromosome X. (*B*) Haplotype groups of affected and unaffected F2 progeny, isolating the *brown* mutation to distal chromosome X. (*C*) DNA sequence chromatogram indicates the mutated nucleotide in *Atp7a*. (*D*) Sequence chromatograms of two independent alleles of *Atp7a*: *Tigrou* and *Tigrou-like*. (*E*) Comparison of the coat color phenotypes of three *Atp7a* mutants. (*F*) Predicted relationship between ATP7A activity and tyrosinase-mediated pigmentation. (*G*) Predicted ATP7A topology and domain structure, indicating the relative positions of each mutation. MBD1 to MBD6 represent the N-terminal metal binding domains, with the copper-binding cysteines indicated. Critical residues thought to bind copper in transmembrane domains 6, 7, and 8 are shown. The canonical actuator (marked as "A") domain and phosphorylation ("P") domain residues are also indicated. The dileucine (LL) and PDZ (PSD-95/Discs-large/ZO-1) binding motif (PBM) in the C-terminal tail are necessary for subcellular localization of ATP7A. Conversion of ATP to ADP by the nucleotide-binding ("N") domain leads to phosphorylation of the P-domain and copper transport. The A-domain dephosphorylates the P-domain. Numbers 1, 2, and 3 indicate the order of copper binding and transport.

marker DXMit121 (Fig. 1 *A* and *B*). Within this 62.5-Mb interval lay 358 protein-coding and 22 miRNA genes, three of which had previously been described to affect coat pigmentation when mutated in the mouse (*Atp7a*, *Eda*, and *Htr2c*). As a result of an absence of ectodermal dysplasia phenotypes [commonly associated with *Eda* mutants (34)] or postnatal growth retardation [as seen in an *Htr2c* mutant (35)], all coding exons and splice junctions of *Atp7a* were sequenced. A single T-to-C missense transition was detected at X:103283830, corresponding to position 1570 of the *Atp7a* transcript, in exon 5 of 23 total exons (Fig. 1*C*). The mutation is predicted to result in an isoleucine to threonine substitution at amino acid 483 of the ATP7A protein.

Allelic Series of *Atp7a* Mutations. Although not the case for $Atp7a^{brown}$, heterozygous *Atp7a* mutants typically present with variegated coat color, a consequence of random X-inactivation

in melanocyte precursors (36). Examples of this phenotype were previously observed in our mutagenesis program, and given their similarity to the classic *mottled* mutants (37, 38), were sequenced at the *Atp7a* locus. The mutants *Tigrou* and *Tigrou-like* were both found to harbor *Atp7a* mutations (Fig. 1*D*), respectively creating a premature termination codon at position 469, and an alanine-to-valine substitution at codon 998. Hemizygous *Tigrou* males were occasionally observed, lacked pigmentation (except at their extremities), and died within 3 wk of birth (Fig. 1*E*). *Tigrou-like* appeared to be entirely lethal in utero, as hemizygous males were not observed postpartum. Similar to *Tigrou-like* and *Tigrou*, the vast majority of *Atp7a* alleles described in mouse are hemizygous lethal in utero or shortly after birth (39). $Atp7a^{Blotchy}$ and the *Pewter* series of alleles are all hemizygous viable, yet, unlike *brown*, cause variegated pigmentation in heterozygous form, making *brown* a uniquely mild allele in the *Atp7a* allelic series.

Based on the pigmentation phenotype of heterozygotes and lethality in hemizygotes, the three alleles could be arranged in a decreasing order of functional severity, with *Tigrou-like* predicted to cause the most severe copper deficiency and *brown* the least (Fig. 1*F*; protein schematic shown in Fig. 1*G*).

Although one might expect the *Tigrou* nonsense allele to be more detrimental than the A998V missense mutation of *Tigrou-like*, skipping of a nonsense mutation-harboring exon has been observed in a patient with Menkes disease (40). In the case of *Tigrou*, such a splice product would remove exon 5 yet remain in frame, but would do so at the expense of the fifth metal binding domain. Nevertheless, the effects of each missense mutation were consistent with PolyPhen-2 predictions, with respective scores of 1 and 0.476 for *Tigrou-like* and *brown*.

Reduced Quantities of Copper and Delayed Onset of Prion Disease. The brains of $Atp7a^{brown/Y}$ and $Atp7a^{+/Y}$ littermates were analyzed for copper content. The amount of copper in the brains of $Atp7a^{brown/Y}$ mice was reduced by 60% compared with $Atp7a^{+/Y}$ littermates [1.6 ± 0.2 μg Cu^{2+}/g of brain (mean ± SEM) vs. 3.9 ± 0.4 μg Cu^{2+}/g; $P < 0.0001$; Fig. 2*A*].

$Atp7a^{brown/Y}$ and $Atp7a^{+/Y}$ littermates were inoculated intracranially with the Rocky Mountain Laboratory (RML) strain of mouse scrapie. All 10 $Atp7a^{+/Y}$ mice became ill with clinical signs of scrapie, including altered gait, kyphosis, ataxia, disorientation, and lethargy within 161 d after infection. In contrast, only one of 10 $Atp7a^{brown/Y}$ mice developed disease within the same period. The remaining $Atp7a^{brown/Y}$ mice became terminally ill by 180 d after infection ($P < 0.0001$; Fig. 2*B*). Moribund mice from both groups were killed, and their brains were harvested for detection of abnormally folded PrP^{res} protein (Fig. 2*C*). Proteinase K-resistant PrP was detected by Western blot in the brains of clinically ill $Atp7a^{+/Y}$ (Fig. 2*C*, lanes 6, 8, and 10) and $Atp7a^{brown/Y}$ mice (Fig. 2*C*, lanes 12, 14, and 16), confirming prion disease. No proteinase K-resistant PrP was detected in the brains of uninfected $Atp7a^{+/Y}$ or $Atp7a^{brown/Y}$ mice (Fig. 2*C*, lanes 2 and 4).

Histological analysis showed that the brains of clinically ill $Atp7a^{brown/Y}$ and $Atp7a^{+/Y}$ mice displayed spongiosis typical of transmissible spongiform encephalopathies, particularly in the cerebellum (Fig. 3, *Top*). Brain sections from both RML scrapie-infected $Atp7a^{+/Y}$ and $Atp7a^{brown/Y}$ mice displayed considerable loss of MAP2-immunoreactive dendrites in the neocortex and hippocampus (Fig. 3, *Middle*), most apparent in the CA1–CA3 regions, suggestive of selective damage to pyramidal neurons. Analysis of reactive astrocytes by GFAP staining showed that both groups of RML scrapie-infected mice also showed extensive astrogliosis (Fig. 3, *Bottom*). Consistent with the widespread neurodegenerative alterations observed by MAP2 and GFAP staining, analysis of neuronal cells with NeuN showed rarefaction and loss of neurons in the CA1–CA3 regions in both RML scrapie-infected groups, and was accompanied by microgliosis as determined by Iba1 staining (not shown).

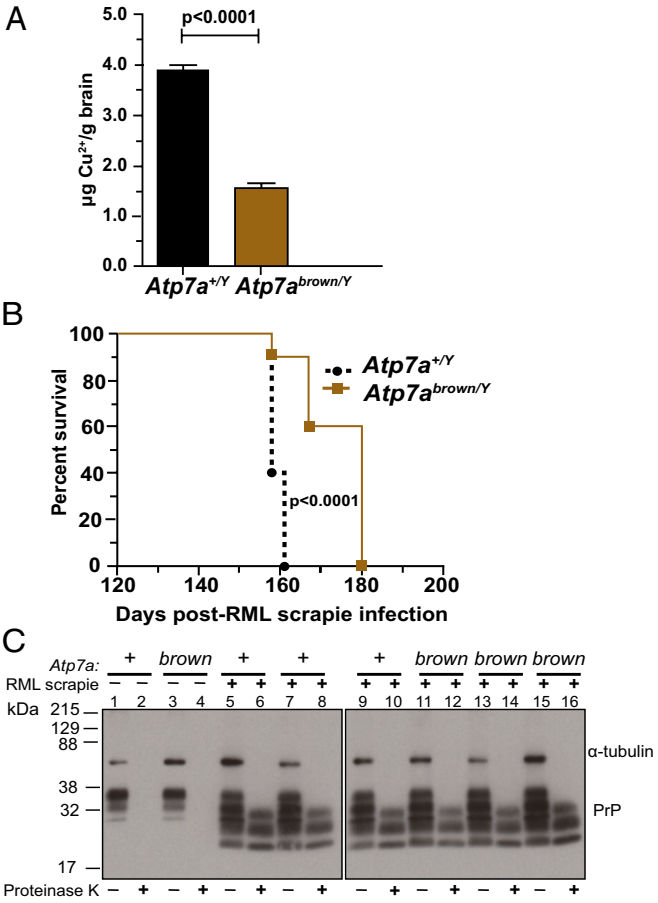


Fig. 2. Reduced copper content in $Atp7a^{brown}$ mutant brains is associated with prolonged survival after intracranial RML scrapie infection. (*A*) The amount of copper in the brains of uninfected $Atp7a^{+/Y}$ and $Atp7a^{brown/Y}$ littermates was determined by ICP-MS ($n = 5$; error bars represent SEM). (*B*) $Atp7a^{+/Y}$ and $Atp7a^{brown/Y}$ mice were inoculated intracranially with RML scrapie and killed when clinical signs of prion disease were observed ($n = 10$). (*C*) The presence of PrP^{res} in the brains of clinically ill $Atp7a^{+/Y}$ and $Atp7a^{brown/Y}$ mice was confirmed by Western blot ($n = 3$). Similar results to those shown were obtained for all other samples analyzed in each experiment.

However, substantially less PrP^{res} was detected by immunohistochemistry in the brains of clinically ill $Atp7a^{brown/Y}$ mice compared with those of $Atp7a^{+/Y}$ (Fig. 4*A*). Upon further analysis, when equal amounts of protein from the brains of clinically ill mice were analyzed by Western blot (Fig. 4*B*), 41% less total PrP ($P < 0.01$; Fig. 4*C*) and 50% less PrP^{res} ($P < 0.01$; Fig. 4*D*) was detected in the brains of infected $Atp7a^{brown/Y}$ mice compared with those of $Atp7a^{+/Y}$. No significant difference was seen between the amount of PrP in the brains of uninfected $Atp7a^{brown/Y}$ and $Atp7a^{+/Y}$ mice (Fig. 4 *B* and *C*).

In summary, we observed widespread degeneration in the cortex, hippocampus, basal ganglia, and cerebellum of RML scrapie-infected $Atp7a^{+/Y}$ and $Atp7a^{brown/Y}$ mice. The degree of neuronal loss, astrocytosis, and microgliosis in infected $Atp7a^{brown/Y}$ mice was equivalent to that observed in infected $Atp7a^{+/Y}$ mice, yet the amount of PrP^{res} in the brains of $Atp7a^{+/Y}$ mice was significantly higher than in their $Atp7a^{brown/Y}$ littermates, as measured by Western blotting and immunohistochemistry.

Discussion

This report describes the characterization of a hypomorphic allele of the Menkes disease gene orthologue, *Atp7a*, characterized by coat hypopigmentation and an insufficiency of copper in the

IMMUNOLOGY

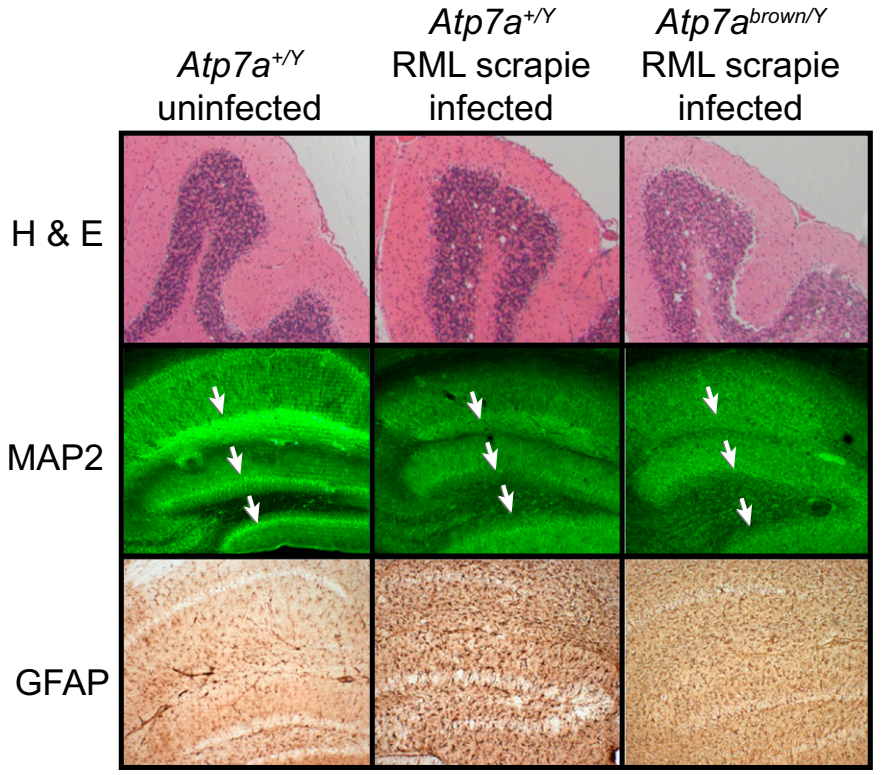


Fig. 3. Normal spongiosis, dendrite loss, and astrogliosis in the brains of RML scrapie-infected *Atp7a*^{brown} mutants. Brain sections from uninfected *Atp7a*$^{+/Y}$, RML scrapie-infected *Atp7a*$^{+/Y}$, and RML scrapie-infected *Atp7a*$^{brown/Y}$ mice killed when clinically ill were stained with H&E, antibodies against the dendrite marker MAP2, and antibodies against the astroglial marker GFAP. Arrows indicate areas of MAP2 staining and highlight dendrite loss in the RML scrapie-infected sections. Similar results to those shown were obtained for all other samples in each group (n = 3).

brain. The *Atp7a*^{brown} mutation significantly increased the incubation period of intracranial RML scrapie infection, supporting earlier reports that copper chelation can delay the onset of scrapie disease (17). *Atp7a*^{brown} mutant mice had twice the reduction in brain copper content compared with mice treated with copper chelation, with the incubation period extended in a commensurate manner (10% longer vs. 7% after chelation) (17).

In addition to the delay in disease onset, the amount of PrP^{res} in the brains of clinically ill *Atp7a*$^{brown/Y}$ mice was significantly lower than that of clinically ill *Atp7a*$^{+/Y}$ mice by Western blot and immunohistochemistry, consistent with previous reports implicating copper in the conversion of PrP to PrP^{res} (17). Nevertheless, the amount of neuronal loss and astrocytosis was similar in both groups in the cortex, hippocampus, cerebellum, and brainstem, indicating that residual PrP^{res} remains capable of causing neurodegeneration and death. The existence of proteinase-sensitive infectious prion protein (PrP^{Sc}) has been reported by others, and copper is known to influence the proteinase resistance of PrP (41–43). It is possible that, although accumulated PrP^{Sc} in a copper-deficient environment may be more sensitive to digestion by proteinases, it may remain toxic enough to cause disease. Equivalent pathology might also be a result of the reduced activity of neuroprotective copper-dependent enzymes such as SOD1. Others have previously reported that copper induces the expression of PrP in vivo (3, 4), yet we observed no difference in the amount of PrP in the brains of uninfected *Atp7a*$^{brown/Y}$ and *Atp7a*$^{+/Y}$ mice.

Our results are consistent with earlier reports of copper-induced PrP proteinase resistance (6, 7, 44) and the delay of disease onset by copper chelation (17). Although copper chelation or an *Atp7a* mutation can delay the onset of prion disease, it cannot prevent it, even given the 60% reduction in brain copper observed in *Atp7a*^{brown} mice. A reduction as great as this also has the potential to cause clinically undesirable side effects, and, as such, copper chelation therapy in humans should be approached cautiously.

Materials and Methods

Mice and Positional Cloning. *Atp7a*^{brown}, *Atp7a*^{Tigrou}, and *Atp7a*$^{Tigrou\text{-}like}$ alleles were all generated on a pure C57BL/6J background by *N*-ethyl-*N*-nitrosourea mutagenesis as previously described (45). The index *brown* mutant (C57BL/6J, male) was outcrossed to C3H/HeN females (Taconic), and F1 daughters were backcrossed to their father. Mice were grouped into mutant and WT cohorts (11 and six mice, respectively) based on coat color. Individual mice were typed at 128 microsatellite markers spaced across the genome (46), with expected and observed genotype frequencies used to calculate logarithm of odds scores at each position. *Atp7a* gene amplicons from WT, *brown*, *Tigrou*, and *Tigrou-like* genomic DNA were sequenced by using an ABI 3730xl capillary sequencer. The deleterious effect of *Atp7a* mutations were predicted by using the HumDiv-trained PolyPhen-2 server (version 2.1.0) (47). C57BL/6J males used for mutagenesis were obtained from The Jackson Laboratory. All other C57BL/6J mice were obtained from The Scripps Research Institute breeding colony. All animal procedures were in accordance with guidelines of the institutional animal care and use committee of The Scripps Research Institute.

Scrapie Inoculation. Mice were inoculated intracranially with 30 μL of a 2% (wt/vol) RML C57BL/6J mouse scrapie brain homogenate in PBS solution. Inoculated mice were monitored daily for clinical signs of scrapie, including weight loss, lethargy, ataxia, and paralysis. Mice showing severe clinical signs of scrapie were killed, and brains were taken for biochemical and histological analysis.

Western Blotting. Brains from scrapie-infected and noninfected control mice were homogenized in PBS solution at 100 mg of tissue/mL. Homogenate was then diluted with an equal volume of 1% Triton X-100 (Sigma) in PBS solution, sonicated, and cleared by centrifugation at 500 × g for 15 min. For diagnostic purposes, an equal volume of 5% brain homogenate from each mouse was untreated or treated with 50 μg/mL of proteinase K in 1%

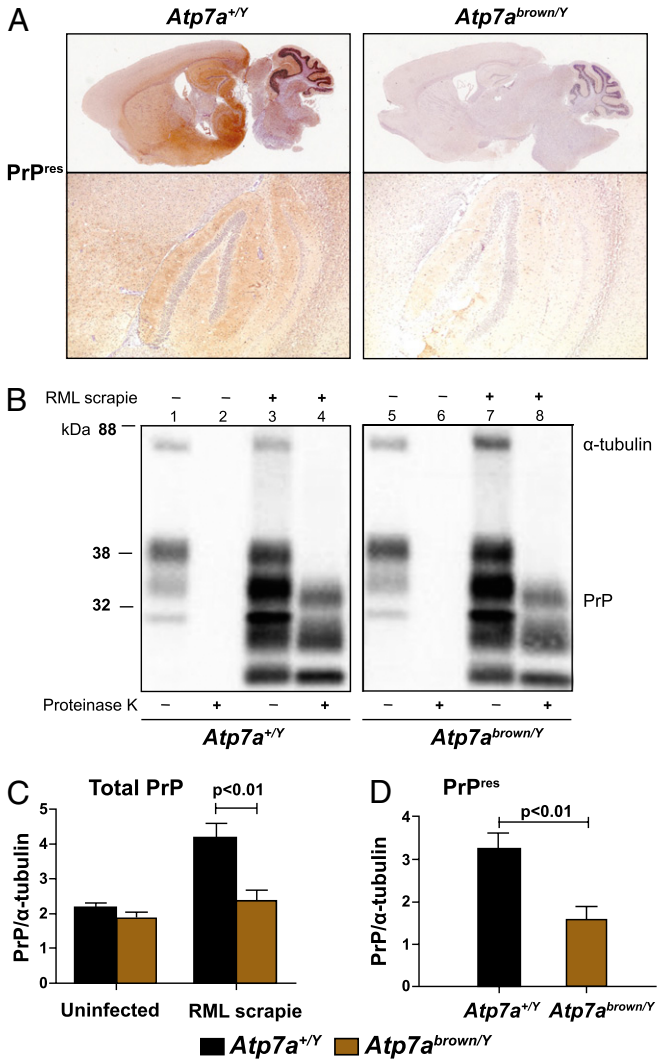


Fig. 4. Reduced PrP and PrP^{res} in the brains of RML scrapie-infected *Atp7a*^{brown} mutants. (*A*) Brain sections from clinically ill RML scrapie-infected *Atp7a*$^{+/Y}$ and *Atp7a*$^{brown/Y}$ mice were stained for proteinase K-resistant PrP (i.e., PrP^{res}; n = 3). Low-magnification (*Upper*) and high-magnification (*Lower*) images are shown. (*B*) Representative Western blots of PrP and PrP^{res} levels in the brains of uninfected and RML scrapie-infected *Atp7a*$^{+/Y}$ (lanes 1–4) and *Atp7a*$^{brown/Y}$ (lanes 5–8) mice. (*C* and *D*) Quantification of total PrP (*C*) and PrP^{res} (*D*) in the brains of uninfected and RML scrapie-infected *Atp7a*$^{+/Y}$ and *Atp7a*$^{brown/Y}$ mice as determined by Western blot by using GE ImageQuant software (n = 5; error bars represent SEM). Similar results to those shown were obtained for all other samples analyzed in each experiment.

Triton X-100 solution for 1 h at 37 °C. For quantitative purposes, total protein concentration of each sample was determined by bicinchoninic acid assay (Pierce), and 20 μg of total protein from each sample was untreated or treated with 50 μg/mL of proteinase K. Reactions were stopped by adding an equal volume of 2× SDS loading buffer (Invitrogen) and heating to 95 °C for 5 min. The samples were then run on a 16% Tris-glycine gel (Invitrogen) and transferred to Invitrolon PVDF membrane (Invitrogen). The membrane was blocked and all antibodies were diluted in 5% nonfat milk. Human anti-PrP antibody D13 was used at 3 μg/mL to detect PrP, followed by peroxidase-conjugated goat anti-human antibody (Jackson ImmunoResearch) used at a 1:10,000 dilution. For quantitative Western blots, a mouse anti–α-tubulin antibody was used at 1:10,000, followed by peroxidase-conjugated anti-mouse IgG antibody (Jackson ImmunoResearch) used at 1:5,000. Blots were developed with SuperSignal West Pico Chemiluminescent Substrate (Thermo Scientific) and exposed to X-ray film or imaged by using a GE ImageQuant LAS 4000. Signal intensities were analyzed with GE ImageQuantTL software.

Analysis of Brain Copper Content. Brains were analyzed individually for copper content using inductively coupled plasma mass spectroscopy (ICP-MS). Whole brain was homogenized in ddH_2O at 100 mg of tissue/mL. The tissue homogenate was cleared by ultrasonication and centrifugation at 500 × *g* for 15 min. One milliliter of cleared brain homogenate was digested with 3 mL of 70% nitric acid by using a microwave acid digestion vessel (Parr). Each sample was microwaved for 30 s at full power in a 1,200-W household microwave oven and allowed to cool for 30 min before opening. Separate microwave digestion vessels were used for mutant and WT samples. The digested sample was then diluted 1:2 with ddH_2O before analysis. Standard concentrations of Cu used were 0, 10, 25, 50, 75, 100, and 200 parts per billion. Each standard and sample contained 100 parts per billion yttrium as an internal standard. Each sample was analyzed three times, with 2% (vol/vol) nitric acid run for 2 min between each sample. The ICP-MS was recalibrated, and standards were rerun after every 15 samples.

Histology and PrP^{res} Immunohistochemistry. Brain hemispheres were fixed in 4% paraformaldehyde containing zinc for a minimum of 24 h before being dehydrated, embedded in paraffin wax, cut into 6-μm sections, and placed on glass slides. Sections were deparaffinized with xylene and rehydrated with ethanol and water. For H&E staining, sections were stained with Shandon hematoxylin (Thermo Scientific) and differentiated in 1% HCl (in 70% isopropanol). Hematoxylin-stained sections were blued with Scott tap water substitute before being stained with Shandon eosin (Thermo Scientific), dehydrated with ethanol, cleared with xylene, and mounted with Permount. For PrP^{res} immunohistochemistry, antigen retrieval was performed by autoclaving in PBS solution for 12 min at 250 °F. Proteinase-sensitive PrP was removed by treatment with 50 μg/mL of proteinase K for 20 min at room temperature. The sections were then blocked with 10% normal goat serum overnight, avidin–biotin blocked (Vector Laboratories), and incubated in 3% hydrogen peroxide for 20 min. PrP was detected with 3 μg/mL antibody D13, biotinylated anti-human IgG (Jackson ImmunoResearch), and avidin-conjugated peroxidase (Jackson ImmunoResearch). After PrP staining, sections were counterstained with Shandon hematoxylin and Scott tap water substitute. The sections were dehydrated with ethanol and xylene and mounted using Permount (Fisher Scientific).

MAP2, GFAP, NeuN, and Iba1 Immunohistochemistry. Vibratome sections (40 μm) were immunolabeled overnight with antibodies against the neuronal marker NeuN (1:1,000; Millipore), the astroglial marker GFAP (1:500; Millipore), the dendritic marker MAP2 (1:200; Millipore), and the microglial cell marker Iba1 (1:500; Wako), followed by incubation with species-appropriate secondary antibodies conjugated to HRP or FITC (1:2,000; Vector Laboratories). Sections labeled with HRP (NeuN, Iba1, and GFAP) were incubated with DAB and analyzed with a bright-field digital Olympus microscope. Signal intensities were assessed by optical density measurements by using the Image Quant 1.43 program (National Institutes of Health) and corrected against background. FITC-labeled sections (i.e., MAP2) were analyzed with an MRC1024 laser scanning confocal microscope (Bio-Rad).

ACKNOWLEDGMENTS. The authors thank M. Gutierrez for animal care; C. Domingo, L. Hanley, and E. Pirie for *N*-ethyl-*N*-nitrosourea pedigree generation; C. Ross for sequencing; Y. Xia for bioinformatics support; D. LaVine for illustrations; A. Murray and V. Webster for manuscript preparation; and M. G. Finn and Z. Polonskaya for help with inductively coupled plasma MS. This work was supported by National Institute of Allergy and Infectious Diseases/National Institutes of Health Grants HHSN272200700038C (to B.B.), AG04342 (to M.B.A.O.), AG18440 (to E.M.), AG022074 (to E.M.), and NS057096 (to E. M.); and by the General Sir John Monash Foundation (O.M.S.). This is Scripps Research Institute publication no. 21636.

1. Brown DR, et al. (1997) The cellular prion protein binds copper in vivo. *Nature* 390: 684–687.
2. Zidar J, Pirc ET, Hodoscek M, Bukovec P (2008) Copper(II) ion binding to cellular prion protein. *J Chem Inf Model* 48:283–287.
3. Varela-Nallar L, et al. (2006) Induction of cellular prion protein gene expression by copper in neurons. *Am J Physiol Cell Physiol* 290:C271–C281.
4. Armendariz AD, Gonzalez M, Loguinov AV, Vulpe CD (2004) Gene expression profiling in chronic copper overload reveals upregulation of Prnp and App. *Physiol Genomics* 20:45–54.
5. Aronoff-Spencer E, et al. (2000) Identification of the Cu2+ binding sites in the N-terminal domain of the prion protein by EPR and CD spectroscopy. *Biochemistry* 39: 13760–13771.

6. Hornshaw MP, McDermott JR, Candy JM (1995) Copper binding to the N-terminal tandem repeat regions of mammalian and avian prion protein. *Biochem Biophys Res Commun* 207:621–629.
7. Hornshaw MP, McDermott JR, Candy JM, Lakey JH (1995) Copper binding to the N-terminal tandem repeat region of mammalian and avian prion protein: Structural studies using synthetic peptides. *Biochem Biophys Res Commun* 214:993–999.
8. Stevens DJ, et al. (2009) Early onset prion disease from octarepeat expansion correlates with copper binding properties. *PLoS Pathog* 5:e1000390.
9. Qin K, et al. (2000) Copper(II)-induced conformational changes and protease resistance in recombinant and cellular PrP. Effect of protein age and deamidation. *J Biol Chem* 275:19121–19131.
10. Jones CE, Abdelraheim SR, Brown DR, Viles JH (2004) Preferential Cu2+ coordination by His96 and His111 induces beta-sheet formation in the unstructured amyloidogenic region of the prion protein. *J Biol Chem* 279:32018–32027.
11. Kuczius T, et al. (2004) Cellular prion protein acquires resistance to proteolytic degradation following copper ion binding. *Biol Chem* 385:739–747.
12. Quaglio E, Chiesa R, Harris DA (2001) Copper converts the cellular prion protein into a protease-resistant species that is distinct from the scrapie isoform. *J Biol Chem* 276: 11432–11438.
13. Younan ND, et al. (2011) Copper(II)-induced secondary structure changes and reduced folding stability of the prion protein. *J Mol Biol* 410:369–382.
14. Orem NR, Geoghegan JC, Deleault NR, Kascsak R, Supattapone S (2006) Copper (II) ions potently inhibit purified PrPres amplification. *J Neurochem* 96:1409–1415.
15. McKenzie D, et al. (1998) Reversibility of scrapie inactivation is enhanced by copper. *J Biol Chem* 273:25545–25547.
16. Brown DR, et al. (1999) Normal prion protein has an activity like that of superoxide dismutase. *Biochem J* 344:1–5.
17. Sigurdsson EM, et al. (2003) Copper chelation delays the onset of prion disease. *J Biol Chem* 278:46199–46202.
18. Mitteregger G, Korte S, Shakarami M, Herms J, Kretzschmar HA (2009) Role of copper and manganese in prion disease progression. *Brain Res* 1292:155–164.
19. Hijazi N, Shaked Y, Rosenmann H, Ben-Hur T, Gabizon R (2003) Copper binding to PrPC may inhibit prion disease propagation. *Brain Res* 993:192–200.
20. Bennetts HW (1932) Enzootic ataxia of lambs in Western Australia. *Aust Vet J* 8: 137–142.
21. Bennetts HW, Chapman FE (1937) Copper deficiency in sheep in Western Australia: A preliminary account of the etiology of enzootic ataxia of lambs and an anemia of ewes. *Aust Vet J* 13:138–149.
22. Danks DM, Campbell PE, Stevens BJ, Mayne V, Cartwright E (1972) Menkes's kinky hair syndrome. An inherited defect in copper absorption with widespread effects. *Pediatrics* 50:188–201.
23. Kühlbrandt W (2004) Biology, structure and mechanism of P-type ATPases. *Nat Rev Mol Cell Biol* 5:282–295.
24. Kaler SG (2011) ATP7A-related copper transport diseases-emerging concepts and future trends. *Nat Rev Neurol* 7:15–29.
25. Vulpe C, Levinson B, Whitney S, Packman S, Gitschier J (1993) Isolation of a candidate gene for Menkes disease and evidence that it encodes a copper-transporting ATPase. *Nat Genet* 3:7–13.
26. Mercer JF, et al. (1993) Isolation of a partial candidate gene for Menkes disease by positional cloning. *Nat Genet* 3:20–25.
27. Chelly J, et al. (1993) Isolation of a candidate gene for Menkes disease that encodes a potential heavy metal binding protein. *Nat Genet* 3:14–19.
28. Kaler SG, et al. (1994) Occipital horn syndrome and a mild Menkes phenotype associated with splice site mutations at the MNK locus. *Nat Genet* 8:195–202.
29. Kennerson ML, et al. (2010) Missense mutations in the copper transporter gene ATP7A cause X-linked distal hereditary motor neuropathy. *Am J Hum Genet* 86: 343–352.
30. Bull PC, Thomas GR, Rommens JM, Forbes JR, Cox DW (1993) The Wilson disease gene is a putative copper transporting P-type ATPase similar to the Menkes gene. *Nat Genet* 5:327–337.
31. Tanzi RE, et al. (1993) The Wilson disease gene is a copper transporting ATPase with homology to the Menkes disease gene. *Nat Genet* 5:344–350.
32. de Bie P, Muller P, Wijmenga C, Klomp LW (2007) Molecular pathogenesis of Wilson and Menkes disease: correlation of mutations with molecular defects and disease phenotypes. *J Med Genet* 44:673–688.
33. Siggs OM, Smart NG, Murray AR, Beutler B (2012) Record for brown. MUTAGENETIX (TM), B Beutler and Colleagues, Center for the Genetics of Host Defense, UT Southwestern, Dallas, TX. Available at http://mutagenetix.utsouthwestern.edu/phenotypic/phenotypic_rec.cfm?pk=469. Accessed July 12, 2012.
34. Srivastava AK, et al. (1997) The Tabby phenotype is caused by mutation in a mouse homologue of the EDA gene that reveals novel mouse and human exons and encodes a protein (ectodysplasin-A) with collagenous domains. *Proc Natl Acad Sci USA* 94: 13069–13074.
35. Morabito MV, et al. (2010) Mice with altered serotonin 2C receptor RNA editing display characteristics of Prader-Willi syndrome. *Neurobiol Dis* 39:169–180.
36. Lyon MF (1961) Gene action in the X-chromosome of the mouse (Mus musculus L.). *Nature* 190:372–373.
37. Mercer JF, et al. (1994) Mutations in the murine homologue of the Menkes gene in dappled and blotchy mice. *Nat Genet* 6:374–378.
38. Levinson B, Packman S, Gitschier J (1997) Mutation analysis of mottled pewter. *Mouse Genome* 95:163–165.
39. Mercer JF (1998) Menkes syndrome and animal models. *Am J Clin Nutr* 67(5 suppl): 1022S–1028S.
40. Das S, et al. (1994) Diverse mutations in patients with Menkes disease often lead to exon skipping. *Am J Hum Genet* 55:883–889.
41. Gambetti P, Puoti G, Zou WQ (2011) Variably protease-sensitive prionopathy: A novel disease of the prion protein. *J Mol Neurosci* 45:422–424.
42. Pastrana MA, et al. (2006) Isolation and characterization of a proteinase K-sensitive PrPSc fraction. *Biochemistry* 45:15710–15717.
43. Thackray AM, Hopkins L, Bujdoso R (2007) Proteinase K-sensitive disease-associated ovine prion protein revealed by conformation-dependent immunoassay. *Biochem J* 401:475–483.
44. Miura T, Hori-i A, Takeuchi H (1996) Metal-dependent alpha-helix formation promoted by the glycine-rich octapeptide region of prion protein. *FEBS Lett* 396:248–252.
45. Georgel P, Du X, Hoebe K, Beutler B (2008) ENU mutagenesis in mice. *Methods Mol Biol* 415:1–16.
46. Siggs OM, Li X, Xia Y, Beutler B (2012) ZBTB1 is a determinant of lymphoid development. *J Exp Med* 209:19–27.
47. Adzhubei IA, et al. (2010) A method and server for predicting damaging missense mutations. *Nat Methods* 7:248–249.